

THE EFFECT OF EXPERIMENTAL CONDITIONS ON NATURAL GAS HYDRATE
FORMATION

A THESIS SUBMITTED TO
THE GRADUATE SCHOOL OF NATURAL AND APPLIED SCIENCES
OF
MIDDLE EAST TECHNICAL UNIVERSITY

BY

SOTIRIOS LONGINOS

IN PARTIAL FULFILLMENT OF THE REQUIREMENTS
FOR
THE DEGREE OF DOCTOR IN PHILOSOPHY
IN
PETROLEUM AND NATURAL GAS ENGINEERING

JULY 2020

Approval of the Thesis:

**THE EFFECT OF EXPERIMENTAL CONDITIONS ON NATURAL GAS
HYDRATE FORMATION**

submitted by **SOTIRIOS LONGINOS** in partial fulfillment of the requirements for the degree of **Doctor of Philosophy in Petroleum and Natural Gas Engineering Department, Middle East Technical University** by,

Prof. Dr. Halil Kalıpçılar
Dean, Graduate School of **Natural and Applied Sciences** _____

Assoc. Prof. Dr. Çağlar Sınayuç
Head of Department, **Petroleum and Natural Gas Engineering** _____

Prof. Dr. Mahmut Parlaktuna
Supervisor, **Petroleum and Natural Gas Eng. Dept., METU** _____

Asst. Prof. Dr. İnci Ayrancı Tansık
Co-Supervisor, **Chemical Eng. Dept., METU** _____

Examining Committee Members:

Prof. Dr. Ülkü Mehmetoğlu
Chemical Engineering Dept., Ankara University _____

Prof. Dr. Mahmut Parlaktuna
Petroleum and Natural Gas Engineering Dept., METU _____

Assoc. Prof. Dr. Çağlar Sınayuç
Petroleum and Natural Gas Engineering Dept., METU _____

Prof. Dr. Günay Çifci
Inst. of Marine Sciences and Technology, Dokuz Eylül University _____

Asst. Prof. Dr. İsmail Durgut
Petroleum and Natural Gas Engineering Dept., METU _____

Date: 13.7.2020

I hereby declare that all information in this document has been obtained and presented in accordance with academic rules and ethical conduct. I also declare that, as required by these rules and conduct, I have fully cited and referenced all material and results that are not original to this work.

Name, Last name: Sotirios Longinos

Signature:

ABSTRACT

THE EFFECT OF EXPERIMENTAL CONDITIONS ON NATURAL GAS HYDRATE FORMATION

Sotirios Longinos

Ph.D., Department of Petroleum and Natural Gas Engineering

Supervisor: Prof. Dr. Mahmut Parlaktuna

Co-Supervisor: Asst. Prof. Dr. İnci Ayrancı Tansık

July 2020, 260 pages

Natural gas hydrates (NGH) are proposed as gas storage and transportation media owing to their high gas content and long-term stability of hydrate crystal structure at common refrigeration temperatures and atmospheric pressure. Technically feasible, cost efficient hydrate production is one of the crucial items of the whole chain of storage and transportation of gas by means of NGH technology. This study investigated the effects of types of impellers and baffles, and the use of promoters on natural gas hydrate formation.

Up-pumping pitched blade turbine (PBTU) and Rushton turbine (RT) were the two types of impellers tested. The reactor was equipped with different designs of baffles: full, half and surface baffles, or no baffles. In total 48 experiments were completed with different impeller – baffle combinations. Single (PBTU or RT), dual (PBTU/PBTU or RT/RT) and dual-mixed (PBTU/RT or RT/PBTU) use of impellers with full (FB), half (HB), surface (SB) and no baffle (NB) combinations formed two sets of 24 experiments. The first set was completed with the use of pure methane as hydrate forming gas and in the second set methane – propane mixture (95% - 5%) was used.

Experimental data was analyzed in terms of induction time, hydrate formation rate, overall power consumption, hydrate productivity and conversion of water to hydrate. In addition, split fraction of methane and propane in free gas and solid hydrate during hydrate formation from mixture gas is determined. The reactor was operated in batch mode in all the experiments.

Single impeller experiments with methane showed that Rushton turbine has better performance than up-pumping pitched blade turbine, for all kind of baffles. Use of dual impellers, either the same type or mixed, produced similar results of single impeller. The initial hydrate formation rate is generally higher with the use of Rushton turbine, but the decline rate of hydrate formation was also high compared to up-pumping pitched blade turbine (PBTU). The higher amount of hydrate formed at the gas-water interface initially restricts the mass transfer between gas and water phases and results in a higher decline in the formation rate of hydrate. The other fact causing the decline in hydrate formation rate is the exothermic nature of hydrate formation. Hydrate formation process by gas mixtures become more complex because of different partition of gas components in free gas and solid hydrate phases. Propane is consumed more if hydrate is formed from a gas mixture of methane – propane. This fact brings another complexity of varying hydrate equilibrium curve during hydrate formation. As propane is consumed, hydrate equilibrium pressure gets higher for the given process temperature. Aqueous solutions of amino acids tested in this study showed shorter induction time and generally higher hydrate formation rates compared to distilled water. This indicates a potential of finding hydrate promoters among these amino acids.

Keywords: natural gas hydrates, rate of hydrate formation, induction time, amino acids.

ÖZ

DENEYSEL KOŞULLARIN DOĞAL GAZ HİDRAT OLUŞUMUNA ETKİLERİ

Longinos, Sotirios

Doktora, Petrol ve Doğal Gaz Mühendisliği Bölümü

Tez Yöneticisi: Prof. Dr. Mahmut Parlaktuna

Yardımcı Tez Yöneticisi: Dr. Öğretim Üyesi İnci Ayrancı Tansık

Temmuz 2020, 260 sayfa

Doğal gaz hidratları (NGH), yapılarındaki yüksek gaz içeriği ve hidrat kristal yapısının günümüz derin dondurucu teknolojisinde kullanılan sıcaklık ve atmosferik basınç şartlarındaki uzun süreli kararlı yapısı nedeniyle doğal gazın depolanması ve taşınması için önerilmektedir. Teknik olarak uygulanabilir ve ekonomik bir hidrat üretim süreci, NGH teknolojisi ile gaz depolama ve taşıma zincirinin önemli öğelerden birisidir. Bu çalışmada karıştırıcı ve engel türleri ile kimyasal hızlandırıcıların doğal gaz hidrat oluşumu üzerindeki etkileri araştırılmıştır.

Yukarı pompalayan eğimli bıçaklı karıştırıcı (PBTU) ve Rushton türbini (RT) çalışmada kullanılan iki karıştırıcı türüdür. Deneyler sırasında reaktör tam (FB), yarım (HB) veya yüzey (SB) engellerinden biriyle donatılmış ya da engel kullanılmamıştır. Çalışmada farklı karıştırıcı – engel kombinasyonları ile 48 adet deney gerçekleştirilmiştir. Tek karıştırıcı (PBTU veya RT), aynı türden çift karıştırıcı (PBTU/PBTU veya RT/RT) ve son olarak farklı türden çift karıştırıcı (PBTU/RT veya RT/PBTU) kullanılan deneylerde tam (FB), yarım (HB), yüzey (SB) veya engelsiz (NB) engel türleriyle iki adet 24 deneylik grup oluşmuştur. İlk grupta hidrat oluşturan gaz saf metan iken ikinci grupta % 95 metan - % 5 propandan oluşan gaz karışımı hidrat oluşumu için kullanılmıştır.

Deneysel veri, indüklenme zamanı, hidrat oluşum hızı, tüketilen güç, hidrat üretkenliği ve suyun hidrata dönüşme yüzdesi açısından analiz edilmiştir. Ayrıca karışım gazından hidrat oluşumu sırasında serbest gaz ve katı hidratta metan ve propanın paylaşımları hesaplanmıştır. Tüm deneylerde kesikli reaktör kullanılmıştır.

Saf metan kullanılarak gerçekleştirilen tek karıştırıcı deney sonuçları, tüm engeller için, Rushton türbin tipi karıştırıcının yukarı pompalayan eğimli bıçaklı karıştırıcıdan daha iyi performansa sahip olduğunu göstermiştir. Aynı türden veya farklı türden ikili karıştırıcılarla gerçekleştirilen deneylerde de benzer sonuçlar elde edilmiştir. Rushton türbinle yapılan deneylerde ilk an hidrat oluşum hızı, genel olarak, yukarı pompalayan eğimli bıçaklı karıştırıcı deneylerin ilk an hidrat oluşum hızlarından yüksek olmasına rağmen hidrat oluşum hızının değişim hızı da yüksektir. Yüksek ilk an hızıyla gaz – su arayüzünde oluşturulan yüksek miktardaki hidrat fazlar arası kütle transferini kısıtlamakta ve ilerleyen zamanla hidrat oluşum hızını düşürmektedir. Hidrat oluşum hızının düşmesinin bir diğer nedeni de hidrat oluşumunun ekzotermik bir süreç olmasıdır. Gaz karışımları kullanılarak hidrat oluşum süreci, karışım gazı bileşenlerinin serbest gaz ve hidrat fazlarında farklı oranlarda paylaşılıyor olması nedeniyle daha da karmaşık olmaktadır. Metan- propan karışımları kullanılarak gerçekleştirilen hidrat oluşum sürecinde propan daha çok tüketilmektedir. Propanın daha yüksek oranda tüketilmesiyle, hidrat oluşum süresince, hidrat denge eğrisi değişmektedir. Serbest gaz içinde propan yüzdesi düştükçe, deneyin gerçekleştirildiği sıcaklıktaki hidrat denge basıncı daha yükseğe çıkmaktadır. Son olarak, amino asit çözeltileri kullanılarak gerçekleştirilen hidrat oluşum deneylerinin indüklenme zamanları saf su ile yapılan deneyin indüklenme zamanından kısa ve hidrat oluşum hızları ise daha yüksek bulunmuştur. Bu sonuçlar, test edilen amino asitler içinde hidrat oluşum hızlandırıcıları bulma potansiyeli olduğuna işaret etmektedir.

Anahtar Kelimeler: doğal gaz hidratları, hidrat oluşum hızı, indüklenme zamanı, amino asitler.

To My Father Nikolao, My Mother Anastasia & My Sister Dionisia-Dimitra

ACKNOWLEDGEMENTS

I would like to acknowledge and express my sincere gratitude to my thesis advisor Prof. Dr. Mahmut Parlaktuna for his supervision and support throughout the study. Dr. Parlaktuna was not just a supervisor but also a mentor with his actions in my personal life. I would also like to thank Mrs. Nevruz Parlaktuna for her behavior during my six years in Ankara. Many thanks to my thesis committee members for their contributions.

I would also like to thank one person that was very close and helped me during the process of my thesis who is Özgür Çoban, General Manager of Hydecon. Moreover, I would like to say a big thank to technician Murat Çalışkan for his assistance during my experimental process. I also appreciate the assistance of Naci Doğru during my experiments. One special thanks to Dr Sevtaç Bülbül (Miss Angel) for his kindness to help me any time I asked her assistance.

During my six years in Ankara I made a lot, very good and important friends. One thank for them from the depth of my heart is little but imposed. I would like to thank Emre (first roommate), Duygu, Deniz (yoldaş), Şükrü, Burak, İnanç, Gökhan (project mate), Fikret, Caner, Emre, Murat, Erdem, Serkhan, Behrang, Can, Hasan (lab mate), Kamila, Buğra, Elif, Ozan (Greek Muslim minority), Ayşegül, Fatma, Ayşegül,

I would also like to thank all the professors and instructors of petroleum and natural gas engineering department for their kindness to help me and solve any of my queries during my student life. Special thanks to Mr. Can Bakiler the most kind and gentle person that I met in Turkey. Important thanks to Dr. Uğur Murat Leloğlu, Dr. İsmail Durgut and Dr. Çağlar Sinayuç for their help and kindness during my stay. Last but not least, I would like to say special thanks to Professor Dr. Serhat Akın for his courses that I took during my study.

This study is financially supported by TUBITAK through the project 117M158. Most of the equipment of the experimental setup were purchased by the project budget. In addition, monthly fellowships from the project financially eased by stay in Ankara. Those financial supports are highly appreciated.

I also thank to the administration of the Petroleum Research Center of Middle East Technical University for the chromatographic analysis of gas mixtures. Laboratory technician Mr. Mutlu Uğurlu also deserves a special thank.

Above all, I would like to say a big thank and dedicate this thesis to my parents and the other half of my life, my beloved sister. These three persons are the foundation stone and the lighthouse of my life and without their love, support and encouragement this work would not be finished.

TABLE OF CONTENTS

ABSTRACT	v
ÖZ.....	vii
ACKNOWLEDGEMENTS	x
TABLE OF CONTENTS	xii
LIST OF TABLES	xv
LIST OF FIGURES.....	xvi
NOMENCLATURE.....	xxxiii
CHAPTERS	
1 INTRODUCTION.....	1
2 GAS HYDRATES.....	5
2.1 Properties of Gas Hydrates.....	8
2.2 Hydrate Structures	10
2.2.1 Structure I.....	13
2.2.2 Structure II.....	14
2.2.3 Structure H	14
2.3 Location of Gas Hydrates	14
2.4 Gas Hydrates in Pipelines.....	18
2.5 Gas Hydrates in Tanks.....	20
2.6 Hydrates as Potential Source Energy.....	22
2.7 Motivation of Studying Gas Hydrates	24
3 GAS HYDRATE INHIBITORS AND PROMOTERS	27
3.1 Thermodynamic Inhibitors	30
3.2 Kinetic Inhibitors.....	34
3.3 Anti-agglomerates	36
3.4 Hydrate Promoters.....	39
4 STATEMENT OF PROBLEM	41

5 EXPERIMENTAL SET-UP AND PROCEDURE	43
5.1 Experimental set-up.....	43
5.1.1 Reactor	43
5.1.2 Control unit	55
5.1.3 Cooler – circulator.....	55
5.1.4 Data acquisition system.....	55
5.1.5 Cold room	56
5.2 Experimental procedure	56
5.2.1 High-pressure steel reactor – methane	56
5.2.2 High-pressure steel reactor – methane propane mixture.....	58
5.2.3 Medium-pressure PMMA reactor – methane propane mixture	60
6 RESULTS AND DISCUSSION OF METHANE HYDRATE FORMATION.....	63
6.1 Presentation of raw data	63
6.2 Interpretation of experimental data	67
6.2.1 Gas consumption rate.....	67
6.2.2 Overall power consumption.....	70
6.2.3 Hydrate yield.....	70
6.2.4 Hydrate Productivity	71
6.3 Kinetic Analysis of methane hydrate formation.....	71
7 RESULTS AND DISCUSSION OF METHANE – PROPANE MIXTURE HYDRATE FORMATION.....	95
8 RESULTS AND DISCUSSION OF METHANE – PROPANE MIXTURE HYDRATE FORMATION WITH AMINO ACIDS.....	111
9 CONCLUSIONS.....	115
10 RECOMMENDATIONS	117
REFERENCES.....	119
APPENDICES	139
APPENDIX-A.....	139
APPENDIX-B	193
CURRICULUM VITAE	257

LIST OF TABLES

TABLES

Table 2.1 Properties of different hydrates [25].....	8
Table 2.2 Physical properties of gas hydrates compared with ice (^b Calculated from.....	9
Table 2.3 Elastic properties of solid methane (sI) and propane (sII) hydrate with comparison to that of water ice [34]	10
Table 2.4 Structure of gas hydrate cells. Space group reference numbers from the International Table of Crystallography [5]	12
Table 2.5 Guest molecules and hydrate cages; ratio of guest molecule diameter versus cavity diameter [5].	13
Table 3.1 Comparison between KHIs and AAs for Gulf of Mexico Field [192]	39
Table 5.1 Dimensions and positions of mixing elements during single impeller experiments of steel reactor	49
Table 5.2 Dimensions and positions of mixing elements during single impeller experiments of transparent reactor	55
Table 6.1 Gas consumption rates of experiment CH4-SI-PBT-FB	68
Table 6.2 Summary of results of single impeller experiments	77
Table 6.3 Summary of results of dual impeller experiments	84
Table 6.4 Comparison of duration of hydrate formations.....	85
Table 6.5 Summary of results of dual-mixed impeller experiments.....	89
Table 6.6 Results of repeatability tests	93
Table 7.1 Summary of results of single impeller, methane – propane mixture experiments	100
Table 7.2 Summary of results of dual impeller, methane – propane mixture experiments	108
Table 8.1 Properties of amino acids.....	112

LIST OF FIGURES

FIGURES

<i>Figure 2.1</i> Temperature reductions along with the MH dissociation in depressurization method [27].	6
<i>Figure 2.2</i> Gas hydrate production methods [27].	7
<i>Figure 2.3</i> Heat dissociation of different hydrates [25].	8
<i>Figure 2.4</i> Structures of gas hydrates [5].	11
<i>Figure 2.5</i> Natural Gas Hydrate Reservoir Distributions in the World [43].	15
<i>Figure 2.6</i> Gas hydrate stability conditions for a) marine hydrates b) permafrost hydrates (Orange curve: hydrate equilibrium curve, Blue curve: thermal gradient curve) [47].	16
<i>Figure 2.7</i> Estimates of global gas hydrate inventories in marine sediments. The corresponding estimated ranges are labeled in Gt C [46].	17
<i>Figure 2.8</i> Worldwide natural gas consumption [74].	20
<i>Figure 2.9</i> Comparison of gas transportation with different methods [77].	21
<i>Figure 2.10</i> Energy consumption in the 20 th century [81].	22
<i>Figure 2.11</i> World Energy Balance [81].	23
<i>Figure 2.12</i> Timeline charts of gas hydrate field projects in the world [84].	24
<i>Figure 2.13</i> Technology maturity curve of gas hydrates [85].	25
<i>Figure 2.14</i> Distribution of organic carbon in earth excluding dispersed organic carbon such as kerogen and bitumen. Modified from different sources [86].	26
<i>Figure 3.1</i> Hydrate management strategies [104].	29
<i>Figure 3.2</i> Design of different behaviors from inhibitors.	30
<i>Figure 3.3</i> Phase boundary of methane hydrates [117].	31
<i>Figure 3.4</i> Structures of amino acids [175].	36
<i>Figure 3.5</i> Structure of the ethoxylated sorbitan tween surfactants. The EO groups are randomly distributed over the four available sites [184].	37

Figure 5.1 Experimental set-up for hydrate formation.....	45
Figure 5.2 High-pressure stainless steel reactor.....	46
Figure 5.3 Some components of High-pressure stainless steel reactor.....	46
Figure 5.4 Dimensions and position of mixing elements for PBT impeller.....	49
Figure 5.5 Different impeller arrangements.....	50
Figure 5.6 Types of baffles used in this study, Left: FB, Middle: HB, Right: SB.....	50
Figure 5.7 Placement of baffles. Left: FB, Middle: HB and Right: SB.....	51
Figure 5.8 Types of impellers used in this study,.....	52
Figure 5.9 Experimental setup of transparent reactor.....	53
Figure 5.10 Transparent reactor.....	54
Figure 5.11 Single impeller for transparent reactor.....	54
Figure 5.12 Experimental conditions of methane experiments.....	58
Figure 5.13 Experimental conditions of gas mixture experiments.....	59
Figure 5.14 Steel tubes for gas sampling.....	60
Figure 5.15 Agilent system 6890 series GC for gas analysis.....	60
Figure 6.1 Pressure – temperature vs. time graph of hydrate formation experiment.....	66
Figure 6.2 Pressure vs. torque graph of hydrate formation experiment.....	66
Figure 6.3 Pressure vs. temperature graph of hydrate formation experiment.....	67
Figure 6.4 Calculated number of moles of free gas during hydrate formation.....	69
Figure 6.5 Gas consumption rate equation.....	69
Figure 6.6 Diagram showing the impeller – baffle configurations of 24 methane hydrate experiments.....	72
Figure 6.7 Rate of hydrate formation in single impeller experiments.....	78
Figure 6.8 Hydrate productivity of single impeller experiments.....	79
Figure 6.9 Overall power consumption of single impeller experiments.....	80
Figure 6.10 Recorded torque values of single impeller experiments.....	81
Figure 6.11 Overall power consumption of dual impeller experiments.....	85
Figure 6.12 Recorded torque values of single impeller experiments.....	86

Figure 6.13 Rate of hydrate formation of PBT/PBT and RT/RT dual impellers for time period of 1, 600, 1200 and 1800 seconds	86
Figure 6.14 Overall power consumption of dual-mixed impeller experiments	90
Figure 6.15 Recorded torque values of dual-mixed impeller experiments	90
Figure 6.16 Rate of hydrate formation of dual mixed impellers for time period of 1, 600, 1200 and 1800 seconds.	91
Figure 6.17 Repeatability test of CH ₄ -SI-PBT-NB in terms of gas consumption rate ...	93
Figure 6.18 Repeatability test of CH ₄ -DMI-RT/PBT-FB in terms of gas consumption rate	94
Figure 6.19 Repeatability test of CH ₄ -DI-RT-FB in terms of gas consumption rate	94
1. Figure 7.1 Repeatability Diagram showing the impeller – baffle configurations of 24 methane -propane mixture hydrate experiments	97
Figure 7.2 Split fraction of methane of single impeller mixture hydrate experiments ..	101
Figure 7.3 Split fraction of propane of single impeller mixture hydrate experiments ..	101
Figure 7.4 Separation factor of propane of single impeller mixture hydrate experiments	102
Figure 7.5 Composition of feed gas and free gas at the end of single impeller experiments (lower driving force).....	102
Figure 7.6 Composition of feed gas and free gas at the end of single impeller experiments (higher driving force).....	103
Figure 7.7 Pressure – temperature diagram of mixture gas of SI-RT-FB (lower driving force)	103
Figure 7.8 Pressure – temperature diagram of mixture gas of SI-RT-FB (higher driving force)	104
Figure 7.9 Rate of hydrate formation of mixture gas with single impeller and lower driving force (experimental temperature 8.5 °C)	105
Figure 7.10 Rate of hydrate formation of mixture gas with single impeller and higher driving force (experimental temperature 2 °C)	105

Figure 7.11 Split fraction of methane for single and dual impeller experiments (experimental temperature 2 °C).....	109
Figure 7.12 Split fraction of propane for single and dual impeller experiments (experimental temperature 2 °C).....	109
Figure 7.13 Separation factor of propane for single and dual impeller experiments (experimental temperature 2 °C).....	110
Figure 7.14 Rate of hydrate formation of mixture gas with dual impeller (experimental temperature 2 °C).....	110
Figure 8.1 Induction time of methane-propane hydrate formation in the presence of only water, L-Leucine, L-Lysine, L-Serine, L-Histidine and L-Alanine.....	113
Figure 8.2 Hydrate formation rates of methane-propane mixture and amino acid solutions	114
Figure 8.3 Overall power consumption of water and 5 amino acids during hydrate formation process	114
Figure A.1 Raw data of experiment CH4-PBT-FB-SI-500. A: Pressure – temperature vs. time graph, B: Pressure – torque vs. time graph, C: Pressure vs. temperature graph	139
Figure A.2 Raw data of experiment CH4-PBT-HB-SI-500. A: Pressure – temperature vs. time graph, B: Pressure – torque vs. time graph, C: Pressure vs. temperature graph	140
Figure A.3 Raw data of experiment CH4-PBT-SB-SI-500. A: Pressure – temperature vs. time graph, B: Pressure – torque vs. time graph, C: Pressure vs. temperature graph ...	141
Figure A.4 Raw data of experiment CH4-PBT-NB-SI-500. A: Pressure – temperature vs. time graph, B: Pressure – torque vs. time graph, C: Pressure vs. temperature graph	142
Figure A.5 Raw data of experiment CH4-RT-FB-SI-500. A: Pressure – temperature vs. time graph, B: Pressure – torque vs. time graph, C: Pressure vs. temperature graph ...	143
Figure A.6 Raw data of experiment CH4-RT-HB-SI-500. A: Pressure – temperature vs. time graph, B: Pressure – torque vs. time graph, C: Pressure vs. temperature graph ...	144

Figure A.7 Raw data of experiment CH4-RT-SB-SI-500. A: Pressure – temperature vs. time graph, B: Pressure – torque vs. time graph, C: Pressure vs. temperature graph ...145

Figure A.8 Raw data of experiment CH4-RT-NB-SI-500. A: Pressure – temperature vs. time graph, B: Pressure – torque vs. time graph, C: Pressure vs. temperature graph ...146

Figure A.9 Raw data of experiment CH4-PBT-FB-DI-500. A: Pressure – temperature vs. time graph, B: Pressure – torque vs. time graph, C: Pressure vs. temperature graph147

Figure A.10 Raw data of experiment CH4-PBT-HB-DI-500. A: Pressure – temperature vs. time graph, B: Pressure – torque vs. time graph, C: Pressure vs. temperature graph148

Figure A.11 Raw data of experiment CH4-PBT-SB-DI-500. A: Pressure – temperature vs. time graph, B: Pressure – torque vs. time graph, C: Pressure vs. temperature graph149

Figure A.12 Raw data of experiment CH4-PBT-NB-DI-500. A: Pressure – temperature vs. time graph, B: Pressure – torque vs. time graph, C: Pressure vs. temperature graph150

Figure A.13 Raw data of experiment CH4-RT-FB-DI-500. A: Pressure – temperature vs. time graph, B: Pressure – torque vs. time graph, C: Pressure vs. temperature graph151

Figure A.14 Raw data of experiment CH4-RT-HB-DI-500. A: Pressure – temperature vs. time graph, B: Pressure – torque vs. time graph, C: Pressure vs. temperature graph152

Figure A.15 Raw data of experiment CH4-RT-SB-DI-500. A: Pressure – temperature vs. time graph, B: Pressure – torque vs. time graph, C: Pressure vs. temperature graph153

Figure A.16 Raw data of experiment CH4-RT-NB-DI-500. A: Pressure – temperature vs. time graph, B: Pressure – torque vs. time graph, C: Pressure vs. temperature graph154

Figure A.17 Raw data of experiment CH4-PBT-RT-FB-MIX-DI-500. A: Pressure – temperature vs. time graph, B: Pressure – torque vs. time graph, C: Pressure vs. temperature graph.....	155
Figure A.18 Raw data of experiment CH4-PBT-RT-HB-MIX-DI-500. A: Pressure – temperature vs. time graph, B: Pressure – torque vs. time graph, C: Pressure vs. temperature graph.....	156
Figure A.19 Raw data of experiment CH4-PBT-RT-SB-MIX-DI-500. A: Pressure – temperature vs time graph, B: Pressure – torque vs. time graph, C: Pressure vs. temperature graph.....	157
Figure A.20 Raw data of experiment CH4-PBT-RT-NB-MIX-DI-500. A: Pressure – temperature vs. time graph, B: Pressure – torque vs. time graph, C: Pressure vs. temperature graph.....	158
Figure A.21 Raw data of experiment CH4-RT-PBT-FB-MIX-DI-500. A: Pressure – temperature vs. time graph, B: Pressure – torque vs. time graph, C: Pressure vs. temperature graph.....	159
Figure A.22 Raw data of experiment CH4-RT-PBT-HB-MIX-DI-500. A: Pressure – temperature vs. time graph, B: Pressure – torque vs. time graph, C: Pressure vs. temperature graph.....	160
Figure A.23 Raw data of experiment CH4-RT-PBT-SB-MIX-DI-500. A: Pressure – temperature vs. time graph, B: Pressure – torque vs. time graph, C: Pressure vs. temperature graph.....	161
Figure A.24 Raw data of experiment CH4-RT-PBT-NB-MIX-DI-500. A: Pressure – temperature vs. time graph, B: Pressure – torque vs. time graph, C: Pressure vs. temperature graph.....	162
Figure A.25 Raw data of experiment CH4-C3H8-PBT-FB-SI-500. A: Pressure – temperature vs. time graph, B: Pressure – torque vs. time graph, C: Pressure vs. temperature graph. (Driving force=8.5).....	163

Figure A.26 Raw data of experiment CH4-C3H8-PBT-HB-SI-500. A: Pressure – temperature vs. time graph, B: Pressure – torque vs. time graph, C: Pressure vs. temperature graph. (Driving force=8.5)164

Figure A.27 Raw data of experiment CH4-C3H8-PBT-SB-SI-500. A: Pressure – temperature vs. time graph, B: Pressure – torque vs. time graph, C: Pressure vs. temperature graph. (Driving force=8.5)165

Figure A.28 Raw data of experiment CH4-C3H8-PBT-NB-SI-500. A: Pressure – temperature vs. time graph, B: Pressure – torque vs. time graph, C: Pressure vs. temperature graph. (Driving force=8.5)166

Figure A.29 Raw data of experiment CH4-C3H8-RT-FB-SI-500. A: Pressure – temperature vs. time graph, B: Pressure – torque vs. time graph, C: Pressure vs. temperature graph. (Driving force=8.5)167

Figure A.30 Raw data of experiment CH4-C3H8-RT-HB-SI-500. A: Pressure – temperature vs. time graph, B: Pressure – torque vs. time graph, C: Pressure vs. temperature graph. (Driving force=8.5)168

Figure A.31 Raw data of experiment CH4-C3H8-RT-SB-SI-500. A: Pressure – temperature vs. time graph, B: Pressure – torque vs. time graph, C: Pressure vs. temperature graph. (Driving force=8.5)169

Figure A.32 Raw data of experiment CH4-C3H8-RT-NB-SI-500. A: Pressure – temperature vs. time graph, B: Pressure – torque vs. time graph, C: Pressure vs. temperature graph. (Driving force=8.5)170

Figure A.33 Raw data of experiment CH4-C3H8-PBT-FB-SI-500. A: Pressure – temperature vs. time graph, B: Pressure – torque vs. time graph, C: Pressure vs. temperature graph. (Driving force=16)171

Figure A.34 Raw data of experiment CH4-C3H8-PBT-HB-SI-500. A: Pressure – temperature vs. time graph, B: Pressure – torque vs. time graph, C: Pressure vs. temperature graph. (Driving force=16)172

Figure A.35 Raw data of experiment CH4-C3H8-PBT-SB-SI-500. A: Pressure – temperature vs. time graph, B: Pressure – torque vs. time graph, C: Pressure vs. temperature graph. (Driving force=16).....	173
Figure A.36 Raw data of experiment CH4-C3H8-PBT-NB-SI-500. A: Pressure – temperature vs. time graph, B: Pressure – torque vs. time graph, C: Pressure vs. temperature graph. (Driving force=16).....	174
Figure A.37 Raw data of experiment CH4-C3H8-RT-FB-SI-500. A: Pressure – temperature vs. time graph, B: Pressure – torque vs. time graph, C: Pressure vs. temperature graph. (Driving force=16).....	175
Figure A.38 Raw data of experiment CH4-C3H8-RT-HB-SI-500. A: Pressure – temperature vs. time graph, B: Pressure – torque vs. time graph, C: Pressure vs. temperature graph. (Driving force=16).....	176
Figure A.39 Raw data of experiment CH4-C3H8-RT-SB-SI-500. A: Pressure – temperature vs. time graph, B: Pressure – torque vs. time graph, C: Pressure vs. temperature graph. (Driving force=16).....	177
Figure A.40 Raw data of experiment CH4-C3H8-RT-NB-SI-500. A: Pressure – temperature vs. time graph, B: Pressure – torque vs. time graph, C: Pressure vs. temperature graph. (Driving force=16).....	178
Figure A.41 Raw data of experiment CH4-C3H8-PBT-FB-DI-500. A: Pressure – temperature vs. time graph, B: Pressure – torque vs. time graph, C: Pressure vs. temperature graph. (Driving force=16).....	179
Figure A.42 Raw data of experiment CH4-C3H8-PBT-HB-DI-500. A: Pressure – temperature vs. time graph, B: Pressure – torque vs. time graph, C: Pressure vs. temperature graph. (Driving force=16).....	180
Figure A.43 Raw data of experiment CH4-C3H8-PBT-SB-DI-500. A: Pressure – temperature vs. time graph, B: Pressure – torque vs. time graph, C: Pressure vs. temperature graph. (Driving force=16).....	181

Figure A.44 Raw data of experiment CH ₄ -C ₃ H ₈ -PBT-NB-DI-500. A: Pressure – temperature vs. time graph, B: Pressure – torque vs. time graph, C: Pressure vs. temperature graph. (Driving force=16).....	182
Figure A.45 Raw data of experiment CH ₄ -C ₃ H ₈ -RT-FB-DI-500. A: Pressure – temperature vs. time graph, B: Pressure – torque vs. time graph, C: Pressure vs. temperature graph. (Driving force=16).....	183
Figure A.46 Raw data of experiment CH ₄ -C ₃ H ₈ -RT-HB-DI-500. A: Pressure – temperature vs. time graph, B: Pressure – torque vs. time graph, C: Pressure vs. temperature graph. (Driving force=16).....	184
Figure A.47 Raw data of experiment CH ₄ -C ₃ H ₈ --RT-SB-DI-500. A: Pressure – temperature vs. time graph, B: Pressure – torque vs. time graph, C: Pressure vs. temperature graph. (Driving force=16).....	185
Figure A.48 Raw data of experiment CH ₄ -C ₃ H ₈ -RT-NB-DI-500. A: Pressure – temperature vs. time graph, B: Pressure – torque vs. time graph, C: Pressure vs. temperature graph. (Driving force=16).....	186
Figure A.49 Raw data experiment PBT-FB-SI-WATER-MIX, A: Pressure, temperature vs time graph, B: Pressure, torque vs time graph.....	187
Figure A.50 Raw data experiment PBT-FB-SI-L LYSINE-MIX, A: Pressure, temperature vs time graph, B: Pressure, torque vs time graph.....	188
Figure A.51 Raw data experiment PBT-FB-SI-L HISTIDINE-MIX, A: Pressure, temperature vs time graph, B: Pressure, torque vs time graph.....	189
Figure A.52 Raw data experiment PBT-FB-SI-L SERINE-MIX, A: Pressure, temperature vs time graph, B: Pressure, torque vs time graph.....	190
Figure A.53 Raw data experiment PBT-FB-SI-L ALANINE-MIX, A: Pressure, temperature vs time graph, B: Pressure, torque vs time graph.....	191
Figure A.54 Raw data experiment PBT-FB-SI-L LEUCINE-MIX, A: Pressure, temperature vs time graph, B: Pressure, torque vs time graph.....	192
Figure B.1 Change in number of moles of free gas in CH ₄ -PBT-FB-SI experiment. ...	193
Figure B.2 Gas consumption rate equation for CH ₄ -PBT-FB-SI experiment	193

Figure B.3	Change in number of moles of free gas in CH ₄ -PBT-HB-SI experiment ..	194
Figure B.4	Gas consumption rate equation for CH ₄ -PBT-HB-SI experiment	194
Figure B.5	Change in number of moles of free gas in CH ₄ -PBT-SB-SI experiment ...	195
Figure B.6	Gas consumption rate equation for CH ₄ -PBT-SB-SI experiment	195
Figure B.7	Change in number of moles of free gas in CH ₄ -PBT-NB-SI experiment ..	196
Figure B.8	Gas consumption rate equation for CH ₄ -PBT-NB-SI experiment	196
Figure B.9	Change in number of moles of free gas in CH ₄ -RT-FB-SI experiment	197
Figure B.10	Gas consumption rate equation for CH ₄ -RT-FB-SI experiment	197
Figure B.11	Change in number of moles of free gas in CH ₄ -RT-HB-SI experiment...	198
Figure B.12	Gas consumption rate equation for CH ₄ -RT-HB-SI experiment.....	198
Figure B.13	Change in number of moles of free gas in CH ₄ -RT-SB-SI experiment ...	199
Figure B.14	Gas consumption rate equation for CH ₄ -RT-SB-SI experiment	199
Figure B.15	Change in number of moles of free gas in CH ₄ -RT-NB-SI experiment...	200
Figure B.16	Gas consumption rate equation for CH ₄ -RT-NB-SI experiment.....	200
Figure B.17	Change in number of moles of free gas in CH ₄ -PBT-FB-DI experiment	201
Figure B.18	Gas consumption rate equation for CH ₄ -PBT-FB-DI experiment	201
Figure B.19	Change in number of moles of free gas in CH ₄ -PBT-HB-DI experiment	202
Figure B.20	Gas consumption rate equation for CH ₄ -PBT-HB-DI experiment.....	202
Figure B.21	Change in number of moles of free gas in CH ₄ -PBT-SB-DI experiment	203
Figure B.22	Gas consumption rate equation for CH ₄ -PBT-SB-DI experiment	203
Figure B.23	Change in number of moles of free gas in CH ₄ -PBT-NB-DI experiment	204
Figure B.24	Gas consumption rate equation for CH ₄ -PBT-NB-DI experiment.....	204
Figure B.25	Change in number of moles of free gas in CH ₄ -RT-FB-DI experiment...	205
Figure B.26	Gas consumption rate equation for CH ₄ -RT-FB-DI experiment.....	205
Figure B.27	Change in number of moles of free gas in CH ₄ -RT-HB-DI experiment..	206
Figure B.28	Gas consumption rate equation for CH ₄ -RT-HB-DI experiment	206
Figure B.29	Change in number of moles of free gas in CH ₄ -RT-SB-DI experiment...	207
Figure B.30	Gas consumption rate equation for CH ₄ -RT-SB-DI experiment.....	207
Figure B.31	Change in number of moles of free gas in CH ₄ -RT-NB-DI experiment..	208

Figure B.32 Gas consumption rate equation for CH₄-RT-NB-DI experiment208

Figure B.33 Change in number of moles of free gas in CH₄-MIX-RT-PBT-FB-DI experiment.....209

Figure B.34 Gas consumption rate equation for CH₄-MIX-RT-PBT-FB-DI experiment209

Figure B.35 Change in number of moles of free gas in CH₄-MIX-RT-PBT-HB-DI experiment.....210

Figure B.36 Gas consumption rate equation for CH₄-MIX-RT-PBT-HB-DI experiment210

Figure B.37 Change in number of moles of free gas in CH₄-MIX-RT-PBT-NB-DI experiment.....211

Figure B.38 Gas consumption rate equation for CH₄-MIX-RT-PBT-NB-DI experiment211

Figure B.39 Change in number of moles of free gas in CH₄-MIX-RT-PBT-SB-DI experiment.....212

Figure B.40 Gas consumption rate equation for CH₄-MIX-RT-PBT-SB-DI experiment212

Figure B.41 Change in number of moles of free gas in CH₄-MIX-PBT-RT-FB-DI experiment.....213

Figure B.42 Gas consumption rate equation for CH₄-MIX-PBT-RT-FB-DI experiment213

Figure B.43 Change in number of moles of free gas in CH₄-MIX-PBT-RT-HB-DI experiment.....214

Figure B.44 Gas consumption rate equation for CH₄-MIX-PBT-RT-HB-DI experiment214

Figure B.45 Change in number of moles of free gas in CH₄-MIX-PBT-RT-SB-DI experiment.....215

Figure B.46 Gas consumption rate equation for CH₄-MIX-PBT-RT-SB-DI experiment215

Figure B.47 Change in number of moles of free gas in CH ₄ -MIX-PBT-RT-NB-DI experiment.....	216
Figure B.48 Gas consumption rate equation for CH ₄ -MIX-PBT-RT-NB-DI experiment	216
Figure B.49 Change in number of moles of free gas in CH ₄ -C ₃ H ₈ -PBT-FB-SI-8C experiment.....	217
Figure B.50 Gas consumption rate equation for CH ₄ -C ₃ H ₈ -PBT-FB-SI-8C experiment	217
Figure B.51 Change in number of moles of free gas in CH ₄ -C ₃ H ₈ -PBT-HB-SI-8C experiment.....	218
Figure B.52 Gas consumption rate equation for CH ₄ -C ₃ H ₈ -PBT-HB-SI-8C experiment	218
Figure B.53 Change in number of moles of free gas in CH ₄ -C ₃ H ₈ -PBT-SB-SI-8C experiment.....	219
Figure B.54 Gas consumption rate equation for CH ₄ -C ₃ H ₈ -PBT-SB-SI-8C experiment	219
Figure B.55 Change in number of moles of free gas in CH ₄ -C ₃ H ₈ -PBT-NB-SI-8C experiment.....	220
Figure B.56 Gas consumption rate equation-1 for CH ₄ -C ₃ H ₈ -PBT-NB-SI-8C experiment.....	220
Figure B.57 Gas consumption rate equation-2 for CH ₄ -C ₃ H ₈ -PBT-NB-SI-8C experiment.....	221
Figure B.58 Change in number of moles of free gas in CH ₄ -C ₃ H ₈ -RT-FB-SI-8C experiment.....	221
Figure B.59 Gas consumption rate equation for CH ₄ -C ₃ H ₈ -RT-FB-SI-8C experiment	222
Figure B.60 Change in number of moles of free gas in CH ₄ -C ₃ H ₈ -RT-HB-SI-8C experiment.....	222

Figure B.61 Gas consumption rate equation-1 for CH₄-C₃H₈-RT-HB-SI-8C experiment223

Figure B.62 Gas consumption rate equation-2 for CH₄-C₃H₈-RT-HB-SI-8C experiment223

Figure B.63 Change in number of moles of free gas in CH₄-C₃H₈-RT-SB-SI-8C experiment.....224

Figure B.64 Gas consumption rate equation-1 for CH₄-C₃H₈-RT-SB-SI-8C experiment224

Figure B.65 Gas consumption rate equation-2 for CH₄-C₃H₈-RT-SB-SI-8C experiment225

Figure B.66 Change in number of moles of free gas in CH₄-C₃H₈-RT-NB-SI-8C experiment.....225

Figure B.67 Gas consumption rate equation-1 for CH₄-C₃H₈-RT-NB-SI-8C experiment226

Figure B.68 Gas consumption rate equation-2 for CH₄-C₃H₈-RT-NB-SI-8C experiment226

Figure B.69 Change in number of moles of free gas in CH₄-C₃H₈-PBT-FB-SI-2C experiment.....227

Figure B.70 Gas consumption rate equation-1 for CH₄-C₃H₈-PBT-FB-SI-2C experiment.....227

Figure B.71 Gas consumption rate equation-2 for CH₄-C₃H₈-PBT-FB-SI-2C experiment.....228

Figure B.72 Change in number of moles of free gas in CH₄-C₃H₈-PBT-HB-SI-2C experiment.....228

Figure B.73 Gas consumption rate equation for CH₄-C₃H₈-PBT-HB-SI-2C experiment229

Figure B.74 Change in number of moles of free gas in CH₄-C₃H₈-PBT-SB-SI-2C experiment.....229

Figure B.75 Gas consumption rate equation for CH ₄ -C ₃ H ₈ -PBT-SB-SI-2C experiment	230
Figure B.76 Change in number of moles of free gas in CH ₄ -C ₃ H ₈ -PBT-NB-SI-2C experiment	230
Figure B.77 Gas consumption rate equation-1 for CH ₄ -C ₃ H ₈ -PBT-NB-SI-2C experiment	231
Figure B.78 Gas consumption rate equation-2 for CH ₄ -C ₃ H ₈ -PBT-NB-SI-2C experiment	231
Figure B.79 Change in number of moles of free gas in CH ₄ -C ₃ H ₈ -RT-FB-SI-2C experiment	232
Figure B.80 Gas consumption rate equation-1 for CH ₄ -C ₃ H ₈ -RT-FB-SI-2C experiment	232
Figure B.81 Gas consumption rate equation-2 for CH ₄ -C ₃ H ₈ -RT-FB-SI-2C experiment	233
Figure B.82 Change in number of moles of free gas in CH ₄ -C ₃ H ₈ -RT-HB-SI-2C experiment	233
Figure B.83 Gas consumption rate equation-1 for CH ₄ -C ₃ H ₈ -RT-HB-SI-2C experiment	234
Figure B.84 Gas consumption rate equation-2 for CH ₄ -C ₃ H ₈ -RT-HB-SI-2C experiment	234
Figure B.85 Change in number of moles of free gas in CH ₄ -C ₃ H ₈ -RT-SB-SI-2C experiment	235
Figure B.86 Gas consumption rate equation-1 for CH ₄ -C ₃ H ₈ -RT-SB-SI-2C experiment	235
Figure B.87 Gas consumption rate equation-2 for CH ₄ -C ₃ H ₈ -RT-SB-SI-2C experiment	236
Figure B.88 Change in number of moles of free gas in CH ₄ -C ₃ H ₈ -RT-NB-SI-2C experiment	236

Figure B.89 Gas consumption rate equation-1 for CH ₄ -C ₃ H ₈ -RT-NB-SI-2C experiment	237
Figure B.90 Gas consumption rate equation-2 for CH ₄ -C ₃ H ₈ -RT-NB-SI-2C experiment	237
Figure B.91 Change in number of moles of free gas in CH ₄ -C ₃ H ₈ -PBT-FB-DI-2C experiment	238
Figure B.92 Gas consumption rate equation-1 for CH ₄ -C ₃ H ₈ -PBT-FB-DI-2C experiment	238
Figure B.93 Gas consumption rate equation-2 for CH ₄ -C ₃ H ₈ -PBT-FB-DI-2C experiment	239
Figure B.94 Change in number of moles of free gas in CH ₄ -C ₃ H ₈ -PBT-HB-DI-2C experiment	239
Figure B.95 Gas consumption rate equation-1 for CH ₄ -C ₃ H ₈ -PBT-HB-DI-2C experiment	240
Figure B.96 Gas consumption rate equation-2 for CH ₄ -C ₃ H ₈ -PBT-HB-DI-2C experiment	240
Figure B.97 Change in number of moles of free gas in CH ₄ -C ₃ H ₈ -PBT-SB-DI-2C experiment	241
Figure B.98 Gas consumption rate equation-1 for CH ₄ -C ₃ H ₈ -PBT-SB-DI-2C experiment	241
Figure B.99 Gas consumption rate equation-2 for CH ₄ -C ₃ H ₈ -PBT-SB-DI-2C experiment	242
Figure B.100 Change in number of moles of free gas in CH ₄ -C ₃ H ₈ -PBT-NB-DI-2C experiment	242
Figure B.101 Gas consumption rate equation-1 for CH ₄ -C ₃ H ₈ -PBT-NB-DI-2C experiment	243
Figure B.102 Gas consumption rate equation-2 for CH ₄ -C ₃ H ₈ -PBT-NB-DI-2C experiment	243

Figure B.103 Change in number of moles of free gas in CH ₄ -C ₃ H ₈ -RT-FB-DI-2C experiment.....	244
Figure B.104 Gas consumption rate equation-1 for CH ₄ -C ₃ H ₈ -RT-FB-DI-2C experiment.....	244
Figure B.105 Gas consumption rate equation-2 for CH ₄ -C ₃ H ₈ -RT-FB-DI-2C experiment.....	245
Figure B.106 Change in number of moles of free gas in CH ₄ -C ₃ H ₈ -RT-HB-DI-2C experiment.....	245
Figure B.107 Gas consumption rate equation-1 for CH ₄ -C ₃ H ₈ -RT-HB-DI-2C experiment.....	246
Figure B.108 Gas consumption rate equation-2 for CH ₄ -C ₃ H ₈ -RT-HB-DI-2C experiment.....	246
Figure B.109 Change in number of moles of free gas in CH ₄ -C ₃ H ₈ -RT-SB-DI-2C experiment.....	247
Figure B.110 Gas consumption rate equation-1 for CH ₄ -C ₃ H ₈ -RT-SB-DI-2C experiment.....	247
Figure B.111 Gas consumption rate equation-2 for CH ₄ -C ₃ H ₈ -RT-SB-DI-2C experiment.....	248
Figure B.112 Change in number of moles of free gas in CH ₄ -C ₃ H ₈ -RT-NB-DI-2C experiment.....	248
Figure B.113 Gas consumption rate equation for CH ₄ -C ₃ H ₈ -RT-NB-DI-2C experiment	249
Figure B.114 Change in number of moles of free gas in PBT-FB-SI-WATER-MIX experiment.....	249
Figure B.115 Gas consumption rate equation for PBT-FB-SI-WATER-MIX experiment	250
Figure B.116 Change in number of moles of free gas in PBT-FB-SI-L LYSINE-MIX experiment.....	250

Figure B.117 Gas consumption rate equation for PBT-FB-SI-L LYSINE-MIX experiment.....251

Figure B.118 Change in number of moles of free gas in PBT-FB-SI-L HISTIDINE-MIX experiment.....251

Figure B.119 Gas consumption rate equation for PBT-FB-SI-L HISTIDINE-MIX experiment.....252

Figure B.120 Change in number of moles of free gas in PBT-FB-SI-L SERINE-MIX experiment.....252

Figure B.121 Gas consumption rate equation for PBT-FB-SI-L SERINE-MIX experiment.....253

Figure B.122 Change in number of moles of free gas in PBT-FB-SI-L ALANINE-MIX experiment.....253

Figure B.123 Gas consumption rate equation for PBT-FB-SI-L ALANINE-MIX experiment.....254

Figure B.124 Change in number of moles of free gas in PBT-FB-SI-L LEUCINE-MIX experiment.....254

Figure B.125 Gas consumption rate equation for PBT-FB-SI-L LEUCINE-MIX experiment.....255

NOMENCLATURE

A	Average cavity radius
A^0	Cavity Diameter
AA	Anti-agglomerate
ABS	Acrylonitrile butadiene styrene
AFP	Antifreeze protein
BOP	Blowout preventers
$C_{16}H_{31}NO$	N-dodecylpyrrolidone
$C_{18}H_{33}NaO_2$	Sodium oleate
$C_{20}H_{44}BrN$	Tetrapentylammonium bromide
$C_4H_9O_4$	Butyl sulphate
$C_5H_9NaO_2$	Sodium valerate
$C_6H_{14}O_2$	Butoxy ethanol
CAPEX	Capital expenditures
CNG	Compressed natural gas
C_p	Heat capacity
C_{st}	Distance of sparger from the bottom of reactor
CTAB	Cetyl trimethyl ammonium bromide
C_{tr}	Distance of impeller from the bottom of reactor
DI	Dual impeller

DMI	Dual mixed impeller
DAH	Dodecyl amine hydrochloride
DAM	Quaternary ammonium salt
DBSA	Dodecyl benzene sulfonic acid
DEG	Di-ethyl glycol
D_g	Sparger diameter
DN2Cl	N-dodecylpropane-1,3-diamine hydrochloride
DOE	Department of Energy
D_{st}	Diameter of impeller
D_{tr}	Diameter of impeller
E	Young's Modulus
EG	Ethylene glycol
ENP	Ethoxylated nonylphenol
FB	Full baffle
G	Shear modulus
GC	Gas chromatography
GHSZ	Gas hydrate stability zone
GOS	Gas/Oil ratio
GPa	Giga Pascal
Gt C	Gigaton carbon

GWAA	Gas wells anti-agglomerate
HB	Half baffle
h_g	Thickness of sparger
h_{st}	Thickness of impeller
H_{st}	Height of impeller
HTABr	Hexadecyl-trimethyl-ammonium bromide
H_{tr}	Height of transparent reactor
h_{tr}	Thickness of impeller
I.F.P	Institute Francais du Petrole
I.T.	Induction time
IL	Ionic liquids
IPMA	N-Isopropylmethacrylamide
ISP	Ice-structuring proteins
KH	Kinetic inhibitors
KHI	Kinetic hydrate inhibitors
kJ	Kilojoule
LABS	Linear alkyl benzene sulfonate
LABSA	Linear alkyl benzene sulfonic acid
LC	Large cage
LDHI	Low dose hydrate inhibitors

LDI	Low dosage inhibitors
LDS	Lithium dodecyl sulfate
LNG	Liquefied natural gas
MEG	Mono-ethylene glycol
MEG	Methanol glycol
MH	Methane hydrate
MPa	Mega Pascal
N	Rotational speed
NB	No baffle
NGH	Natural gas hydrates
N_H	Hydration number
n_{H0}	Moles consumed at induction time
n_{Ht}	Moles consumed end of experiment
NR_{30}	Hydrate productivity
OECD	Organization for Economic Co-operation and Development
OPEX	Operating expenses
P	Pressure
PBT	Pitched blade turbine
PBTU	Up-pumping pitched blade turbine
P_c	Overall power consumption

P_{equib}	Pressure at the equilibrium
P_{exp}	Experimental pressure
PLC	Programmable logic controller
PMMA	p-Polymethyl methacrylate
POC	Particulate organic carbon
POVACO	Polyvinylazacyclooctanone
P_r	Reservoir pressure
PVA	Poly vinyl alcohol
PVCap	Polyvinylcaprolactam
PVP	Polyvinylpyrrolidone
PVP	Polyvinylpyrrolidine
PVPPip	Polyvinylpiperidone
r	Interfacial radius of curvature
R	Gas constant
R_{30}	Rate growth first 30 minutes
rpm	Revolutions per minute
rps	Revolutions per second
RT	Rushton turbine
R_t	Rate of hydrate growth
S.F	Separation factor

S.Fr.	Split fraction
SI	Single impeller
SB	Surface baffle
SC	Small cage
SDSN	Sodium dodecyl sulfonate
sH	Structure (H)
SHS	Sodium hexadecyl sulfate
sI	Structure (I)
sII	Structure (II)
SNG	Solidified natural gas
SR	Sedimentation rate
T	Temperature
t	Time
TBAB	Tetrabutylammonium
TEG	Triethylene glycol
Teq	Hydrate equilibrium temperature in water
T _{eq,s}	Hydrate equilibrium temperature in brine
THF	Tetrahydrofuran
THI	Thermodynamic inhibitors
Tq	Torque

US	United States
V	Volume
V _p	Compressional wave velocity
V _s	Shear wave velocity
V _{water}	Volume of water
wt	For weight
z	Compressibility factor

Greek Letters

ΔH	Heat Configuration
$\Delta T_{\text{freezing}}$	Freezing point depression by brine
θ	Occupancy
κ	Thermal diffusivity
K	Bulk modulus
λ	Thermal conductivity
π	The ratio of a circle's circumference to its diameter
ρ	Density
T _{st}	Internal diameter of steel reactor
T _{tr}	Internal diameter of transparent reactor

CHAPTER 1

INTRODUCTION

Planetary request will increase considerably in the following decades as population of the earth proliferates. US DOE 2016 International Energy Outlook, claims that the universal energy consumption will augment from 549 quadrillion BTU in 2012 to 815 quadrillion BTU in 2040, indicating 48% increase. The primarily countries that contribute to this augmentation in demand are non-OECD developing economies, such as China and India, where request is prognosticated to raise by 112% between 2010 and 2040 [1]. Whereas the expectation is that non hydrocarbon sources such nuclear and renewables can generate more power the following years, the quantity generated is presumably still far from meeting the huge augmentation in energy request. By 2040, the prognoses nominate that more than 76% of energy will be of carbon based source, despite expansion in not carbon sources [2]. Therefore, unconventional sources will have a significant place and more specifically, gas hydrates will play the primary role [3].

There are certain sets of high pressure and low temperature conditions under which gas hydrates are formed [4,5]. Methane storage enclosed in cages formed by water molecules via gas hydrates is highly auspicious due to its many advantages [6,7]. Its benefits comprise (i) notable storing action capacity of 165 volumes of methane in a unit volume of hydrate; [8] (ii) temperature and pressure conditions of hydrate formation and storage compared to conventional natural gas storage methods; (iii) relevant comfort and nigh complete recovery of SNG; (iv) ecologically acceptable method utilizing only water with very low concentrations of gas hydrate promoters; and (v) non peril manner of NG storage as it is “non-eruptive” [9,10].

Fast hydrate formation is very crucial for the mercantile performance of SNG technology. Kinetics of hydrate formation can be augmented firstly by appropriate chemicals (promoters) such as surfactants and amino acids, that assist in ameliorating the rate of hydrate formation, secondly by new reactor design that assists at ameliorating gas-liquid contact to manage a higher rate of hydrate formation and thirdly by combination of both approaches. Current experimental and modelling efforts try to manage the kinetic augmentation during hydrate formation by implementing any of the previous listed ways in order to allow the process of SNG technology on a large scale [11-22].

As an outcome this thesis focuses on the following topics:

Chapter 2 is a theoretical approach of gas hydrates and describing the fundamental knowledge about gas hydrates such their chemical structure, properties, location of gas hydrates in nature, utilization of gas hydrates, gas hydrates in tanks and in pipelines, gas hydrates as source of energy and on-going research about gas hydrates.

Chapter 3 makes a summary about hydrate inhibitors and promoters. There is a literature review in the three different kind of inhibitors such as thermodynamic inhibitors, kinetic inhibitors and anti-agglomerates and also presents past and recent chemicals that have been used as promoters.

Chapter 4 presents a definite statement of the current issues

Chapter 5 presents the experimental procedures that took place for three different applications, namely experiments with pure methane, mixture gas and amino acids.

Chapter 6 discusses the experimental results of hydrate formation tests in which methane was used as hydrate forming gas. 24 experiments with different impeller – baffle configurations under fixed rotational speed (500 rpm) were conducted. The graphs of pressure and temperature versus time, torque versus time, moles versus time and hydrate formation are presented.

Chapter 7 is dedicated to discuss the experimental results of hydrate formation tests with methane-propane (95%-5%) mixture as hydrate forming gas. Again, 24 experiments with different impeller – baffle configurations under fixed rotational speed (500 rpm) were conducted and the same interpretation procedure of methane tests is followed.

Chapter 8 presents the interpretation of experiments with the same mixture gas (95 % methane – 5% propane), but this time with some amino acids in water phase. 6 experiments, 5 with different amino acids and one with pure water, were conducted.

Chapter 9 presents the conclusions of this thesis.

Chapter 10 presents the recommendations for future studies.

CHAPTER 2

GAS HYDRATES

Gas Hydrates (GH) commonly called, as clathrates are non-stoichiometric crystalline place when water forms a cage-like structure around small size gas molecules [23]. Gas hydrates form as the constituents get in touch with at low values of temperature and high values of pressure [24]. Gas hydrates are synthesized of water and principally the retainer gas compounds and elements: methane, ethane, propane, iso-butane, normal butane, nitrogen, carbon dioxide and hydrogen sulfide [23]. Makogon [25] exemplified methane hydrate formation reaction as:



(Methane) (Liquid) (Hydrate)



Where N_{H} is the hydration number approximately equal to 6.1 for methane (CH_4) hydrates [5]. The hydrate configuration reaction is an exothermic operation, which generates heat while the hydrate dissociation reaction is an endothermic operation, which imbibes heat. The heat of modulation of methane hydrate from methane and liquid water (H_2O) is $\Delta H_1=54.2$ kJ/mol and the heat of modulation of methane hydrate from methane and ice is $\Delta H_2=18.1$ kJ/mol [26].

In methane Hydrate (MH) reservoirs in nature, temperature and pressure conditions have to be in MH stability region in the initial phase. In order to segregate MH and manufacture gas from a MH reservoir, pressure and temperature conditions should be in MH separation area. Consequently, three methods of thermal injection, depressurization

and inhibitor injection have been suggested as primarily operations for separating MH [27,28].

In depressurization operation, the bottom-hole pressure is diminished by a pump settled down hole and this low pressure is moved to reservoir to prompt the dissociation of MH. By diminishing the bottom hole pressure of a well, the reservoir pressure (P_r) in the contiguity of this well diminishes first. The temperature of reservoir diminishes along with dissociation of MH due to dissociation of MH because imbibes energy. The dissociation of MH ceases when the reservoir temperature concludes alike to the 3-phase equilibrium temperature analogous to the reservoir pressure shown in Figure 2.1.

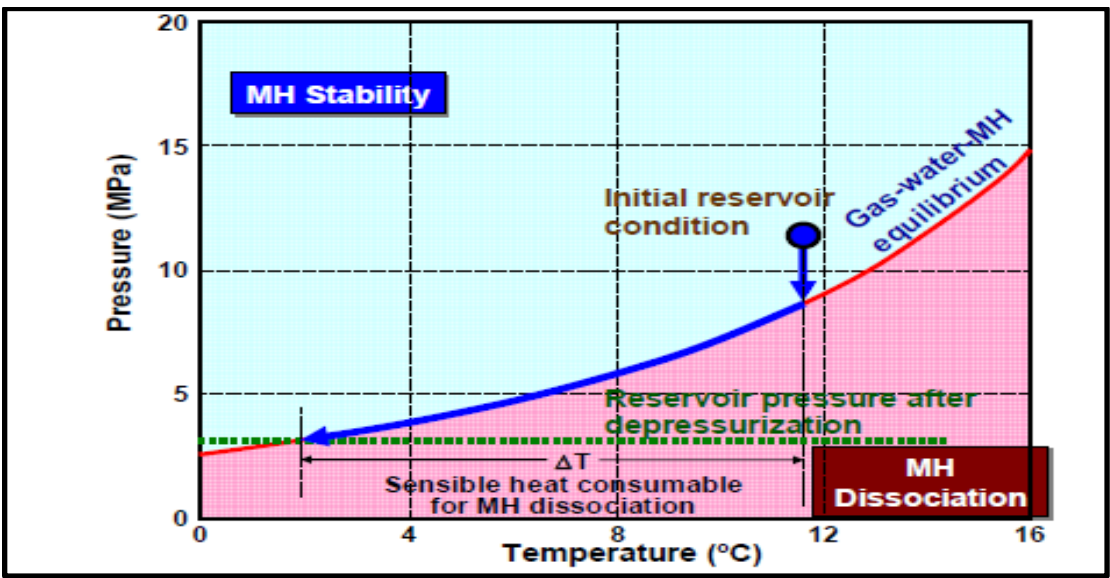


Figure 2.1 Temperature reductions along with the MH dissociation in depressurization method [27].

Although depressurization was suggested as a promising method, the methane recovery from a MH reservoir by this method highly relies on reservoir properties and is prognosticated to be up to about 60% even in the propitious occasion [29].

Thermal operation is the comprehensive phrase for the operations supporting the dissociation of MH by augmenting the reservoir temperature. This method also contains thermal stimulation method and thermal flooding method. The thermal stimulation

operations intend to the augmentation in the temperature near a well. These operations comprise a hot water circulation process, circulating hot water in a wellbore to increase bottom hole temperature. In thermal flooding, the heat such as hot water is injected from a well and is flooded toward other wells augmenting the degree of warmth and hence dissociating the MH between wells (hot water flooding method) [28,29].

From hot water circulation only a few per cent of methane retrieval is anticipated since bottom-hole pressure should be higher than inceptive reservoir pressure to circulate water. On the contrary in depressurization and other thermal methods approximately 100% of methane recovery is anticipated by synergistic effect of depressurization and heating if the conditions are favorable. However, since energy supplied is big enough, the quality of being appropriate of thermal methods is questioned from the point of energy ability. In the inhibitor injection method, important MH dissociation is not anticipated solely. Over and above, it should be hard to supply an inhibitor smoothly into a reservoir because of very low initial effective permeability to water. The effect of the inhibitor injection method, however, comes into doubt because of the high expenditure and dilution/dispersion of inhibitors [27,30].

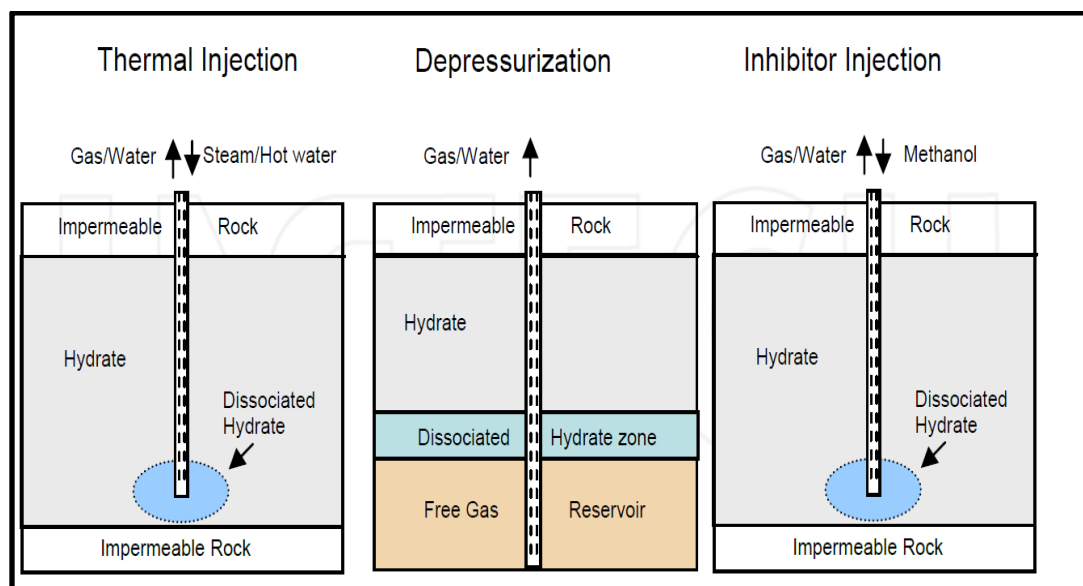


Figure 2.2 Gas hydrate production methods [27]

2.1 Properties of Gas Hydrates

Gas hydrates look like compact ice, can be burnt and they usually smell like natural gas. One cubic foot of methane hydrate can compress around 164 ft³ of methane at standard pressure and temperature [31,32]. The density for gas hydrates varies, according firstly to the composition of the gas, secondly according to temperature T and finally due to pressure P, which they are used to form, hydrates.

Table 2.1 Properties of different hydrates [25]

Gas	Formula of Hydrate	Hydrate density@273K(gr/cm ³)
CH ₄	CH ₄ .6H ₂ O	0.910
CO ₂	CO ₂ .6H ₂ O	1.117
C ₂ H ₆	C ₂ H ₆ .7H ₂ O	0.959
C ₃ H ₈	C ₃ H ₈ .17H ₂ O	0.866
C ₄ H ₁₀	iC ₄ H ₁₀ .17H ₂ O	0.901

The hydrate dissociation is an endothermic reaction. In figure 2.3 is shown the heat of dissociation of different hydrates [26].

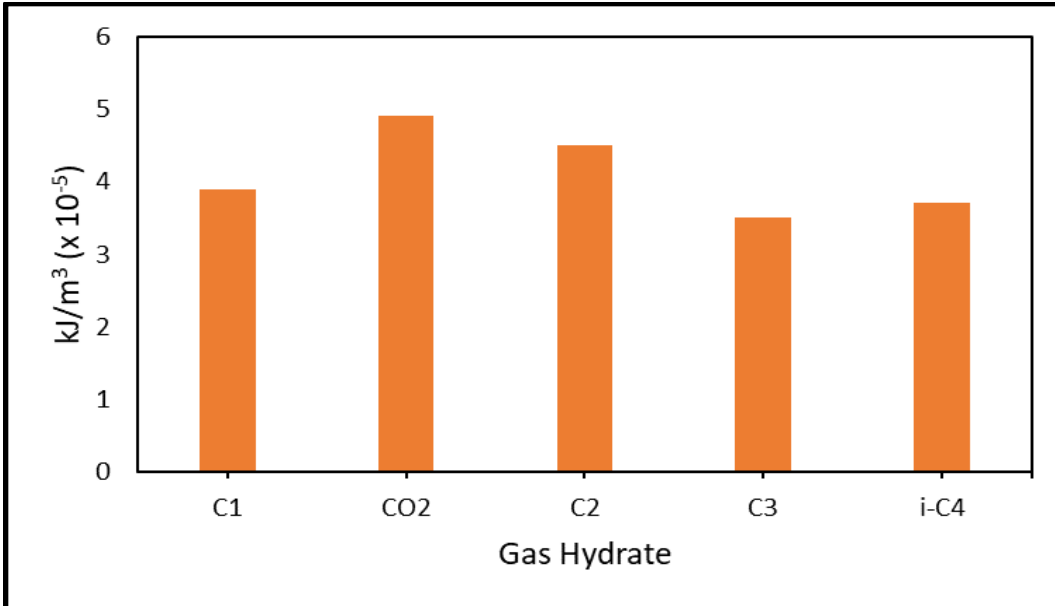


Figure 2.3 Heat dissociation of different hydrates [25]

Table 2.2 Physical properties of gas hydrates compared with ice (^bCalculated from $k=1/(r \cdot C_p)$, ^cCalculated from Reference [5]) [32]

Property	Water	Ice Ih	Structure I (sI)	Structure II (sII)
Thermal conductivity λ ($Wm^{-1}K^{-1}$)	0.58 (283K)	2.21 (283K)	0.57 (263K)	0.51 (261K)
Thermal diffusivity κ (m^2s^{-1})	1.38×10^{-7b}	11.7×10^{-7b}	3.35×10^{-7}	2.60×10^{-7}
Heat capacity C_p ($Jkg^{-1}K^{-1}$)	4,192 (283K)	2,051 (270K)	2,0319 (263K)	2,020 (261K)
Linear thermal expansion at 200K (K^{-1})	-	56×10^{-6}	77×10^{-6}	52×10^{-6}
Compressional wave velocity V_p (kms^{-1})	1.5	3.87 (5MPa, 273 K)	3.77 (5MPa, 273K)	3.821 (30.4-91.6MPa, 258-288K; C ₁ -C ₂)
Shear wave velocity V_s (kms^{-1})	0	1.94 (5MPa, 273K)	1.96 (5MPa, 273K)	2.001 (26.6-62.1MPa, 258-288K; C ₁ -C ₂)
Bulk modulus K (GPa)	0.015	9.09 (5MPa, 273 K)	8.41 (5MPa, 273K)	8.482 (30.4-91.6MPa, 258-288K; C ₁ -C ₂)
Shear modulus G (GPa)	0	3.46 (5MPa, 273 K)	3.54 (5MPa, 273K)	3.666 (30.4-91.6MPa, 258-288K; C ₁ -C ₂)
Density ρ (kgm^{-3})	999.7 (283K)	917 (273K)	929 (273K)	971 ^c (273K); 940(C ₁ -C ₂ -C ₃)

Table 2.2 summarizes the fundamental properties for solid methane and solid propane by using Brillouin spectroscopy on a small volume of relatively pure propane hydrate samples, whereas Waite et al. made experiments by the use of pulse wave transmission through dense polycrystalline methane hydrate to obtain results. The same also table 2.3 presents the properties of pure methane hydrate [33].

Table 2.3 Elastic properties of solid methane (sI) and propane (sII) hydrate with comparison to that of water ice [34]

Properties	Water Ice	Methane Hydrate ^a	Propane Hydrate ^a	Methane Hydrate ^b
Density (gcm ⁻³)	0,916	0.91	0.88	0.89
Shear Modulus G (GPa)	3.5	3.3	2.4	4.3
Bulk Modulus K (GPa)	8.8	7.7	5.6	-
Young's Modulus E (GPa)	9.3	8.5	8.3	11.07
Vp/Vs	1.96	1.93	1.95	1.80
Poisson's Ratio	0.325	0.317	0.32	0.2776

The results show that the density of gas hydrate is a little bit lower than the density which has been measured in the laboratory. The results also propose that Young's moduli of methane hydrate are higher than that of water ice [34].

2.2 Hydrate Structures

Water molecules compose the cavities, which are constituted of pentagonal and hexagonal faces, mold hydrates. The merging of different parts of alternative faces assists for the formation of different hydrate structures to the fact that geometric structures are notable to realize the nature of hydrates. Two structures (types) of hydrates are the most common in chemical and petroleum industry and these are, structure I (sI) and structure II (sII). Another structure (type) that is less ordinary than the two preceding structures are the structure H [35]. The tetrahedral positioning of water molecules, which are held together by hydrogen bonds, is the common property of the three structures of hydrates. The tetrahedral bonded waters in hydrates resemble the tetrahedral positioning of water molecules in hexagonal ice, which is the most ordinary

solid form of water. The bond lengths of the hydrates vary only less than 1%. From the other side the angles between oxygen atoms deviate by less than 4 % [36]. The gas hydrate structure contains a number of polyhedral cages while ice includes a compilation of non-planar “puckered” hexagonal rings. Due to the difference the guest molecules inside the lattice can be trapped by the hydrates. It is obvious from the previous difference that the thermodynamic conditions required for ice formation and gas hydrate have the ability to form at temperature above the freezing point of water as long as the sufficient gas molecule and water is available [37].

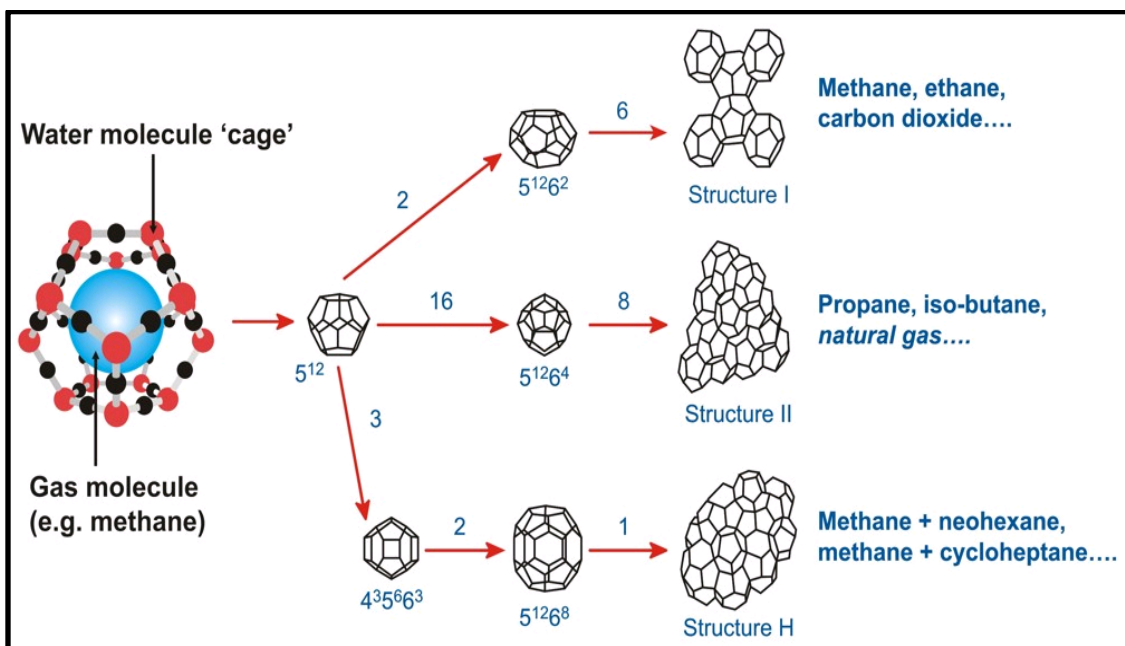


Figure 2.4 Structures of gas hydrates [5]

The structures (sI, sII and sH) are described by the parameters of figure 2.4. The small cage (SC) of sI is connected in space by the vertices of the cages. The SC of structure sII the faces are shared. The spaces for both of the structures between the SC are formed by large cage (LC). As far as it concerns the structure sH the face sharing occurs in two dimensions such that a layer of SC connects to a layer of medium and LC [5,38]. The three structures of gas hydrate embody alternative guest molecules into a single cell but sH needs two different-sized molecules to form: one small molecule as a helping gas

such as methane accomplishing the small cage and a large molecule [39]. Table 2.4 represents the structures of gas hydrates according to Sloan and Koh in 2008.

Table 2.4 Structure of gas hydrate cells. Space group reference numbers from the International Table of Crystallography [5]

Structure	I		II		H		
Crystal system	Cubic		Cubic		Hexagonal		
Space group	Pm3n(No.223)		Fd3m(No.227)		P6/mmm(No.191)		
Ideal unit cell	$2(5^{12})6(5^{12}6^2) \times 46\text{H}_2\text{O}$		$16(5^{12})8(5^{12}6^4) \times 136\text{H}_2\text{O}$		$3(5^{12})2(4^35^{16}6^3) \times 34\text{H}_2\text{O}$		
Ideal hydration number	5.750		5.667		5.667		
Cages	Cages		Cages		Cages		
	Small	Large	Small	Large	Small	Medium	Large
Average cavity radius[A]	3.95	4.33	3.91	4.73	3.94	4.04	5.79
Variation in radius[%]	3.4	14.4	5.5	1.71	4.0	8.5	15.1
Water molecules per cavity	20	24	20	28	20	20	36

The ratio of water molecules to gas molecules within a unit cell is expressed by the hydration number (n). It has mutual connection to the cage occupancy (θ), as each unoccupied cage adds more water but no gas molecule to the equation, therefore a high n implies a low θ . The cage occupancy (θ) is significant to define the amount of gas captured in hydrates [29]. As far as, it concerns the presence of two or more gases, the crystal structure is depended not only by the size of the biggest guest molecule present

but also by the concentrations of the guests. Ethane suits into LC of both sI and sII. Methane as single gas also suits in both structures of sI and sII. If methane and ethane occurred together, both of them can be formed as sI or sII depending: firstly, on temperature, secondly on Pressure and lastly on relative concentrations of the potential guests. A mixture of methane and ethane at various conditions of P, T insist as sI if the CH₄ concentration stays below 72-75 mol% [40] or above 99.2-99.4 mol % [41]. Table 2.5 shows the guest molecules and hydrate cages; ratio of guest molecule diameter versus cavity diameter.

Table 2.5 Guest molecules and hydrate cages; ratio of guest molecule diameter versus cavity diameter [5].

Guest molecule	Guest molecule	sI	sII	sI	sII
Molecule	Diameter[A ⁰]	SC	LC	SC	LC
N ₂	4.1	0.804	0.7	0.817	0.616
O ₂	4.2	0.824	0.717	0.837	0.631
CH ₄	4.36	0.855	0.744	0.868	0.655
H ₂ S	4.58	0.898	0.782	0.912	0.687
CO ₂	5.12	1.00	0.834	1.02	0.769
C ₂ H ₆	5.5	1.08	0.939	1.10	0.826
C ₃ H ₈	6.28	1.23	1.07	1.25	0.943
i-C ₄ H ₁₀	6.5	1.27	1.11	1.29	0.976
n-C ₄ H ₁₀	7.1	1.39	1.21	1.41	1.07

2.2.1 Structure I

Structure I gas hydrates contain 46 water molecules per unit cell arranged in 2 dodecahedral voids and 6 tetrakaidecahedral voids which can accommodate at most 8 guest molecules. The hydration number ranges from 5.75 to 7.67. The average hydration number in the Structure I hydrates is 6 and the lowest hydration value is obtained when all crystal units are occupied whereas highest value is obtained for large guest molecules that cannot fill small cage. Structure I hydrates are formed by gas molecules such as methane, ethane, carbon dioxide and hydrogen sulfide [5,23,32].

2.2.2 Structure II

Structure II gas hydrates contain 136 water molecules per unit cell arranged in 16 dodecahedral voids and 8 hexakaidecahedral voids, which can also accommodate up to 24 guest molecules. The hydration number is 5.67 when all crystal units are occupied, whereas 17 when large guest molecules are not able to fill the small cages. This allows inclusion of propane and iso-butane in addition to methane and ethane but not pentane [5,23,32].

2.2.3 Structure H

The rarer structure of gas hydrates, which contain 34 water molecules per unit cell arranged in 3 pentagonal dodecahedral voids, 2 irregular dodecahedral voids, and 1 icosahedral void, can accommodate even larger guest molecules such as iso-pentane. The hydration number of sH is 5.67 like sII. The structure H of gas hydrates was discovered by Ripmeester et al. in 1987 [42]. It is possible that Structure H was first prepared (but not found) by de Forcrand in 1883 during his laboratory experiments. Binary (double) hydrates with iso-butyl chloride or bromide as the big guest were mingled by de Forcrand, where these guest molecules were contiguous in size to iso-pentane, now known to be a sH hydrate former. Formation of this structure necessitates minor guest molecules like methane, nitrogen or carbon dioxide for the 5^{12} and $4^35^66^3$ cages, but the molecules in the $5^{12}6^8$ cage should be bigger than 0.7 nm but smaller than 0.9 nm like methyl cyclohexane. These hydrate structures consist of three 5^{12} , two $4^35^66^3$ and one $5^{12}6^8$ crystal units in a unit cube. When the cages of structure H are concerned, there would be 6 gas molecules per 34 water molecules in other words, the guest to water ratio becomes $1: 5 \frac{2}{3}$ [5,23,32].

2.3 Location of Gas Hydrates

More comprehension about gas hydrates operations initiated after 1920 when the pipelines commenced to transport methane from gas reservoirs. In low temperature there was obstruction in pipelines which sometimes put impediments for the gas to flow

through them. Primarily these obstructions were expounded as frozen water. The advisable designation about these obstructions was given in the 1930s, and it was hydrate. On the other hand, in 1946, Russian specialists claimed that the conditions and resources for hydrate formation and stability subsist in nature, in districts covered by permafrost and their first discovery suggestion was in Western Antarctica [25,34]. Figure 2.5 shows the marine and onshore hydrate locations. About 98% of the gas hydrate resources are concentrated in marine sediments, with the other 2% beneath permafrost. Seismic processes and scientific drilling programs are responsible for interfered gas hydrate accumulations (red) and discovered gas hydrates (blue) respectively [43].

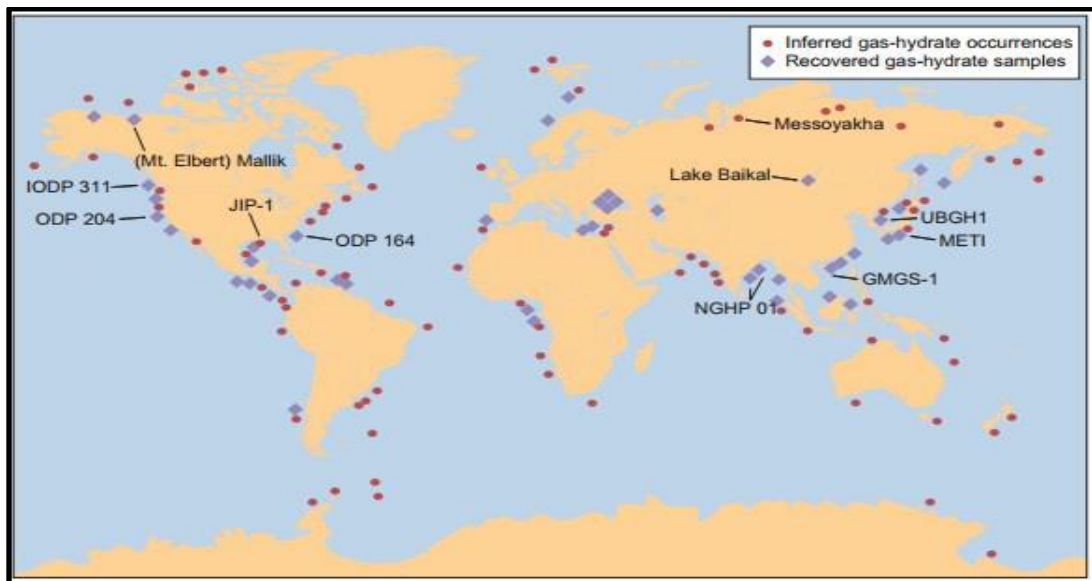


Figure 2.5 Natural Gas Hydrate Reservoir Distributions in the World [43]

Other regions that have been indicated for gas hydrates are Gulf of Mexico, Pacific Coast of Canada, North Slope of Alaska, Japan, China, India and in South Korea [45].

Boswell's group suggested a new way to classify hydrate reservoirs and they divided in four categories. According to these scientists, their classification is based on geological framework and lithology of hydrate bearing sediments. The four significant plays that hydrates could be located were sand-dominated plays, fractured clay dominated plays; massive gas hydrate formations exposed at sea floor and low concentrations hydrates

disseminated in a clay matrix. It is also found that hydrates exist in fracture fillings in clay dominated systems in shallow sediments [26]. The natural gas hydrates in marine sediments are regulated by the hoardings of Particulate Organic Carbon (POC) which is microbial transformed into methane, the thickness of the gas hydrate stability zone (GHSZ) that methane (CH_4) can be ensnared, the sedimentation rate (SR) that checks the time that POC and the produced methane (CH_4) stays within the GHSZ [46]. Figure 2.6 presents the gas hydrate stability conditions for both marine and permafrost hydrates.

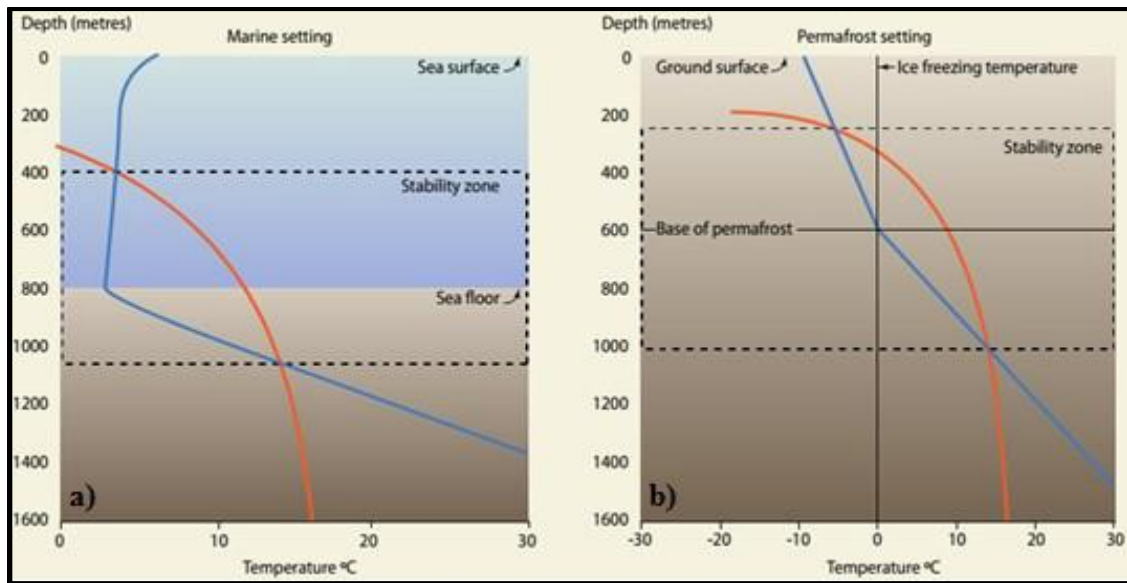


Figure 2.6 Gas hydrate stability conditions for a) marine hydrates b) permafrost hydrates (Orange curve: hydrate equilibrium curve, Blue curve: thermal gradient curve) [47]

Recently, Wallmann et al. in 2012, introduced transfer functions to show the gas hydrate inventory in diffusion-controlled geological systems based on SR, POC and GHSZ thickness for two alternative plans: normal and full compacting sediments [48]. In Figure 2.7 is presented the global gas hydrate inventories in marine sediments.

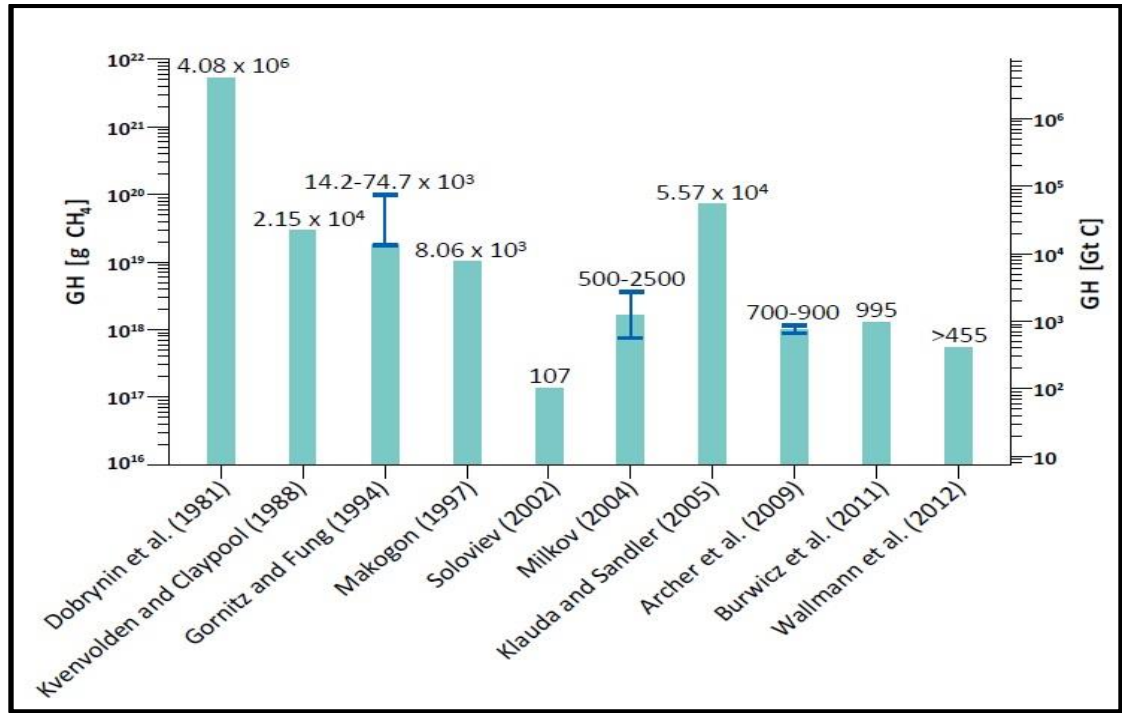


Figure 2.7 Estimates of global gas hydrate inventories in marine sediments. The corresponding estimated ranges are labeled in Gt C [46].

Hydrates have changed derived the current semantic about untapped hydrocarbon source, as an icy compound in outer solar system environments, and as a manufactured material that is a contingent way for not dangerous storage and transport of natural gas [49]. Many tries of different researchers in the world that attempted to obtain the solution to the problem of natural gas transportation and storage in a solid hydrate state. It is safer to store or ship gas in hydrate state than liquefy it [50]. Parlaktuna and Gudmundsson first proposed storage and shipping of natural gas in 1992 in Trondheim University [51]. This idea continued by Stern et al. who made experiments and proposed an anomalous self-preservation effect of hydrates. Stern claimed that only mild refrigeration (268 K) was needed to maintain the hydrates for longer time at atmospheric pressure [49].

Hydrate formation is a key factor for safety reasons in deep water oil/gas production. In 2010 hydrate was the major restrained reason of the oil leak following blow out of the Macondo well in Mexico. Other utilizations of gas hydrates contain storage of natural

gas and hydrogen (H_2). The competence to store natural gas in the form of hydrate pellets has the tendency to be done where there is secluded gas in small quantities and the need for building a liquefied natural gas plant is not economic viable [52,53]. The storage and transportation of gas hydrates are to commercialization by developing and optimizing efficient production of large volumes/scale up of gas hydrate pellets [54].

Attempts have also been done to evolve gas hydrates for hydrogen storage applications. The hydrogen molecules conceive the small and the large cages of structure II of hydrates. Tetrahydrofuran (THF) which works as promoter molecule, it enables H_2 hydrates to be formed and stabilized at lower pressure conditions than those needed by pure hydrogen hydrates. The incentive in this occasion is to store H_2 in clathrates materials in as possible lower values of temperature and pressure as well as at high capacity [55,56]. Gas hydrates can be implemented to separation procedures such as separation of flue gas and desalination of water. Flue gases such as carbon dioxide (CO_2) are captured in gas hydrates while precluding nitrogen (N_2) and other not harmful molecules. There is no commercialization use until now [57]. On the other side desalination is very significant for fresh water for both domestic and agricultural factors. In the desalination procedure, gas hydrate will be formed by sea water such that salt ions are blocked [58,59]. Albeit that first time desalination procedure was proposed some decades ago, it is still unsearchable and it will be needed further research and evolvment to explore the technical and economic expediency of this process [60,61].

2.4 Gas Hydrates in Pipelines

The exploitation of gas hydrates seems beneficial to untie upcoming energy problems. Moreover, gas hydrates play a significant role in gas transportation and gas storage in pipelines, particularly in conduits and valves, gas hydrates are created and prevent the gas flow. This phenomenon is called “plugging” and congests high operational expenditures as well as vague not dangerous circumstances [62]. It is obvious that the gas hydrate formation in oil and gas pipelines is an unwelcome condition, undermining the flow assurance programs in addition to posing menace to the staff and equipment

[63]. Blocking by gas hydrates can be shunned in pipelines by the utilization of alternative operations of inhibition such as heating or insulating the critical pipeline expanses or by adding inhibiting chemicals e.g. methanol. These hydrate inhibition operations are both pricey and not environmental acceptable [62].

Various transportation options of natural gas from off-take include long pipelines transport, liquefied natural gas (LNG), compressed natural gas (CNG) of pressure between 207 and 248 bar (3,000 and 3,600 psi) and methanol. Long pipelines and LNG are the ordinary utilization. The unit expense of pipeline selection is obvious higher than LNG due to the demanded huge charge of refrigeration and liquefaction of boiled-off liquids and the high peril of over pressurization for LNG. Transportation by methanol and CNG evince unit costs which are similar to pipelines but these are in theory nowadays [64]. Water is of 90% composition of the hydrate lattice while other components constitute 10%. The solid hydrate may be formed at high pressures and low temperatures (even above the normal melting point of ice) due to the weak Van der Waals forces and the hydrogen bonding properties of water [65,66]. Below sea, gas transportation pipelines frequently have thermodynamically conditions to generate hydrates. Formed hydrates can obstruct pipelines, subsea transfer lines and in the event of gas kick during drilling, hydrate can be formed in the wellbore riser, blow-out preventer and choke-lines [67]. As far as it concerns the economic situation, expenses that originate from gas hydrates, cost billions of dollars (\$) in upstream industry. Every year upstream industry tries to moderate these expenses with no stable solutions in focus [68]. Hydrates can also influence alternative types of natural gas pipeline's internal corrosion which is a long term trouble through physical and chemical functions based on hydrate size, stage and contact period [69]. H_2S , CO_2 and Cl^- that are components of hydrate, are acidic gases which conduce to internal gas pipeline corrosion rate [70]. Methane, the major component of natural gas, also participates as a diminishing agent for metal corrosion [71]. Water is another known corrosive agent [72]. Corrosion apart from the financial aftermaths will also generate political and environmental corollaries and will lead to consolidate substitution of the pipe-length at extra production rate. The

corrosion types that could be initiated by physical means include cavitation, erosion, pitting, galvanized and stress cracking corrosions. Worldwide oil and gas industry instead to put efforts how to solve the problem about hydrates creation of corrosion (main problem), they insist to put efforts how to remove hydrates after its formation with so many discoveries about its properties and abilities to rapture a service pipe [73].

2.5 Gas Hydrates in Tanks

Natural gas is one of the significant energy resources and lately its worldwide consumption is promptly amplifying due to the growing demand for clean energy and environmental concerns. It is prognosticated that the natural gas demand is raised at an average rate of 2.4% annually until 2030 in the world [73]. Figure 2.8 shows the worldwide trend natural gas consumption up to 2025 [74].

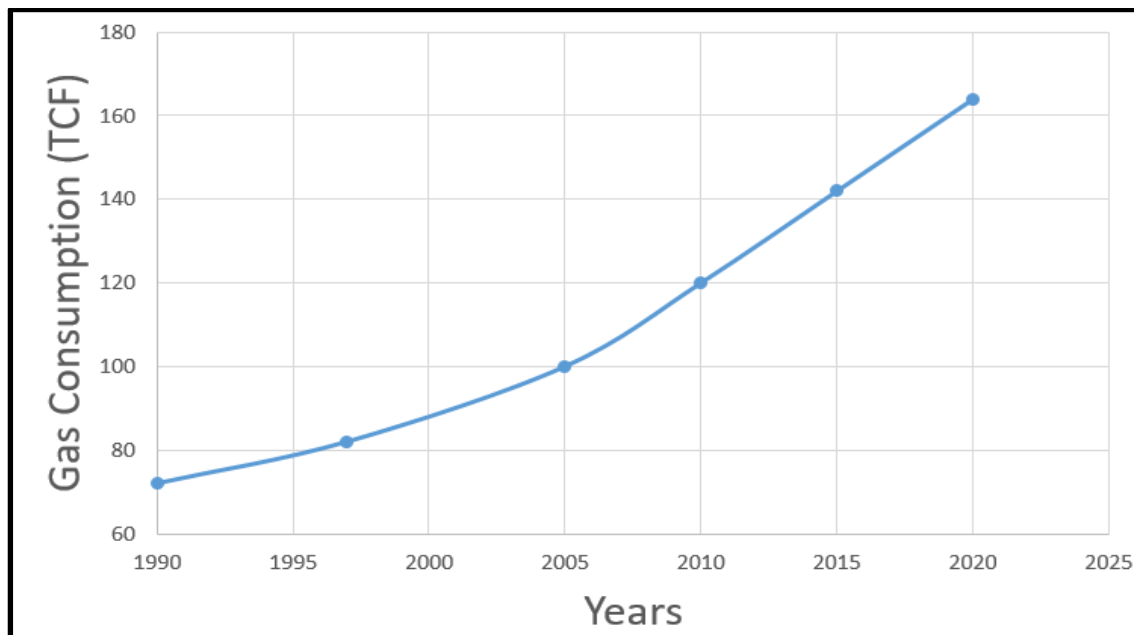


Figure 2.8 Worldwide natural gas consumption [74]

To satisfy such a demand, there are plans to transport natural gas to potential markets. Apart from transportation of hydrates through pipelines, there are other methods such LNG and CNG. In LNG occasion, natural gas is liquefied at atmospheric pressure and

temperature approximately 113K. Transforming natural gas to LNG decreases the gas to 160 of its volume permitting transportation by specialized LNG tanker ships over long distances. The storage of LNG is commonly guided in onshore facilities LNG carriers can also be profitable for shipping big volumes of gas over long distances [75,76]. Although offshore transportation of compressed natural gas CNG have been begun from long time ago up to lately, the studies and researches for commercial outcomes have not been successful. The main reason is the cost of the required pressure vessels. However, commercial CNG carriers are on the stage of the implementation [74]. In CNG projects, most of the capital investment is consumed on creating the ships. Due to the fact that LNG is complicated and capital intensive cooling and re-gasification, CNG loading and unloading terminals would conditionally be simpler and cheaper than those used for LNG [75]. Generally, it is obvious that the transportation of gas is cheaper by ships compared to pipelines [77]. Figure 2.9 presents the cost for gas transportation with different methods.

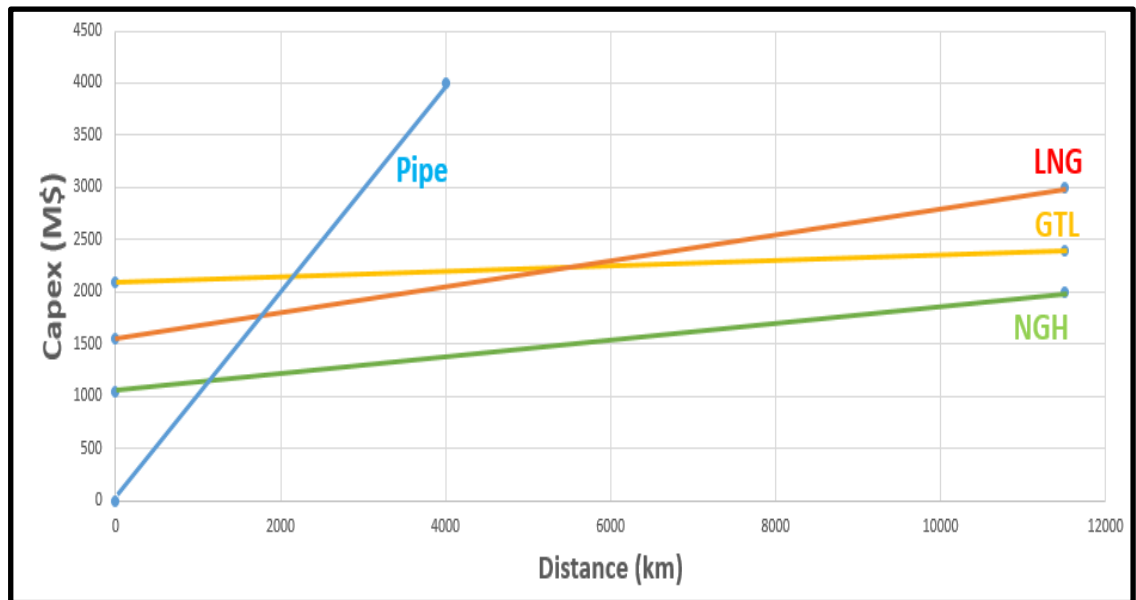


Figure 2.9 Comparison of gas transportation with different methods [77]

2.6 Hydrates as Potential Source Energy

It is obvious that oil and gas industry face many problems in hydrate operations. All of efforts from researchers and companies have been spent about the determination of hydrate crystal structure, thermodynamic behavior, kinetics of hydrate formation and ways to face plug formations [78]. Potential reserves of gas hydrates are over 1.5×10^{16} m³ and are distributed all over the earth both offshore and onshore. If only 17-20% of this resource can be produced feasibly, it can be sufficient supply energy for 200 years [79]. More than 220 gas hydrate deposits have been discovered, more than a hundred well have been drilled and kilometers of hydrated cores recovered. The most significant fact is not the amount of gas hydrate potential reserves but the volume of gas that can be commercially produced. The rate of modern civilization development in future hinge on different considerations but the quality and especially the quantity of energy will be among the most significant considerations. The data presented in figure 2.10 shows that in the 20th century the energy consumption came from coal instead of oil and gas [80].

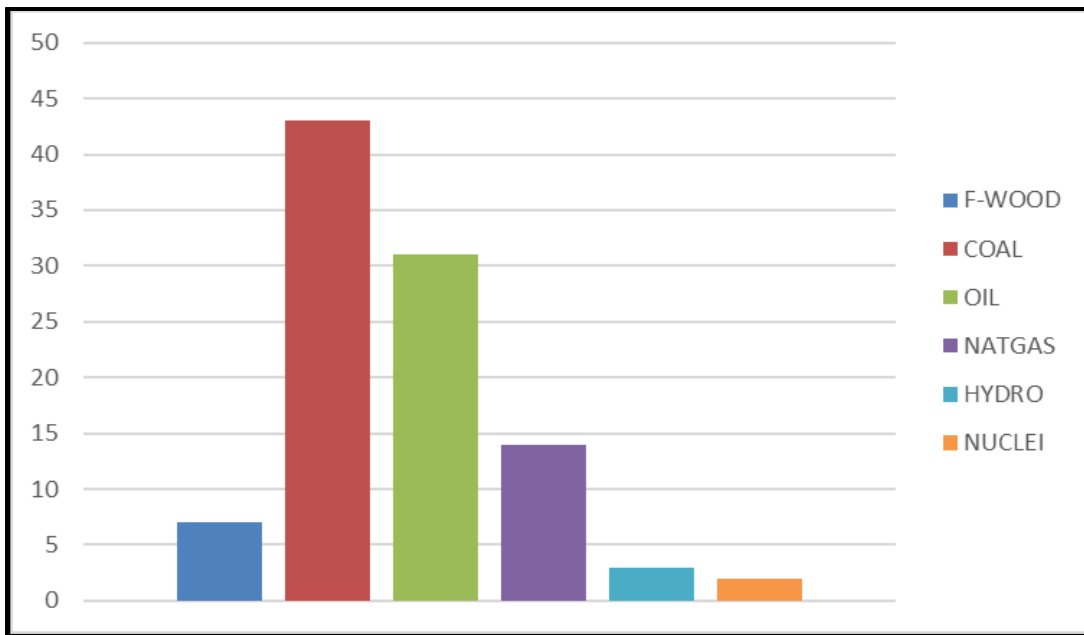


Figure 2.10 Energy consumption in the 20th century [81]

The winning performance of natural gas transport like NGH may confine the operational expense drastically by shunning extremely low temperature process cost in LNG production and compressing demand in CNG production. On the contrary, firmness of the end product is a significant disquiet. It has been demonstrated that the firmness of the end NGH product remained stable up to 2 years in solid hydrate form in cold climates such as Russia and Norway [82]. It should not be forgotten that natural gas, primarily methane, is a splendid fuel for combustion many reasons. Methane generates less carbon dioxide per mole than any other fossil fuel when it is used as fuel. Figure 2.11 is summarizes the world energy balance until 2050

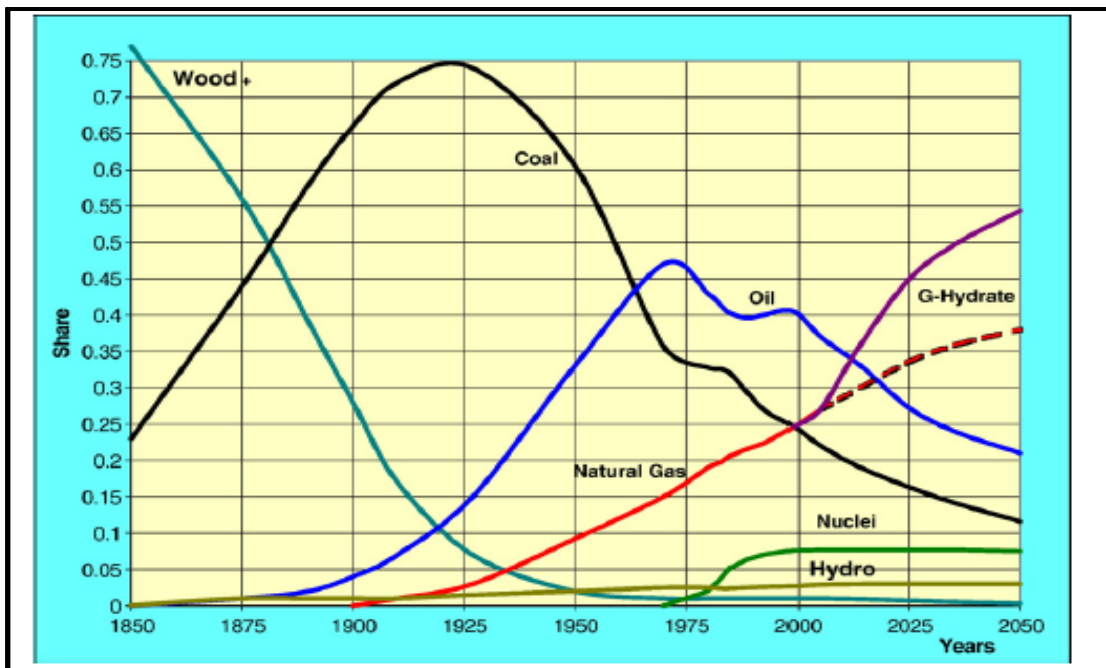


Figure 2.11 World Energy Balance [81]

Thus, it can decrease the quantity of emissions originating in human activities of carbon dioxide gas, which may cause a greenhouse effect. Moreover, the quantity of fossil fuel in hydrate form is around double as large as in all other fossil fuels combined [83]. In Figure 2.12 is depicted the timeline graphs for the essential gas hydrate projects worldwide.

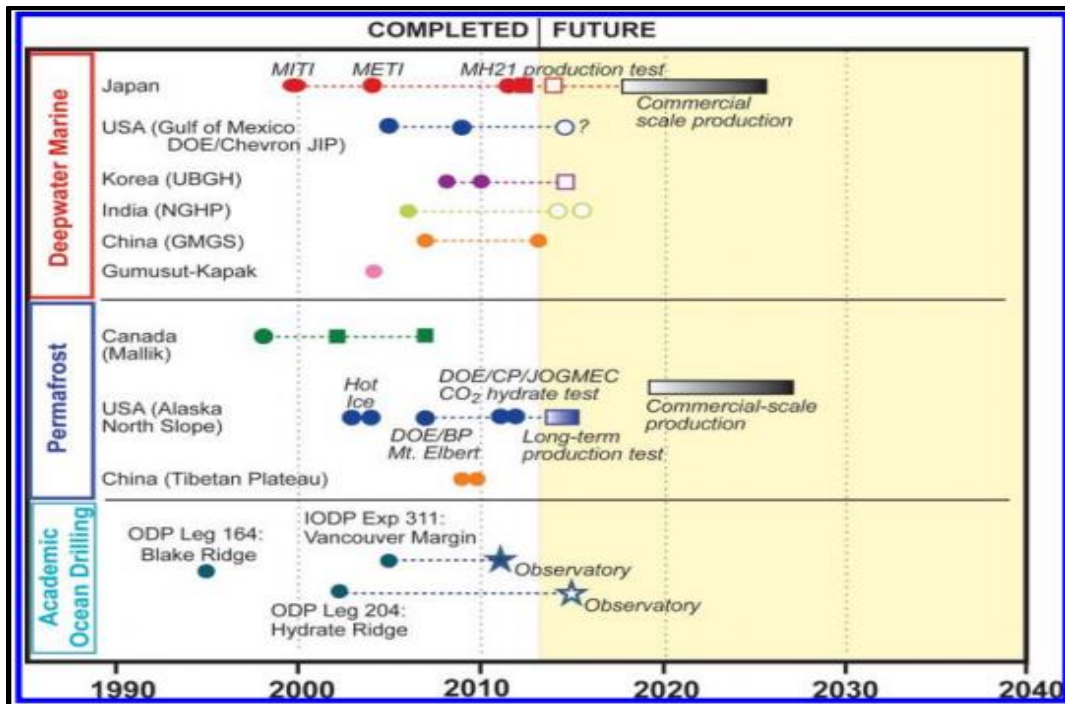


Figure 2.12 Timeline charts of gas hydrate field projects in the world [84]

Natural gas hydrates are more evenly distributed on the planet than sources of hydrocarbons. The most crucial anxiety is the generation of highly-effective technologies of transporting the natural gas from its solid state into free gas [79].

2.7 Motivation of Studying Gas Hydrates

It is obvious over the past years that complexity and important inability there are in the relationship between crystal structure and size of hydrate formers if more than one gas is present. This makes important the search about the structural information together with thermodynamic parameters, especially in multicomponent. Nowadays importance in hydrate persistence and decomposition requires application of new technologies that permit acquiring high resolved structural and statistically important crystallizes size information. Moreover, new information about thermodynamic behavior and kinetics of hydrate formation will play significant role in the researcher's future studies [32]. Figure

2.13 indicates that gas production from gas hydrates are still at the early stages of development.

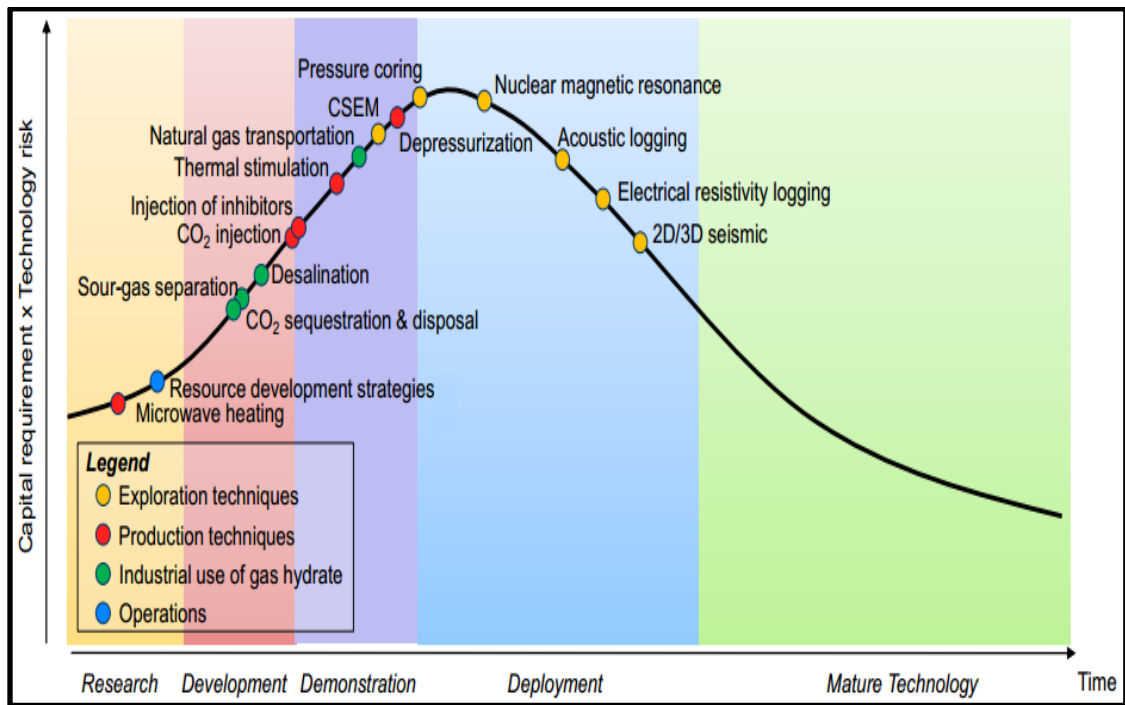


Figure 2.13 Technology maturity curve of gas hydrates [85]

It is apparent that gas hydrates postulate more research to be comprehended, and this is indeed taking place. Willingness and persistence of both scientists and industry will optimistically take gas hydrates away from the legendary cloud that covers them, to something closer to a well-comprehended actuality [86]. Figure 2.14 shows the dispensation of organic carbon in earth blocking scattered organic carbon such as kerogen and bitumen.

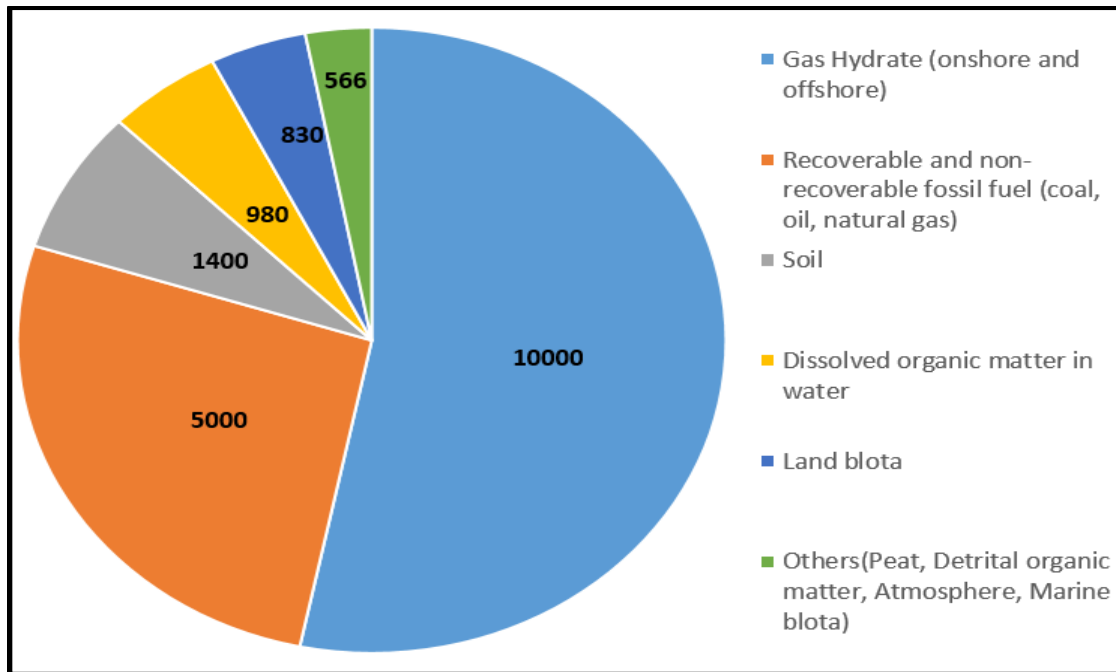


Figure 2.14 Distribution of organic carbon in earth excluding dispersed organic carbon such as kerogen and bitumen. Modified from different sources [86]

CHAPTER 3

GAS HYDRATE INHIBITORS AND PROMOTERS

Formation of gas hydrates is known to cause rigorous problems in wellbores and more specifically in drilling [87], well completion [88,89] as well as transportation through gas pipelines [90,91]. Because production goes into deeper water, hydrate control grows in importance. Ideally, operators want total hydrate control without the problems associated with Thermodynamic Inhibitors (THI) and/or Low Dose Hydrate Inhibitors (LDHI) [92].

Kinetics of hydrate formation is always a significant scientific subject for more explorations. Since this scientific field is not well comprehended, various theories and models have been evolved explicating the mechanisms of hydrate formation. Miscellaneous correlations have been introduced in the literature for prognosticating the hydrate generation conditions. These correlations can be categorized into five major processes [93]. The first method is K-value method which uses the vapor-solid equilibrium constants for predicting hydrate forming conditions [94]. The second method is Gas-Gravity plot developed by Katz [95]. The third method consists of empirical correlations developed according to the following form by Holder [96] and Makogon [97] for selected pure gases. The fourth method contains the charts of permissible expansion that natural gas can undergo without risk of hydrate formation. These charts were redrawn with the aid of the gas gravity charts using the Joule Thomson cooling curves [98]. The fifth method is based on statistical thermodynamic approach developed by van der Waals and Platteeuw and accounts for the interactions between water molecules forming the crystal lattice and gas molecules [99]. However new hydrate phase measurement methods such as Raman, NMR and Diffraction

Spectroscopy have enabled van der Waals and Platteeuw model corrections to provide predictions which are almost accurate as the measurements themselves [100]. Apart from these five methods Ostegaard in 2000 presented an idea similar to gas gravity idea practicable to all reservoir fluids, in the attendance of distilled water from natural gas to black oil which requires simply knowledge on the specific gravity and the concentration of the hydrate forming components in the system. The effect of non-hydrocarbon gases such as CO₂, N₂ in the petroleum fluid can be taken into account for the above approach [101].

Hydrates may be formed in the drilled wells if fresh water based drilling fluids are used in low temperature and pressure intervals [102]. In water-based drilling muds, hydrates can defy difficulties in two ways. The first way is when hydrates create a ‘plug’ or solid mass in wellbore. The plug will start from areas with little or no circulation such as choke lines; kill lines and blowout preventers (BOP). The second way where hydrates cause problems with drilling mud comes from their physical makeup. The loss of water from mud causes flow properties to impair strictly [103]. Consequently, stunting the generation of gas hydrates is an essential problem in upstream industry. There are two selections to answer this exigent situation: hydrate avoidance (no entry in hydrate domain) or hydrate management (operate with risk in hydrate domain). The management of hydrate obstacle comprises actions that are shown in figure 3.1. [104].

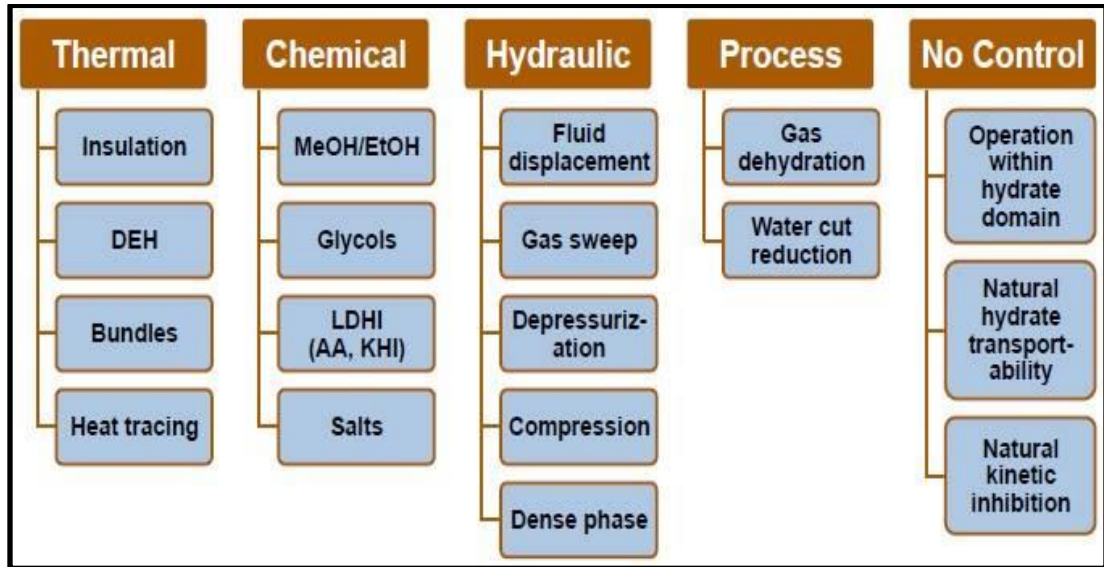


Figure 3.1 Hydrate management strategies [104]

Through any of these actions can be efficacious in inhibiting hydrates, some may not be attainable or covetable for deep water operations. For example, dehydration is weak as action for subsea wells or small platforms with limited space. Heating and insulation can be used independently or jointly; however, it may not be cost effective for longer flow lines to convey high GOR (gas/oil ratio) fluids. Chemical inhibition is by far the most commonly used method for audit hydrates [105].

The chemical methods can be divided in two main categories thermodynamic inhibitors and low dosage inhibitors. The most common thermodynamic inhibitors are the organic compounds such as glycols (MEG, DEG, TEG). Other known thermodynamic inhibitors are the salts (NaCl, CaCl₂, CaBr₂ etc.) [106-110]. Low Dosage Inhibitors are divided in two categories: kinetic inhibitors (KHs) and anti-agglomerates (AAs). Prominent kinetic inhibitors are polymers such as PVP, TBAB, amino acids such as Tyrosine, salts with two or more n-butyl, n-pentyl, and iso-pentyl groups, copolymers and similar ones [111,112]. Moreover, well known anti-agglomerants are surfactants such as LABSA anionic type, DAM cationic type and Ethoxalate non-ionic and salts such as NaCl and similar ones [113]. Figure 3.2 shows the different functions of hydrate inhibitors.

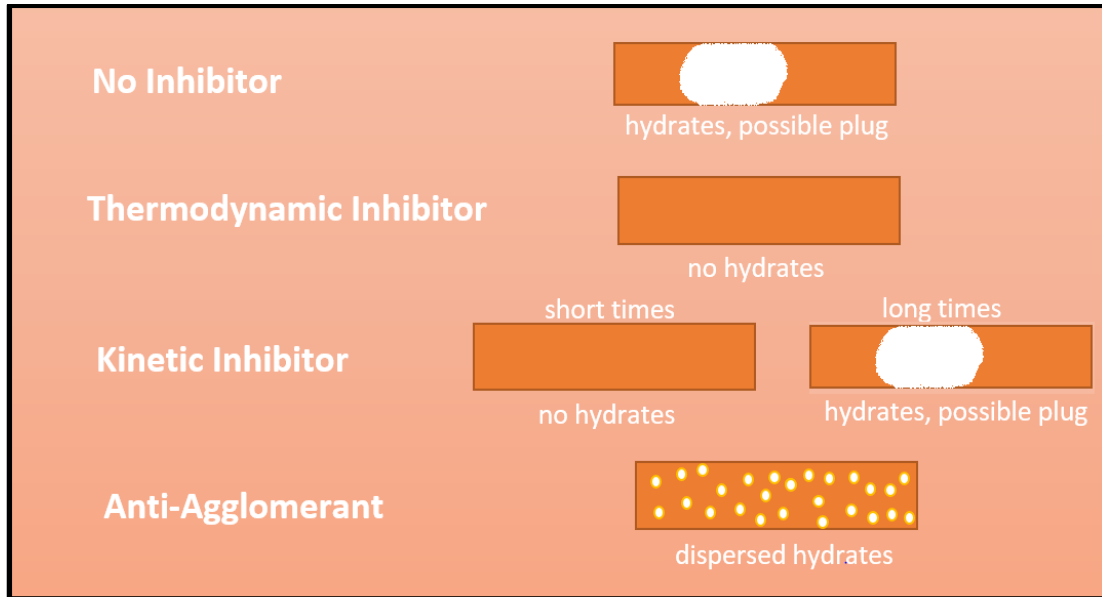


Figure 3.2 Design of different behaviors from inhibitors

3.1 Thermodynamic Inhibitors

Many researchers such as Parrish and Plausnitz in 1972, Sloan et al. in 1976, Robinson in 1976, 1977 and 1980, Holder in 1980 and John in 1980 discussed the thermodynamics of hydrate formation. All the researchers, apart from John et al., made use of the statistical thermodynamic theory presented by van der Waals and Platteeuw in 1959. With the exception of Sloan in 1984, all previous works have been restricted to selected parts of a general multiphase problem; and not the multiphase problem within a molecular thermodynamic framework [114]. Hydrates, which are compounds with low molecular weight, are in equilibrium with water at low temperature and high pressure. Water molecules form regular crystalline lattices that include cavities. These cavities encage gas molecules that stabilize the lattice by van der Waals forces [115].

Inhibitors such as methanol act by lowering the fugacity of water in coexisting phases; as a result hydrates are formed at lower temperatures and higher pressures than those encountered in the absence of methanol. This behavior is analogous to the freezing point depression of water by methanol [116]. Hydrates are most frequently encountered

in gas transportation and processing. Well known method to inhibit generation of hydrates in pipelines, is to use ‘thermodynamic’ inhibitors, such as methanol, broadly at high quantities (e.g. 40 vol%). THIs functions by alternating the hydrate formation phase limit elsewhere from the temperature and pressure conditions of the process in question, augmenting the driving force demanded for hydrate generation (see figure 3.3). Nevertheless, the implementation of thermodynamic inhibitors is both not good from financially perspective and ecologically hazardous and not acceptable. Nowadays that upstream sector goes to profound waters where hydrates prefer to be generated; up to 60 vol% methanol could be demanded for valid hydrate audit [117].

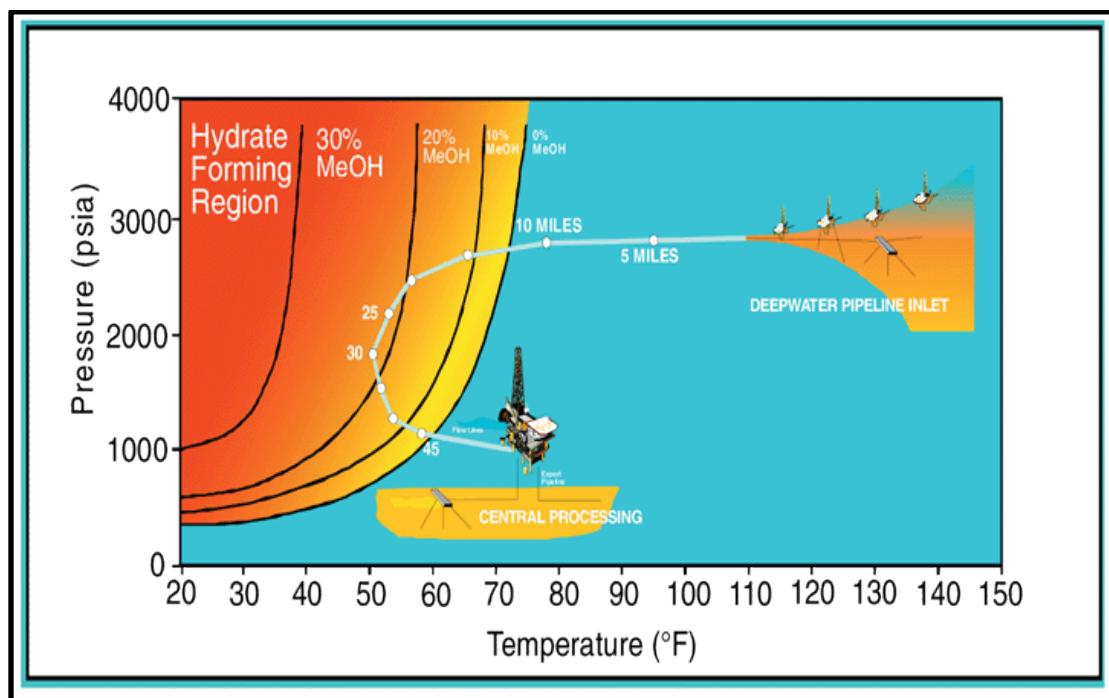


Figure 3.3 Phase boundary of methane hydrates [117]

Historically as it has already mentioned the most common thermodynamic hydrate inhibitors are glycols and salts. The thermodynamic inhibitors shift the formation of hydrates curve to the left so the system can bear lower temperatures and high pressures [118,119]. Apart from glycerol, Hale and Dewan [120] reported the felicitous use of salt together with glycerol so as to impede the hydrate formation in 1990. Quigley and

Hubbar conducted experiments with high concentrations of salt, alcohols, surfactants and their mixtures at 3,100 ft water depth and 5°C sea floor. Inhibition capacity of 26-wt % NaCl and its combinations proved safe choice apart from the mixture of 26-wt % NaCl and 20-wt % glycerol, which did not procure adequate safety at these conditions. Generally, salts are much more corrosive and less effective than methanol or glycols as pure thermodynamic inhibitor [121].

In 1992 Kotkoskie et al. [103] run a series of experiments with three different salts as thermodynamic inhibitors. The outcomes show that (NaCl) and sodium bromide (NaBr) have crucial inhibiting properties and could displace the equilibrium. Another salt, calcium chloride (CaCl₂) induces desirable hydrate formation, but due to the corrosive outcomes, it is not preferable. Nevertheless, CaCl₂ acquires the best result for inhibition among the pure salts. Howard in 1995 nominated how to calculate the effect of salts on hydrate formation temperature by freezing point depression data for the salts. Howard used the formula that was presented by Sloan in 1990. With this formula you could foretell the outcome on hydrate formation temperature for any natural gas [122]:

$$T_{eq,s} = T_{eq} * \Delta T_{freezing} \quad (3.1)$$

where:

$T_{eq,s}$ = hydrate equilibrium temperature in brine, °C

T_{eq} = hydrate equilibrium temperature in water, °C

$\Delta T_{freezing}$ = freezing point depression by brine, °C

In 1997 Ebeltoft et al. tested the salt polymer system by comparing drilling fluids in terms of hydrate inhibiting outcome. Apart from the three salts that were used before (NaCl, NaBr, CaCl₂), potassium chloride (KCl) was used for the first time. The effect of glycol was under consideration as thermodynamic inhibitor. The best outcomes depended on composition of salt and glycols were the 10-wt % ethylene glycol+15-wt % NaCl+5-wt % KCl [123]. Fadnes et al. in 1998 assured that salts could behave as

thermodynamic inhibitors. They ionized the solution and interacted with water molecules by bonds, resulting as clusters. Hence, they formed clustering around the polar solute molecule and the potential hydrate formation molecule diminished in water. This procedure is the “salting out” which was mentioned before [118].

Dominique Richon (2006) used thermodynamic inhibitors that have been used before such as salts of (NaCl) and (KCl) together with thermodynamic models. Generally, there was a good agreement between independent experimental data (using reliable isochoric technique) and predictions demonstrated the reliability of the developed model [108,124]. Calcium Chloride (CaCl_2) was also used as thermodynamic inhibitors together with ethylene glycol in different concentrations. Reliable hydrate dissociation data for quaternary system $\text{CH}_4\text{-H}_2\text{O-CaCl}_2\text{-EG}$ had been estimated at pressures up to 50 MPa. Also in CaCl_2 salt there was an acceptable accordance between model prognoses and irrespective experimental data on; water freezing point depression, vapor pressure reducing, salt solubility and hydrate constancy zone [109].

Another effort of thermodynamic inhibitors took place in 2009 again from Dominique Richon et al., where they used salts such as Sodium Bromide (NaBr), Potassium Bromide (KBr), Calcium Bromide (CaBr_2), Potassium Carbonate (K_2CO_3) and Magnesium Chloride (MgCl_2) for different concentrations and temperatures. The acceptable agreements for dissociation conditions between the experimental data measured and the data reported in literature helped to confirm the reliability of the experimental results for all salts, but MgCl_2 , which showed an unusual behavior at higher concentration [125].

Methanol is the most common thermodynamic inhibitor at oil/gas complex due to its availability and cheapness as chemical compound. Nevertheless, it is not implied that methanol is the most appropriate in use. Availability, low cost and guaranteed outcome from its use are not always the determining factors for the choosing of an inhibitor. Methanol has very high toxicity contiguously to ethyl spirit. Moreover, due to its high toxicity there is problem in recycling the water solutions of methanol. Hence, this

situation is required unprecedented security measures at purchase, transportation storage and use of methanol that are comparable to the cost of product itself [126].

3.2 Kinetic Inhibitors

Kinetic Hydrate Inhibitors (KHIs) are Low Dosage Inhibitors (LDIs) that are added at low concentrations (<1-wt %) and they do not influence the thermodynamics of hydrate formation [127]. However, these kinetic hydrate inhibitors dissipate hydrate particles as they generate such as special surfactants or some of them suspend hydrate formation for more chronological inking by prolonging the induction time for hydrate generation [128]. KHIs are generally water-soluble polymers. However, there are a number of non-polymeric hydrate crystal growth inhibitions that are poor anti-nucleates (e.g. $C_{20}H_{44}BrN$, $C_6H_{14}O_2$). KHIs allow transportation of hydrate forming fluids for specific chronological limits up to hydrates commence to form. The chronological limit to the generation of the first hydrate crystals is called induction time [129,130]. A wide range of Operating Expenses savings, possible extended field lifetime and multi-million-dollar Capital Expenditures savings, are financial leaders for selecting LDHIs as a substitute of other hydrate impeding practices [131].

Good performance of KHIs has been noticed for different fluid systems such as gas, condensate and black oil [132,133]. In case it was necessary for actual multiphase reservoir fluid in oil and gas pipelines, salts could be added to make saline solutions and heptane or decane could be added as a liquid hydrocarbon phase [134-136]. Apart from multiphase applications, KHIs are also used during drilling while compromised to the drilling fluid [137,138]. Porous media such as silica sand have also been tested. Interstitial pores can be very different from that in the usual liquid gas hydrate system in the hydrate formation dissociation conduct. Kelland in 2014 presented a comprehensive research on gas hydrate control with special target on synthesis, chemistry and laboratory performances on new KHIs. On the other hand the industrial research has been completed by Klomp [139,140].

Apart from chemistry of KHIs, many researchers targeted the tools and the processes for experimental KHIs in natural gas hydrate systems the previous years. KHIs inhibition based on both experimental and computational data are: Antifreeze proteins (AFPs) [141-143], Ionic Liquids (ILs) [144,145], Tetrahydrofuran (THF) or cyclopentane hydrate systems [146-149], Recycling [150] or removal [151] of KHIs for future field applications. For upstream applications implemented three different KHIs polymer groups such as Poly (N-vinyl lactam) polymers [152-158], hyper-branched poly (ester amide) [159,160] and N-Isopropylmethacrylamide [161] (IPMA) polymers and copolymers.

Other polymeric KHIs that have been tested contain pyroglutamate polymers, maleic copolymers and alkyl amide derivatives [163,164], polyalkyloxazolines [165], polymaleimides [166], polyallylamides [167], polyaspartamides [168,169] modified starch, starch derivatives and proteins. Recently, sodium chloride, an inorganic and well-known THI, was mentioned to possess kinetic inhibition properties toward hydrate formation in porous media. Nevertheless, it seems to only slow the growth rate of hydrate formation and has no influence on the induction time [170].

In late years, amino acids play important role as kinetic inhibitors but still in the lab environment. Hydrophobic amino acids such as glycine, L-alanine, and L-valine to be applied as thermodynamic hydrate inhibitors (THIs) [171]. L-serine, L-proline, asparagine, L-threonine, L-valine, L-histidine, glycine, alanine, serine, proline, arginine, L-leucine, L-tryptophan, Lysine, valine, methionine, phenylalanine, alanine, serine, glycine+ethylene glycol and glycine+1-ethyl-3-methylimidazolium chloride have also been used as inhibitors for methane gas hydrates [172]. Other amino acids that have been used for CO₂ hydrate inhibition are L-phenylalanine, L-cysteine, L-methionine L-threonine, proline, glycine, threonine, glutamine, histidine, alanine, arginine, L-methionine, L-norvaline, L-norleucine, 2 amino heptanoic acid, n-hexylamine, lysine, phenylalanine, methionine, Cysteine, isoleucine, aspartic acid, asparagine, histidine, L-histidine, PVP and L-Tyrosine [173,174].

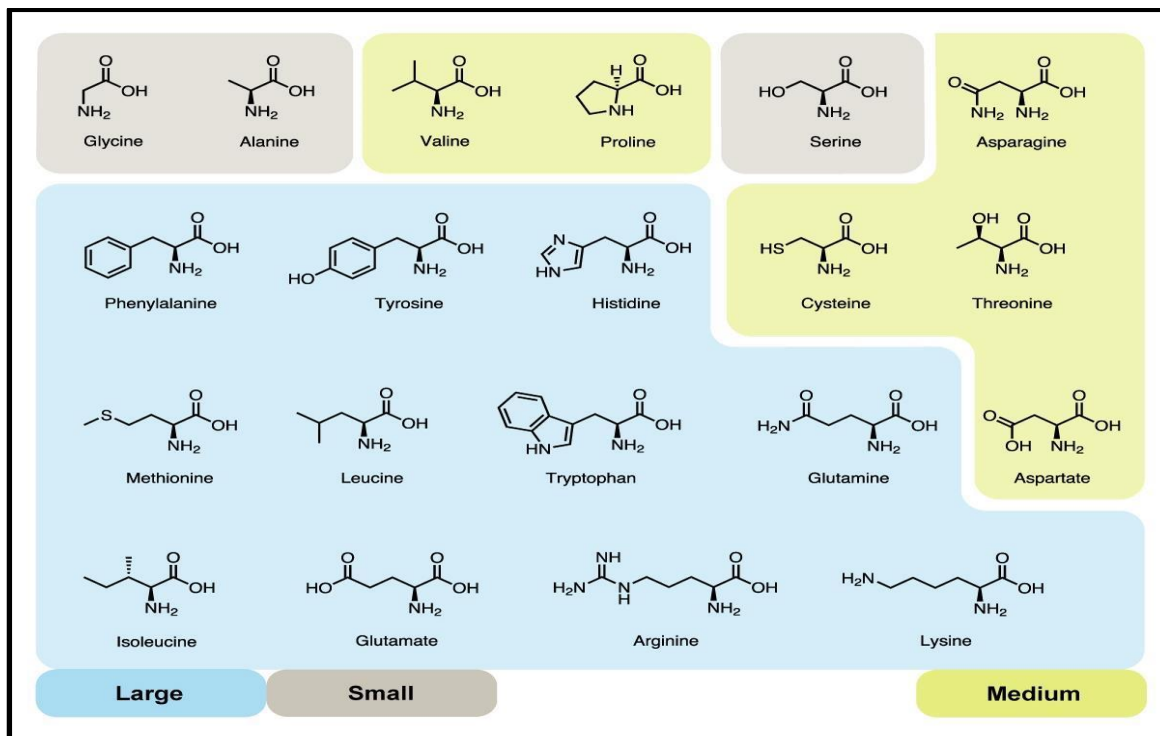


Figure 3.4 Structures of amino acids [175].

In field applications, there were enough examples that the use of kinetic inhibitors leading to positive outcomes such as in GoM in 1990 [176] and the other in Peru in 1995 [177,178]. In both occasions [VIMA/VCAP] was injected to audit hydrates.

3.3 Anti-agglomerates

Anti-agglomerates low dosage inhibitor (LDHI's) confers to researchers and companies an additional tool for checking the formation of hydrates in their systems. Unlike the kinetic and thermodynamic inhibitors, anti-agglomerates LDHI's inhibit hydrate plugging rather than hydrate formation. Anti-agglomerates permit hydrates to form but retain the particles small and well dissipated. In other words, AAs have a hydrophilic head and a hydrophobic tail [179]. According to Koh et al. in 2002, AAs were described as emulsifying agents, which suspend hydrate crystals in condensate because the ends of AA molecules have qualities attractive to both hydrates and oil [180]. The amount of

AA required for hydrate blockage impeding is almost only a fraction of the THI dosage and therefore AA does not appreciably shift the hydrate thermodynamic equilibrium curve of the system. Due to the mechanisms by which AA works, its felicitous application requests the presence of hydrocarbon phase [181]. AAs as chemicals are polymers and surfactants which are added at low concentrations (<1 wt %). The first try to control the hydrates by the use of surfactants was by Yuliev in 1972 before any other relevant work has been published [182]. In the last years of 1980 and the early years of 1990, Institute Francais du Petrole (I.F.P) made experiments with many surfactants but only some of them were for commercial use. Some of the chemicals were ethoxylated sorbitan monolaurate, ethylene diamine based block PO-EO copolymers, polymers of isobutylene succinate diester of monomethylpolthylene glycol which could behave as anti-agglomerates [183].

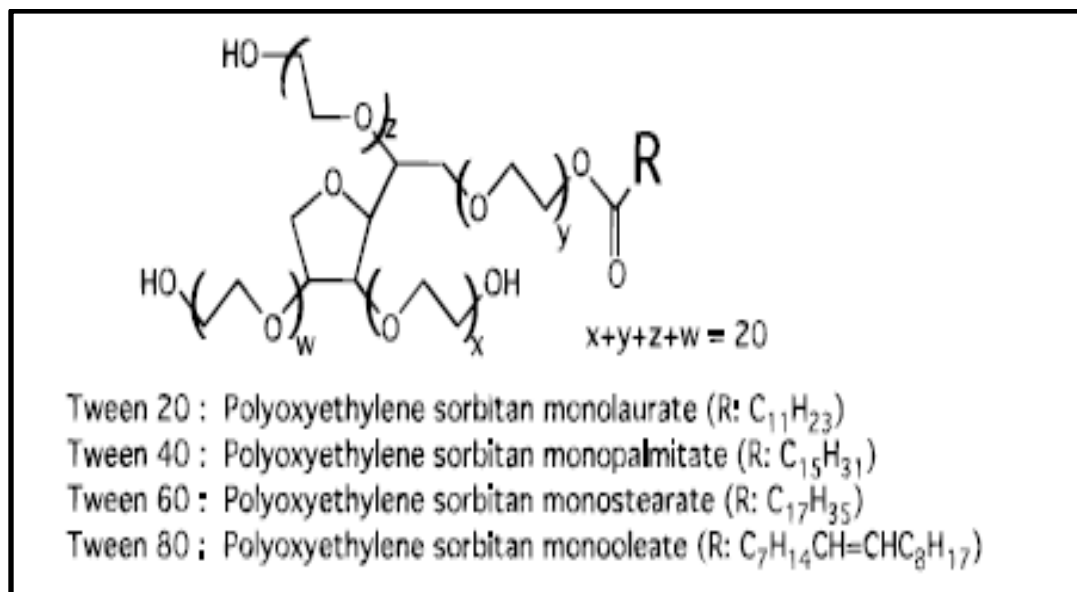


Figure 3.5 Structure of the ethoxylated sorbitan tween surfactants. The EO groups are randomly distributed over the four available sites [184]

Apart from I.F.P, Shell has also patented some other classes of surfactants. These include alkyl aromatic sulphonates (Dobanax series) and alkyl polyglycosides (Dobanol). Stat Oil, SINTEF and NTH had published work on surfactants containing alkyl phenylethoxy lates. One of these, Berol 26 showed logical outcomes in the high-

pressure wheel, but the concentrations used were very high (up to 7 wt. %). Sodium dodecyl sulphate (SDS), some polyacrylamides and tyrosine gave not desirable outcomes [185]. More specifically Exxon presented a formal request for two patents in 1994 about surfactants with hydrophobic tail of 12 carbons or less as AAs [199] and in 1995 covered their use as synergists with KHI polymers [186]. The surfactants that were used by their own in the THF ball-stop rig and they had desirably performance contained $C_4H_9O_4$, $C_5H_9NaO_2$, zwitterionics such as butyl-dimethyl ammonium butylene sulfonate and $C_{16}H_{31}NO$. When they also used together with alkyl amide polymer KHIs, they gave desirably outcomes [187].

BJ Unichem Chemical Services found that polyether polyamines and polyether diamines lowered the blocking temperature or gave a longer time to blocking than a test with no additives [188]. BJ Unichem also patented quaternized polyether polyamines by reaction of polyamines with long chain alkyl bromide. These products behaved better in the THF hydrates [189]. At least four field applications have been reported in gas wells. It is difficult to categorize BJ's products or indeed understand the mechanism for their action [190]. Gao tested hydrate formation with an anti-agglomerate hydrate inhibitor and methanol, which was conducted on rocking cell apparatus to investigate the feasibility, and the strategy for managing gas hydrates at high water cuts with AA. Outcomes showed that brine salinity plays important role in hydrate management at water cuts with AA. A minor raise in salinity causes a step change in AA performance. It was also noticed that the addition of a small dosage of AA could considerably retrench the amount of methanol required for hydrate blockage anticipation; in case AA reaches, its water cut limitation. Outcomes declared that sub cooling is not an accurate term in depicting the inconvenience of treating hydrate problems with AA technology [191].

Swanson et al. [192] studied the implementation of LDIHs in Gulf of Mexico. All kind of inhibitors were used such methanol (THI), two anti-agglomerates and at the end kinetic inhibitors. The anti-agglomerates behaved successfully until the water cut increased to 50% so there was the necessity for the kinetic inhibitors. According to field

data, there was a thorough analysis of benefits and drawbacks for both anti-agglomerates and kinetic inhibitors. Table 3.1 shows the analysis of LDIHs [192]

Table 3.1 Comparison between KHIs and AAs for Gulf of Mexico Field [192]

KHI Advantages	More compatible with changing water cut	Reduced Emulsion	Acceptable environmental impact
KHI Drawbacks	Sensitive to brine salinity with respect to solubility	Higher doe rate than AAs	Limited sub cooling possible
AA Advantages	Longer shut in times	Better Solubility in highly saline brines	Higher sub cooling
AA Drawbacks	Obligatory presence of h/c liquid	Typically limited to water cuts of 50% or less	Environmental concerns

3.4 Hydrate Promoters

Surfactants can also play the role of kinetic promoters. Kalogerakis et. al was the first that investigated the performance of surfactants in methane hydrate formation without any influence in the thermodynamics [193]. Anionic surfactants that have been used to promote methane hydrates are LABS, DBSA, SDSN), LDS, SO, SHS), SDBS, STS, sand other sodium alkyl sulfates like sodium butyl sulfate [194-198]. Cationic surfactants that play the role of promoter in methane hydrates are DAH, HTABr, CTAB, DN₂Cl while ENP, tergitol have also been tested successfully as methane hydrate promoters [199-203]. Another group of chemicals that are used as hydrate promoters are amino acids. Hydrophobic amino acids such as glycine, L-alanine, and L-valine to be applied as thermodynamic hydrate inhibitors (THIs) [204]. L-serine , L-proline, asparagine, L-threonine, L-valine, L-histidine, glycine, alanine, serine, proline, arginine, L-leucine, L-tryptophan, Lysine, valine, methionine, phenylalanine, alanine, serine, glysine+ethylene glycol and glysine+1-ethyl-3-methy limidazolium chloride have also been used as inhibitors for methane gas hydrates [205]. Other amino acids that have

been used for CO₂ hydrate inhibition are L-phenylalanine, L-cysteine, L-methionine L-threonine, proline, glycine, threonine, glutamine, histidine, alanine, arginine, L-methionine, L-norvaline, L-norleucine, 2 amino heptanoic acid, n-hexylamine, lysine , phenylalanine, methionine, Cysteine, isoleucine, aspartic acid, asparagine, histidine, L-histidine, PVP and L-Tyrosine [206,207].

Polymers and starches also have been tested successfully as hydrate promoters. Polymers that have been used for promoting hydrates are soluble hydroxyethyl cellulose [208], poly (2-acrylamido-2-methylpropane sulfonic acid and poly (acrylic acid) [209] and poly vinyl alcohol (PVA) [210]. Starches that successfully functioned as hydrate promoters are potato starch [211], xanthan gum and starch [212], and Maize starch [213].

CHAPTER 4

STATEMENT OF PROBLEM

For decades, oil and gas industry considered natural gas hydrates as nuisance since hydrates have the potential to plug the production lines, pipelines and stop the production which can be resumed by costly operations. After the discovery of natural gas deposits in deep sea but shallow sea bed formations and permafrost regions, oil and gas industry started to study on the production of natural gas from hydrate bearing formations. But, hydrates also exhibit other characteristics which make them as the potential players of some industrial processes.

Owing to their high gas storage capacities (1 m³ solid hydrate can contain 150 – 170 Sm³ of gas) and the long-term stability of hydrate crystal structure at standard refrigeration temperatures and atmospheric pressure, oil industry started to look at the possibility of using hydrates as gas storage and transportation media.

Among several other factors to make the storage and transportation of gas in hydrate form, hydrate formation rate has crucial importance. The faster formation of hydrates in a hydrate forming reactor can play important role on the economics of operation. Good mixing of hydrate forming components (gas and water) can accelerate the formation process. This can partly be achieved by correct selection of tank interiors. Several water soluble chemicals can also be used to alter the hydrate formation rate. This study aims to promote hydrate formation by investigating the effects of impeller – baffle configurations, and use of water soluble chemicals on the rate of hydrate formation. In that respect, two types of impellers (up-pumping pitch blade turbine and Rushton

turbine) were utilized. As baffles, full, half, surface and no baffle alternatives were studied. As water soluble chemicals five different amino acids were tested.

CHAPTER 5

EXPERIMENTAL SET-UP AND PROCEDURE

5.1 Experimental set-up

An experimental set-up designed and constructed to carry out the kinetic studies of hydrate formation. The schematic diagram of the experimental set-up is shown in Figure 5.1. Five main components of the experimental set-up are:

1. Reactor
2. Control Unit
3. Cooler – controller
4. Data acquisition system
5. Cold room

Details of each main component are described in the following paragraphs.

5.1.1 Reactor

Two different stirred-tank reactors, one high-pressure steel reactor and one medium-pressure polymethyl methacrylate reactor, have been designed and built to carry out studies on the scale up of gas hydrate formation. The high-pressure cylindrical AISI 316 L stainless steel reactor has internal dimensions of 150 mm in diameter and 312 mm in length, and total available volume of 5.7 liter. It was designed for working pressures up to 150 bars. Figure 5.2 and Figure 5.3 show different components of the reactor. Those components namely are; pressure transducers, thermocouples, gas injection valve,

cooling water, shaft, baffle, impeller, servo motor and gear mechanism. The functions of each item are as follows:

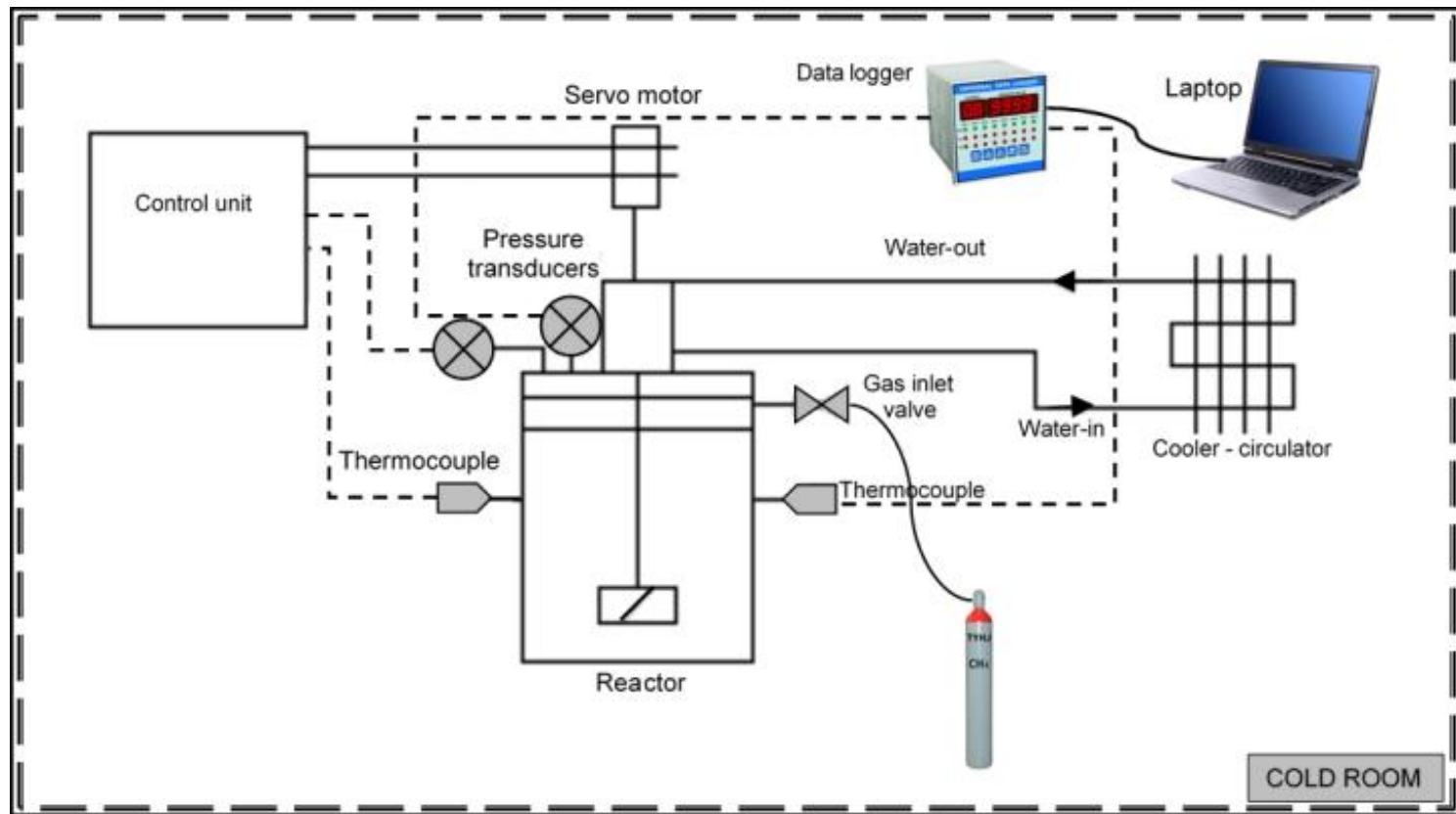


Figure 5.1 Experimental set-up for hydrate formation

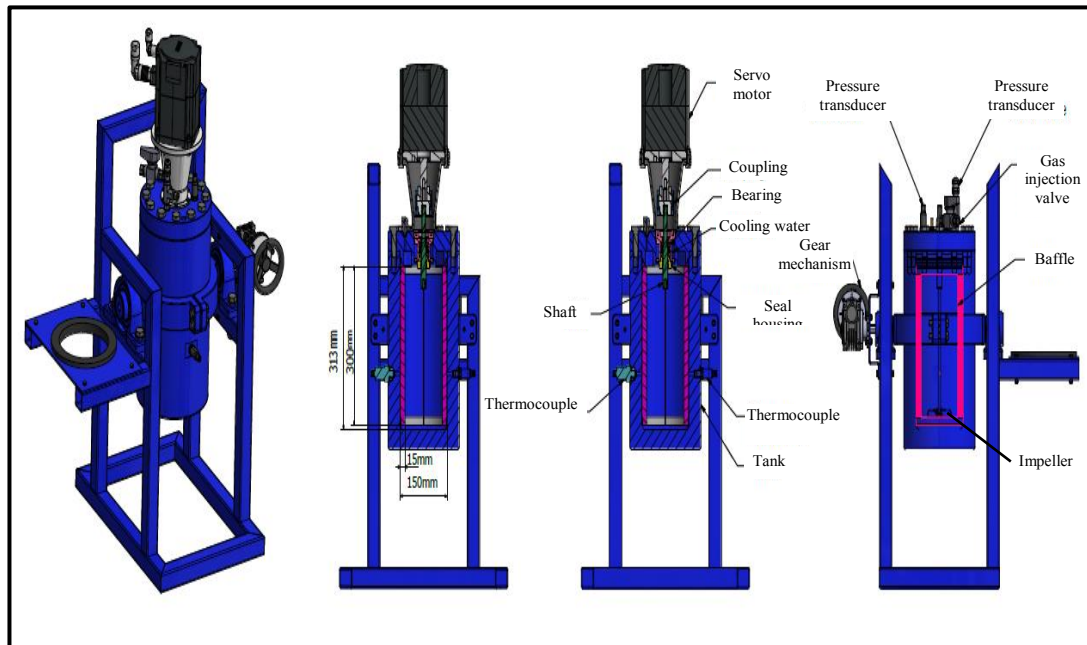


Figure 5.2 High-pressure stainless steel reactor

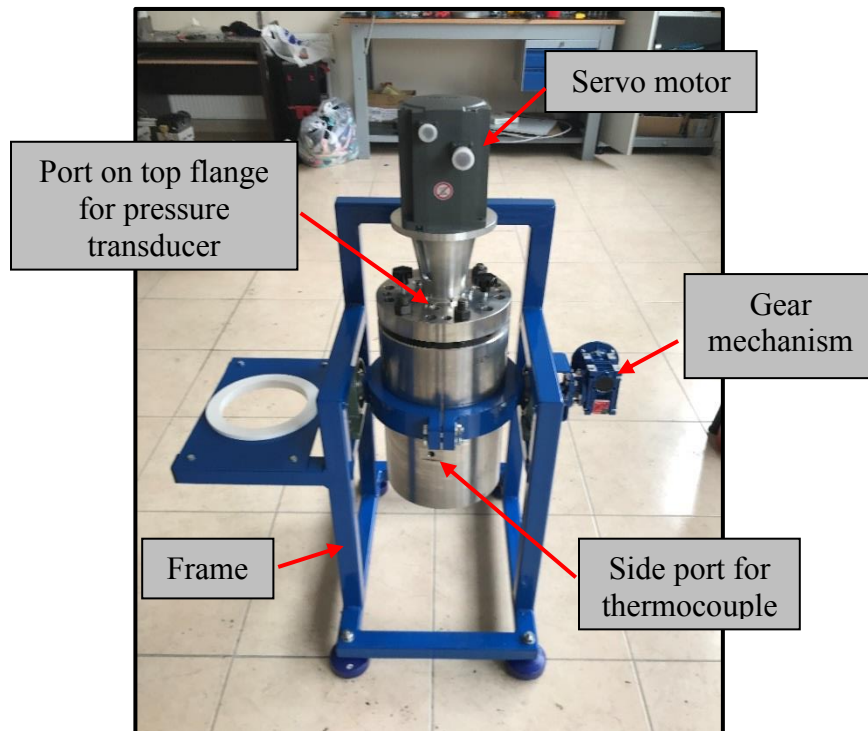


Figure 5.3 Some components of High-pressure stainless steel reactor

Pressure transducers: There are five ports (three on top flange and two on the main body of the reactor) on high-pressure steel reactor to attach the measuring devices and gas injection valve. Two pressure transducers with measuring range of 0 – 100 barg and accuracy of $\pm 0.25\text{FS}$ % are attached to the top flange of the reactor to measure the pressure throughout the hydrate formation tests.

Thermocouples: Two thermocouples, one mineral insulated type TW/T (Threaded Type Thermowells) with accuracy of ± 0.2 % and one Pt100 with accuracy of $\pm 0.25\%$ are attached to the ports at the main body of the reactor to measure the temperature throughout the hydrate formation tests. Those ports are located at a level in the main body that thermocouples are always in contact with liquid.

Gas injection valve: This needle valve is connected to the top flange of reactor to facilitate the gas injection into reactor which already contains distilled water to form hydrate. Gas is supplied from high-pressure gas bottles through pressure a regulator that provides adjustment of the pressure to the gas injection line.

Gear mechanism: The gear mechanism makes it easier to empty and clean the heavy reactor after each experiment. Reactor and gear mechanism are placed on a frame to make the easy handling of reactor.

Servo motor: One of the characteristic components of hydrate formation experiments is the mixing of hydrate forming liquid and gas to maximize the interfacial area between hydrate forming components (gas and liquid), thus minimizing mass transfer barriers. Both reactors that are used in this study are batch reactors equipped with different types of impeller – baffle configurations to provide efficient mixing. Rotation of impeller in this study is achieved by a High Inertia permanent-magnet synchronous motor (Siemens model SIMOTICS S-1FL6). Rotational speed of the motor is kept constant at 500 RPM throughout the study.

Cooling water: Relatively high rotational speed of shaft attached to servo motor created frictional heat at the early trials of experimental study. In order to overcome this

drawback of the system, a cooling water circulation system was added to remove the heat around the shaft.

Shaft, impeller and baffle: Shaft is a hollow pipe made by steel AISI 316L with an inner diameter of 6 mm and was attached to the servo motor. A one mm hole was opened on the shaft at a level close to top of the flange (within gas bearing section of the reactor) to allow the induction of gas through the shaft. A sparger was attached to the tip of the shaft to distribute the induced gas within liquid.

Two different types of impellers, namely Pitch-Blade-Turbine (PBT) and Rushton Turbine (RT) were used. They were made by acrylonitrile butadiene styrene (ABS) plastic and printed by a 3D printer. The effects of type of impellers on hydrate formation was studied with single impeller (SI) or dual impeller (DI) arrangements. In case of single impeller arrangement, the impeller is attached on the shaft to a position just above the sparger to break down the gas bubbles efficiently. This corresponds to a distance of 6.6 cm from the tank bottom. Figure 5.4 and Table 5.1 give the dimensions and position of mixing elements during single impeller experiments. There are four types of impeller arrangements in case of dual impeller experiments, PBT-PBT, RT-RT, PBT-RT and RT-PBT. In the first two arrangements the same type of impellers are used but in the remaining two, which are called as Dual Mixed Impellers (DMI), two different types of impellers are used. Figure 5.5 shows all impeller arrangements used in this study.

The shaft and baffles are made of AISI 304. Baffles are used to provide axial motion and to eliminate vortex formation in the reactor. Three different baffles were used in this study. These are named as Full-Baffle (FB), Half-Baffle (HB) and Surface-Baffle (SB) (Figure 5.6). Figure 5.7 shows the placement of baffles as reference to gas-liquid interface. Finally, Figure 5.8 shows the height of gas-liquid interface for single and dual impeller experiments as well as the placement distance of baffles with respect to this interface. As seen, the gas-liquid interface is at 150 mm for single impeller experiments and 225 mm for dual impellers from the bottom of reactor (NB stands for No-Baffle).

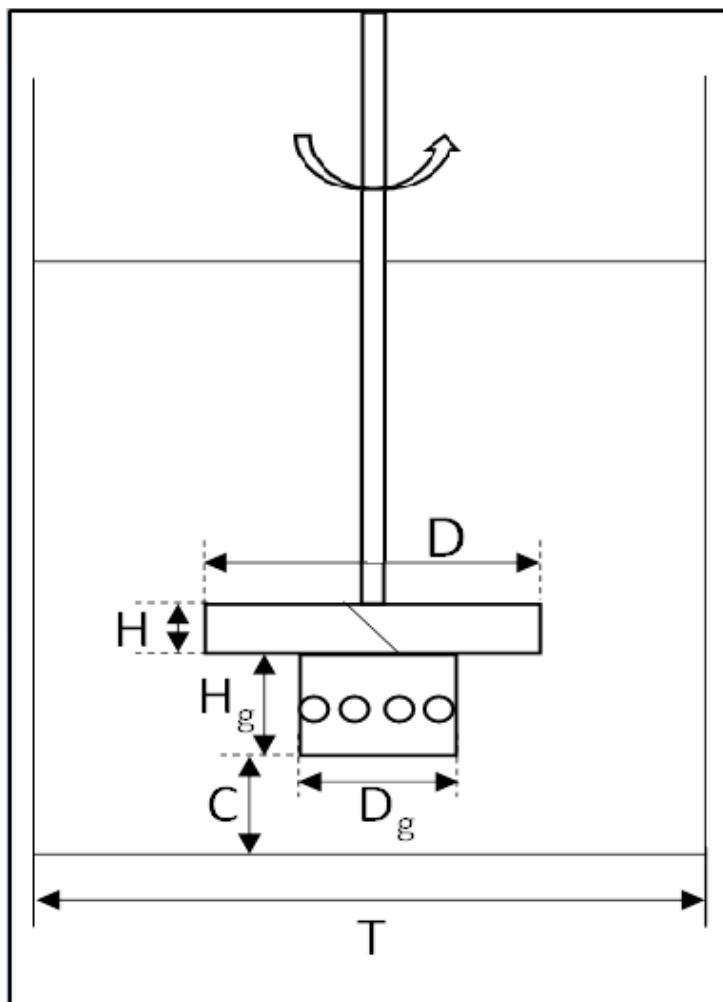


Figure 5.4 Dimensions and position of mixing elements for PBT impeller

Table 5.1 Dimensions and positions of mixing elements during single impeller experiments of steel reactor

Symbol	Explanation	Length (cm)
T	Internal diameter of reactor	15.0
D	Diameter of impeller	7.5
D_g	Sparger diameter	3.5
H	Thickness of impeller	1.0
H_g	Thickness of sparger	2.6
C	Distance of sparger from the bottom of reactor	4.0

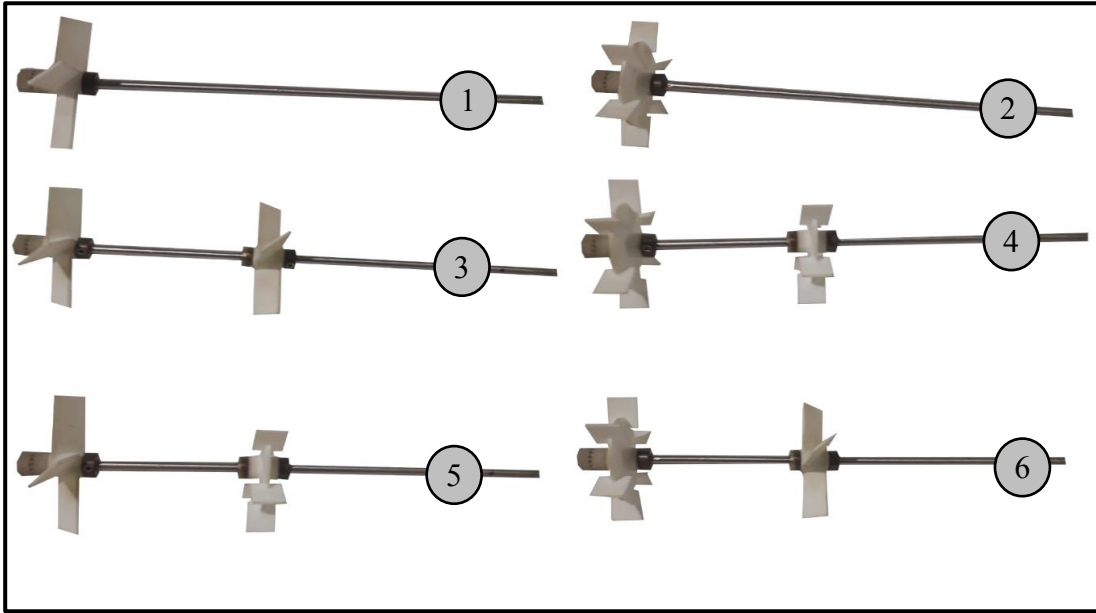


Figure 5.5 Different impeller arrangements

1: SI-PBT, 2: SI-RT, 3: DI-PBT-PBT, 4: DI-RT-RT, 5: DMI-PBT-RT, 6: DMI-RT-PBT



Figure 5.6 Types of baffles used in this study, Left: FB, Middle: HB, Right: SB

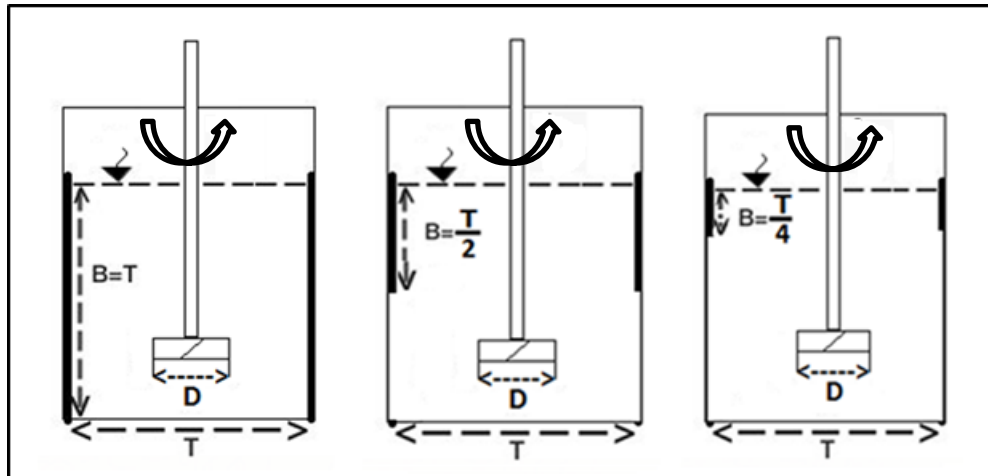


Figure 5.7 Placement of baffles. Left: FB, Middle: HB and Right: SB

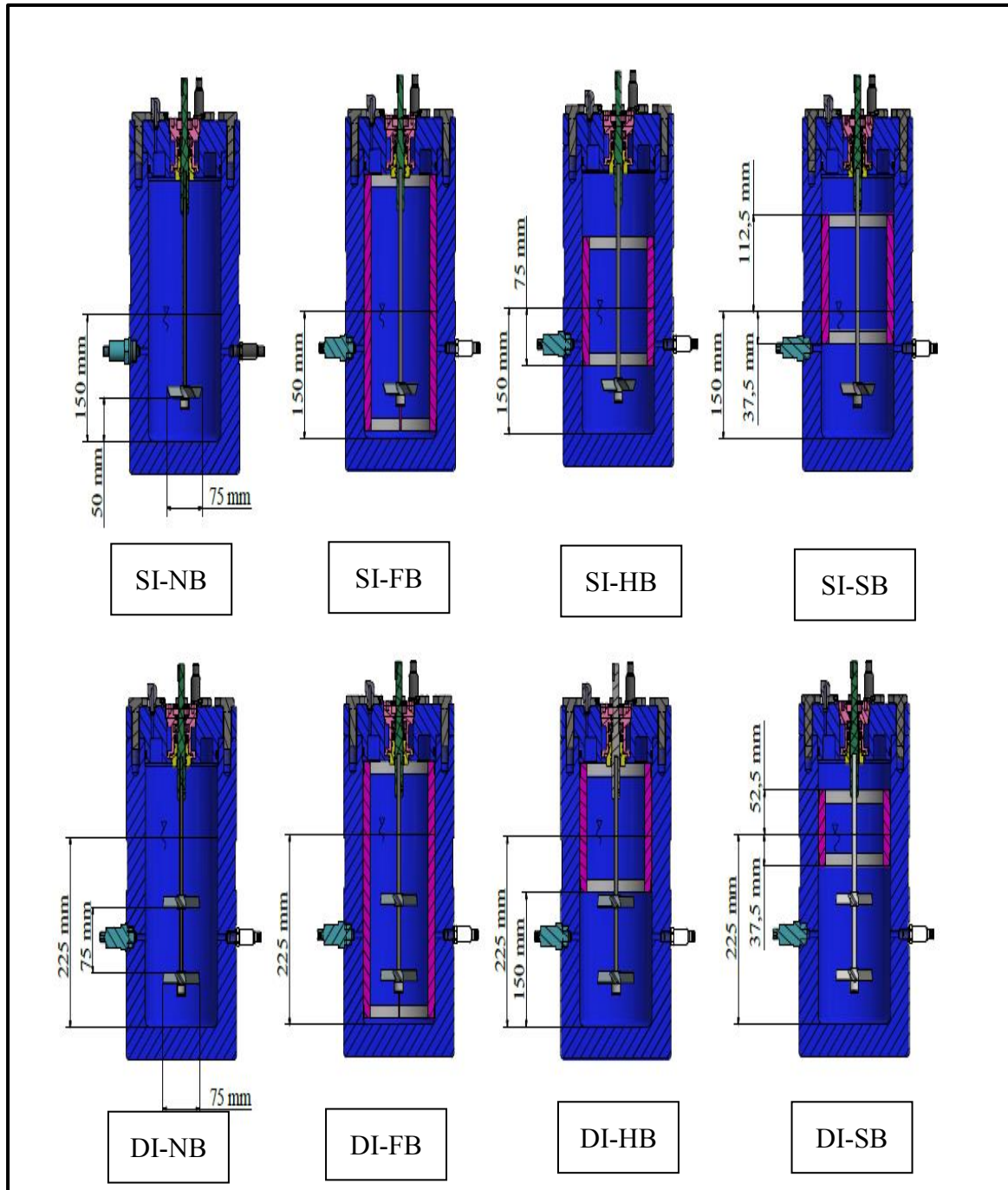


Figure 5.8 Types of impellers used in this study,
 Upper row: PBT-SI, Lower row: PBT-DI

As mentioned earlier, a second reactor – a transparent one – was designed and built to carry out some of the experiments of gas hydrate formation (Figure 5.9). The main body of the reactor is made of polymethyl methacrylate (PMMA) with internal dimensions of 80 mm in diameter and 310 mm in length, and total available volume of 1.56 liter. It was designed for working pressures up to 30 bars. There are two steel (AISI 316L) outer circular disks which are mounted in the main body of the reactor where there are 4 inlets for the pressure transducers and thermocouples. The top and bottom flanges are serving as servo motor receptacle and as the base of the reactor, respectively. Flanges and discs are mounted with 8 steel studs, hence to function as the frame of the main body (Figure 10). Transparent nature of this reactor made it possible to make eye observations and video recording during hydrate formation. All other elements of transparent reactor are the same of high-pressure steel reactor except impellers and baffles. Only single impellers of PBTU and RT are used with 40 mm in diameter and no baffles are used (Figure 5.11). Table 5.2 give the dimensions elements of transparent reactor.

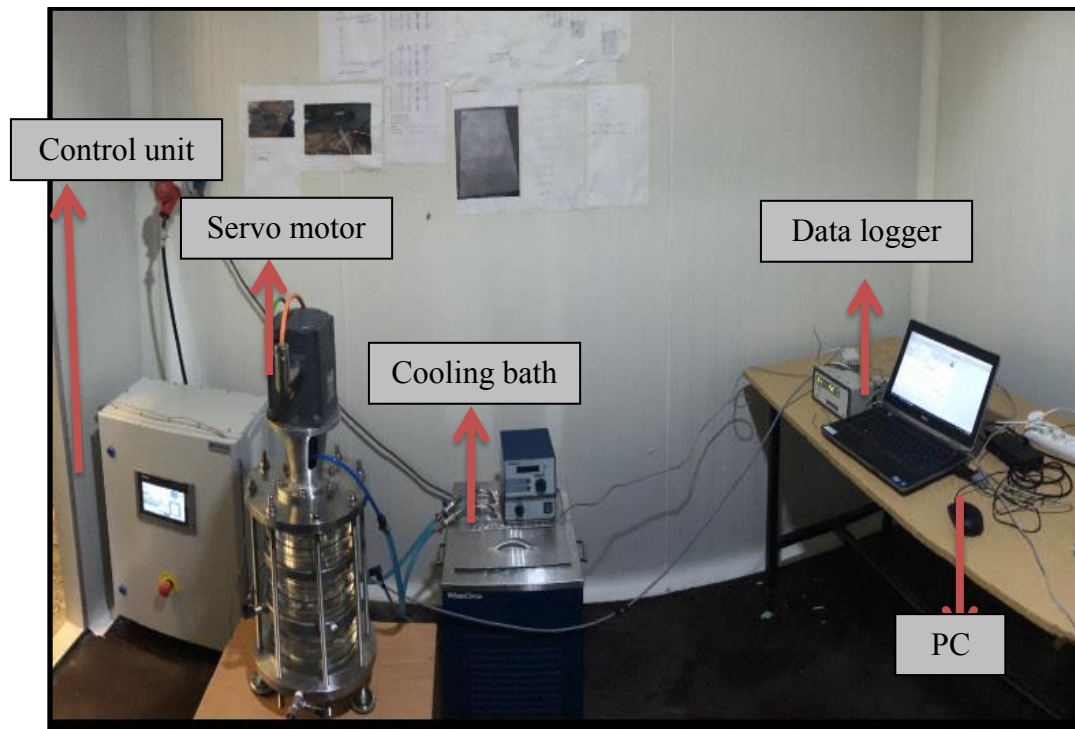


Figure 5.9 Experimental setup of transparent reactor



Figure 5.10 Transparent reactor

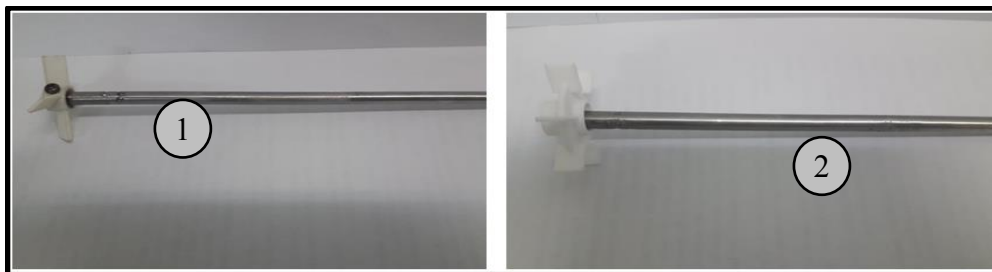


Figure 5.11 Single impeller for transparent reactor
1: PBT, 2: RT

Table 5.2 Dimensions and positions of mixing elements during single impeller experiments of transparent reactor

Symbol	Explanation	Length (cm)
T	Internal diameter of reactor	8.0
D	Diameter of impeller	4.0
H	Height of transparent reactor	30.0
H _g	Thickness of impeller	0.2
C	Distance of impeller from the bottom of the reactor	5.0

5.1.2 Control unit

This unit is mainly used to control the servo motor. This PLC unit has the capabilities to start / stop servo motor, set the duration, direction (clockwise or counter clockwise) and speed (RPM) of mixing. In addition, one of the pressure transducers and thermocouples are connected to this unit to record the data at every second. Finally, the voltage output of servo motor is converted to torque and recorded at every second.

5.1.3 Cooler – circulator

As mentioned earlier, rotation of shaft created heat due to friction which can retard / stop hydrate formation. In order to remove this heat, cooling water is circulated around the bearing of the shaft by a special design. A Refrigerated Cooling Bath is utilized to circulate anti-freeze added cooling water (2 °C) with a flow rate of 12L/min.

5.1.4 Data acquisition system

As explained in Reactor subsection, there are two pressure transducers and two thermocouples to measure the pressure and temperature during hydrate formation. While control unit is recording one pressure and one thermocouple, others are connected to a second data logger and laptop to record the data. This is actually a back-up to minimize the risk to lose the data. The data logger model is Elimko: E-680-08-2-0-00-1-0.

5.1.5 Cold room

One of the characteristics of hydrate formation experiments is cooling since hydrate forms at low temperatures. Cooling requirement is achieved by a cold room having dimensions of 3 x 3 x 2.5 m. Working range of the room are -5 °C - +10 °C.

5.2 Experimental procedure

Pure methane (99.995 % - Hat Grup Company, Kocaeli-Turkey) and methane – propane mixture (95 % methane and 5 % propane – Hat Grup Company, Kocaeli-Turkey) were used to form hydrates either at high-pressure steel reactor or medium-pressure PMMA reactor. Distilled water is the liquid phase to form hydrate. In addition, the hydrate formation kinetics of the aqueous phases containing amino acids was studied experimentally. In that respect, depending on the type of gas and aqueous phase different experimental procedures were applied.

5.2.1 High-pressure steel reactor – methane

The following procedure has been applied during the course of 24 experiments where high-pressure steel reactor was used to form methane hydrate with distilled water.

- Turn on cooling unit to adjust the room temperature to 10 °C.
- Put distilled water (2.65 liter for single impeller or 3.8 liter for dual impeller experiments) while the top lid of the reactor is open.
- Insert the selected baffle and adjust the height of it with respect to gas – liquid interface.
- Connect the selected impeller(s) to the shaft then close the top lid and make necessary connections for data recording and gas injection. Start data recording.
- Inject methane into reactor via gas injection valve and adjust the reactor pressure to 46 ± 0.2 bar-g.
- Then, after closing the gas injection line set the cooling unit temperature to – 5 °C to start the cooling of cold room.

- Continuously observe the reactor pressure and temperature until reactor temperature is about 2 ± 0.2 °C.
- At this point reset the cooling unit temperature to 0 °C and start servo motor with a rotational speed of 500 RPM for a period of 10 hours.
- Hydrate formation generally starts within few minutes after the start of rotation. But, in some cases, depending on impeller – baffle configuration, it may take hours (induction time). Keeping this fact in mind, the reactor pressure and temperature trends are observed carefully. A change in the pressure decline rate (an increase in rate) and a sharp increase in temperature indicate the initiation of hydrate formation. Record this time and keep rotation 3 hours more, then stop rotation.
- Transfer the recorded data from two data logging units and release the pressure to prepare the system for the next experiment.

Figure 5.12 shows the pressure – temperature traverse during hydrate formation process with a reference line showing the methane hydrate equilibrium. Hydrate equilibrium line is obtained from CSMHYD (Research Center for Hydrates, Chemical Engineering Department, Colorado School of Mines). The decrease in pressure from initial condition to start of rotation is due to cooling and dissolution of gas in water. On the other, the change in pressure and temperature after rotation is due to formation of hydrate which is an exothermic reaction with consumption of gas into solid phase.

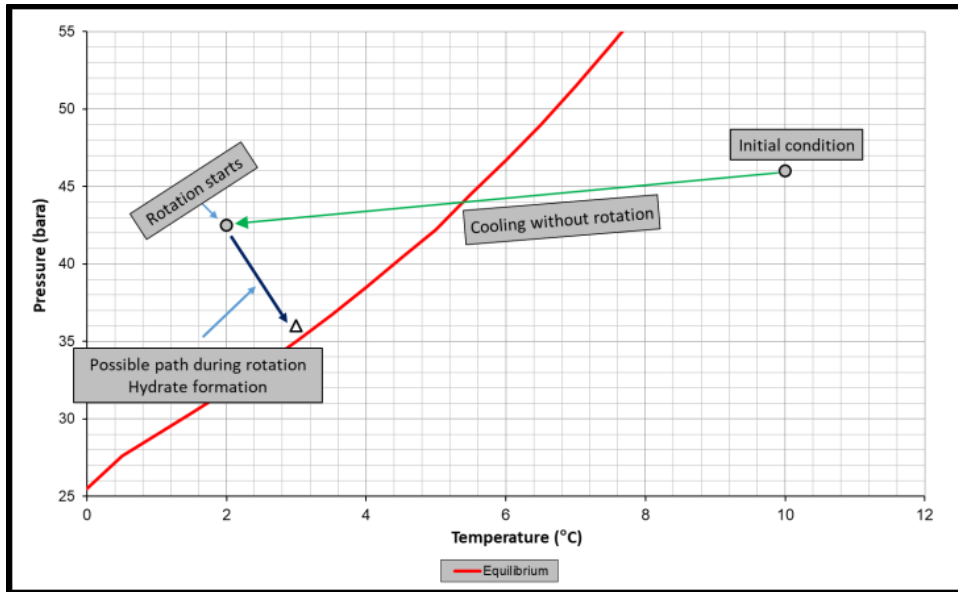


Figure 5.12 Experimental conditions of methane experiments

5.2.2 High-pressure steel reactor – methane propane mixture

Sixteen hydrate formation experiments (8 with single impellers, 8 with dual impellers) were carried out with the use of gas mixture to form hydrates. The experimental procedure of mixture gas experiments is almost the same of methane experiments except the differences given below.

- The first difference is the initial conditions at which the mixture gas was injected into the reactor. Since methane – propane mixture forms hydrate at a lower pressure compared to methane at the given temperature, the initial pressure was lowered from 46 ± 0.2 bar-g to 26 ± 0.2 bar-g at $13\text{ }^{\circ}\text{C}$. Therefore the first step of the experiment was adjusting the cold room temperature to $13\text{ }^{\circ}\text{C}$ by the help of cooling unit.
- The other difference was the temperature at which the rotation was started. It is known from literature that use of gas mixtures to form hydrates results with difference in fractionation of mixture components in gas phase and hydrate phase. This fractionation actually results with the change in equilibrium

conditions since one of the components of gas phase is spent more in hydrate formation than the other component. In order to test this phenomenon some of the gas mixture hydrates formation carried out at a higher temperature (8 °C) while the rest had the same temperature of methane experiments (2 °C). Figure 5.13 shows the experimental conditions of gas mixture hydrate formations.

- At the end of each hydrate formation experiment of gas mixture the composition of free gas was determined by taking gas samples in sampling tubes (Figure 5.14) aiming to quantify the fractionation of gas components. Gas composition analyses were carried out at Petroleum Research Center Gas Analysis Laboratory by using Agilent 6890 series GC (Figure 5.15).

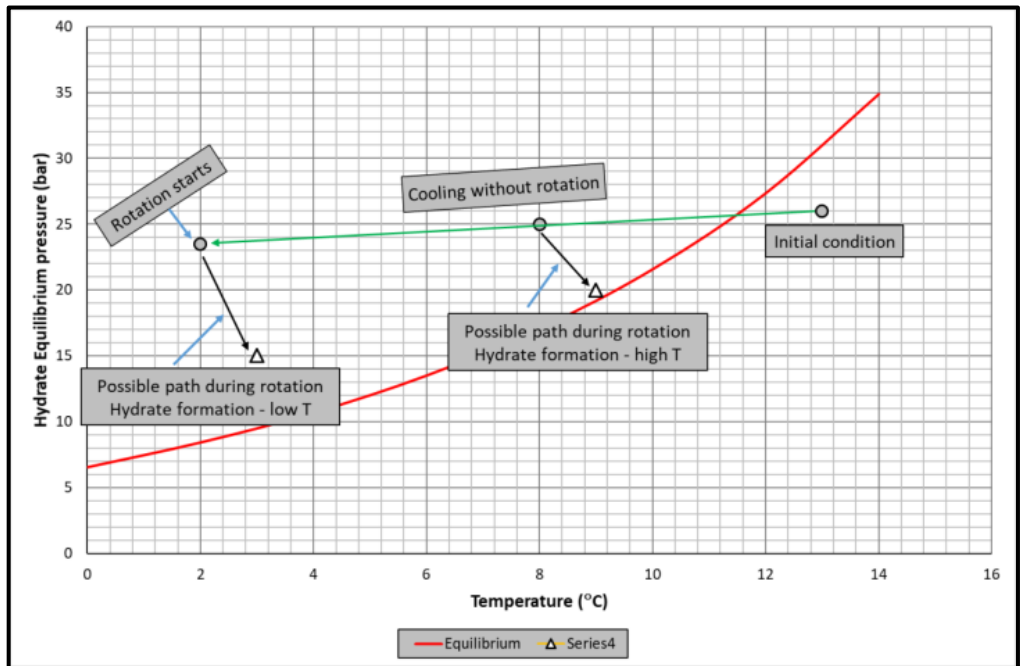


Figure 5.13 Experimental conditions of gas mixture experiments



Figure 5.14 Steel tubes for gas sampling

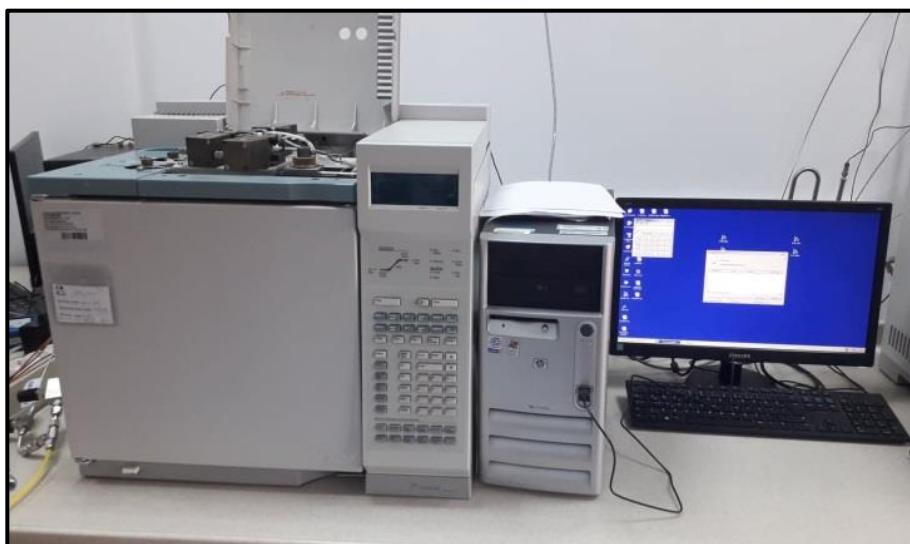


Figure 5.15 Agilent system 6890 series GC for gas analysis

5.2.3 Medium-pressure PMMA reactor – methane propane mixture

The last part of the study aims to see the effect of some selected amino acids on natural gas hydrate formation. In that respect, the following 5 different amino acids from EMD Milipore Co. were added to hydrate forming water at certain concentrations.

- L-Lysine monochloride,
- L-Serine,
- L-Histidine monohydrochloride monohydrate,
- L-Leucine and
- L-Alanine.

The initial pressure and the temperature for these experiments were 24 bar-g and 2 °C while the water in transparent reactor was 300 cm³. The experimental procedure was the same of methane and methane-propane hydrate formation experiments with the advantage of eye observation.

CHAPTER 6

RESULTS AND DISCUSSION OF METHANE HYDRATE FORMATION

As mentioned in Chapter 5, pure methane and methane – propane mixture (95 % methane and 5 % propane) hydrates are formed either at high-pressure steel reactor or medium-pressure PMMA reactor. In addition, some amino acids are tested on their promotion potential for hydrate formation. Experimental procedure for those tests was already given in Chapter 5. This chapter is dedicated on the discussion of experimental findings of methane hydrate formation.

At first, the raw data of a selected test will be presented as the sample of all experimental raw data, and then the raw data of all other tests will be given in Appendix A.

Later, again the same set of data is utilized to describe how the experimental data is interpreted to study the kinetics of hydrate formation.

Then, results of pure methane hydrate formation experiments are discussed, in detail.

6.1 Presentation of raw data

Pressure and temperature within the hydrate formation reactor and the torques during rotation of impellers are the three parameters recorded during any hydrate formation test. Those raw data are presented in three figures:

1. Pressure and temperature vs. time (Figure 6.1)
2. Pressure and torque vs. time (Figure 6.2)
3. Pressure vs. time with a reference line of hydrate equilibrium of hydrate forming gas (Figure 6.3)

Figures 6.1, 6.2 and 6.3 are showing the experimental data of hydrate formation test with following conditions:

- Hydrate forming gas: Methane (CH₄)
- Number of impeller: Single impeller (SI)
- Type of impeller: Pitched –Blade Turbine (PBT)
- Type of baffle: Full (FB)
- Rotational speed: 500 RPM (500)

Each experiment will have a coding based on those parameters. As an example, the coding of this experiment is **CH4-SI-PBT-FB**.

The whole raw data of a given hydrate formation experiment has three distinct intervals as indicated in Figure 6.1.

1. After preparing the system to run a hydrate formation test, cooling is started without rotating the impeller. Decrease in temperature as response of cooling causes a decrease in pressure based on real gas law as well as in the increase of gas solubility. This period ends when temperature reaches to the determined hydrate formation temperature.
2. The second interval is the period in which hydrate formation is achieved. In order to initiate the hydrate formation and keep it continuous, the impeller is rotated at a speed of 500 RPM. The duration of this interval is dependent on the INDUCTION TIME which is known as the starting time of hydrate formation. Figure 6.1 shows that INDUCTION TIME of **CH4-SI-PBT-FB** experiment is almost ZERO and hydrate formation started immediately after the start of rotation. A three-hour rotation after induction time is set a standard for this study. After initiating the hydrate formation, a steep pressure decline is observed as a response of losing the free gas into solid hydrate structure. Another observation

is a slight increase in temperature due to exothermic characteristic of hydrate formation.

3. Three hours after INDUCTION TIME, rotation and cooling are stopped and the system is let to warm up. A longer waiting under these conditions will end of dissociation of hydrate. Since the main focus of this study is to determine the kinetics of hydrate formation, this period is generally kept short. Therefore, many of experiments ended before having a full cycle of hydrate formation – dissociation.

Figure 6.2 shows the pressure – torque data of experiment **CH4-SI-PBT-FB**. Measured torque (N/m) values will be utilized to calculate the overall power consumption during hydrate formation.

The last graph drawn from raw data is the pressure vs. temperature graph (Figure 6.3). The hydrate equilibrium line of hydrate forming gas (methane for **CH4-SI-PBT-FB**) is drawn as a reference to indicate the position of any pressure – temperature pair during experiment. The hydrate equilibrium line of hydrate forming gas/water mixture is obtained from CSMHYD (Sloan, 1990). As indicated in Figure 6.3 the initial condition of experiment is outside the hydrate formation region. Red arrows on the figure show the direction of pressure – temperature change by time. As cooling progresses, pressure – temperature pairs come closer to equilibrium line and at some point it crosses the hydrate equilibrium line. Further cooling without rotation makes the system temperature far inside the hydrate formation region. The difference between the hydrate equilibrium temperature at experimental pressure and experimental temperature is known as SUB-COOLING (black arrow line in the figure). The higher the SUB-COOLING the stronger the driving forces to initiate the hydrate formation. In order to have comparable kinetic data a fixed SUB-COOLING is applied throughout this study.

As hydrate formation progresses, pressure decreases and a slight increase in temperature is observed. The final step is letting the system to warm up after stopping the rotation and cooling to allow hydrate dissociation.

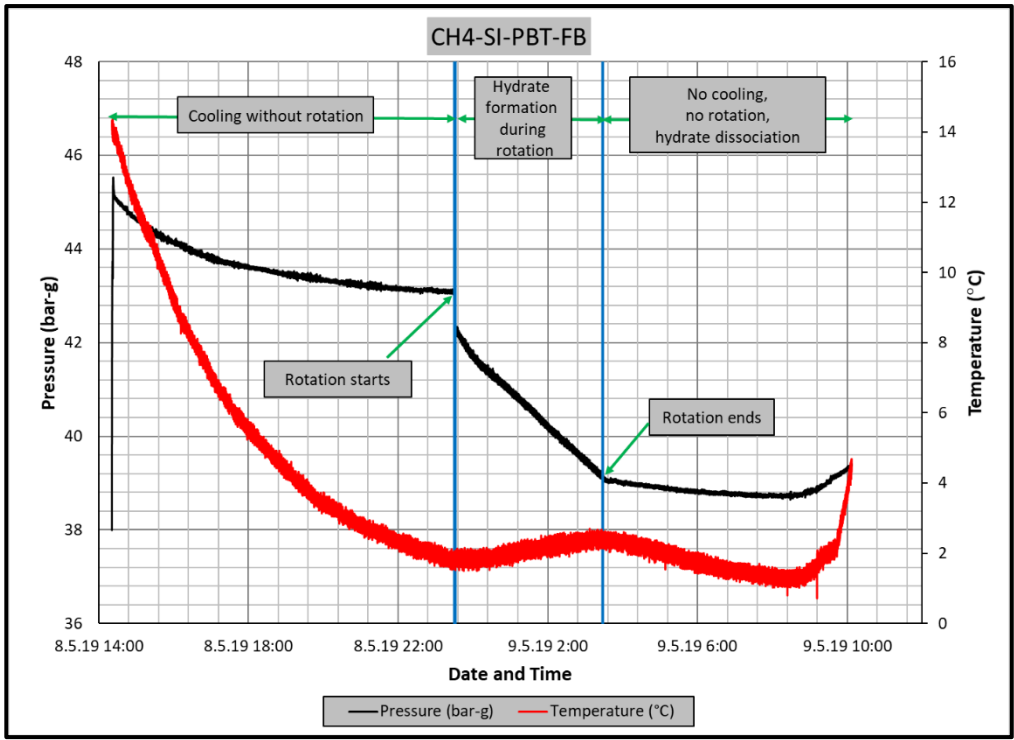


Figure 6.1 Pressure – temperature vs. time graph of hydrate formation experiment

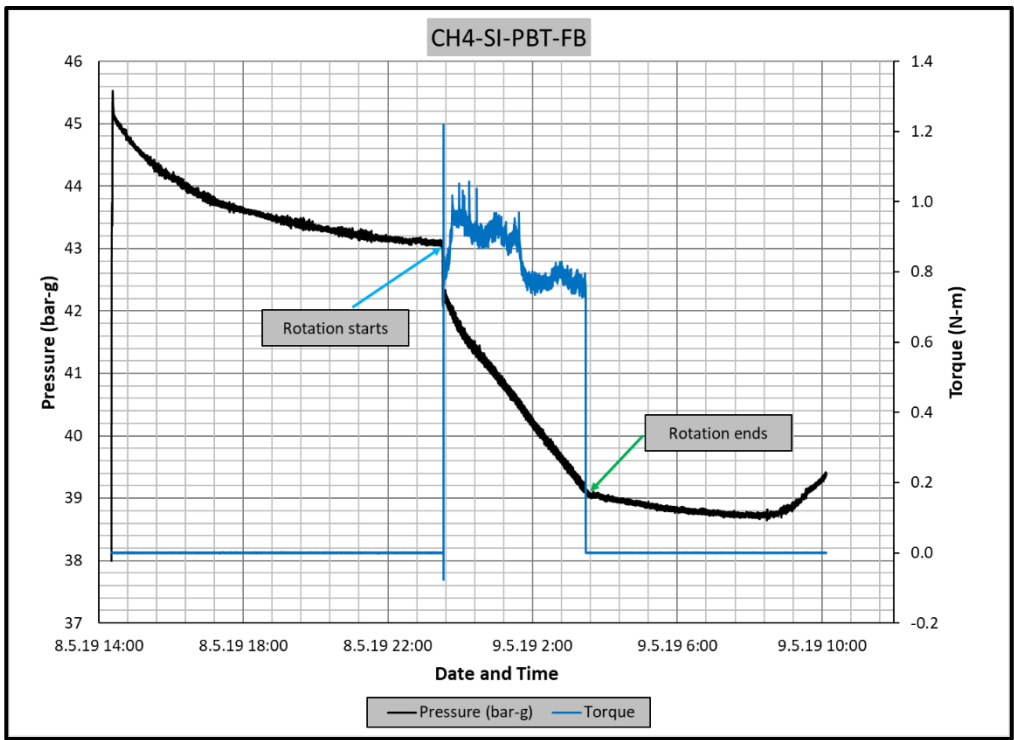


Figure 6.2 Pressure vs. torque graph of hydrate formation experiment

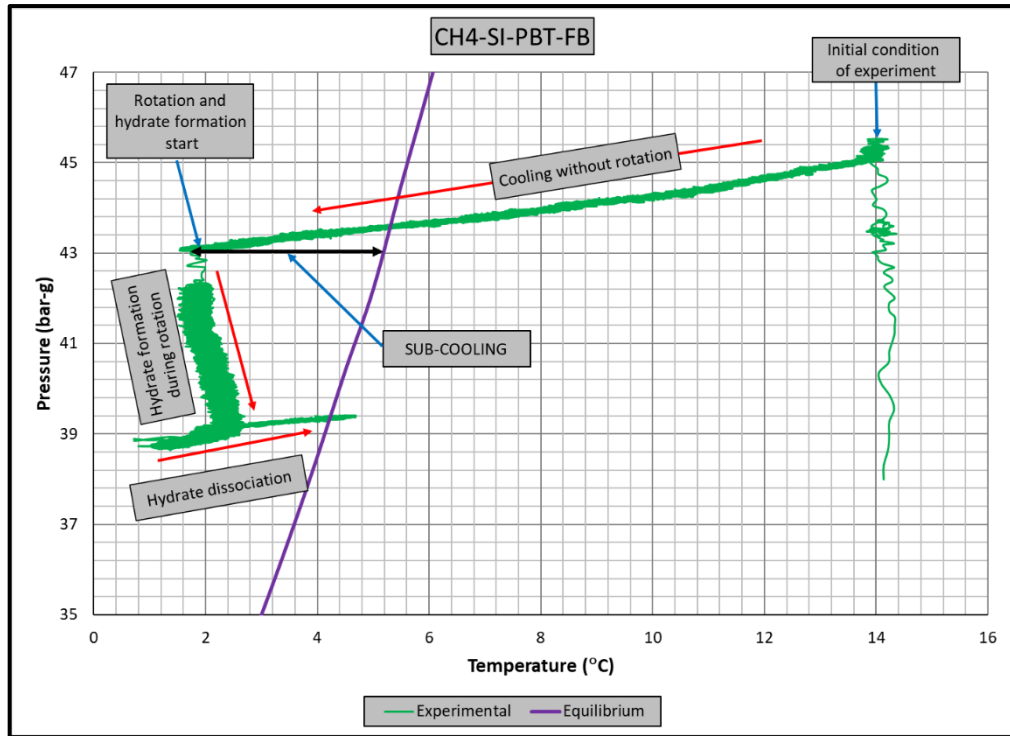


Figure 6.3 Pressure vs. temperature graph of hydrate formation experiment

6.2 Interpretation of experimental data

6.2.1 Gas consumption rate

The main objective of this study is to investigate the effect of different impeller – baffle configurations on hydrate formation kinetics. Therefore, a tool must be devised to extract the kinetic data from raw experimental data. Application of real gas law ($PV = znRT$) for each data point with known pressure, temperature and free gas volume gives the change in number of moles of free gas with time. The gas compressibility factor of the real gas law Z is estimated by using Lee and Kesler's (1975) compressibility factor expression. A sample plot of change in free gas number of moles is given in Figure 6.4 for **CH4-SI-PBT-FB**.

Figure 6.5 is plotted with the same data of Figure 6.4 but covering only hydrate formation period. A third-order polynomial fit of experimental data result with Equation 6.1.

$$n = 1.0295 \times 10^{-15}t^3 + 1.4283 \times 10^{-11}t^2 - 1.3373 \times 10^{-7}t + 1.3441 \times 10^{-2}$$

(Eq. 6.1)

where:

n = Number of moles of free gas, lb-mol

t = Time, sec

The derivative of Equation 6.1 results with the gas consumption rate (Equation 6.2) which can be considered as the hydrate formation rate.

$$\frac{dn}{dt} = 3 \times 1.0295 \times 10^{-15}t^2 + 2 \times 1.4283 \times 10^{-11}t - 1.3373 \times 10^{-7} \quad (\text{Eq. 6.2})$$

where:

$\frac{dn}{dt}$ = Gas consumption rate, lb-mol/sec

t = Time, sec

Comparison of gas consumption rates of different experiments will be done by utilizing gas consumption rate equations (Equation 6.2 is an example) with four different time values, namely 1, 600, 1200 and 1800 seconds. Table 6.1 presents the gas consumption rates of experiment **CH4-SI-PBT-FB**, as an example.

Table 6.1 Gas consumption rates of experiment **CH4-SI-PBT-FB**

Time (sec)	1	600	1200	1800
Gas consumption rate (lb-mole/sec)	-1.34E-07	-1.15E-07	-9.50E-08	-7.23E-08

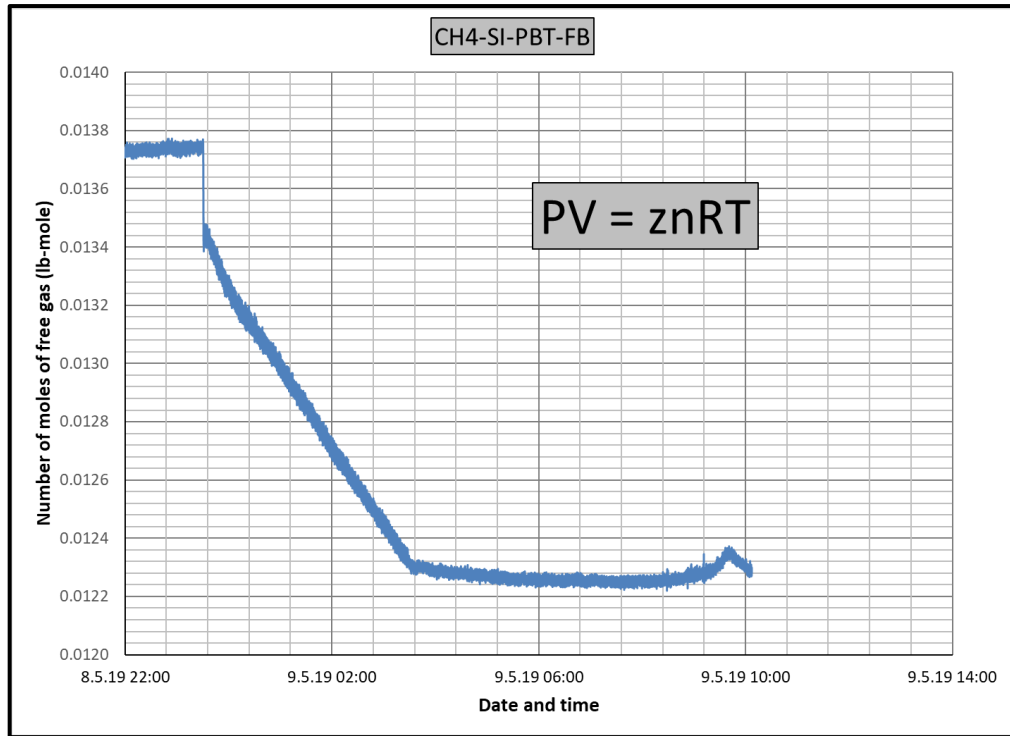


Figure 6.4 Calculated number of moles of free gas during hydrate formation

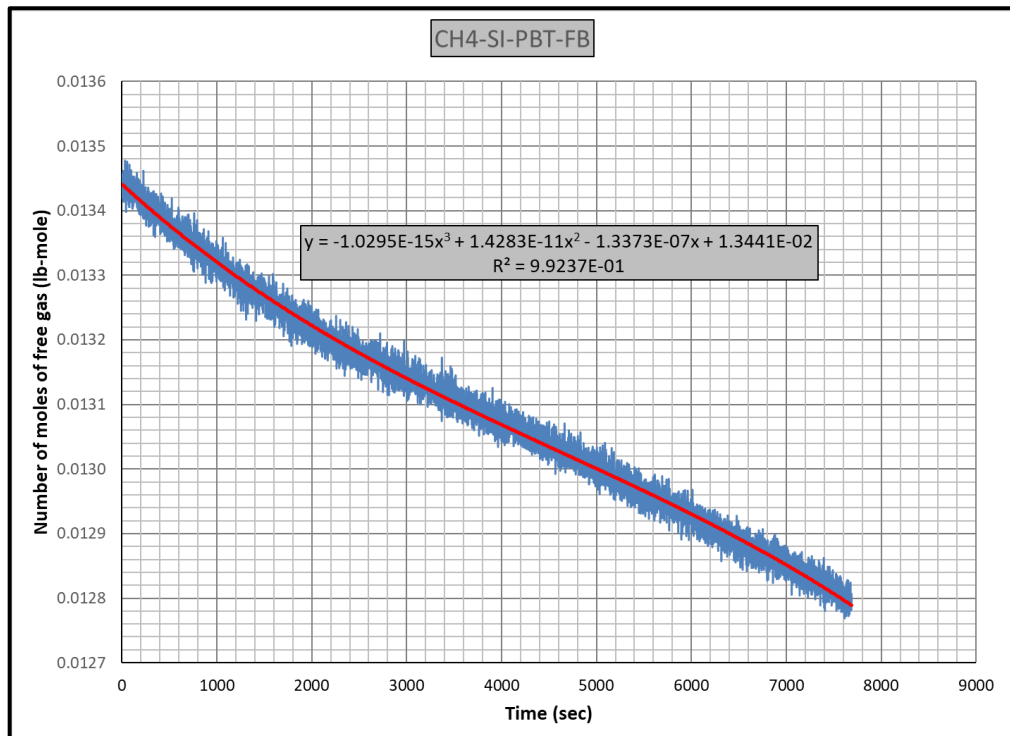


Figure 6.5 Gas consumption rate equation

6.2.2 Overall power consumption

Power consumption was calculated based on the torque measured every second based on the following equation:

$$P_c = T_q \times 2\pi N \quad (\text{Eq. 6.3})$$

where T_q is the Torque in N-m and N is the rotational speed in rps and power consumption is in Watt.

The power consumption at every second over the duration of hydrate formation for each experiment was summed to obtain overall power consumption during the experiment. The duration for the calculation of overall power consumption is the sum of the induction time of a given experiment and the hydrate formation duration of the experiment with shortest duration.

6.2.3 Hydrate yield

The percent of water conversion to hydrate or hydrate yield is defined from the information of hydrate growth rate obtained from gas uptake and the experimental conditions using Equation 6.4:

$$\text{Conversion of water to hydrate (mol\%)} = \frac{\Delta n_{H,\downarrow} \times \text{HydrationNumber}}{n_{H_2O}} \times 100 \quad (\text{Eq. 6.4})$$

where

$$\Delta n_{H,\downarrow} = n_i - n_{end}$$

n_i = moles of free gas when hydrate formation starts or moles of free gas at induction time,

n_{end} = moles at free gas at the end of hydrate formation

n_{H_2O} = moles of water in the reactor

The hydration number is the number of water molecules required per guest methane molecule which is taken as 6.1 from literature [214].

6.2.4 Hydrate Productivity

Hydrate productivity is defined by the formula $NR_{30} = \frac{R_{30}}{V_{water}} (\text{mol lt}^{-1} \text{s}^{-1})$ (Eq. 6.5)

where

V_{water} is the volume of water (lt) in the reactor,

R_{30} is the rate of hydrate growth (mol s^{-1}) calculated by fitting the gas uptake due to hydrate growth versus time for the first 30 minutes after the induction time.

6.3 Kinetic Analysis of methane hydrate formation

Twenty-four experiments with different impeller – baffle configurations given in Figure 6.6 were conducted to determine their effect on kinetics and efficiency of methane hydrate formation.

The twenty-four experiments were divided in eight experiments with single impellers (SI) and sixteen experiments with dual impellers. The single eight experiments conducted with two different impellers: up-pumping pitched blade turbine (PBTU) which generates mixed flow and with Rushton turbine (RT) which generates radial flow. The sixteen experiments of dual impellers were divided in dual impellers (DI) when the impellers are the same and in dual mixed impellers (DMI) when the two types of impellers are mixed. Hence the experiments with dual impellers conducted with the four possible combinations such as PBTU-PBTU, RT-RT, PBTU-RT and RT-PBTU where the first impeller named is the one that was positioned lower on the shaft. Each impeller combinations are tested with four baffle types as full baffle (FB), half baffle (HB), surface baffle (SB) and no baffle (NB).

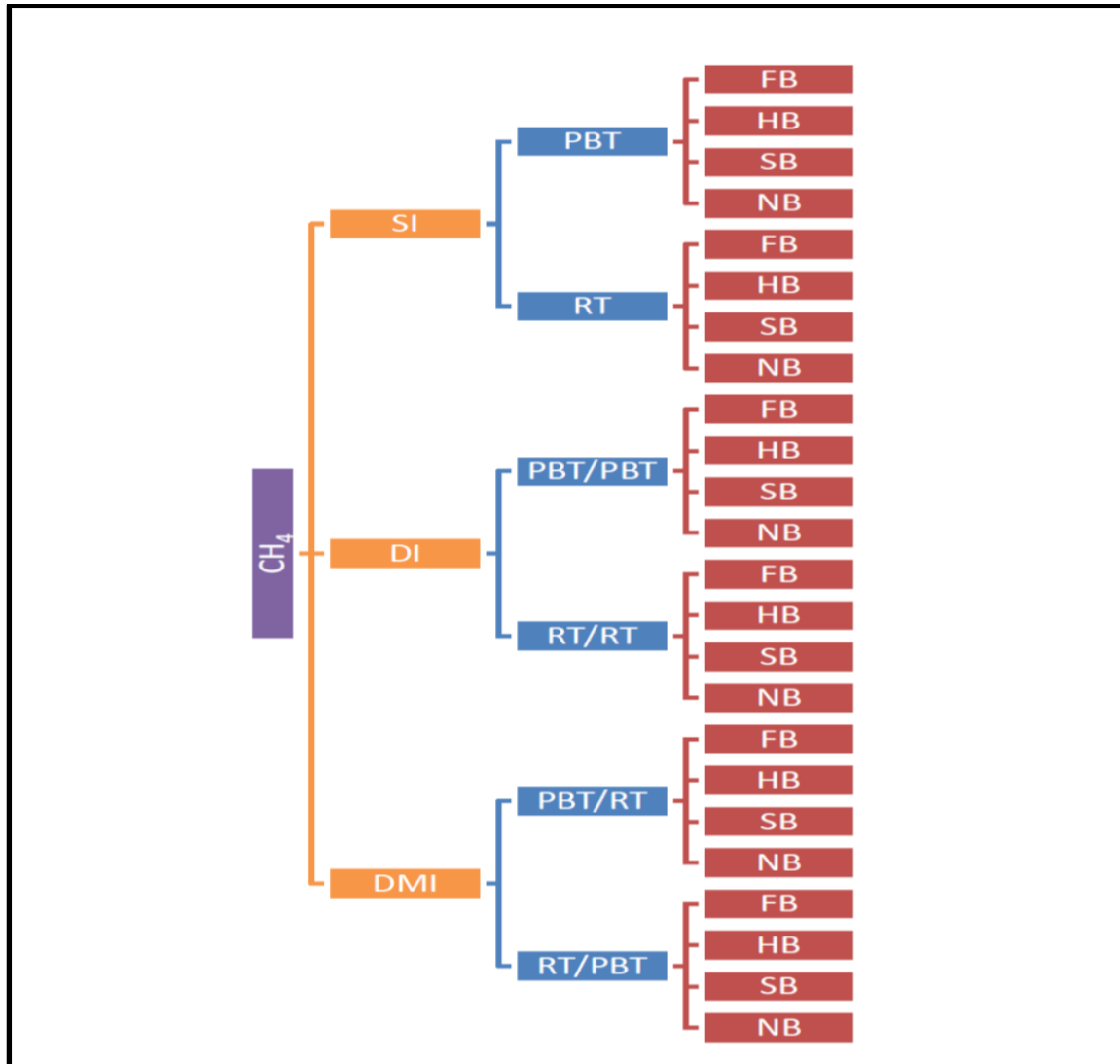


Figure 6.6 Diagram showing the impeller – baffle configurations of 24 methane hydrate experiments

As referred before in this chapter, the recorded data during hydrate formation are pressure, temperature and torque during rotation, at every second. By the use of temperature and pressure with the assistance of Lee and Kesler's (1975) compressibility factor expression, the number of moles of free gas in the reactor (n) at the time of interest during hydrate formation and z compressibility factor are calculated since we also know the volume for each experiment. The graphs of pressure and temperature vs time, pressure and torque vs time and pressure vs time in methane hydrate equilibrium

curve for all eight single experiments are presented in Appendix A, (Figures A.1 to A.4 are for PBTU and Figures A.5 to A.8 are for RT experiments).

Table 6.2 summarizes the results of single impeller (SI) experiments. Stirring is started at the same pressure and temperature conditions (42.5 bar-g and 2 °C) in all experiments. Since the hydrate equilibrium temperature (T_{eq}) of pure methane is 10.5 °C at 42.5 bar-g, the driving force at the start of stirring is 8.5 °C for all experiments.

Analysis of the raw data of PBTU experiments indicate different induction times depending on the type of baffle used. The shortest induction time was 3 minutes with full baffles (FB) while it was 50 minutes and 42 minutes for half (HB) and surface baffles (SB), respectively. On the other hand, it took 10 hours and 15 minutes to observe the start of hydrate formation in no baffles (NB) case. After having such a long induction time for PBTU with NB, this test was repeated and an induction time of 12 hours and 34 minutes was obtained.

The baffles provide axial flow and eliminate the central vortex in a stirred tank. When full baffles are used, it is expected to observe the axial motion of the reactor contents beginning from the bottom of the tank. When shortened baffles such as half and surface baffles are used, however, the tangential flow would be dominant at the bottom of the tank. The axial motion would begin where or whereabouts of the start of the baffles. When there are no baffles in the system, the tangential flow is dominant everywhere, and a central vortex would form. The central vortex could be useful in incorporating gas if the vortex reaches the impeller; however, excessive entrance of the gas would have a significant effect on the hydrodynamics in the tank and the gas entrance through the vortex can become an undesired situation. Based on these, it is seen here that when full baffles are used, there is sufficient gas entrance to the system and the axial flow provided by the baffles allow for the induction to begin much faster. As the baffles become shorter, the possible disconnect between the bottom of the tank and the top where baffles are present do not allow for such efficient gas-liquid contact, and

induction time increases. When no baffles are used, the hydrodynamics completely change, in no favor of the induction time, and a substantial increase is seen.

In all experiments, an increase in the temperature of the system is observed with the initiation of hydrate since the reaction is exothermic. This effect is more pronounced in the experiments with no baffles, indicating a serious heat transfer limitation (Appendix A and Figure A.4).

The results of induction time for RT experiments are closer to each other, but they follow a similar trend. In the full baffles (FB) experiment, the induction time is 4 minutes while it is 25 and 23 minutes in the half (HB) and surface (SB) baffles experiments, respectively. In no baffles (NB) experiment the induction time is 53 minutes and it is the highest value. It is seen that when half and surface baffles are used and no baffles inserted, with the RT impeller hydrates begin to be formed more quickly compared to PBTU. This difference may result in from the different flow patterns the two impellers generate. PBTU is a mixed flow impeller which gives both radial and axial flow and RT is a radial impeller. RT is known to be a shear intensive impeller. This means that whether there are baffles or not, RT is better in producing smaller gas bubbles that enter the reactor either through the surface or through the hollow shaft and as a result, from the sparger. The smaller bubbles allow for the induction time to decrease. It should, however, be noted that RT is not advantageous compared to the PBTU when full baffles are used. This is probably because the mixed flow generated by the PBTU, combined with full baffles allows for better interaction between the gas and the liquid phases, even though the bubbles generated are possibly larger compared to the RT. This also shows that the combination of the type of the impeller and baffle configuration is important in the decision of tank interiors for hydrate production.

Although it was aimed to continue hydrate formation at least 3 hours after the initiation of hydrate formation, this was not achieved for all single impeller experiments. Column 6 in Table 6.2 reports the duration of hydrate formation for single impeller experiments. It is seen that it was possible to form hydrates as long as 3 hours for all PBTU

experiments but none of the RT experiments lasted 3 hours although stirring continued more than 3 hours after initiation of hydrate formation. The main reason of shortened hydrate formation duration in RT experiments is the higher increase in temperature subsequent to hydrate formation compared to PBTU experiments (Appendix A, Figures A.1 to A.8). This phenomenon will be discussed further in the following sections when the hydrate formation rate data is presented.

The change in the number of moles of free gas after the initiation of hydrate formation was used to calculate the rate of hydrate formation at four different times (1 second, 10, 20 and 30 minutes). The graphs of number of moles of free gas vs time and gas consumption rate equations for all single impeller experiments for each configuration are presented in Appendix B (Figures B.1 to B.16).

Figure 6.7 presents the hydrate formation rates of single impeller experiments. The following results are deduced from the analysis of Figure 6.7.

1. The initial hydrate formation rate (rate at 1 sec) of any experiment is always the highest for the given experiment and there exists continuous decrease in hydrate formation rate by time. The possible reasons of the decline in hydrate formation rate are:
 - a) Although hydrate is initially started to form at the gas – water interface and tried to be removed from the interface by mixing, some of the hydrate may stay at the interface. This may result with the restriction of mass transfer between phases,
 - b) As mentioned earlier hydrate formation is an exothermic process. If the heat of hydrate formation is not removed efficiently from the reactor an increase in reactor temperature may occur. An increase in reactor temperature result with reduction in driving force.
2. Hydrate formation rates of RT experiments are always higher than hydrate formation rates of PBTU experiments, for all types of baffles.

3. Although the initial hydrate formation rates of RT experiments are higher compared to PBTU experiments, the hydrate formation rates of RT experiments decrease faster than PBTU experiments. Reasons mentioned in 1a and 1b would be the responsible for this phenomenon. The higher hydrate formation rate results with more hydrate formation in short period of time causing higher restriction of mass transfer between phases. On the other hand, there is little decline in hydrate formation rate with time for PBTU experiments which started with relatively low hydrate formation rate. This difference actually created the shortening of the duration of hydrate formation in RT experiments.

Table 6.2 Summary of results of single impeller experiments

System	Stirring starts at		Driving Force* (°C)	Induction time (hours - minutes)	Duration of hydrate formation (hours - minutes)	Hydrate growth rate for 30 minutes, R ₃₀ (10 ⁻⁸ mol/sec)	Hydrate Yield / Conversion of water to hydrate (mol%)
	P (bar-g)	T (°C)					
SI-PBT-FB	42.5	2	8.5	3 min	3 h	7.2	0.00368
SI-PBT-HB	42.5	2	8.5	50 min	3 h	11.8	0.00483
SI-PBT-SB	42.5	2	8.5	42 min	3 h	34.9	0.00900
SI-PBT-NB	42.5	2	8.5	10 h - 15 min	3 h	17.5	0.00473
SI-RT-FB	42.5	2	8.5	4 min	1 h - 40 min	37.4	0.00972
SI-RT-HB	42.5	2	8.5	25 min	2 h - 5 min	36.2	0.00789
SI-RT-SB	42.5	2	8.5	23 min	2 h - 23 min	39.0	0.00918
SI-RT-NB	42.5	2	8.5	53 min	1 h - 50 min	25.7	0.00520

* Driving force = $T_{\text{exp}} - T_{\text{eq}}$

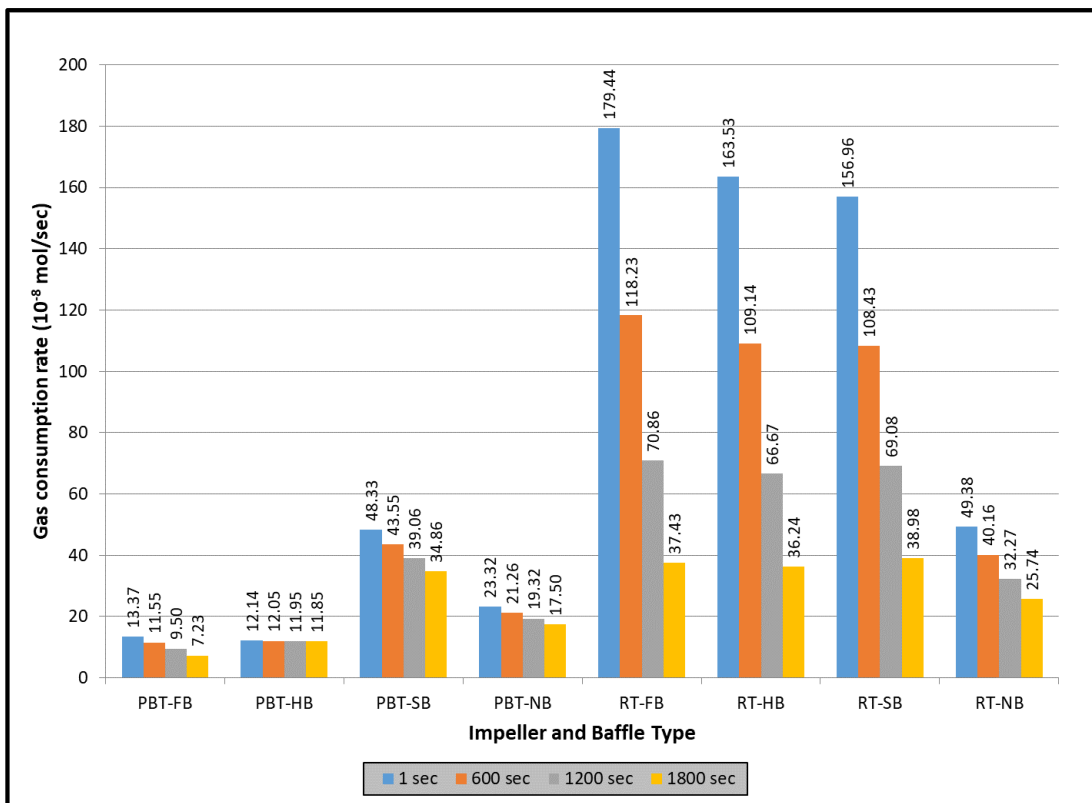


Figure 6.7 Rate of hydrate formation in single impeller experiments

Hydrate growth rate for the first 30 minutes divided by the volume of water in the system is defined as hydrate productivity (Equation 6.5). The results of hydrate productivity of single impeller experiments are presented in Figure 6.8.

Hydrate productivity has an analogy with the rate of hydrate formation. RT experiments have higher hydrate productivity compared to PBTU experiments.

Conversion of water into hydrate (hydrate yield) is calculated based on the hydration number (6.1) and the change in the number of moles of gas during hydrate formation (Equation 6.4). The results are presented at the last column of Table 6.2. It is clear from the hydrate yield values that the amount of water that is converted to hydrates is very small. The main reason of this is the excessive water used in experiments. In a batch type experiment with excessive water, the hydrate formation is hindered by time in response to exothermic nature of hydrate formation if the heat of formation is not fully

removed from the system. In addition, the hydrate layer at the gas – water interface would have an obstructive effect to decrease the mass transfer between hydrate forming phases. These observations actually indicate some of the drawbacks of stirred tank reactors in hydrate formation.

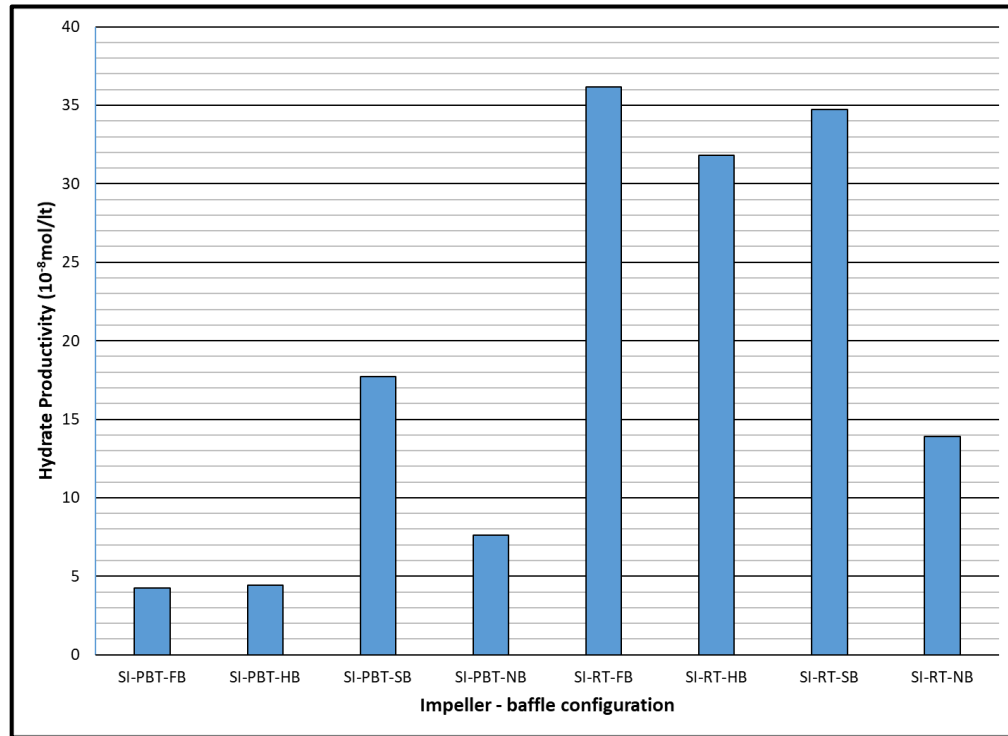


Figure 6.8 Hydrate productivity of single impeller experiments

Overall power consumption during hydrate formation is the last outcome obtained from experimental data. Equation 6.3 is utilized to calculate the power consumption at every second and the summation of all these gave the overall power consumption. The duration for the calculation of overall power consumption is the sum of the induction time of a given experiment and the hydrate formation duration of the experiment with shortest duration. The experiment with Ruston turbine (RT) and no baffle (NB) had the shortest hydrate formation duration among this group experiments as 1 hour and 50 minutes. Figure 6.9 shows the overall power consumptions of all single impeller experiments.

It is obvious from Figure 6.9 that hydrate formation experiment with PBT impeller and no baffle case is an outlier owing to the fact that this experiment had a very long induction time (10 hours and 15 minutes). This long induction with no hydrate production increased the overall power consumption of this particular experiment.

Apart from PBTU impeller – no baffle case, RT experiments have higher overall power consumptions compared to PBTU experiments although RT experiments produced hydrate for shorter periods than PBTU experiments. This difference comes from the higher torque values measured in RT experiments than PBTU experiments. The RT impeller has higher power number; therefore, higher torque requirement. Figure 6.10 plots the torque values of all single impeller experiments after the initiation of stirring. It is seen that all PBTU experiments generally have torque values smaller than 0.9 N-m while RT experiments have higher than 0.9 N-m, even very high at the start of stirring reaching to 1.9 N-m.

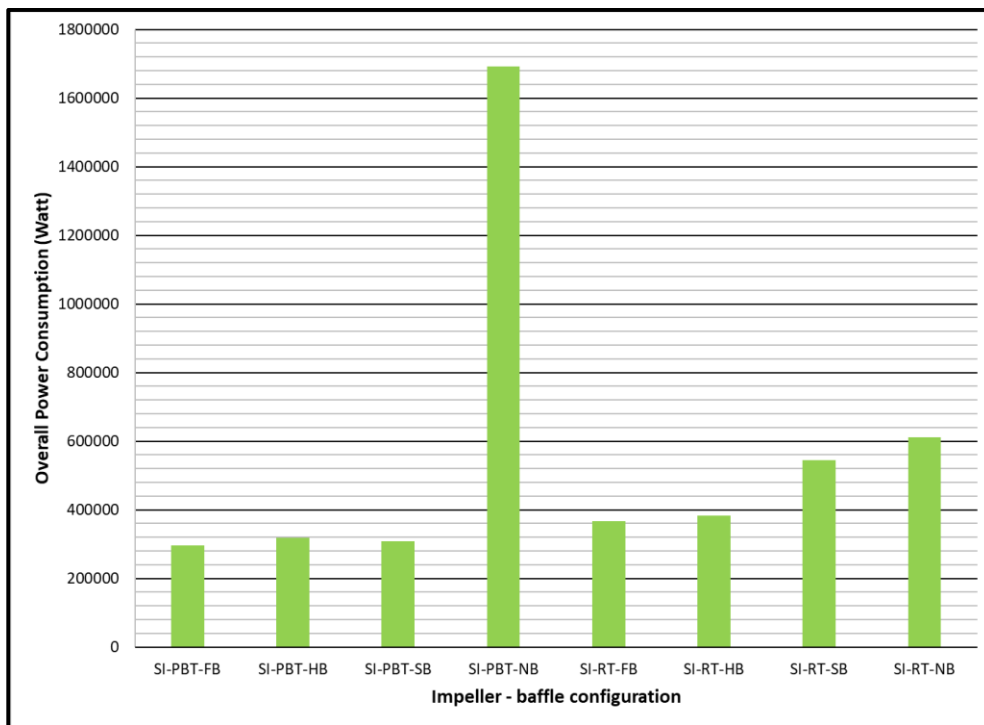


Figure 6.9 Overall power consumption of single impeller experiments

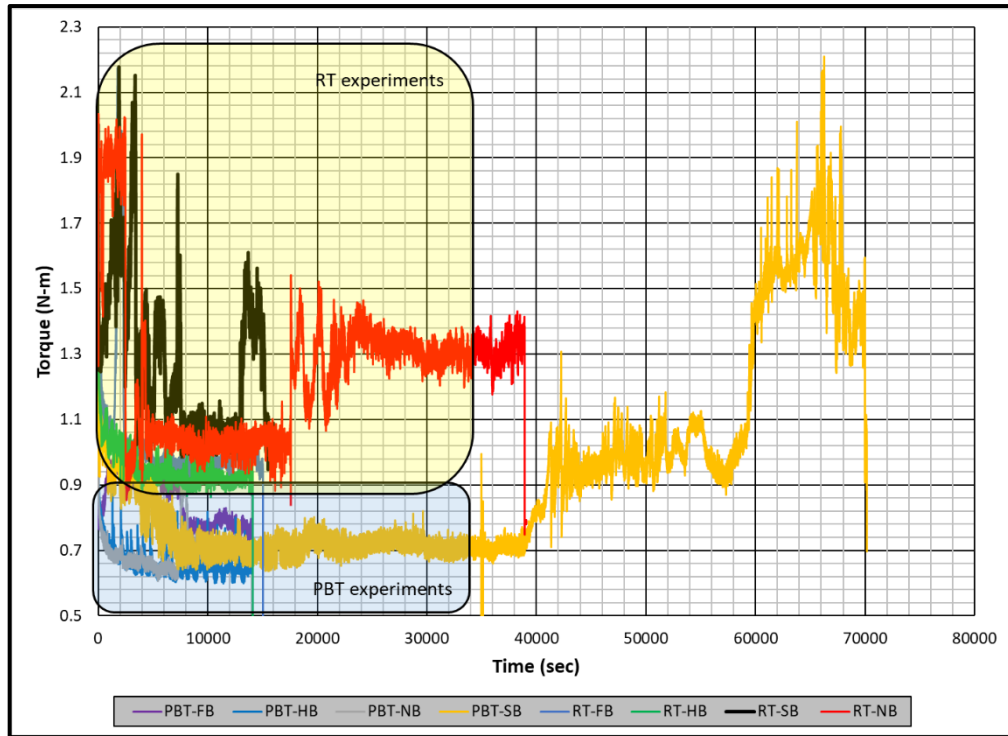


Figure 6.10 Recorded torque values of single impeller experiments

In the second group of experiments with pure methane dual impellers of the same type (PBT-PBT or RT-RT) were used. Table 6.3 gives the summary of results for dual impeller experiments. Pressure and temperature conditions at the starting time of stirring are the same of single impeller experiments (42.5 bar-g, 2 °C). The graphs of pressure and temperature vs time, pressure and torque vs time and pressure vs time in methane hydrate equilibrium curve for all eight dual impeller experiments are presented in Appendix A, (Figures A.9 to A.12 are for PBTU/PBTU and Figures A.13 to A.16 are for RT/RT experiments).

Analysis of the raw data of PBTU/PBTU and RT/RT dual impeller experiments for induction time shows the same trend of single impeller experiments. The shortest induction time are with full baffles (FB) (3 minutes for PBTU/PBTU and 4 minutes for RT/RT). Then induction times are increasing in the same order half baffles (HB), surface baffles (SB) and no baffles cases (NB). Therefore, the discussion made for the effect of

baffle types on the induction time of single impeller experiments is also valid for dual impeller experiments.

Column 6 in Table 6.3 lists the duration of hydrate formation for dual impeller experiments. It is seen that it was possible to form hydrate as long as 3 hours for only two experiments and others last shorter than 3 hours of hydrate formation although stirring continued more than 3 hours after initiation of hydrate formation. Comparison of duration of hydrate formation for single and dual impellers indicates that use of dual impellers generally shortened the duration of hydrate formation (Table 6.4).

Figure 6.11 shows the overall power consumption during hydrate formation with dual impellers. In order to find the duration for the calculation of overall power consumption of a given experiment, the shortest hydrate formation duration of dual Rushton turbine (RT/RT) with full baffle (FB) (22 minutes) was added to the induction time of the particular experiment. It is clear from Figure 6.11, two experiments with very short induction times had relatively low overall power consumption. On the other hand, the longer the induction time resulted with higher overall power consumptions. This clearly shows the importance of shorter induction time to reduce the overall power consumption. On the other hand, although PBT/PBT-HB experiment had shorter induction time compared to PBT/PBT-SB and PBT/PBT-NB experiments, its overall power consumption higher. PBT/PBT-HB experiment had the highest torque values (Figure 6.12) recorded among this group of experiments causing an increase in overall power consumption.

As in the case of single impeller experiments, the change in the number of moles of free gas after the initiation of hydrate formation was used to calculate the rate of hydrate formation at four different times (1 second, 10, 20 and 30 minutes). The graphs of number of moles of free gas vs time and gas consumption rate equations for all single impeller experiments for each configuration are presented in Appendix B (Figures B.17 to B.32).

Figure 6.13 presents the hydrate formation rates of dual impeller experiments. The following results are obtained from the analysis of Figure 6.13.

1. The initial hydrate formation rate (rate at 1 sec) of any experiment is always the highest for the given experiment and there exists continuous decrease in hydrate formation rate by time. The same reasoning of single impeller experiments is valid for dual impeller case.
2. Hydrate formation rates of RT/RT experiments are always higher than hydrate formation rates of PBTU/PBTU experiments, for all types of baffles.
3. On the other hand, although the initial hydrate formation rates of RT/RT experiments are higher compared to PBTU/PBTU experiments, the hydrate formation rates of RT/RT experiments decrease faster than PBTU/PBTU experiments. Reasons mentioned in 1 would be the responsible for this phenomenon. The higher hydrate formation rate results with more hydrate formation in short period of time causing higher restriction of mass transfer between phases. On the other hand, there is little decline in hydrate formation rate with time for PBTU/PBTU experiments which started with relatively low hydrate formation rate. This difference actually created the shortening of the duration of hydrate formation in RT/RT experiments.

Regarding the hydrate yield (the last column of Table 6.4), the percentage of water converted to hydrate gets smaller in dual impeller experiments compared to single impeller experiments. This is an expected result since the amount of water was increased in dual impeller experiments to place the upper impeller in liquid water.

Table 6.3 Summary of results of dual impeller experiments

System	Stirring starts at		Driving Force* (°C)	Induction time (hours - minutes)	Duration of hydrate formation (hours - minutes)	Hydrate growth rate for 30 minutes, R_{30} (10^{-8} mol/sec)	Hydrate Yield / Conversion of water to hydrate (mol%)
	P_{exp} (bars)	T (°C)					
DI-PBT/PBT-FB	42.5	2	8.5	3 min	3 h	24.7	0.00377
DI-PBT/PBT-HB	42.5	2	8.5	31 min	2h - 20 min	24.5	0.00313
DI-PBT/PBT-SB	42.5	2	8.5	43 min	1 h - 20 min	8.8	0.00352
DI-PBT/PBT-NB	42.5	2	8.5	49 min	1 h - 30 min	12.4	0.00148
DI-RT/RT-FB	42.5	2	8.5	4 min	22 min	-	0.00382
DI-RT/RT-HB	42.5	2	8.5	52 min	1 h & 10 min	18.3	0.00334
DI-RT/RT-SB	42.5	2	8.5	1 h - 26 min	1 h	3.9	0.00363
DI-RT/RT-NB	42.5	2	8.5	1 h - 32 min	3 h	19.1	0.00276

*Driving force = $T_{exp} - T_{eq}$

Table 6.4 Comparison of duration of hydrate formations

Single impeller		Dual impeller	
SI-PBT-FB	3 h	DI-PBT/PBT-FB	3 h
SI-PBT-HB	3 h	DI-PBT/PBT-HB	2h - 20 min
SI-PBT-SB	3 h	DI-PBT/PBT-SB	1 h - 20 min
SI-PBT-NB	3 h	DI-PBT/PBT-NB	1 h - 30 min
SI-RT-FB	1 h - 40 min	DI-RT/RT-FB	22 min
SI-RT-HB	2 h - 5 min	DI-RT/RT-HB	1 h & 10 min
SI-RT-SB	2 h - 23 min	DI-RT/RT-SB	1 h
SI-RT-NB	1 h - 50 min	DI-RT/RT-NB	3 h

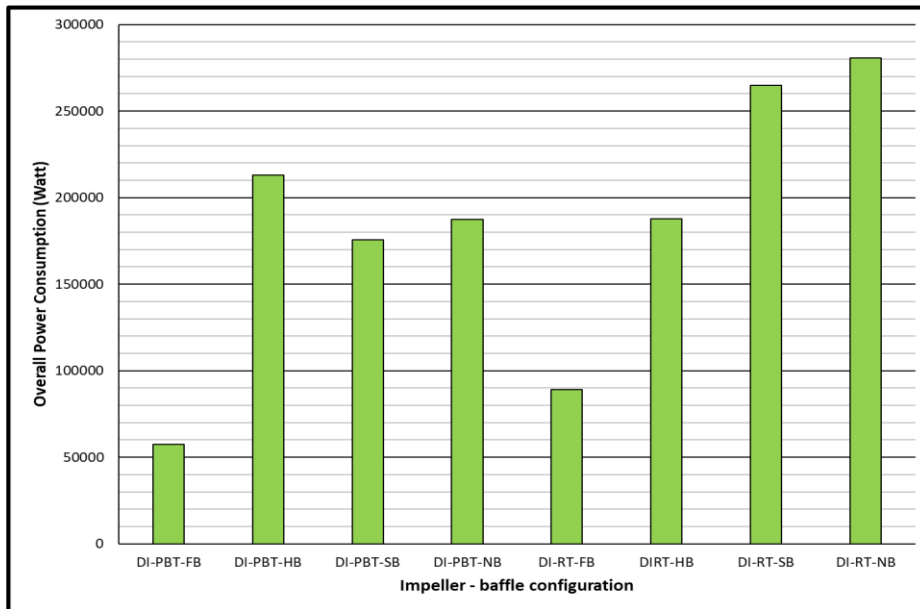


Figure 6.11 Overall power consumption of dual impeller experiments

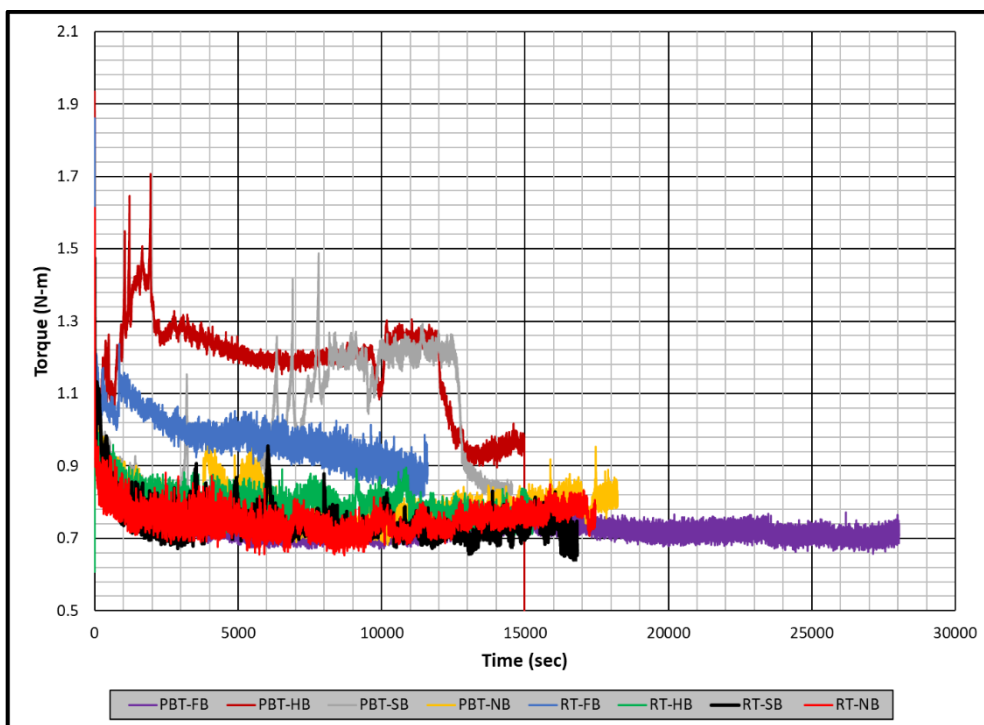


Figure 6.12 Recorded torque values of single impeller experiments

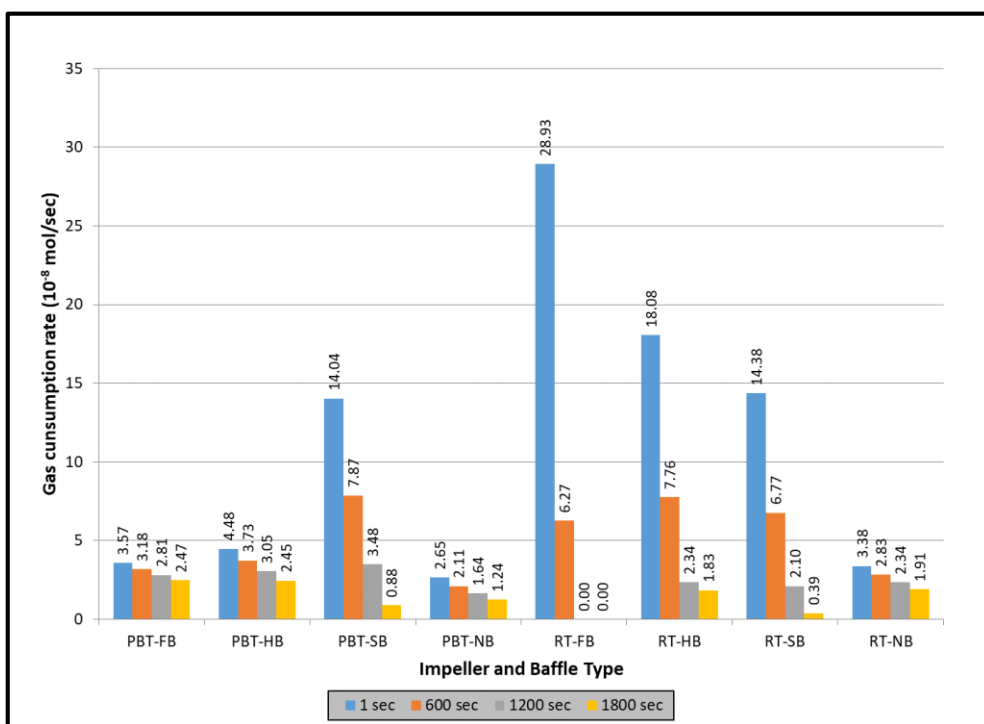


Figure 6.13 Rate of hydrate formation of PBT/PBT and RT/RT dual impellers for time period of 1, 600, 1200 and 1800 seconds

The third and the last group of experiments are the ones with pure methane are dual mixed impellers of different types (PBT/RT or RT/PBT). In the description of any dual mixed experiment the impeller written first is attached to the shaft at a lower position (close to sparger) while the second one is attached to the shaft closer to the gas-liquid interface.

Table 6.5 gives the summary of results for dual mixed impeller experiments. Pressure and temperature conditions at the starting time of stirring are the same of the previous experiments (42.5 bar-g, 2 °C). The graphs of pressure and temperature vs time, pressure and torque vs time and pressure vs time in methane hydrate equilibrium curve for all eight dual impeller experiments are presented in Appendix A (Figures A.17 to A.20 are for PBTU/RT and Figures A.21 to A.24 are for RT/PBTU experiments).

Analysis of the raw data of dual mixed impeller experiments for induction time shows the same trend of single and dual impeller experiments. The shortest induction time are with full baffles (FB) (2 minutes for PBTU/RT and 3 minutes for RT/PBTU). Then induction times are increasing in the same order half baffles (HB), surface baffles (SB) and no baffles cases (NB). Therefore, the discussion made for the effect of baffle types on the induction time of single and dual impeller experiments is also valid for dual mixed impeller experiments.

Column 6 in Table 6.5 lists the duration of hydrate formation for dual impeller experiments. It is seen that it was possible to form hydrate in half of the experiments as long as 3 hours and others lasted shorter than 3 hours of hydrate formation although stirring continued more than 3 hours after initiation of hydrate formation. There is no general trend for the duration of hydrate formation for dual mixed impeller experiments.

The overall power consumption during hydrate formation with dual-mixed impellers is given in Figure 6.14. The duration for the calculation of overall power consumption of a given experiment was obtained by the summation of the induction time of the particular experiment and hydrate formation duration of the experiment having shortest hydrate

formation period (dual-mixed Pitched blade turbine / Rushton turbine (PBT/RT) with full baffle (FB) (24 minutes)). It is clear from Figure 6.14, two experiments with very short induction times had relatively low overall power consumption. On the other hand, the experiments having induction times closer to or longer than an hour had higher overall power consumptions. This clearly shows the importance of shorter induction time to reduce the overall power consumption. A similar observation is made from Figure 6.15 by comparing the measured torque values of dual-mixed impeller experiments. Two experiments of pitched blade turbine / Rushton turbine (PBT/RT) with surface baffle (SB) and no baffle (NB) had the lowest torque values but because of their longer induction times (about two hours) they had the highest overall power consumption.

As in the case of single and dual impeller experiments, the change in the number of moles of free gas after the initiation of hydrate formation was used to calculate the rate of hydrate formation at four different times (1 second, 10, 20 and 30 minutes). The graphs of number of moles of free gas vs time and gas consumption rate equations for all dual mixed impeller experiments for each configuration are presented in Appendix B (Figures B.33 to B.48).

Figure 6.16 presents the hydrate formation rates of dual mixed impeller experiments. Almost all combinations of dual mixed impeller and baffles start with relatively high hydrate formation rates but decrease about the half of the initial rate in a short period of time. This observation indicates that dual impeller arrangement is suitable for hydrate formation but the higher initial rate of hydrate formation limits the mass transfer between phases because of the batch type operation. The highest gas consumption rate is obtained from PBT/RT impellers and FB baffles.

Table 6.5 Summary of results of dual-mixed impeller experiments

System	Stirring starts at		Driving Force* (°C)	Induction time (hours - minutes)	Duration of hydrate formation (hours - minutes)	Hydrate growth rate for 30 minutes, R_{30} (10^{-8} mol/sec)	Hydrate Yield / Conversion of water to hydrate (mol%)
	P_{exp} (bars)	T (°C)					
DMI-PBT/RT-FB	42.5	2	8.5	2 min	24min	-	0.00409
DMI-PBT/RT-HB	42.5	2	8.5	11 min	1 h - 30 min	28.5	0.00339
DMI-PBT/RT-SB	42.5	2	8.5	1 h - 47 min	3 h	11.2	0.00296
DMI-PBT/RT-NB	42.5	2	8.5	1 h - 56 min	3 h	17.8	0.00259
DMI-RT/PBT-FB	42.5	2	8.5	3 min	3 h	18.2	0.00328
DMI-RT/PBT-HB	42.5	2	8.5	30 min	42 min	4.9	0.00333
DMI-RT/PBT-SB	42.5	2	8.5	56 min	40 min	12.2	0.00247
DMI-RT/PBT-NB	42.5	2	8.5	1 h - 39 min	3 h	15.9	0.00222

*Driving force = $T_{exp} - T_{eq}$

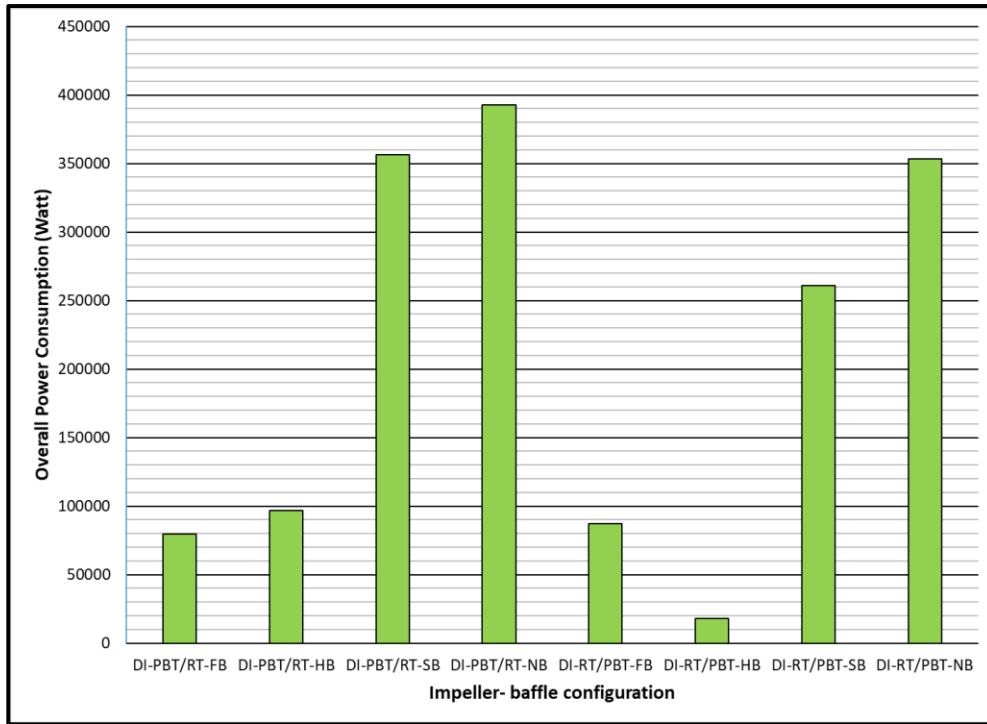


Figure 6.14 Overall power consumption of dual-mixed impeller experiments

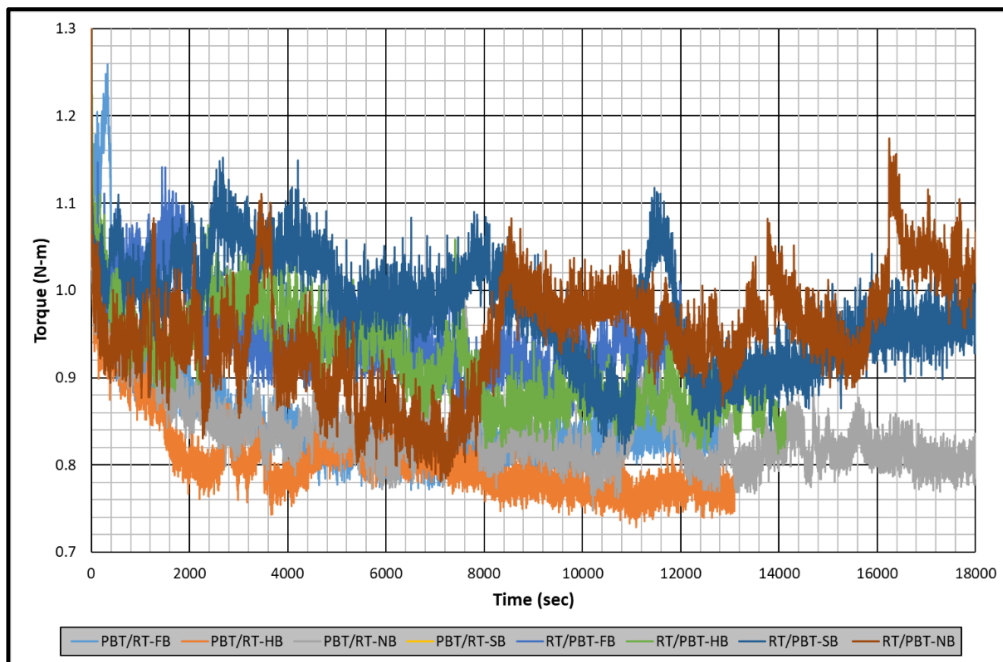


Figure 6.15 Recorded torque values of dual-mixed impeller experiments

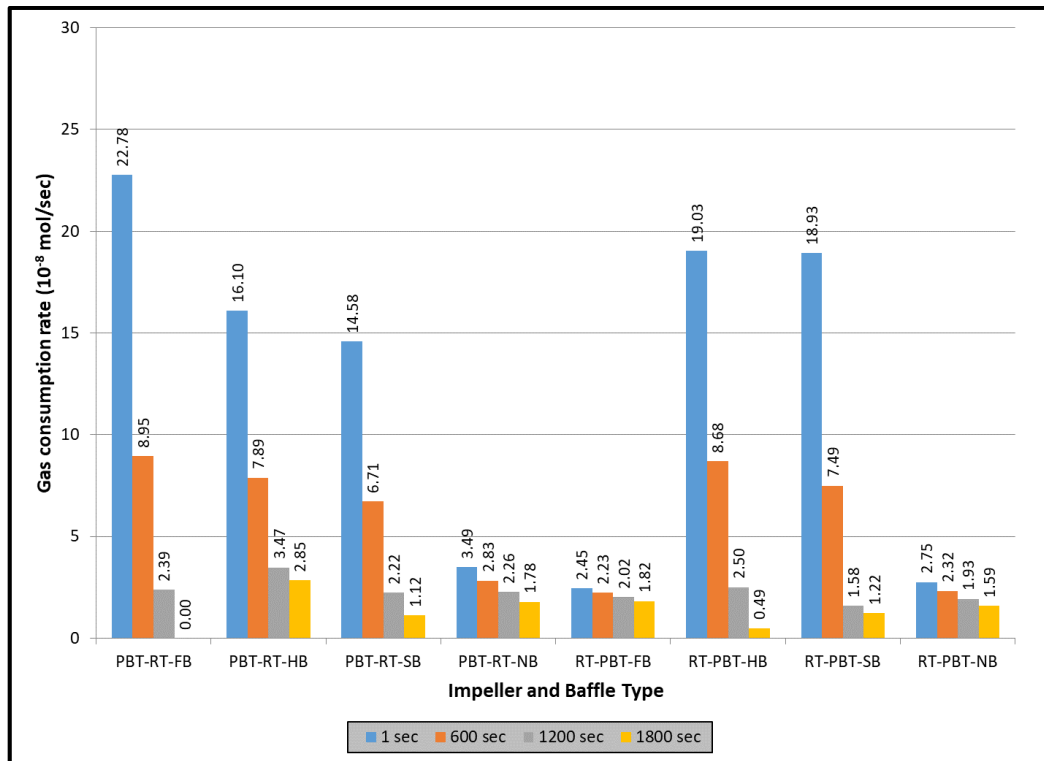


Figure 6.16 Rate of hydrate formation of dual mixed impellers for time period of 1, 600, 1200 and 1800 seconds.

Two important parameters dictating the suitability of a given impeller – baffle configuration on natural gas hydrate formation are induction time and the rate of hydrate formation. Although experimental results indicate a regular change in the induction time with the type of baffle (shortest with full baffle and in an increasing order with half, surface and no baffle) it is not possible to assign a numerical value because of its stochastic nature. On the other hand, experimental results indicated that it is possible to define the hydrate formation rate with a third order polynomial. Experimental data of 24 methane hydrate formation experiments fit to a 3rd order polynomial with correlation coefficients (R^2) close to 1. But, there is still a question about the repeatability of the tests. **Repeatability** is defined as the closeness of agreement between independent test results, obtained with the same method, on the same test material, in the same

laboratory, by the same operator, and using the same equipment within short intervals of time. In order to check the repeatability of hydrate formation experiments of this study three tests were repeated. Then their induction times and hydrate formation rates were compared. Those tests were chosen as one test for each of the single, dual and dual mixed impeller arrangements. Table 6.6 lists the gas consumption rates and induction times for comparison which are also shown as bar charts in Figures 6.17 to 6.19.

Regarding the induction time, although it has a stochastic nature the results show similarity. On the other hand, gas consumption rates of repeatability tests are quite close to each other. Gas consumption rates of experiments with single impeller and no baffle almost the same (Figure 6.17). Repeatability tests with dual and dual mixed impellers show some differences in gas consumption rates (Figure 6.18 and 6.19). Gas consumption rates of two repeatability tests with dual mixed impeller with full baffle have small differences but exhibit the same trend. Although the numerical values differ slightly the behavioral change with time is considered as the sign of repeatability. The last pair for repeatability are the experiments with dual Rushton turbine impellers with full baffle. This arrangement has the highest gas consumption rates among all other impeller – baffle configurations. Figure 6.19 shows that both repeatability tests resulted with higher gas consumption rates, again showing the sign of repeatability.

Table 6.6 Results of repeatability tests

Experiment	Gas consumption rate (10^{-8} mol/sec)				Induction time (hours – minutes)
	1 sec	600 sec	1200 sec	1800 sec	
CH4-SI-PBT-NB (1)	23.3	21.3	19.3	17.5	10 hours – 15 minutes
CH4-SI-PBT-NB (2)	23.5	21.4	19.4	17.6	12 hours – 34 minutes
CH4-DMI-PBT/RT-FB (1)	24.5	22.3	20.2	18.2	2 min
CH4-DMI-PBT/RT-FB (2)	27	24.6	22.3	20.2	2 min
CH4-DI-RT/RT-FB (1)	289.3	62.7	-	-	22 min
CH4-DI-RT/RT-FB (2)	185.8	72.7	20.7	-	18 min

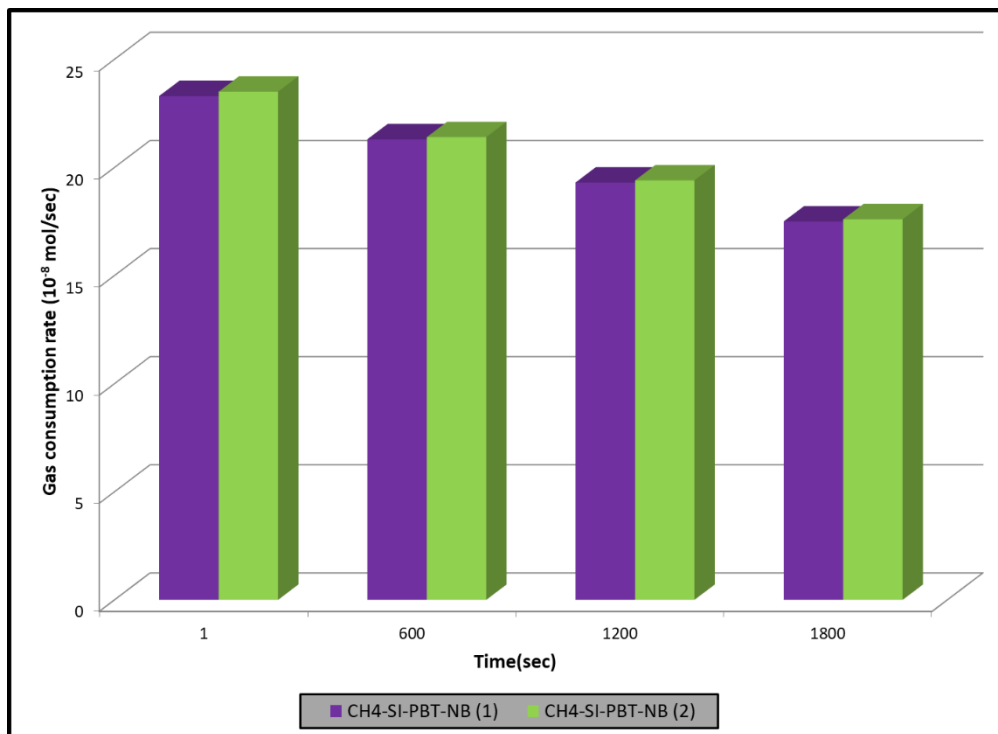


Figure 6.17 Repeatability test of CH4-SI-PBT-NB in terms of gas consumption rate

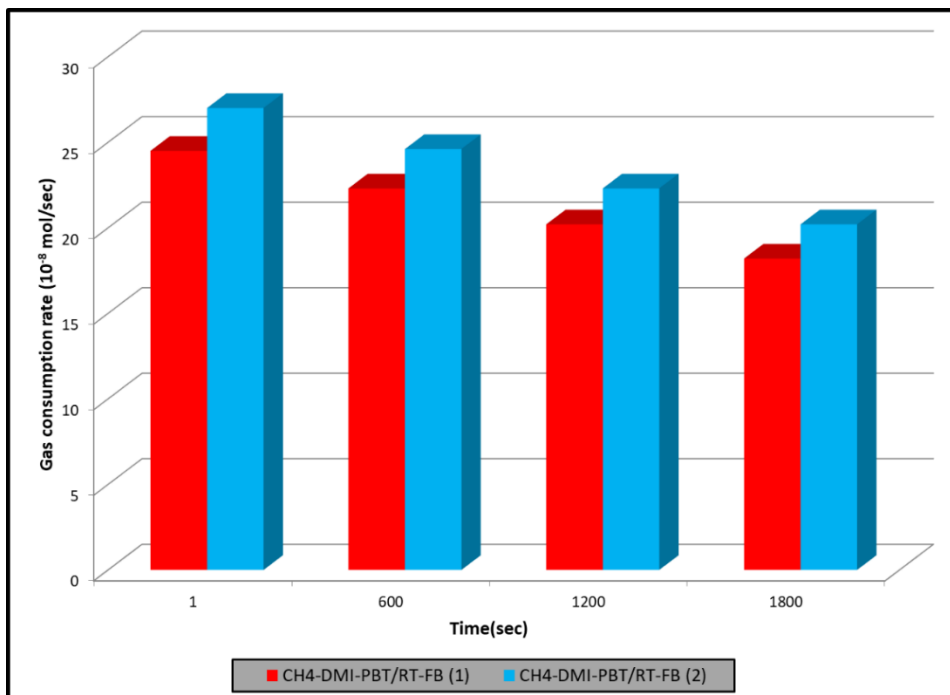


Figure 6.18 Repeatability test of CH4-DMI-RT/PBT-FB in terms of gas consumption rate

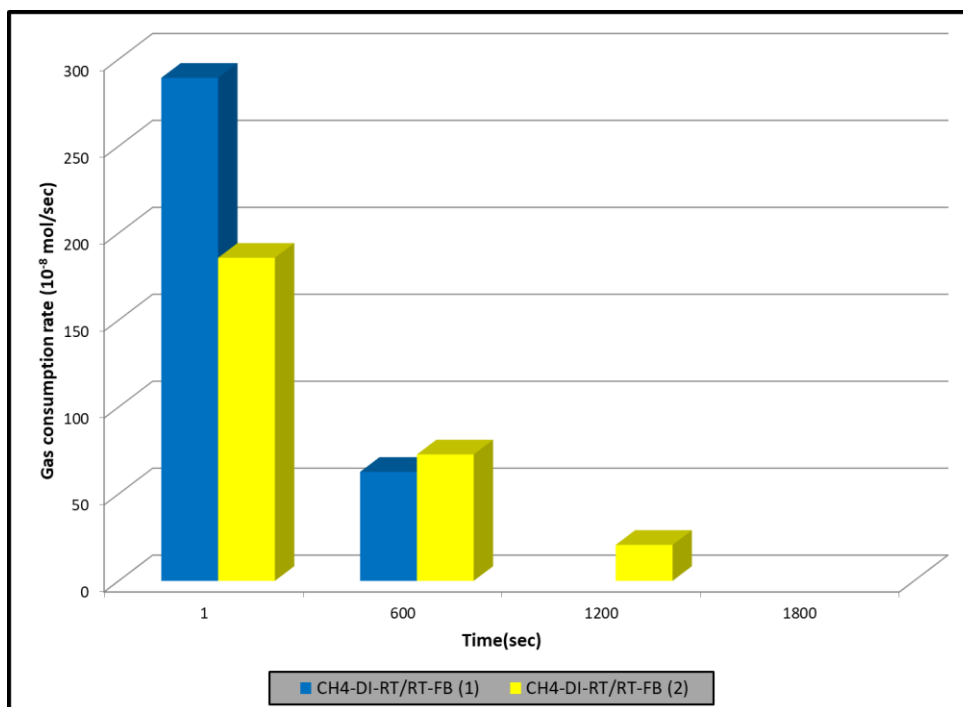


Figure 6.19 Repeatability test of CH4-DI-RT-FB in terms of gas consumption rate

CHAPTER 7

RESULTS AND DISCUSSION OF METHANE – PROPANE MIXTURE HYDRATE FORMATION

As far as it concerns, hydrate formation experiments of methane – propane mixture (95% methane-5% propane) experimental data is interpreted as in methane hydrate experiments with some additional steps to take into account the fractionation of the gas components in the gas and hydrate phases. Chromatographic analysis of free gas at the end of hydrate formation process was carried out to determine the partition of methane and propane in free gas and hydrate structure. Split fraction of methane and propane and separation factor of propane are calculated based on kinetic analysis of experimental data and chromatographic analysis of gas sample taken at the end of hydrate formation [215].

Split fraction

Split fraction (S.Fr) given in equations 7.1 and 7.2 are used to quantify the partition of hydrate forming gases in free gas and solid hydrate phases,.

The split fraction of methane is calculated as follows:

$$\text{S.Fr.CH}_4 = \frac{n_{\text{CH}_4}^{\text{H}}}{n_{\text{CH}_4}^{\text{Feed}}} \quad (\text{Eq. 7.1})$$

where $n_{CH_4}^{Feed}$ is the number of moles of methane in feed gas and $n_{CH_4}^H$ is the number of moles of methane in hydrate phase at the end of the experiment.

Similarly, the split fraction (S.Fr.) of propane is calculated as follows:

$$S.Fr.C_3H_8 = \frac{n_{C_3H_8}^H}{n_{C_3H_8}^{Feed}} \quad (Eq. 7.2)$$

where $n_{C_3H_8}^{Feed}$ is the number of moles of propane in feed gas and $n_{C_3H_8}^H$ is the number of moles of propane in hydrate phase at the end of the experiment.

Separation Factor

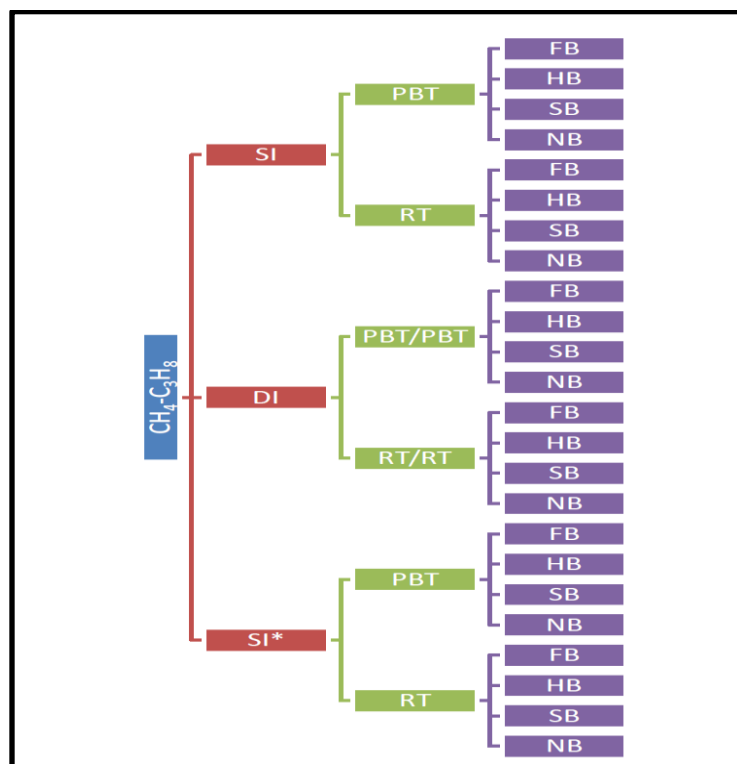
Natural gas hydrates are frequently used to separate gas components of given gas mixtures owing to the fact that those separated components either consumed more into the hydrate structure than the other components of the mixture, or they do not go into the hydrate structure at all. In this study, the mixture that is used to form hydrates are both hydrate formers but it is known from literature that propane is consumed more compared to methane. Since the studied gas is rich in methane, it was decided to analyze how propane is separated from the mixture depending on the experimental conditions. Equation 7.3 is utilized to calculate the separation factor of propane (S.F_{C₃H₈}) [215].

$$S.F_{C_3H_8} = \frac{n_{C_3H_8}^H \times n_{CH_4}^{gas}}{n_{CH_4}^H \times n_{C_3H_8}^{gas}} \quad (Eq. 7.3)$$

where $n_{CH_4}^{gas}$ is the number of moles of methane in the gas phase at the end of hydrate formation, $n_{C_3H_8}^{gas}$ is the number of moles of propane in the gas phase at the end of the hydrate formation, $n_{C_3H_8}^H$ is the number of moles of propane in the hydrate phase.

In total, 24 hydrate formation experiments were conducted with 95 % methane 5% propane mixture (Figure 7.1). The driving force of 8 experiments out of 24 was the same as pure methane experiments (8.5 °C). Since methane – propane mixtures form hydrate at relatively low pressure than pure methane for a given temperature, the pressure at the

starting time of stirring was chosen as 26.5 bar-g which corresponds to the hydrate equilibrium temperature of 17 °C for 95 % methane – 5 % propane mixture. After completing these 8 experiments, it was found that the experimental conditions were not suitable for longer period of hydrate formation. The reason for shorter duration of hydrate formation was the change in hydrate equilibrium curve as most of the propane was consumed in hydrate formation and remaining free gas became richer in methane. The more the methane in free gas the higher the hydrate equilibrium pressure. On the other hand, the reactor pressure decreases by hydrate formation. As a result, the driving force gets smaller by time and at some point hydrate formation stops. After realizing this fact, the remaining 16 experiments were carried out at 2 °C which was the temperature of methane hydrate experiments. Another change in this group of experiments was the pressure at the start of stirring. It was kept at 24.5 bar-g.



1. **Figure 7.1** Repeatability Diagram showing the impeller – baffle configurations of 24 methane -propane mixture hydrate experiments

Another important difference from pure methane experiments was the sampling of free gas at the end of each experiment. Gas samples were analyzed by gas chromatography to determine the degree of fractionation of methane and propane between free gas and solid hydrate phases.

Another parameter for grouping of methane – propane mixture experiments is the type of impeller. Single impellers were used in 16 experiments and dual impellers were used in the remaining 8 experiments. Half of the single impeller experiments were realized at 8.5 °C and the other half at 2 °C.

Interpretation of experimental data is the same as the interpretation of methane experiments. Therefore, the graphs of pressure and temperature vs time, pressure and torque vs time and pressure vs time in methane-propane hydrate equilibrium curve were drawn and presented in Appendix A, (Figure A.25 to A.32 for PBTU and RT experiments with experimental temperature of 8.5 °C and Figure A.33 to A.40 for PBTU and RT experiments with experimental temperature of 2 °C).

Table 7.1 summarizes the results of single impeller, methane – propane mixture experiments. The following findings are drawn from Table 7.1:

- Except in one experiment (Rushton turbine – half baffle), hydrate formation started almost immediately after the start of stirring (very short induction times)
- Duration of hydrate formation was always shorter than 3 hours in experiments with higher experimental temperature (8.5 °C). This is attributed to the lower driving force as explained earlier. Furthermore, experiments with RT last shorter compared to experiments with PBTU.
- Experiments with lower experimental temperature (2 °C) and PBTU type impeller had hydrate formation durations longer than 3 hours. But the change in impeller type from PBTU to RT resulted with shortening of hydrate formation duration.

- Split fraction values of methane are relatively low (between 0.040 and 0.133) indicating that a higher percentage of methane in the original gas still remains in free gas phase. On the other hand, the split fraction of methane values are high in case of higher driving force (Figure 7.2).
- Split fraction values of propane are much higher compared to the split fraction values of methane, as expected. Again, higher driving force resulted with higher split fraction for propane (Figure 7.3) as high as 0.889 (almost 90% of propane consumed for hydrate production).
- Final parameter to be discussed in Table 7.1 is the separation factor of propane. Depending on experimental conditions, propane separated from the mixture with a factor between 8 to 64 compared to methane. The higher the driving force the better the separation of propane from the mixture (Figure 7.4).

Discussion on split fractions and separation factor of propane clearly indicates the change in the composition of hydrate forming gas as hydrate formation progresses. In order to quantify this phenomenon, chromatographic analysis of gas samples after hydrate formation are plotted on Figures 7.5 and 7.6. Arithmetic average of free gas compositions at the end of single impeller experiments with lower driving force is 97.08 % methane and 2.92 % propane (Figure 7.5) indicating an increase in methane mole percentage compared to feed gas composition. Figure 7.7 shows the experimental pressure – temperature data with hydrate equilibrium lines of feed gas and free gas after hydrate formation. As seen, hydrate formation line is shifting closer to experimental conditions. The consequence is a reduced driving force for hydrate formation. Same observation is valid for experiments with higher driving forces but higher consumption of propane, ending up with an average free gas composition of 99.24 % of methane and 0.76 % of propane (Figure 7.6). Again, the experimental condition after hydrate formation is very close to the hydrate equilibrium line of free gas sampled at this condition (Figure 7.8).

Table 7.1 Summary of results of single impeller, methane – propane mixture experiments

System	P _{exp} (bars)	T (°C)	Driving Force (°C)	Duration of hydrate formation	Induction time (min)	S.Fr _{CH₄}	S.Fr _{C₃H₈}	S.F _{C₃H₈}
SI-PBT-FB	26.5	8.5	8.5	2h - 30min	1	0.043	0.286	8.85
SI-PBT-HB	26.5	8.5	8.5	1h - 49min	1	0.040	0.250	8.02
SI-PBT-SB	26.5	8.5	8.5	1h - 59min	1	0.061	0.549	18.73
SI-PBT-NB	26.5	8.5	8.5	2h - 7min	1	0.053	0.397	11.83
SI-RT-FB	26.5	8.5	8.5	1h - 32min	1	0.094	0.606	14.75
SI-RT-HB	26.5	8.5	8.5	1h - 23min	1	0.100	0.630	15.28
SI-RT-SB	26.5	8.5	8.5	1h - 22min	1	0.041	0.518	25.16
SI-RT-NB	26.5	8.5	8.5	1h - 47min	1	0.054	0.451	14.52
SI-PBT-FB	24.5	2	16	3h	1	0.114	0.870	52.41
SI-PBT-HB	24.5	2	16	3h	2	0.114	0.884	59.23
SI-PBT-SB	24.5	2	16	3h	3	0.110	0.889	64.77
SI-PBT-NB	24.5	2	16	3h	2	0.120	0.887	57.40
SI-RT-FB	24.5	2	16	1h - 20min	1	0.129	0.848	37.67
SI-RT-HB	24.5	2	16	1h - 31min	27	0.099	0.860	56.23
SI-RT-SB	24.5	2	16	54min	1	0.133	0.886	50.74
SI-RT-NB	24.5	2	16	1h - 7min	1	0.131	0.854	38.71

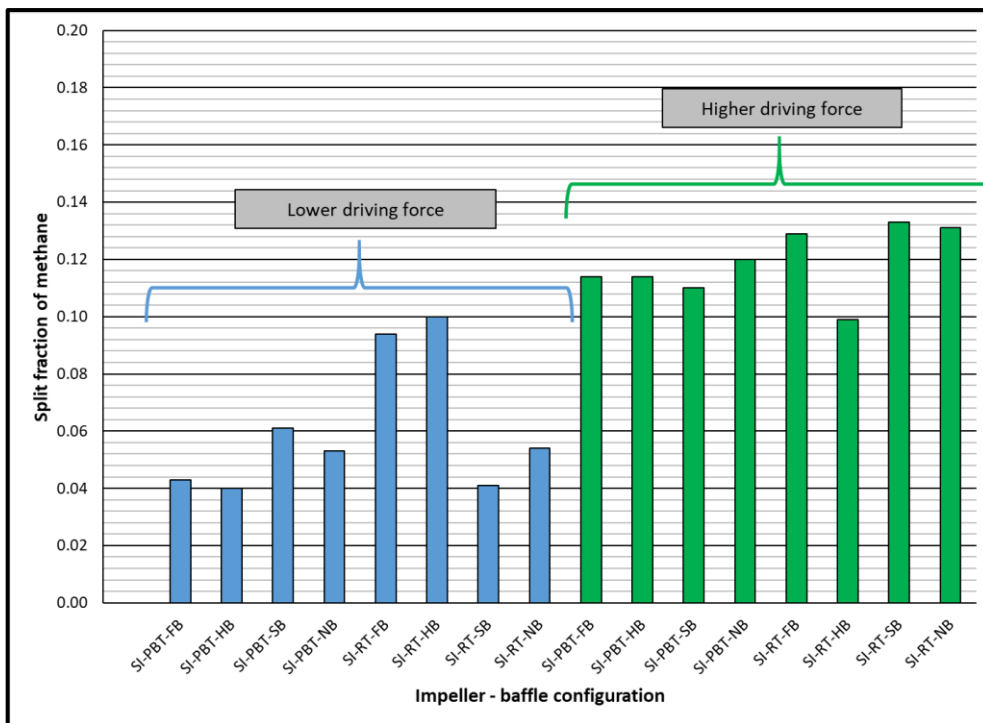


Figure 7.2 Split fraction of methane of single impeller mixture hydrate experiments

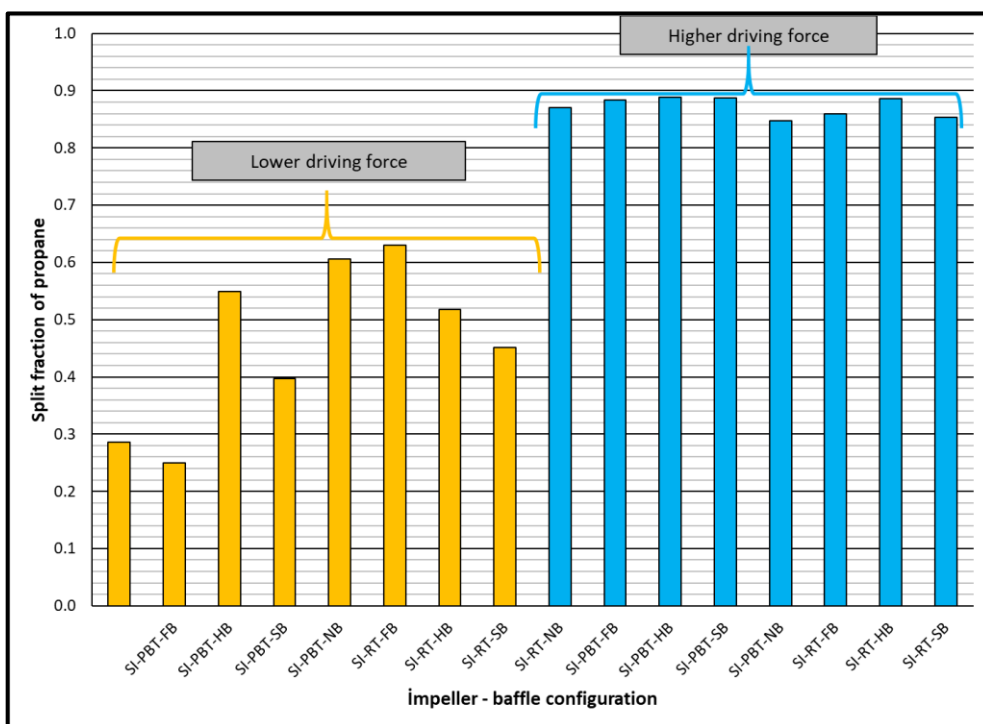


Figure 7.3 Split fraction of propane of single impeller mixture hydrate experiments

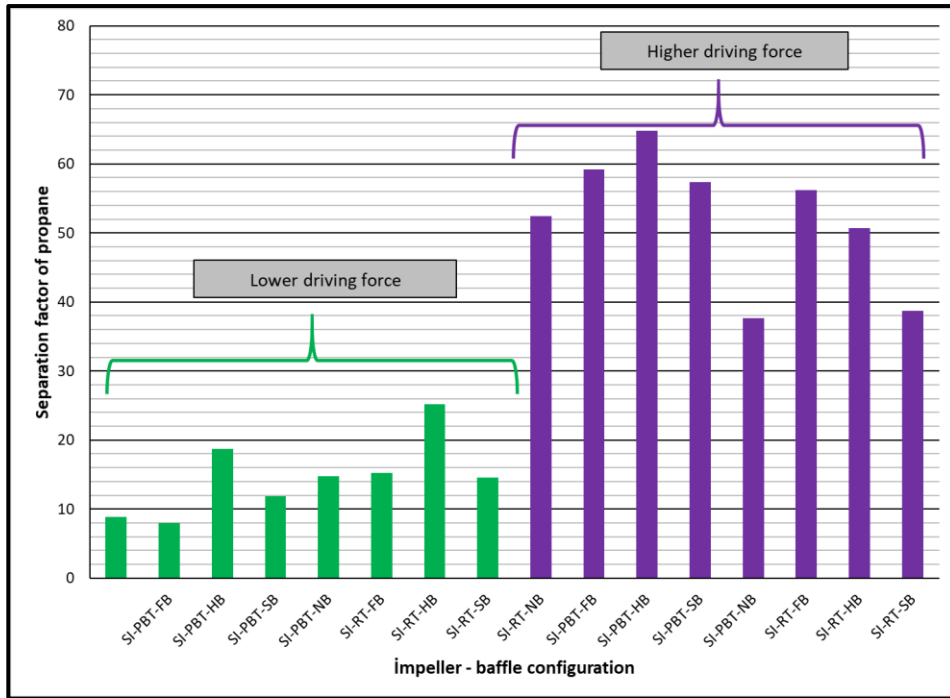


Figure 7.4 Separation factor of propane of single impeller mixture hydrate experiments

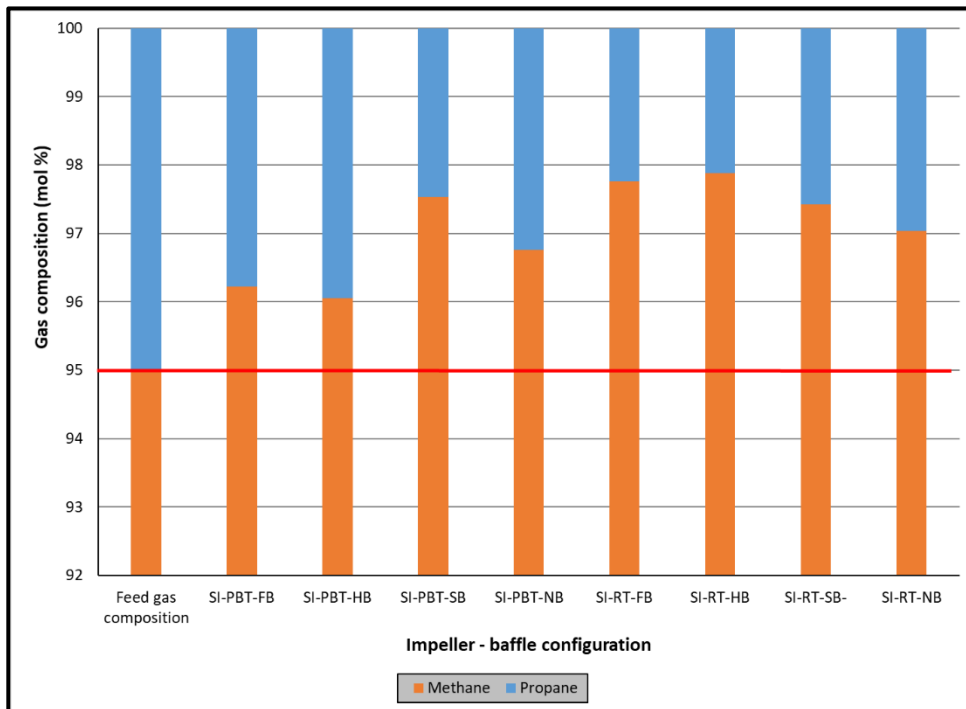


Figure 7.5 Composition of feed gas and free gas at the end of single impeller experiments (lower driving force)

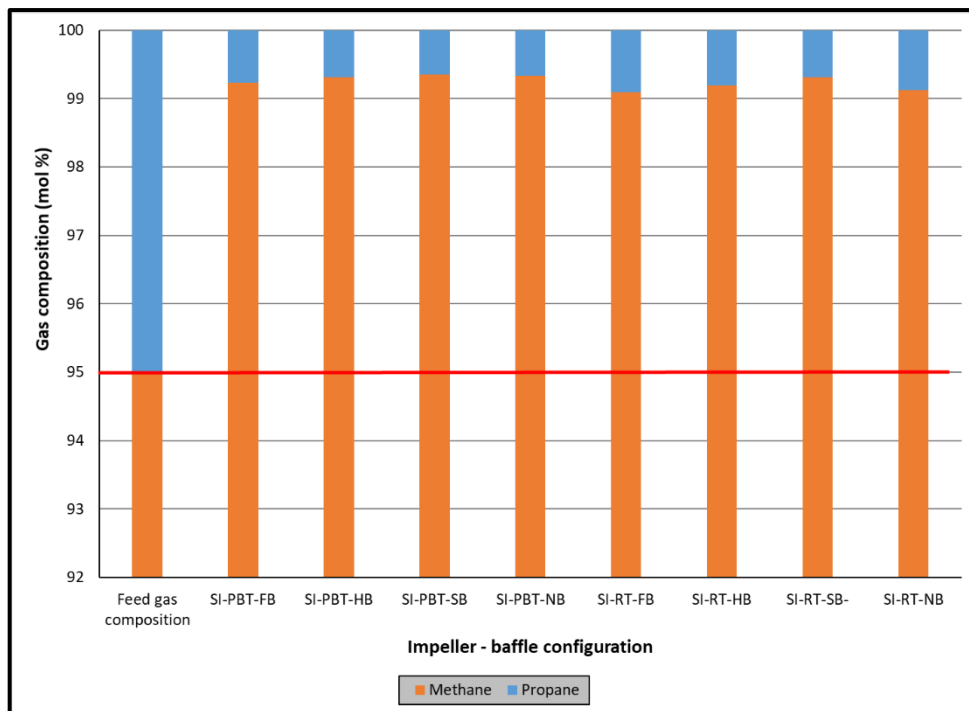


Figure 7.6 Composition of feed gas and free gas at the end of single impeller experiments (higher driving force)

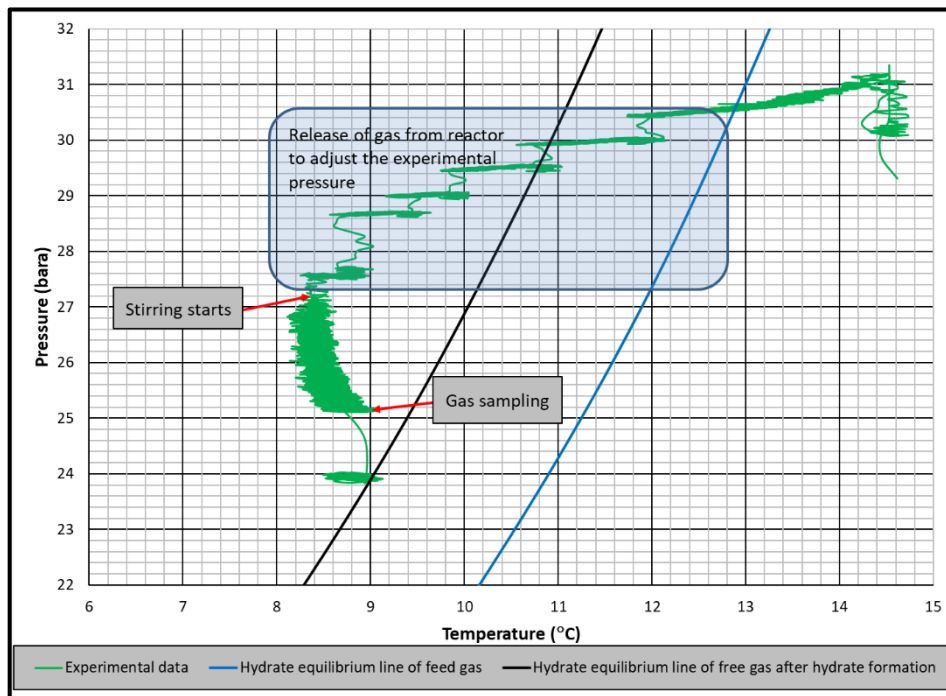


Figure 7.7 Pressure – temperature diagram of mixture gas of SI-RT-FB (lower driving force)

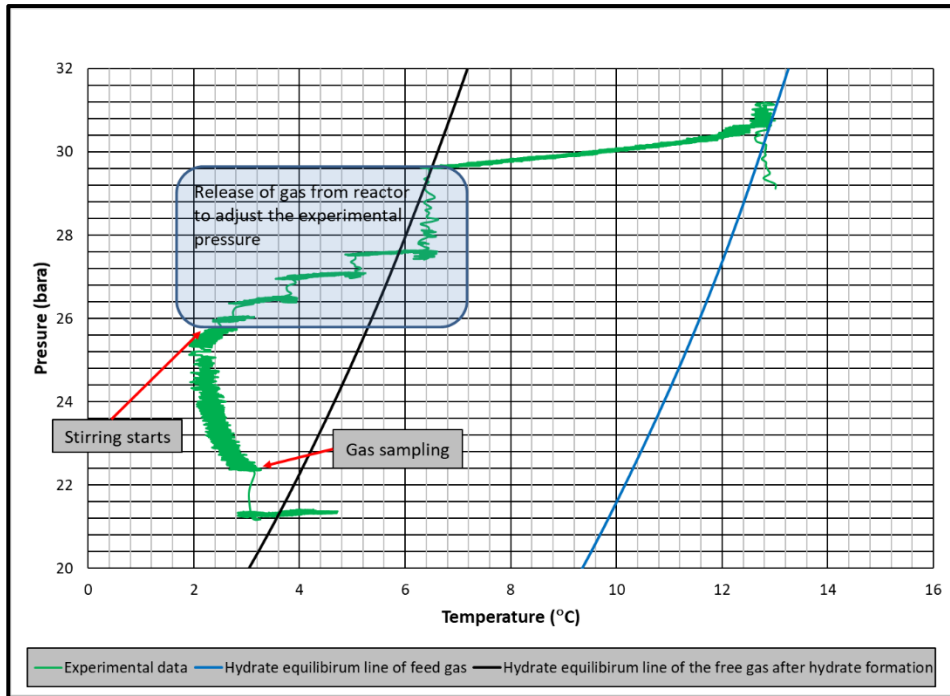


Figure 7.8 Pressure – temperature diagram of mixture gas of SI-RT-FB (higher driving force)

Rate of hydrate formation charts of mixture gas with single impeller for lower and higher driving forces are presented in Figures 7.9 and 7.10, respectively. The graphs of free gas vs time for all single impeller experiments and gas consumption rate equations are presented in Appendix B (Figures B.49 to B.68 for lower driving force and Figures B.69 to B.90 for higher driving force).

The common characteristics of hydrate formation rate changes is the continuous decline of rate by time for a given experiment. Initial hydrate formation rates for RT experiments generally higher than PBTU experiments for the same type of baffle (Figures 7.9 and 7.10). On the other hand, the decline rate of hydrate formation is higher for RT compared to PBTU.

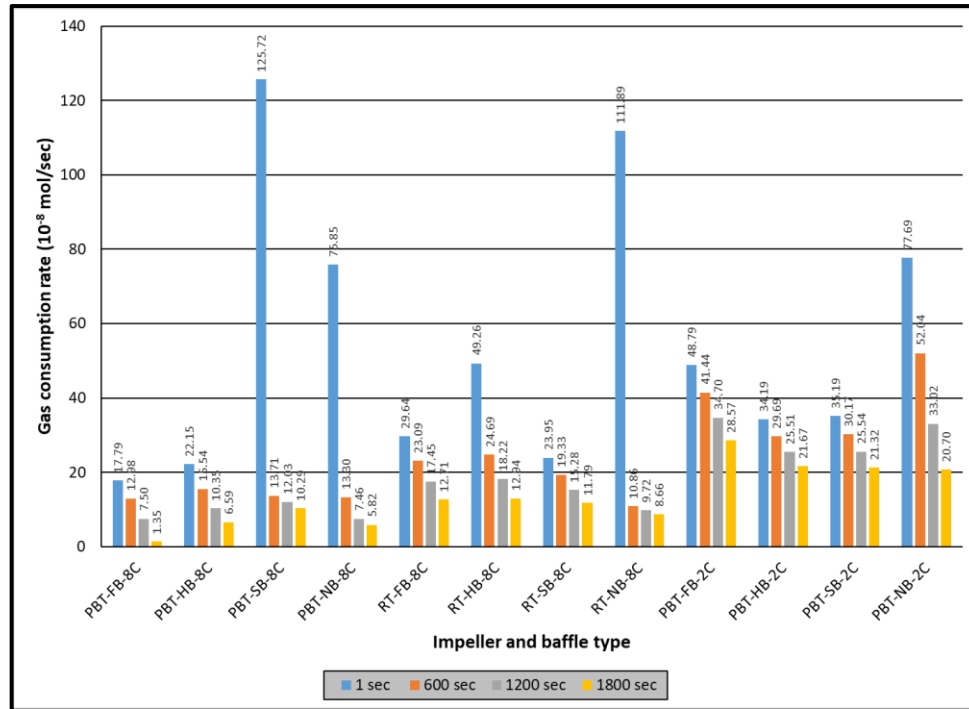


Figure 7.9 Rate of hydrate formation of mixture gas with single impeller and lower driving force (experimental temperature 8.5 °C)

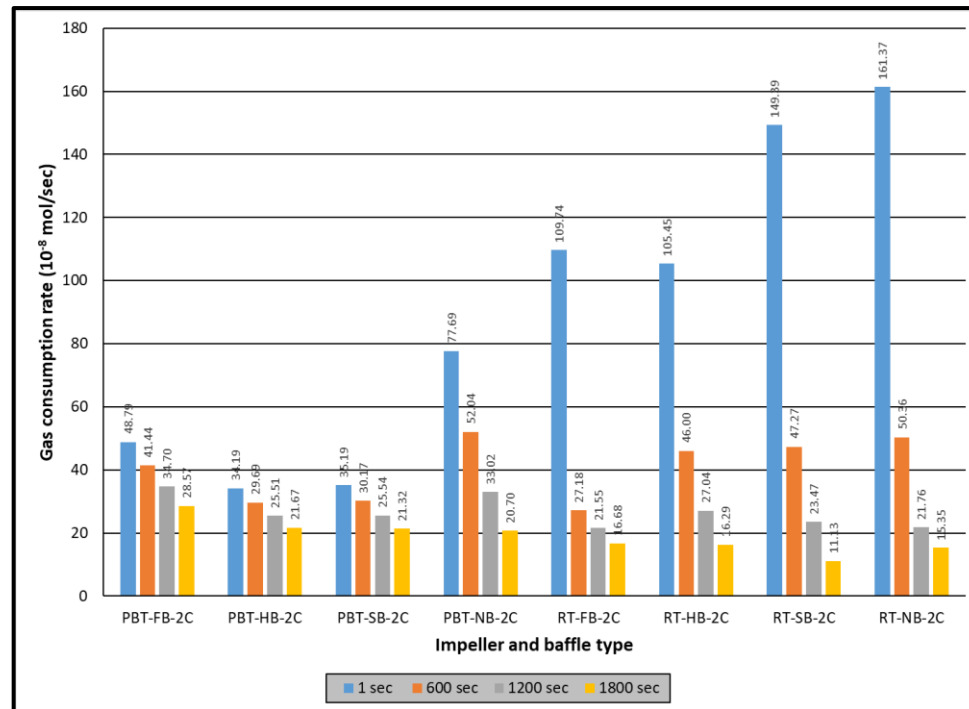


Figure 7.10 Rate of hydrate formation of mixture gas with single impeller and higher driving force (experimental temperature 2 °C)

Table 7.2 summarizes the results of dual impeller, methane – propane mixture experiments. Eight experiments realized with dual impellers at 2 °C experimental temperature. The following findings are drawn from Table 7.1:

- In all dual impeller experiments with mixture gas, hydrate formation started almost immediately after the start of stirring (2 minutes of induction times).
- Duration of hydrate formation was always shorter than 3 hours in all experiments. The effect of baffles for a given impeller type is opposite for dual impellers of PBTU and RT. The duration of hydrate formation decreases in the order of FB, HB, SB and NB for PBTU/PBTU but in opposite direction for RT/RT.
- Split fraction values of methane are again relatively low (between 0.115 and 0.223) but higher in dual impeller experiments compared to single impeller ones (Figure 7.11).
- Split fraction values of propane are much higher compared to the split fraction values of methane, as expected. Again, higher split fractions of propane were observed in dual impeller experiments compared to single impeller experiments (Figure 7.12).
- Depending on experimental conditions, propane separated from the mixture with a factor between 22 to 72 compared to methane. Comparison of separation factors of propane for single and dual impeller experiments did not show a distinct trend (Figure 7.13).

Rate of hydrate formation of mixture by using dual impellers are presented in Figure 7.14. Again, the results are given for 1, 600, 1200 and 1800 seconds. The graphs of free gas vs time for all dual impeller experiments and gas consumption rate equations are presented in Appendix B (Figures B.91 to B.113). The initial hydrate formation of RT/RT experiments with full, half and surface baffles were comparatively high among all other hydrate formation experiments of this study. But, there exists very sharp decline in hydrate formation rate within first 600 seconds. The main reason of such a sharp decline is attributed to the higher amount of hydrate formation which could restrict the

mass transfer between gas and liquid phases if the solid hydrate is not removed efficiently from the gas – liquid interface. Increase in temperature due to exothermic nature of hydrate formation, change in the composition of hydrate forming gas due to different partition of components in free gas and hydrate phases are other reasons to be mentioned.

Table 7.2 Summary of results of dual impeller, methane – propane mixture experiments

System	P _{exp} (bars)	T (°C)	Driving Force (°C)	Duration of hydrate formation	Induction time (min)	S.Fr _{CH₄}	S.Fr _{C₃H₈}	S.F _{C₃H₈}
DI-PBT/PBT-FB	24.5	2	16	2h - 9min	2 min	0.223	0.876	24.710
DI-PBT/PBT-HB	24.5	2	16	1h - 33min	2 min	0.115	0.904	72.591
DI-PBT/PBT-SB	24.5	2	16	1h - 11min	2 min	0.164	0.915	54.496
DI-PBT/PBT-NB	24.5	2	16	53 min	2 min	0.205	0.853	22.546
DI-RT/RT-FB	24.5	2	16	42 min	2 min	0.115	0.886	60.110
DI-RT/RT-HB	24.5	2	16	59 min	2 min	0.144	0.895	51.107
DI-RT/RT-SB	24.5	2	16	1h - 20min	2 min	0.157	0.897	47.000
DI-RT/RT-NB	24.5	2	16	1h - 16min	2 min	0.208	0.835	19.404

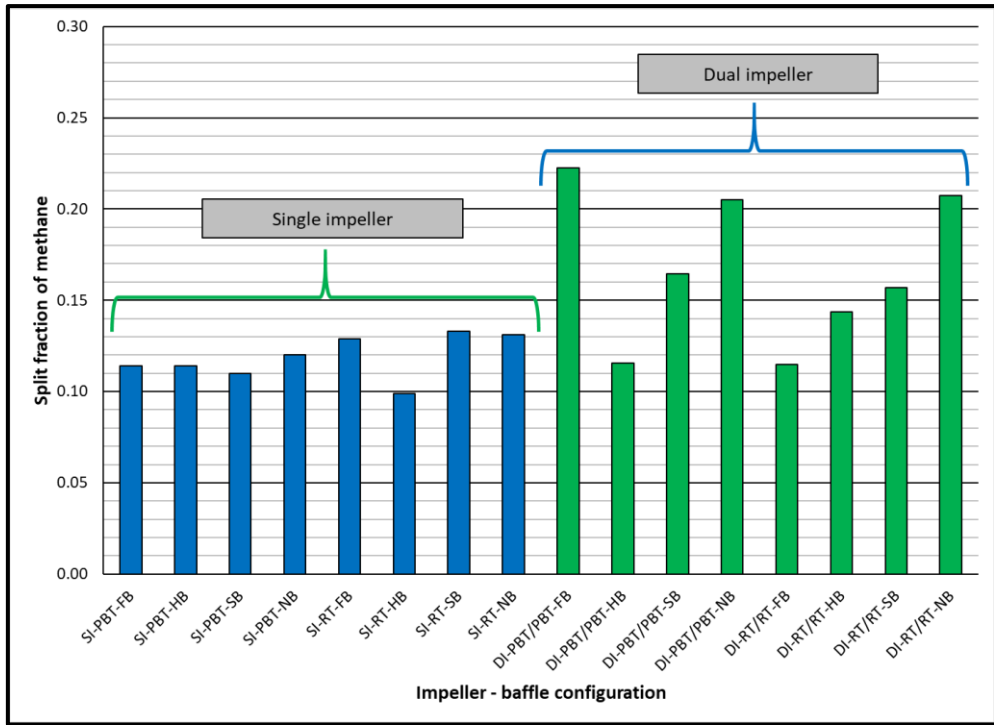


Figure 7.11 Split fraction of methane for single and dual impeller experiments (experimental temperature 2 °C)

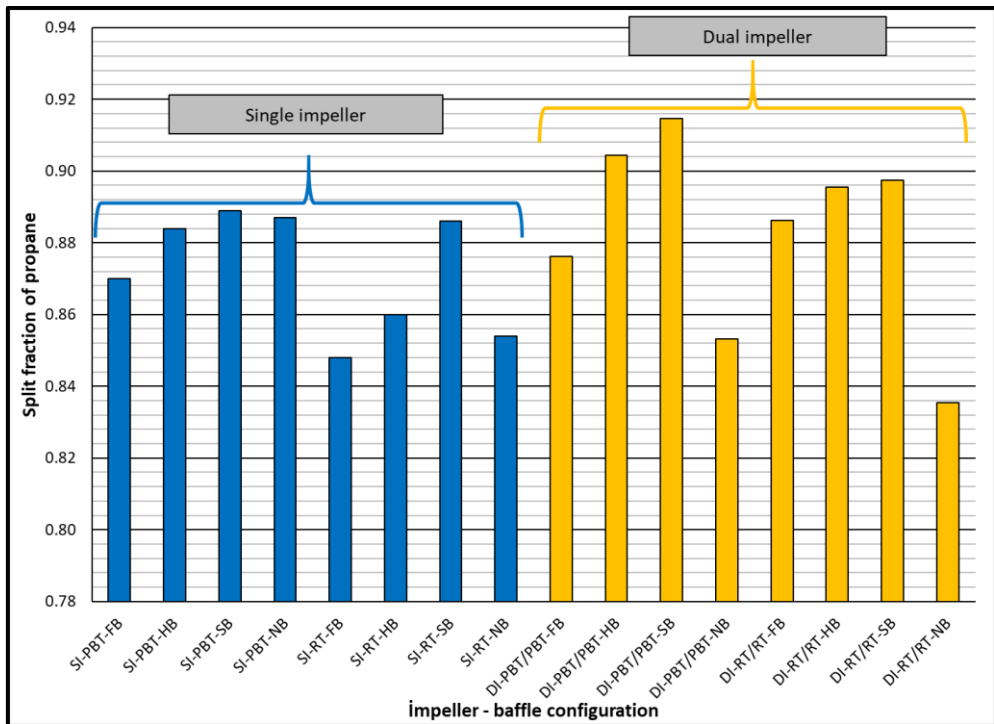


Figure 7.12 Split fraction of propane for single and dual impeller experiments (experimental temperature 2 °C)

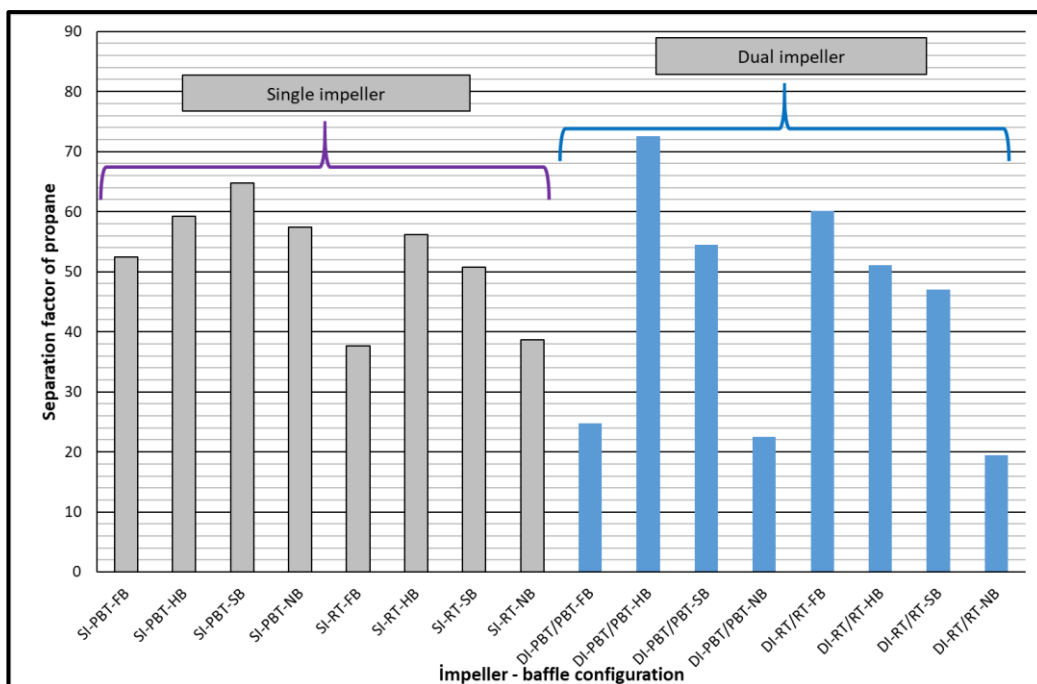


Figure 7.13 Separation factor of propane for single and dual impeller experiments (experimental temperature 2 °C)

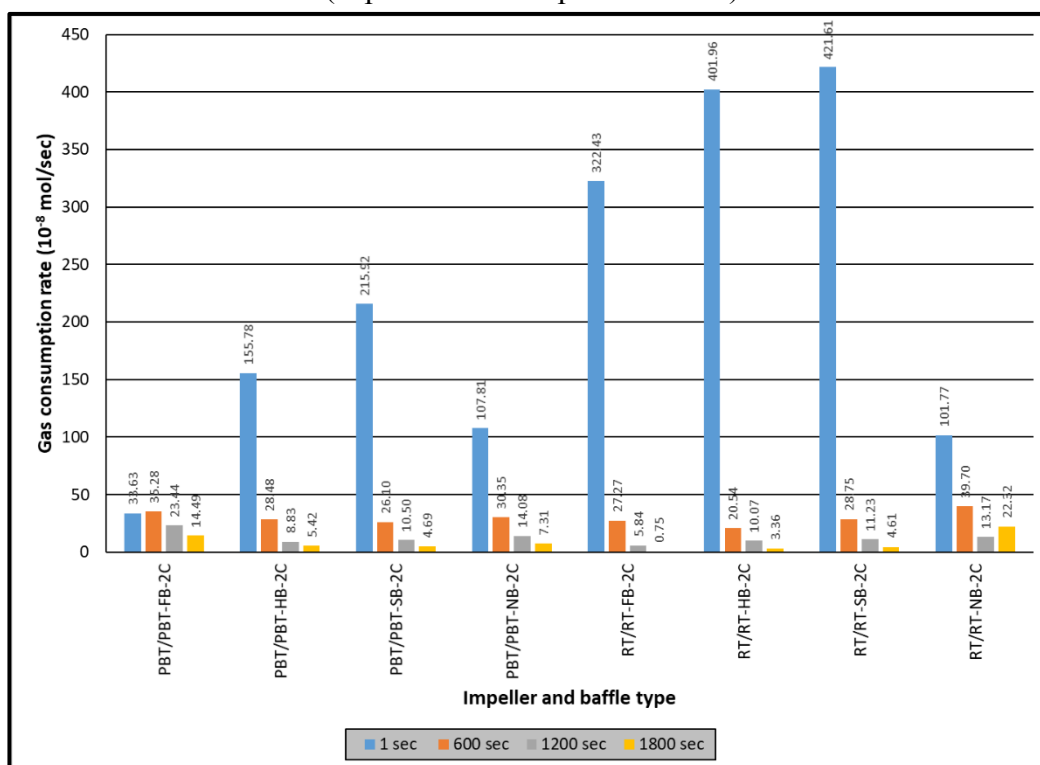


Figure 7.14 Rate of hydrate formation of mixture gas with dual impeller (experimental temperature 2 °C)

CHAPTER 8

RESULTS AND DISCUSSION OF METHANE – PROPANE MIXTURE HYDRATE FORMATION WITH AMINO ACIDS

Previous chapters were dedicated to discuss the effect of impeller – baffle configurations on pure methane and methane – propane gas mixture hydrates formation. Distilled water was used as the aqueous phase while forming hydrates from those gas phases. It is a common application to use some chemicals to change the hydrate equilibrium conditions and/or kinetics of hydrate formation. There are three different classes of chemical inhibitors to prevent hydrate formation. Thermodynamic inhibitors aim to change the hydrate equilibrium conditions of a given system, kinetic inhibitors slow down the hydrate formation process and anti-agglomerants prevent the coagulation of already formed hydrate particles. On the other hand, promoters can also be used to increase the hydrate formation rate.

Recently amino acids have been introduced as hydrate promoters and/or inhibitors. In our study five different amino acids were examined and compared about their effectiveness on induction time, hydrate formation rate and overall power consumption. Table 8.1 gives some of the properties of amino acids used in this study.

In total, six hydrate formation experiments of mixture gas (95% methane and 5% propane) have been conducted by using the transparent reactor introduced in Chapter 5.1.1. Table 5.2 gives the dimensions of transparent reactor. An up-pumping pitch blade turbine (PBTU) - full baffle (FB) configuration was used in all experiments.

Experimental procedure of these tests are given in Chapter 5.2.3. It should be noted that the rotation started when the temperature was 2°C and the pressure was 24 bars. One of the six experiments was carried out by using distilled water as base experiment to study the effect of aqueous solutions of 1 weight percent of amino acids.

Table 8.1 Properties of amino acids

	Hydrophobic Classes	Chemical	Density (gr/cm ³)	Solubility (g/L)
L-Lysine	Hydrophilic	Basic	1.237	>1500
L-Histidine	Neutral	Basic	1.412	38.2
L-Serine	Neutral	Hydroxyl	1.582	360
L-Alanine	Hydrophobic	Aliphatic	1.371	166.5
L-Leucine	Hydrophobic	Aliphatic	1.167	18.9

Figure 8.1 presents the induction time of methane-propane hydrate formation of amino acids experiments. All amino acids had induction times shorter than distilled water experiment.

The raw data of pressure - temperature versus time and pressure - torque versus time of all amino acid experiments are presented in Appendix A (Figures A.49 to A.54). Hydrate formation rates of experiments with amino acids are given in Figure 8.2 for 1, 600, 1200 and 1800 seconds. One conclusion that comes out from the mutual analysis of Figures 8.1 and 8.2 is that although hydrophobic compounds may delay hydrate formation compared to other amino acids, they exhibit higher hydrate formations rates compared to hydrophilic or neutral compounds.

Overall power consumption of hydrate formation with amino acids are presented in Figure 8.3. Except L-Lysine all other amino acids had less overall power consumptions compared to distilled water experiment.

These preliminary investigation of the effect of amino acids show that there is a potential to find some amino acids as hydrate promoters.

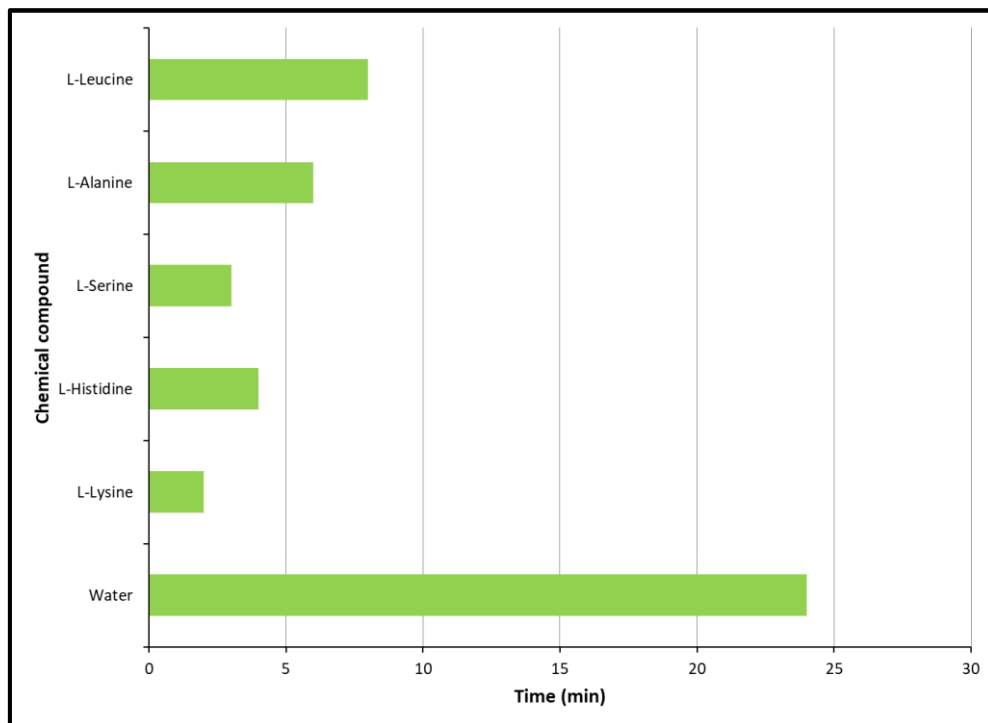


Figure 8.1 Induction time of methane-propane hydrate formation in the presence of only water, L-Leucine, L-Lysine, L-Serine, L-Histidine and L-Alanine.

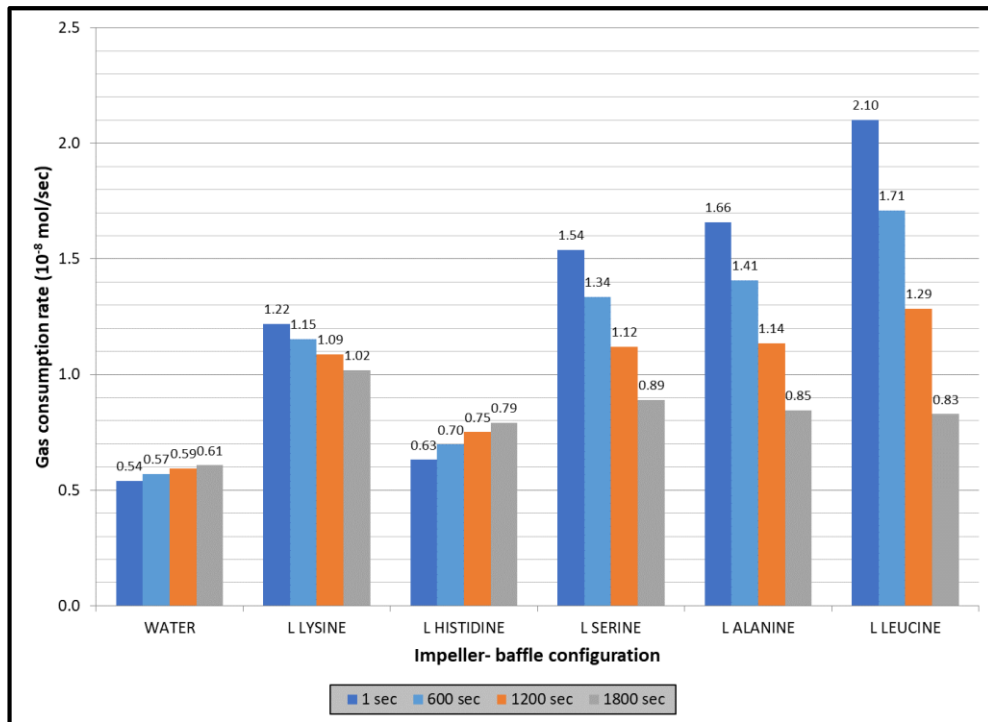


Figure 8.2 Hydrate formation rates of methane-propane mixture and amino acid solutions

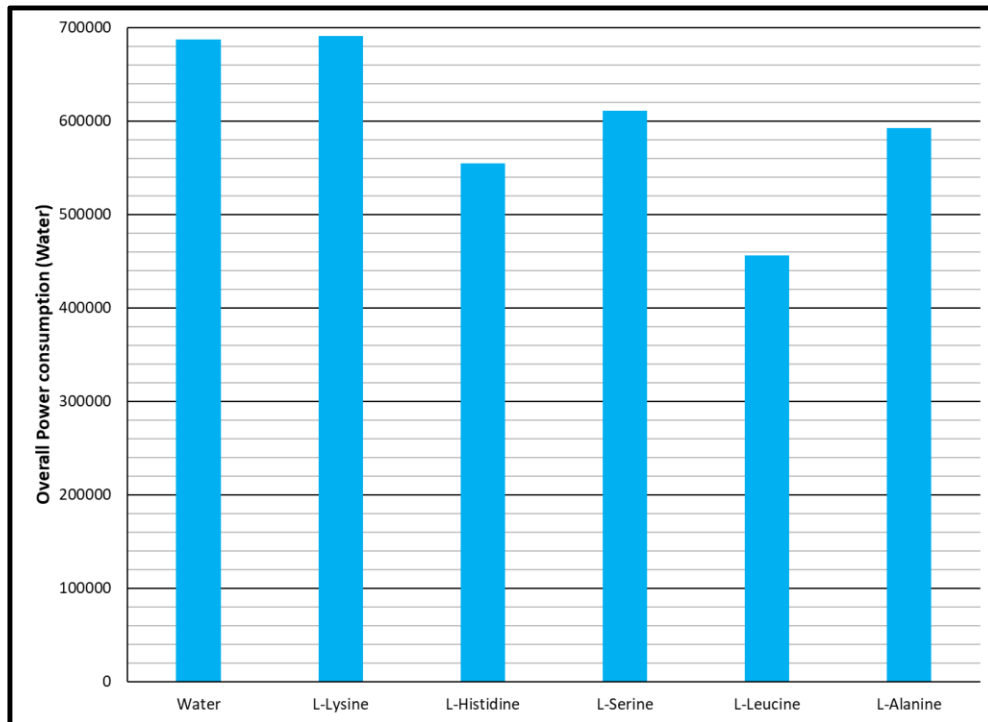


Figure 8.3 Overall power consumption of water and 5 amino acids during hydrate formation process

CHAPTER 9

CONCLUSIONS

This study mainly aimed to promote hydrate formation by investigating the effects of impeller – baffle configurations, and use of water soluble chemicals on the rate of hydrate formation. In order to achieve this goal of study, two stirred tanks were constructed and more than 50 experiments were run by using pure methane or methane – propane mixtures to form hydrates. Distilled water was used in most of the experiments as the water phase of hydrate formation but in 5 experiments, 1 weight percent of different amino acid aqueous solutions were used as the water phase. Under the light of the analysis of the experimental study the following conclusions were drawn:

- Single impeller experiments with methane showed that Rushton turbine (RT) impeller has better performance than up-pumping pitched blade turbine (PBTU) impeller, for all kinds of baffles.
- The produced gas consumption data, from the reactor systems used in this study, fit well to a third order quadratic equation as function of time.
- The initial hydrate formation rate is generally higher with the use of Rushton (RT) turbine as impeller, but the decline rate of hydrate formation also high compared to up-pumping pitched blade turbine (PRBTU).
- The higher decline rate of hydrate formation with higher initial hydrate formation is attributed to the restricted mass transfer between gas and water phases when higher amount of hydrate is formed at the gas - water interface initially. This actually shows the importance of the necessity the immediate and better removal of the solid hydrate particles from the gas – water interface.

- Another important item for the higher decline in hydrate formation is the exothermic nature of hydrate formation. The generated heat by hydrate formation must be removed as efficiently as possible to keep the driving force for hydrate formation at higher values.
- Use of dual impellers, either the same type or mixed, produced similar results of single impeller.
- In pure methane experiments, based on the low overall power consumption and high hydrate productivity, use of RT with full baffles proved to be a better combination for single impeller, for dual impellers and for dual mixed impellers where RT is the lower impeller.
- Hydrate formation process by gas mixtures become more complex because of different partition of gas components in free gas and solid hydrate phases.
- Propane is consumed more if hydrate is formed from a gas mixture of methane – propane. This fact brings another complexity of varying hydrate equilibrium curve during hydrate formation. As propane is consumed, hydrate equilibrium pressure gets higher for the given process temperature.
- Aqueous solutions of amino acids tested in this study showed shorter induction time and generally higher hydrate formation rates compared to distilled water experiment. This indicates a potential of finding hydrate promoters among these amino acids.

CHAPTER 10

RECOMMENDATIONS

This study was carried out by using stirred-tank reactors in batch mode. Although the results are quite satisfactory to delineate the effect of impeller – baffle configurations on the rate of hydrate formation there were some drawbacks mainly arising based on the batch operation mode. It is therefore recommended to operate the system semi-batch or continuous mode of operation.

The first option could be the injection of gas throughout the experiment rather than loading it at the beginning of experiment and run the experiment under constant feed of gas and constant pressure to convert the system into a semi-batch mode.

The second, but more complicated and expensive option is to have continuous mode in which the reactants (aqueous phase and the gas) are continuously flowing into and out of reactor. Since the flowing material out of reactor will be a mixture of water, gas and hydrate a separation operation is needed, firstly to separate the gas. Then, the remaining slurry of water and hydrate can also be separated to sample the hydrate phase for further investigation of hydrate parameters, such as composition of gas trapped in hydrate.

REFERENCES

- [1] E.I.A. US. Annual energy outlook 2016. Washington D.C.: U.S. Department of Energy; 2013.
- [2] ExxonMobil. The outlook for energy: a view to 2040; 2014.
- [3] I.E.A. World energy outlook special report: are we entering the golden age of gas?
Paris, France: International Energy Agency; 2011.
- [4] Englezos P. Clathrate hydrates. *Ind Eng Chem Res* 1993;32:1251–74.
- [5] Sloan Jr ED, Koh CA. Clathrate hydrates of the natural gases. 3rd ed. Boca Raton, FL: CRC Press; 2008.
- [6] Gudmundsson, J. S. Method for production of gas hydrates for transportation and storage. U.S. Patent 5,536,893, July 16, 1996.
- [7] Gudmundsson, J. S.; Parlaktuna, M.; Khokhar, A. Storage of natural gas as frozen hydrate. *SPE Prod. Facil.* 1994, 9, 69–73.
- [8] Kvenvolden, K. A. Gas hydrates-geological perspective and global change. *Rev. Geophys.* 1993, 31, 173–173.
- [9] Veluswamy, H. P.; Kumar, S.; Kumar, R.; Rangsunvigit, P.; Linga, P. Enhanced clathrate hydrate formation kinetics at near ambient temperatures and moderate pressures: Application to natural gas storage. *Fuel* 2016, 182, 907–919.
- [10] Veluswamy, H. P.; Wong, A. J. H.; Babu, P.; Kumar, R.; Kulprathipanja, S.; Rangsunvigit, P.; Linga, P. Rapid methane hydrate formation to develop a cost effective large scale energy storage system. *Chem. Eng. J.* 2016, 290, 161–173.
- [11] Ganji, H.; Manteghian, M.; Sadaghiani zadeh, K.; Omidkhah, M. R.; Rahimi Mofrad, H. Effect of different surfactants on methane hydrate formation rate, stability and storage capacity. *Fuel* 2007, 86, 434–441.
- [12] Kalogerakis, N.; Jamaluddin, A. K. M.; Dholabhai, P. D.; Bishnoi, P. R. Effect of surfactants on hydrate formation kinetics. *Proceedings of the 1993 SPE International Symposium on Oilfield Chemistry, New Orleans, LA, March 2–5, 1993; pp 375–383.*

- [13] Kumar, A.; Bhattacharjee, G.; Kulkarni, B. D.; Kumar, R. Role of Surfactants in Promoting Gas Hydrate Formation. *Ind. Eng. Chem. Res.* 2015, 54, 12217–12232.
- [14] Veluswamy, H. P.; Ang, W. J.; Zhao, D.; Linga, P. Influence of cationic and non-ionic surfactants on the kinetics of mixed hydrogen/ tetrahydrofuran hydrates. *Chem. Eng. Sci.* 2015, 132, 186–199.
- [15] Veluswamy, H. P.; Chen, J. Y.; Linga, P. Surfactant effect on the kinetics of mixed hydrogen/propane hydrate formation for hydrogen storage as clathrates. *Chem. Eng. Sci.* 2015, 126, 488–499.
- [16] Yoslim, J.; Linga, P.; Englezos, P. Enhanced growth of methane–propane clathrate hydrate crystals with sodium dodecyl sulfate, sodium tetradecyl sulfate, and sodium hexadecyl sulfate surfactants. *J. Cryst. Growth* 2010, 313, 68–80.
- [17] Zhong, Y.; Rogers, R. E. Surfactant effects on gas hydrate formation. *Chem. Eng. Sci.* 2000, 55, 4175–4187.
- [18] Mandal, A.; Laik, S. Effect of the Promoter on Gas Hydrate Formation and Dissociation. *Energy Fuels* 2008, 22, 2527–2532.
- [19] Kumar, A.; Kumar, R. Role of Metallic Packing and Kinetic Promoter in Designing a Hydrate-Based Gas Separation Process. *Energy Fuels* 2015, 29, 4463–4471.
- [20] Sa J.H., Kwak G.H., Han K., Ahn D., Cho S.J., Lee D.J., Lee K.H, Inhibition of methane and natural gas hydrate formation by altering the structure of water with amino acids, *Scientific Reports* | 6:31582 | DOI: 10.1038/srep31582
- [21] Prasad P.S.R., Kiran B.S., Are the amino acids thermodynamic inhibitors or kinetic promoters for carbon dioxide hydrates?, *Journal of Natural Gas Science and Engineering* 52 (2018) 461–466
- [22] Bavoh B.C., Lal B., Osei H., Sabil K.M., Mukhar K., A review on the role of amino acids in gas hydrate inhibition, CO₂ capture and sequestration, and natural gas storage, *Journal of Natural Gas Science and Engineering* 64 (2019) 52–71
- [23] Sloan E.D. Natural Gas Hydrates. *JPT SPE Technology Today Series*, SPE 23562, (December 1991), 1414-1417.
- [24] Sloan E.D. *Fundamentals Principles and Applications of Natural Gas Hydrates*. Nature Publishing Group. (20th November 2003), Vol 426, 353-359.

- [25] Makogon, Y. F. Hydrates of Hydrocarbons, Pennwell Books, Tulsa, (1997),482
- [26] Grover T.,Natural Gas Hydrates-Issues for Gas Production And Geomechanical Stability. PhD Thesis.(August 2008), Texas: Texas A & M University, 6.
- [27] Kurihara M., Ouchi H., Narita H., Masuda Y., Gas production from methane hydrate reservoirs, Proceedings of the 7th International Conference on Gas Hydrates (ICGH 2011), Edinburgh, Scotland, United Kingdom, July 17-21, 2011.
- [28] Ikegawa Y., Mitakawa K., Suzuki K., Masuda M., Narita H., Ebinuma T., Hydrates: Experimental Results for Long Term CO₂ Injection Near Methane Hydrate Formations, OTC (Houston 2010), USA 3-6 May 2010
- [29] Fujii K., Yasuda M., Cho B., Ikegami T., Sugiyama H., Imasato Y., Dallimore S.R., Wright F., Development of a Monitoring System For The JOGMEC/NRCAN/AURORA MALLIK Gas Hydrate Production Test Program, Proceedings of the 6th International Conference on Gas Hydrates (ICGH 2008), Vancouver, British Columbia, CANADA, July 6-10, 2008.
- [30] Kurihara M., Sato A., Ouchi H., Narita H., Masuda Y., Saeki T., Fujii T., Prediction of Gas Productivity from Eastern Nankai Trough Methane-Hydrate Reservoirs, SPE 125481
- [31] Makogon, Y.F., Sloan E.D.Phase Equilibrium for Methane Hydrate from 190 to 262 K, J. Chem. Eng. Data 1994, 39, 2, 351-353
- [32] Koh*, Carolyn.A Sloan, E .Dendy, Sum, Amadeu K and Wu, David T.(2011). Fundamentals and Applications of Gas Hydrates.Annu. Rev.Chem.Biomol.Eng vol2, 237-257
- [33] Rees, Emily V.L (March 2009) Methane Gas Hydrate Morphology and its Effect on the Stiffness and Damping of some Sediments. PhD Thesis Southampton: University of Southampton, 9-10
- [34] Miller,Stanley.SL(1969) Clathrate Hydrates of Air in Antarctic Ice, Science New Series, vol 165,No.3892,489-490
- [35] Longinos, Sotirios (May 2015) Analysis of Gas Hydrates by Using Geochemical Instruments. Thesis. Ankara: Middle East Technical University, pp. 6-8

- [36] Sloan E.D., Gas Hydrates: Review of Physical/Chemical Properties, 1998, Energy & Fuels, 12(2)
- [37] Merey, Sukru (May 2014) Instrumental Geochemical Analysis. Thesis. Ankara: Middle East Technical University, 7-8
- [38] Ribeiro C.P., Lage P., Modelling of hydrate formation kinetics: State of the art and future directions, 2008, Chemical Engineering Science 63(8):2007-2034
- [39] Klapp, A. Stephen. (August 2009). Natural Gas Hydrates -from the Microstructure towards a Geological Understanding. PhD Thesis. Bremen: university of Bremen, 1
- [40] Subramanian S., Ballard L.A., Kini R., Dec S.F., Sloan E.D., Structural transitions in methane+ethane gas hydrates - Part I: Upper transition point and applications, 2000a, Chemical Engineering Science 55(23):5763-5771
- [41] Subramanian S., Kini R., Dec S.F., Sloan E.D., Evidence of structure II hydrate formation from methane+ethane mixtures - Part II. Application of statistical mechanics to the study of hydrates of methane, argon, and nitrogen, 2000b, Chemical Engineering Science 55(11)
- [42] Ripmeester, J.A., Tse, J.S., Ratcliffe, C.I., Powell, B.M., 1987. A new clathrate hydrate structure. Nature 325, 135–136.
- [43] Boswell, Ray. Collett, Timothy. Cook, Ann, (2010) Developments in Gas Hydrates, Oil field review, no 1, 18-33
- [44] M. Riedel, R.D. Hyndman, G.D. Spence, N.R. Chapman, I. Novosel, N. Edwards(September 2014) Hydrate on the Cascadia Accretionary margin of North America, AAPG Hedberg Research Conference
- [45] Brooks, JM. Cox, HB. Bryant, WR. Kennicut, MC (1986) Association of Gas Hydrates and Oil Seepage in the Gulf of Mexico, Organic Geochemistry 10, no1-3,221-234
- [46] E. PiNero, M. Marquardt, C. Hensen, M. Haeckel, and K. Wallmann(21 December 2012) Estimation of the global inventory of methane hydrates in marine sediments using transfer functions, Bio geosciences, 10, 959–975
- [47] Merey S., Drilling of Gas Hydrates, Journal of Natural Gas Science and Engineering 35 (2016) 1167-1179

- [48] Wallmann K., Pinero E., Burwicz E., Haeckel M., Hensen C., Dale A., and Ruepke L., The Global Inventory of Methane Hydrate in Marine Sediments: A Theoretical Approach, *Energies* 2012, 5, 2449-2498
- [49] Stern, Laura.A. Circone, Susan. Kirby, Stephen.H. And Durham, William.B. (December 2000) Anomalous Preservation of Pure Methane Hydrate at 1 atm, *J.Phys. Chem.B*, 105, 1756-1762
- [50] Kupeyeva, Aliyeva. (August 2007) Determination of Hydrate Formation Conditions of Drilling Fluids, Master Thesis, Ankara: Middle East Technical University, 7-8
- [51] Gudmundsson, JS. Parlaktuna, M. (1992) Storage natural gas at hydrated conditions. Presented at AIChE Spring Natl. Meet., New Orleans, LA
- [52] Andersson, V. Vibeke, JS. Gudmundsson (2000) Flow Properties of hydrate-in-water slurries. *N.Y.Acad.Sci.* 912:322-29
- [53] Gudmundsson, JS. Andersson, V. Levik, O.I and Mork, M.(2000) Hydrate Technology for capturing stranded gas. *N.Y.Acad.Sci.* 912:403-10
- [54] Watanabe, S. Takahashi, S. Mizubayashi, H. Murata, S. Murakami, H. (2008) A demonstration project of NGH land transportation system. *Proc. Intl. Conf. Gas Hydrates*, 6th, Vancouver. CD-ROM
- [55] Pinnelli S. R. Prasad, Takeshi Sugahara, Amadeu K. Sum E. Dendy Sloan, and Carolyn A. Koh* (2009) Hydrogen Storage in Double Clathrates with tert-Butylamine, *Phys. Chem. A* 113:6540-43
- [56] Kyuchul Shin, Yongkwan Kim, Timothy A. Strobel, P. S. R. Prasad, Takeshi Sugahara, Huen Lee, E. Dendy Sloan, Amadeu K. Sum*, and Carolyn A. Koh* (2009) Tetra-n-butylammonium Borohydride Semiclathrate: A Hybrid Material for Hydrogen Storage, *Phys. Chem. A* 113:6415-18
- [57] Kang, Seong-Pil & Lee*, Huen (2000) Recovery of CO₂ from Flue Gas Using Gas Hydrate: Thermodynamic Verification through Phase Equilibrium Measurements. *Environ.Sci.Technol.* 34:4397-400
- [58] Max MD, Pellenbarg RE. 1999. U.S Patent No 5,873,262
- [59] Max MD, Pellenbarg RE. 2000. U.S Patent No 6,158,239
- [60] Sangwai, JS. Patel, RS. Mekala, Prathyusha. Mech, Deepjyoti. Busch, Marc (December 2013) Desalination Of Sea Water Using Gas Hydrate Technology Current Status & Future Direction, *Proceedings of Hydro 2013 International* 4,

- IIT Madras, Chennai, INDIA XVIII Conference on Hydraulics, Water Resources, Coastal and Environmental Engineering,434-440
- [61] Barduhn, A.J.(1967),Desalination by crystalline process.Chem.Eng.Progr.57:66-71
- [62] Florian Stephan Merkel, Carsten Schmuck, Heyko Jürgen Schultz, Timo Alexander Scholz, and Sven Wolinski (2015)Research on Gas Hydrate Plug Formation under Pipeline-Like Conditions, International Journal of Chemical Engineering, vol 2015,ID:214638,5 pages
- [63] M. Naseer & W. Brandstatter (2011) Hydrate formation in natural gas pipelines, WIT Transactions on Engineering Sciences, Vol 70,261-270
- [64] E.O. Obanijesu, V. Pareek, R. Gubner and M.O. Tade (2011) Hydrate formation and its influence on natural gas pipeline internal corrosion, Nafta 62 (5-6), 164-173
- [65] Jamaluddin, A.K.M. (1991) "Hydrate Plugging Problems in Undersea Natural Gas Pipelines under Shutdown Conditions", J. Pet. Sci. Eng., 5:323-335
- [66] Talaghat, M.R. (2009) Experimental and Theoretical Investigation of Simple Gas Hydrate Formation with or without Presence of Kinetic Inhibitors in a Flow Mini-Loop Apparatus", Fluid Phase Equilibria, Vol 279, Is. 1, 28-40
- [67] Botrel, T. (2001) Offsetting kill and choke lines friction losses, a new method for deep water well control", SPE 67813.
- [68] Jassim, E. and Abdi, M.A. (2008), "A CFD-Based Model to Locate Flow Restriction Induced Hydrate Deposition in Pipelines", Manuscript OTC 19190,Offshore Technology conference, Houston, Texas, USA,OTC 19190
- [69] Obanijesu, E.O. et al., (2010), "Hydrate Formation and its Influence on Natural Gas Pipeline Internal Corrosion Rate", SPE-128544-MS, SPE Oil and Gas India Conference and Exhibition (OGIC), Mumbai,
- [70] Obanijesu, E.O. and Macaulay, S.R.A. (2009), "West African Gas Pipeline (WAGP) Project: Associated Problems and Possible Remedies", E.K Yanful (Ed), Chapter 2, Appropriate Technology for Environmental Protection in the Developing World, Springer Books, Netherlands, 101-112
- [71] McKee. (2007), "Carbon Deposition and the Role of Reducing Agents in Hot-Corrosion Processes", Chemistry and Material Science, 4(8): 1877-1885.

- [72] Kritzer, P. (2004), "Corrosion in High-Temperature and Supercritical Water and Aqueous Solutions: A Review", the Journal of Supercritical Fluids, Vol 29, Is.1-2,1-29.
- [73] International Energy Outlook, Energy Information Administrative, June 2006.
- [74] Seungyong, Chang, (April 2001) Comparing Exploitation and Transportation Technologies for Monetisation of Offshore Stranded Gas, Korea Gas Corporation, R&D Center; SPE 68680
- [75] Subero, Gloria. Sun, Kai. Deshpande, Asim. McLaughlin, John. Economides, Michael.J (2004) A Comparative Study of Sea-Going Natural Gas Transport, SPE Annual Technical Conference and Exhibition held in Houston, Texas, SPE 90243
- [76] H. Najibi*, R. Rezaei, J. Javanmardi, Kh. Nasr far M. Moshfeghian(2008) Economic evaluation of natural gas transportation from Iran's South-Pars gas field to market, Elsevier, Applied Thermal Engineering 29,2009-2015
- [77] Gudmundsson J.S., Oscar F. Graff, Aker Kvaerner (2003) Hydrate Non-Pipeline Technology for Transport of Natural Gas, 22nd World Gas Conference, Tokyo
- [78] Lachet V and Béhar E., (2000) Industrial Perspective on Natural Gas Hydrates, Oil & Gas Science and Technology – Rev. IFP, Vol. 55 (2000), No. 6, 611-616
- [79] Makogon, Y.(2010)Natural Gas Hydrates- A promising source of energy. Natural Gas and Science Engineering, vol 2, 49-59
- [80] Y.F. Makogon*, S.A. Holditch, T.Y. Makogon (2005) Natural gas-hydrates — A potential energy source for the 21st Century, Journal of Petroleum Science and Engineering 56 (2007) ,14–31
- [81] Makogon Y.F.,Holditch S.A.,Perry K.F., Holste J.C., Gas Hydrate Deposits: Formation and Development ,OTC 16677, Houston, Texas, U.S.A., 3–6 May 2004
- [82] Mert, Atilhan. Santiago, Aparicio.Farid, Benyahia and Erhan, Deniz, Natural Gas Hydrates, Advances in Natural Gas Technology, 193-212
- [83] Sang-Yong Lee, Gerald D. Holder* (2001) Methane hydrates potential as a future energy source, Fuel Processing Technology 71,181–186

- [84] Collett, T., Bahk, J. J., Baker, R., Boswell, R., Divins, D., Frye, M., Goldberg, D., Husebø, J., Koh, C., Malone, M., Morell, M., Myers, G., Shipp, C., Torres, M. (2015). Methane hydrates in nature-current knowledge and challenges. *Journal of Chemical and Engineering Data*, 60(2), 319–329.
- [85] Kiani H., A conceptual cost minimization model for estimating methane hydrate upstream activity in NEA for policy-making, *WSEAS Transactions on Business and Economics*, vol 14: 2017, pp. 110-119
- [86] Benoit Beauchamp (2004) Natural gas hydrates: myths, facts and issues, *C. R. Geoscience* 336,751–765
- [87] Power D, Slaterb K, Aldea C, Steve L: Gas Hydrate Inhibited Water-Based Muds for Ultra-Deep water Drilling, AADE-03 -NTCE-48, AADE 2003 Technical Conference, Practical Solutions for Drilling Challenge, Houston, Texas, April 1-3, 2003
- [88] Pakulski M, Qu Q, Pearcy R, Gulf of Mexico Deep water Well Completion with Hydrate Inhibitors, SPE 92971 presented at the 2005 SPE International Symposium on Oilfield Chemistry held in Houston, Texas, U.S.A., 2 – 4 February 2005.
- [89] Nelson R, Flayfall F, Dubois R, A Novel Gas Hydrate Inhibitor for Deep water Frac-Pack and Subsea Environments, SPE 58764 presented at International Formation Symposium on Formation Damage Control, Lafayette, LA Feb. 23-24, 2000
- [90] Talley L.D., Mitchell GF, Application of Proprietary Kinetic Gas Hydrate Inhibitors in Gas Flowlines, OTC 11036, Offshore Technology Conference, Houston TX, May 3-6, 1998
- [91] Sira J.H., Patil S.L. and Kamath V.A, “Study of Hydrate Dissociation by Methanol and Glycol Injection”, SPE 20770, 65th Annual Technical Conference and Exhibition in New Orleans, LA,, 1990
- [92] Pakulski M. and Qu Q. “Hydrate Protection with Heat Producing Three – Component Gas Hydrate Inhibitor” ,7th International Conference on Gas Hydrates (ICGI,2011)Edinburgh, Scotland, United Kingdom, July 17-21, 2011

- [93] Elgibably A.A, Elkamel A.M, "A new correlation for predicting hydrate formation conditions for various gas mixtures and inhibitors", *Fluid Phase Equilibria* 152 (1998) 23-42
- [94] Carson D.B, Katz D.L, Natural gas hydrates, *Trans., AIME* 146 (1942) 150.
- [95] Katz D.L, Predictions of continuous hydrate formation in natural gases, *Trans., AIME* 160 (1945) 140-144
- [96] Holder G.D, Zetts S.P, Pradhan N, Phase behaviour in systems containing clathrate hydrates, *Reviews in Chemical Engineering* 5 (1) (1998)
- [97] Makogon Y.F., Perspectives for the development of Gas Hydrate deposits. Fourth Canadian Permafrost Conference, Calgary, March 2-6, 1981
- [98] Katz D.L., A Look Ahead in Gas Storage Technology. Proceedings AGA Trans. Conference, 1981, T283-T289
- [99] van der Waals J.H., Platteeuw J.C., Clathrate solutions, *Advances in Chemical Physics* 11 (1959) 1-57
- [100] Sloan E.D., A changing hydrate paradigm-from apprehension to avoidance to risk management, *Fluid Phase Equilibria* 228-229 (2005) 67-64
- [101] Ostegaard, K.K., Danesh, A., Tohidi, B., Todd, A.C., Burgass, R.W., 2000. "A general correlation for predicting the hydrate free zone of reservoir fluids" *SPE Prod. Facil.* 15(4), 228-233
- [102] Tahir A.N. "Effect of Polyglycols on Hydrate Formation during Drilling Operations", M.Sc. Thesis, Middle East Technical University, 2005
- [103] Kotkoskle T.S., AL-Ubaldi B., Wildeman T.R., "Inhibition of Gas Hydrates in Water-Based Drilling Muds", *SPE* 20437,1992
- [104] Sum A.K., "Controlling Hydrate Formation in Production Lines", Colorado School of Mines, JEM 2015 Campinas, SP-Brazil
- [105] Fu B., Neff S., Mathur A. and Bakeev K., "Application of Low-Dosage Hydrate Inhibitors in Deep water Operations" Annual Technical Conference and Exhibition, New Orleans, 30 September 2001, *SPE* 78823
- [106] Li G., Li X.S.,* Liang-Guang Tang, and Yu Zhang "Experimental Investigation of Production Behavior of Methane Hydrate under Ethylene Glycol Injection in Unconsolidated Sediment" *Energy & Fuels* 2007,21,3388–3393
- [107] Mohammadi A.H., Afzal W., and Richon D., "Experimental Data and Predictions of Dissociation Conditions for Ethane and Propane Simple Hydrates

- in the Presence of Methanol, Ethylene Glycol, and Triethylene Glycol Aqueous Solutions”, *J. Chem. Eng. Data* 2008,53,683–686
- [108] Mohammadi A.H., Afzal W., and Dominique Richon D.,” Gas hydrates of methane, ethane, propane, and carbon dioxide in the presence of single NaCl, KCl, and CaCl₂ aqueous solutions: Experimental measurements and predictions of dissociation conditions”, *J. Chem. Thermodynamics* 40 (2008) 1693–1697
- [109] Masoudi R., Tohidi B., Anderson R., Burgass R.W., Yang J., “Experimental measurement and thermodynamic modelling of clathrate hydrate equilibria and salt solubility in aqueous ethylene glycol and electrolyte solutions”, *Fluid Phase Equilibria* 219 (2004) 157–163
- [110] Masoudi R., Tohidi B., Danesh A., Todd C.A., Anderson R., Burgass R.W., Jinhai Yang J., “Measurement and prediction of gas hydrate and hydrated salt equilibria in aqueous ethylene glycol and electrolyte solutions”, *Chemical Engineering Science* 60 (2005) 4213–4224
- [111] Kelland A.M., “History of the development of Low Dosage Hydrate Inhibitors”, *Energy and Fuels*, American Chemical Society Journal, Volume 20, Number 3, March 2006
- [112] Villano, L.D., Kommedal, R., Fijten, M.W.M., Schubert, U.S., Hoogenboom, *R., Kelland*, M.A., A Study of the Kinetic Hydrate Inhibitor Performance and Seawater Biodegradability of a Series of Poly(2-alkyl-2-oxazoline)s, *Energy & Fuels* 2009, 23, 3665–3673
- [113] Karaaslan U., Parlaktuna M., “Surfactants as Hydrate Promoters”, *Energy and Fuels* 2000, 14, 1103-1107
- [114] Anderson F.E., Prausnitz J.M., “Inhibition of Gas Hydrates by Methanol”, *AIChE Journal*, August 1986, vol. 32, No 8, pp. 1321-1333.
- [115] Byk, S.S, Fomina V.I., “Gas Hydrates”, *Russ. Chem. Rev.*, 37(6), 469 (1968)
- [116] Chuch, P. L., and J. M. Prausnitz, “Vapor-Liquid Equilibria at High Pressures: Calculation of Partial Molar Volumes in Nonpolar Liquid Mixtures”, *AIChE J.*, 13(6). 1,099 (1967)
- [117] Koh C.A., “Towards a fundamental understanding of natural gas hydrates”, *Chem. Soc. Rev.*, 2002, 31, 157–167

- [118] Amy T.K., Gongmin F., A., Malene W., Mason B.T.,” Effect of Hydrate Inhibitors On Oilfield Scale Formation And Inhibition”, SPE 74657 (2002)
- [119] Fadnes, F.H., Jakobsen, T., Bylov, M., Holset, A., Downs, J.D. (1998): “Studies on the Prevention of Gas Hydrate Formation in Pipelines Using Potassium Formate as a Thermodynamic Inhibitor”, paper SPE 50688, Proc. of the 1998 SPE European Petroleum Conference, The Hague, the Netherlands, 22-22 October, pp. 497-506.
- [120] Hale A.H., Dewan A.K.R., (1990): “Inhibition of Gas Hydrates in Deep water Drilling”, SPEDE June-1990, pp.109-55
- [121] Quigley, M.S. and Hubbard, J.C., (1990), : “Gas Hydrates Formation in Drilling Fluids,” presented at the 1990 Drilling Managers Technical Meeting at Mobil Research and Development Corp., Dallas Research Laboratory (1990).
- [122] Howard, S. K., (1995): “Formate Brine for Drilling and Completion State of the Art”, paper SPE 30498, Proc. of the SPE Annual Technical Conference and Exhibition, Dallas, U.S.A. 22-25 October, pp.483-496.
- [123] Ebeltoft H., Yousif M., Soergaard E., (1997): “Hydrate Control during Deep Water Drilling: Overview and New Drilling Fluids Formulations”, paper SPE 38567, SPE Annual Technical Conference and Exhibition, Texas, 5-8 October.
- [124] Joseph W.K., James B.D., “A Protocol to inhibit the Formation of Natrium Chloride Salt Blocks”, SPE 74662 (2002)
- [125] Amir H. Mohammadi, Ilyas Kraouti, Dominique Richon,”Methane hydrate phase equilibrium in the presence of NaBr, KBr, CaBr₂, K₂CO₃, MgCl₂ aqueous solutions: Experimental measurements and predictions of dissociation conditions”, J. Chem. Thermodynamics 41 (2009) 779-782
- [126] Istomi V.A., Kvon V.G. (2004),” Gas Production: Prevention and Elimination of Gas Hydrates” , Irtc. Gas. Prom.: Moscow.

- [127] M.A. Kelkmd, T.M. Svartaas and L.A. Dybvik, “Control of Hydrate Formation by Surfactants and Polymers” SPE 28506, SPE Annual Technical Conference, New Orleans 1994.
- [128] M.A. Kelland, T.M. Svartaas and L.Dybvik,” A New Generation of Gas Hydrate Inhibitors” , SPE 30695, SPE Annual Technical Conference, Dallas, 1995
- [129] Makogon, T. Y.,Larsen, R.; Knight, C. A.,Sloan, E. D. J.” Crystal Growth “1997, 179, 258-262.
- [130] Zeng, H.; WI, L. D.; Walker, V. K.; Ripmeester, L. A. In Proceedings of the 4th International Conference on Natural Gas Hydrates, Yokohama, Japan, May 19-23, 2002
- [131] Frostman, L. M.; Thieu, V.; Crosby, D. L.; Downs, H. H. “Low-Dosage Hydrate Inhibitors (LDHIs): Reducing Costs in Existing Systems and Designing for the Future” Proceedings of the SPE International Symposium on Oilfield Chemistry, Houston, TX, February 5-8, 2003; SPE 80269
- [132] Sharifi, H. Laboratory Evaluation of Chemical and Biological Kinetic Gas Hydrate Inhibitors. PhD Thesis, University of British Columbia, 2014.
- [133] Klomp, U. “The World of LDHI: From Conception to Development to Implementation”. Proceedings of the 6th International Conference on Gas Hydrates (ICGH 2008); Vancouver, British Columbia, Canada, 2008.
- [134] Sharifi, H.; Ripmeester, J. A.; Walker, V. K.; Englezos, P. “Kinetic Inhibition of Natural Gas Hydrates in Saline Solutions and Heptane”. Fuel 2014, 117, 109–117
- [135] Sharifi, H.; Englezos, P.; Ripmeester, J.; Walker, V. K.,” Evaluation of Kinetic Hydrate Inhibitors in Saline Solutions and n-Heptane”. In Proceedings of the 8th International Conference of Gas Hydrates (ICGH2014); Beijing, China, 2014.
- [136] Shin, K.; Kim, J.; Seo, Y.; Kang, S.-P.” Effect of Kinetic Hydrate Inhibitor and Liquid Hydrocarbon on the Heterogeneous Segregation and Deposition of Gas Hydrate Particles.” Korean J. Chem. Eng. 2014, 31 (12), 2177–2182
- [137] Kelland, M. A. ; Iversen, J. E.” Kinetic Hydrate Inhibition at Pressures up to 760 bar in Deep Water Drilling Fluids”, Energy Fuels 2010, 24 (5), 3003–3013.

- [138] Garcia Chui, J. A.; Ning, F.; Wu, X.; Sun, C.” The Effect of Lecithin and PVP on Gas Hydrate Formation in Water-Based Drilling Fluids for Deep-water Drilling”, In Proceedings of the 8th International Conference on Gas Hydrates; Beijing, China, 2014
- [139] Kelland, M. A.’Production Chemicals for the Oil & Gas Industry’, 2014, second edition, CRC Press
- [140] Klomp, U. “The World of LDHI: From Conception to Development to Implementation”, In Proceedings of the 6th International Conference on Gas Hydrates (ICGH 2008); Vancouver, British Columbia, Canada, 2008
- [141] Ohno, H.; Susilo, R.; Gordienko, R.; Ripmeester, J.; Walker, V. K.” Interaction of Antifreeze Proteins with Hydrocarbon Hydrates”, Chem. - Eur. J. 2010, 16 (34), 10409–10417.
- [142] Gordienko, R.; Ohno, H.; Singh, V. K.; Jia, Z.; Ripmeester, J. A.; Walker, V. K. “Towards a Green Hydrate Inhibitor: Imaging Antifreeze Proteins on Clathrates”, PLoS One 2010, 5 (2), e8953.
- [143] Cruz-Torres, A.; Romero-Martinez, A.; Galano, A.” Computational Study on the Antifreeze Glycoproteins as Inhibitors of Clathrate-Hydrate Formation”, Chem Phys Chem 2008, 9, 1630–1635.
- [144] Nazari, K.; Moradi, M. R.; Ahmadi, A. N.” Kinetic Modeling of Methane Hydrate Formation in the Presence of Low-Dosage-Water- Soluble Ionic Liquids”. Chem. Eng. Technol. 2013, 36 (11), 1915–1923.
- [145] Del Villano, L.; Kelland, M. A.” An Investigation into the Kinetic Hydrate Inhibitor Properties of Two Imidazolium-based Ionic Liquids on Structure II Gas Hydrate”, Chem. Eng. Sci. 2010, 65 (19), 5366–5372.
- [146] Herslund, P. J.; Thomsen, K.; Abildskov, J.; Von Solms, N.; Galfré, A.; Br. ntuas, P.; Kwaterski, M.; Herri, J.-M.” Thermodynamic Promotion of Carbon Dioxide–Clathrate Hydrate Formation by Tetrahydrofuran, Cyclopentane and Their Mixtures”, Int. J. Greenhouse Gas Control 2013, 17, 397–410. (67)
- [147] Llamedo C, M. A.; Yáñez, F.” Innovative Results from the Evaluation of Natural Compounds on Hydrate Formation”, In Proceedings of the 8th International Conference on Gas Hydrates (ICGH8-2014); Beijing, China, 2014.

- [148] Dirdal, E. G.; arulanantham, C.; Sefidroodi, H.; Kelland, M. A. Can ,”Cyclopentane Hydrate Formation Be Used to Rank the Performance of Kinetic Hydrate Inhibitors?” Chem. Eng. Sci. 2012, 82, 177–184.
- [149] Rojas González, Y. V. “Tetrahydrofuran and Natural Gas Hydrates Formation in the Presence of Various Inhibitors”. Ph.D. Thesis, Curtin University of Technology, 2011
- [150] Schrader, G. A. International Patent Application WO/2012/ 041785, 2012.
- [151] Spencer, H. J.; Lehmann, M. N.; Ionescu, T. C.; Garza, T. Z.; Jackson, S. J. International Patent Application WO/2012/135116, 2012.
- [152] Morales, N. L.; Anthony, J.; Garming, J. F. L.; Trompert, R. A.; de Vries, G. J.; Webber, P. A. “A Mature Southern North Sea Asset Considers Conversion to Wet Gas Operation Which Requires the Development of Compatible and Novel Chemistries for Flow- Assurance and Asset Integrity”. In Proceedings of the Offshore Technology Conference; Houston, TX, 2013.
- [153] Menendez, C. M.; Jardine, J.; Mok, W. Y.; Ramachandran, S.; Jovancicevic, V.; Bhattacharya, A. “New Sour Gas Corrosion Inhibitor Compatible with Kinetic Hydrate Inhibitor”, In Proceedings of the International Petroleum Technology Conference; Doha, Qatar, 2014.
- [154] Sloan, E. D. U.S. Patent 5420370, 1995
- [155] O’Reilly, R.; Jeong, N. S.; Chua, P. C.; Kelland, M. A.” Missing Poly (N-vinyl lactam) Kinetic Hydrate Inhibitor: High-Pressure Kinetic Hydrate Inhibition of Structure II Gas Hydrates with Poly- (Nvinylpiperidone) and Other Poly (N-vinyl lactam) Homopolymers”, Energy Fuels 2011, 25, 4595–4599.
- [156] Cohen, J. M.; Wolf, P. F.; Young, W. D. U.S. Patent Application 5723524, 1998.
- [157] Chua, P. C.; Kelland, M. A. “Poly (N-vinyl azacyclooctanone): A More Powerful Structure II Kinetic Hydrate Inhibitor than Poly (Nvinyl caprolactam)”, Energy Fuels 2012, 26, 4481–4485
- [158] O’Reilly R., Jeong N.S., Chua P.C., Kelland M.A., Crystal growth inhibition of tetrahydrofuran hydrate with poly(N-vinyl piperidone) and other poly(N-vinyl lactam) homopolymers, Chemical Engineering Science 66 (2011) 6555–6560
- [159] Klomp, U. C. International Patent Application WO/2001/ 077270, 2001.

- [160] Kelland, M. A.” A Review of Kinetic Hydrate Inhibitors-Tailormade Water-soluble Polymers for Oil and Gas Industry Applications”. In *Advances in Materials Science Research*; Nova Science Publishers, Inc.: New York, NY, 2012; Vol. 8.
- [161] Chua, P. C.; Kelland, M. A.; Ishitake, K.; Satoh, K.; Kamigaito, vM.; Okamoto, Y. “Kinetic Hydrate Inhibition of Poly(Nisopropylmethacrylamide)vs with Different Tacticities”. *Energy Fuels* 2012, 26, 3577–3585.
- [162] Carlise, J. R.; Lindeman, O. E. S.; Reed, P. E.; Conrad, P. G.; Ververs, L. M. International Patent Application WO/2010/045520, 2010.
- [163] Leinweber, D.; Feustel, M. U.S. Patent Application 20090054268, 2009.
- [164] Leinweber, D.; Feustel, M. International Patent Application WO/2007/054226, 2007
- [165] Klug, P.; Kelland, M. A. International Patent Application WO/1998/023843, 1998
- [166] Colle, K. S.; Oelfke, R. H. International Patent Application WO/1996/008673, 1996
- [167] Colle, K. S.; Costello, C. A.; Talley, L. D. Canadian Patent Application 96/2178371, 1996
- [168] Chua, P. C.; Sæbø, M.; Lunde, A.; Kelland, M. A.” Dual Kinetic Hydrate Inhibition and Scale Inhibition by Polyaspartamides”. *Energy Fuels* 2011, 25 (11), 5165–5172.
- [169] Talaghat, M. R.” Experimental Investigation of Gas Consumption for Simple Gas Hydrate Formation in a Recirculation Flow Mini-Loop Apparatus in The presence of Modified Starch as a Kinetic Inhibitor”. *J. Nat. Gas Sci. Eng.* 2013, 14, 42–48.
- [170] Chong, Z. R.; Chan, A. H. M.; Babu, P.; Yang, M.; Linga, P.”Effect of NaCl on Methane Hydrate Formation and Dissociation in Porous Media”. *J. Nat. Gas Sci. Eng.* 2015, 27, 178–189.
- [171] Sa J.H., Lee B.R., Park D.H., Han K., Chun H.D., Lee K.H., Amino Acids as Natural Inhibitors for Hydrate Formation in CO₂ Sequestration, [dx.doi.org/10.1021/es200552c](https://doi.org/10.1021/es200552c) | *Environ. Sci. Technol.* 2011, 45, 5885–5891
- [172] Sa J.H., Kwak G.H., Han K., Ahn D., Cho S.J., Lee D.J., Lee K.H, Inhibition of methane and natural gas hydrate formation by altering the structure

of water with amino acids, Scientific Reports | 6:31582 | DOI: 10.1038/srep31582

- [173] Prasad P.S.R., Kiran B.S., Are the amino acids thermodynamic inhibitors or kinetic promoters for carbon dioxide hydrates?, *Journal of Natural Gas Science and Engineering* 52 (2018) 461–466
- [174] Bavoh B.C., Lal B., Osei H., Sabil K.M., Mukhar K., A review on the role of amino acids in gas hydrate inhibition, CO₂ capture and sequestration, and natural gas storage, *Journal of Natural Gas Science and Engineering* 64 (2019) 52–71
- [175] Royal Society of Chemistry,
<https://www.chemistryworld.com/features/why-are-there-20-amino-acids/3009378.article> [Cited 9 April 2019]
- [176] Fu S.B., Cenegy L.M., Neff C.S., A Summary of Successful Field Applications of A Kinetic Hydrate Inhibitor, SPE 65022
- [177] Kelland, M.A., Svartaas, T.M. and Dybvik, L.A.: “Studies on New Gas Hydrate Inhibitors”, SPE 30420 presented at the 1995 SPE Offshore Europe Conference, Aberdeen, Sept. 5-8.
- [178] Palermo, T. et al.: “Pilot Loop Tests of New Additives Preventing Hydrate Plugs Formation”, paper presented at Multiphase '97 Conference, Cannes.
- [179] Frostman L.M.,”Anti-Agglomerant Hydrate Inhibitors for Prevention of Hydrate Plugs in Deepwater Systems”, SPE 63122, Annual Technical Conference and Exhibition, Dallas, 2000
- [180] Koh C.A., Westacott R.E., Zhang W, Hirachand K, Creek J.L. Soper AK. “Mechanisms of gas hydrate formation and inhibition”, *Fluid Phase Equilibria*. 2002; 194-197 (0): 143-151
- [181] Gao S.,”Hydrate Risk at High Watercuts with Anti-Agglomerant Hydrate Inhibitors”, *Energy & Fuels* 2009, 23, 2118-2121
- [182] Kelland .A., T.M. Svarttaas T.M.M,L. Dybvik L.,” Studies on New Gas Hydrate Inhibitors”, SPE Offshore European Conference, SPE 30420, 1995
- [183] I.F.P.patents:Fr.Pats.2625,527,2625,547,2625,548,2697,264, Eur. Pats .594,579,582,507,323,307, US.Pat.5244,878 and Can.Pats.2036,084)
- [184] Prouzet E., Cot F.,Nabias G., Larbo A., Kooyman P.,

- Pinnavaia T.J., "Assembly of Mesoporous Silica Molecular Sieves Based on Nonionic Ethoxylated Sorbitan Esters as Structure Directors", *Chem. Mater.* 1999, 11, 1498-1503
- [185] Colle, K. S.; Costello, C. A.; Talley, L. D.; Pfeiffer, D. G.; Rabeony, M.; Wright, P. J. WO Patent Application 96/08636, 1996.
- [186] Colle, K. S.; Costello, C. A.; Talley, L. D.; Pfeiffer, D. G.; Rabeony, M.; Wright, P. J. WO Patent Application 96/08456, 1996.
- [187] Malcolm A. Kelland," History of the Development of Low Dosage Hydrate Inhibitors", *Energy & Fuels*, Volume 20, Number 3, 2006
- [188] Pakulski, M. U.S. Patent Application 6331508, 2001.
- [189] Pakulski, M. U.S. Patent European Patent Application 6025302, 2000.
- [190] Pakulski, M.; Dawson, J. C. U.S. Patent Application, 2004/ 0231848, 2004.
- [191] Gao S.,” Hydrate Risk Management at High Watercuts with Anti-agglomerant Hydrate Inhibitors”, *Energy & Fuels* 2009, 23, 2118–2121
- [192] Swanson T.A.,Petrie M., Sifferman T.R.,” The Successful Use of Both Kinetic Hydrate and Paraffin Inhibitors Together in a Deep water Pipeline with a High Water Cut in the Gulf of Mexico” , SPE 93158, Symposium on Oilfield Chemistry, Houston, Texas, 2005
- [193] Kalogerakis N, Jamaluddin AKM, Dholabhai PD, Bishnoi PR. Effect of surfactants on hydrate formation kinetics. Society of Petroleum Engineers; 1993.
- [194] Ando N, Kuwabara Y, Mori YH. Surfactant effects on hydrate formation in an unstirred gas/liquid system: An experimental study using methane and micelle forming surfactants. *Chem Eng Sci* 2012;73:79–85.
- [195] Daimaru T, Yamasaki A, Yanagisawa Y. Effect of surfactant carbon chain length on hydrate formation kinetics. *J Petrol Sci Eng* 2007;56:89–96
- [196] Okutani K, Kuwabara Y, Mori YH. Surfactant effects on hydrate formation in an unstirred gas/liquid system: An experimental study using methane and sodium alkyl sulfates. *Chem Eng Sci* 2008; 63:183–94.
- [197] Dicharry C, Diaz J, Torr  J-P, Ricaurte M. Influence of the carbon chain length of a sulfate-based surfactant on the formation of CO₂, CH₄ and CO₂–CH₄ gas hydrates. *Chem Eng Sci* 2016; 152:736–45.

- [198] Wang F, Jia Z-Z, Luo S-J, Fu S-F, Wang L, Shi X-S, et al. Effects of different anionic surfactants on methane hydrate formation. *Chem Eng Sci* 2015; 137: 896–903
- [199] Di Profio P, Arca S, Germani R, Savelli G. Novel nanostructured media for gas storage and transport: clathrate hydrates of methane and hydrogen. *J Fuel Cell Sci Technol* 2007; 4:49–55
- [200] Du J, Li H, Wang L. Effects of ionic surfactants on methane hydrate formation kinetics in a static system. *Adv Powder Technol* 2014; 25:1227–33.
- [201] Fazlali A, Kazemi S-A, Keshavarz-Moraveji M, Mohammadi AH. Impact of different surfactants and their mixtures on methane-hydrate formation. *Energy Technol* 2013; 1:471–7
- [202] Link DD, Ladner EP, Elsen HA, Taylor CE. Formation and dissociation studies for optimizing the uptake of methane-by-methane hydrates. *Fluid Phase Equilib* 2003; 211:1–10.
- [203] Saw VK, Gudala M, Udayabhanu G, Mandal A, Laik S. Kinetics of methane hydrate formation and its dissociation in presence of non-ionic surfactant Tergitol. *J Unconventional Oil Gas Resources* 2014; 6:54–9.
- [204] Sa J.H., Lee B.R., Park D.H., Han K., Chun H.D., Lee K.H., Amino Acids as Natural Inhibitors for Hydrate Formation in CO₂ Sequestration, [dx.doi.org/10.1021/es200552c](https://doi.org/10.1021/es200552c) | *Environ. Sci. Technol.* 2011, 45, 5885–5891
- [205] Sa J.H., Kwak G.H., Han K., Ahn D., Cho S.J., Lee D.J., Lee K.H, Inhibition of methane and natural gas hydrate formation by altering the structure of water with amino acids, *Scientific Reports* | 6:31582 | DOI: 10.1038/srep31582
- [206] Prasad P.S.R., Kiran B.S., Are the amino acids thermodynamic inhibitors or kinetic promoters for carbon dioxide hydrates?, *Journal of Natural Gas Science and Engineering* 52 (2018) 461–466
- [207] Bavoh B.C., Lal B., Osei H., Sabil K.M., Mukhar K., A review on the role of amino acids in gas hydrate inhibition, CO₂ capture and sequestration, and natural gas storage, *Journal of Natural Gas Science and Engineering* 64 (2019) 52–71

- [208] Mohammad-Taheri M, Moghaddam A.Z., Nazari K, Zanjani N.G., Methane hydrate stability in the presence of water-soluble hydroxyalkyl cellulose. *J Nat Gas Chem* 2012; 21:119–25.
- [209] Al-Adel S. The effect of biological and polymeric inhibitors on methane gas hydrates growth kinetics. Canada: McGill University; 2007.
- [210] Karaaslan U., Parlaktuna M., Promotion effect of polymers and surfactants on hydrate formation rate. *Energy Fuels* 2002; 16:1413–6.
- [211] Fakharian H, Ganji H, Naderi Far A, Kameli M. Potato starch as methane hydrate promoter. *Fuel* 2012; 94:356–60.
- [212] Ganji H, Manteghian M, Rahimi Mofrad H. Effect of mixed compounds on methane hydrate formation and dissociation rates and storage capacity. *Fuel Process Technol* 2007; 88:891–5.
- [213] Maghsoodloo B.S., Alamdari A. Effect of maize starch on methane hydrate formation/dissociation rates and stability. *J Nat Gas Sci Eng* 2015; 26:1–5.
- [214] Linga P., Daraboina N., Ripmeester J.A., Englezos P., Enhanced rate of gas hydrate formation in a fixed bed column filled with sand compared to a stirred vessel, *Chemical Engineering Science* 68 (2012) 617–623
- [215] Linga P., Kumar R., Lee J.D., Ripmeester J., Englezos P., A New Apparatus to Enhance the Rate of Gas Hydrate Formation: Application to capture of carbon dioxide, *International Journal of Greenhouse Gas Control*, 4 (2010) 630-637

APPENDICES

APPENDIX-A

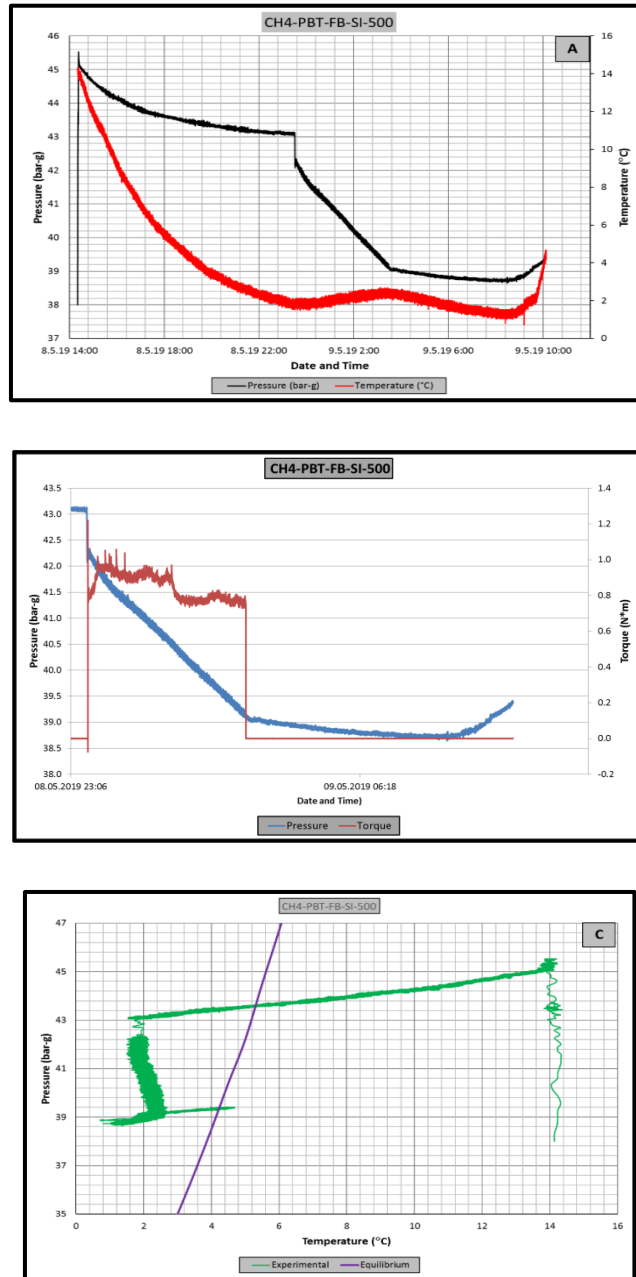


Figure A.1 Raw data of experiment CH4-PBT-FB-SI-500. A: Pressure – temperature vs. time graph, B: Pressure – torque vs. time graph, C: Pressure vs. temperature graph

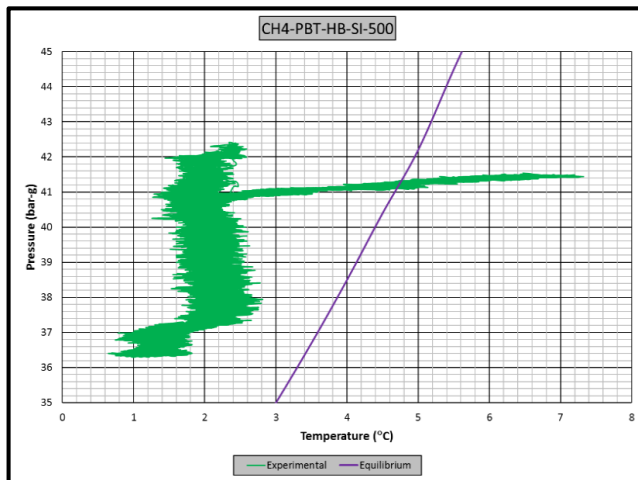
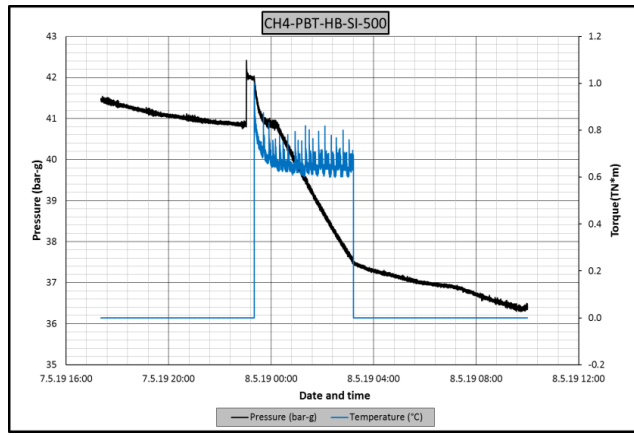
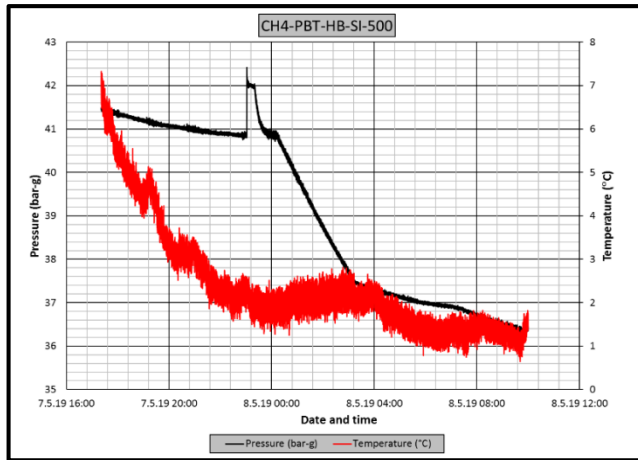


Figure A.2 Raw data of experiment CH4-PBT-HB-SI-500. A: Pressure – temperature vs. time graph, B: Pressure – torque vs. time graph, C: Pressure vs. temperature graph

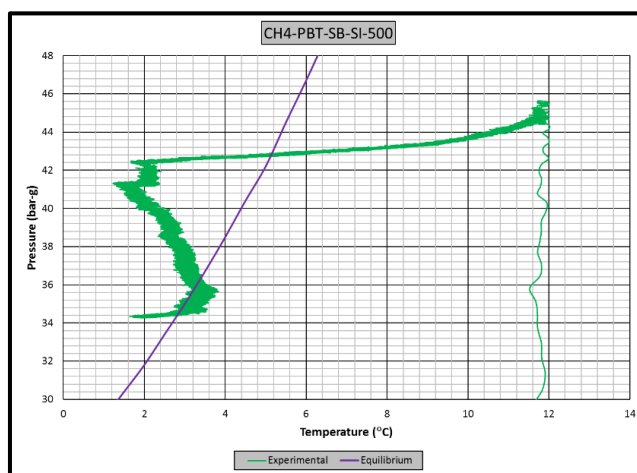
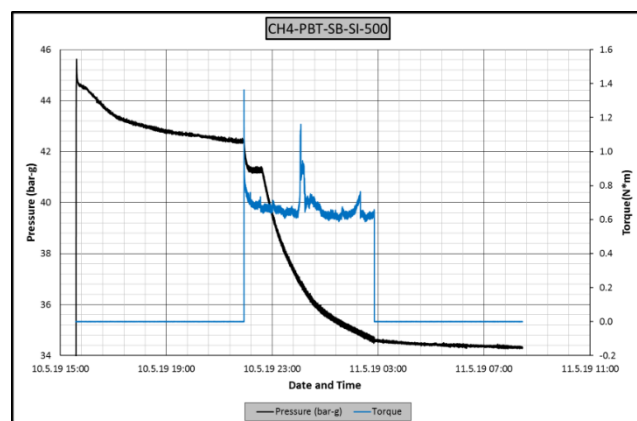
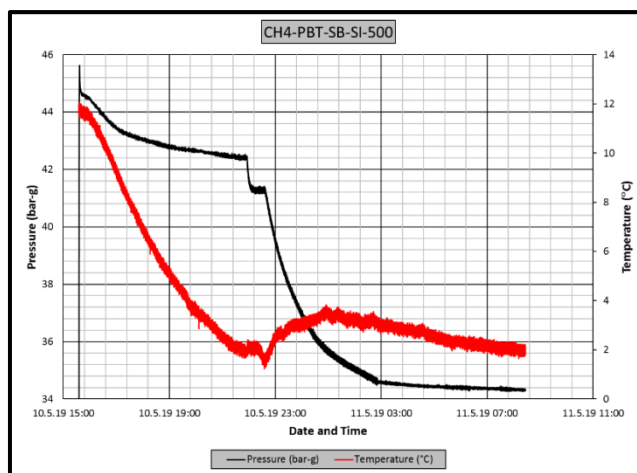


Figure A.3 Raw data of experiment CH4-PBT-SB-SI-500. A: Pressure – temperature vs. time graph, B: Pressure – torque vs. time graph, C: Pressure vs. temperature graph

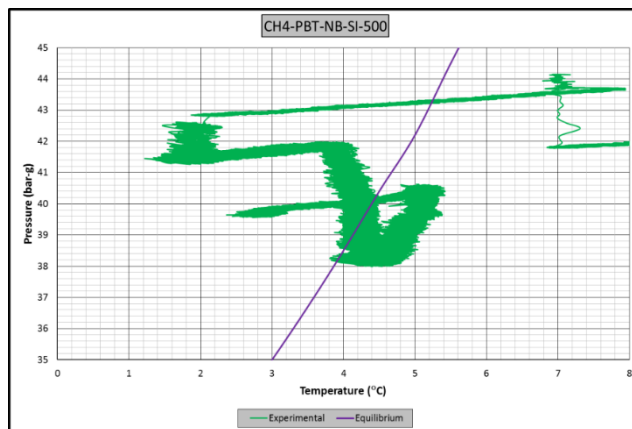
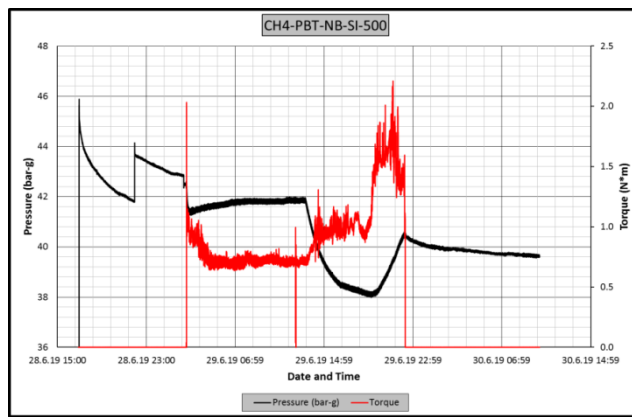
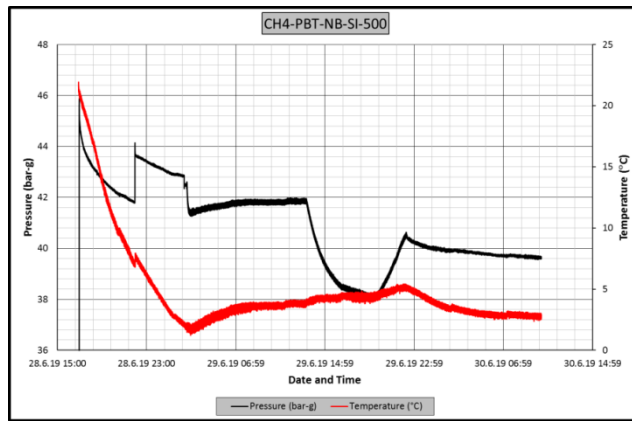


Figure A.4 Raw data of experiment CH4-PBT-NB-SI-500. A: Pressure – temperature vs. time graph, B: Pressure – torque vs. time graph, C: Pressure vs. temperature graph

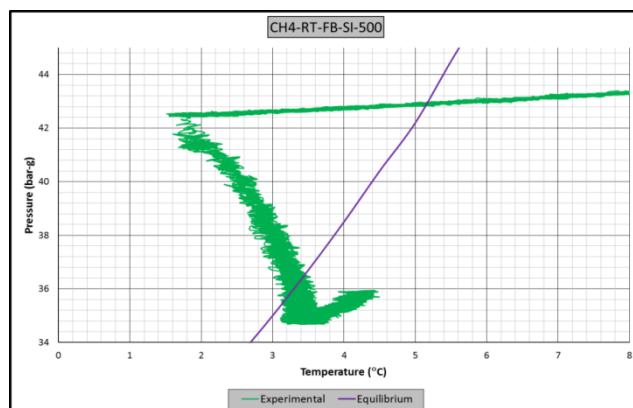
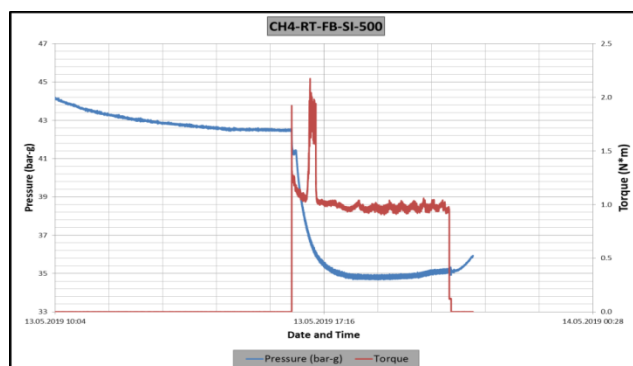
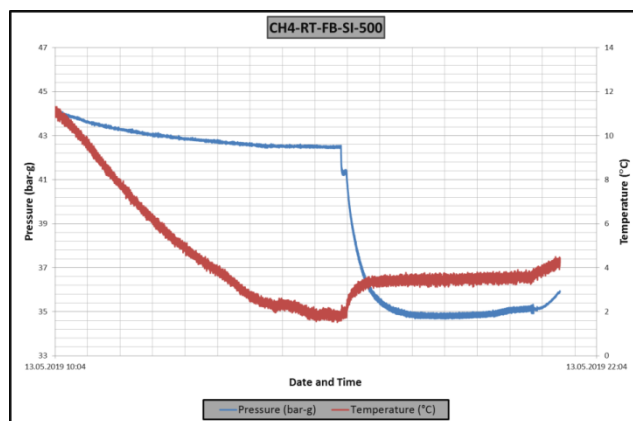


Figure A.5 Raw data of experiment CH4-RT-FB-SI-500. A: Pressure – temperature vs. time graph, B: Pressure – torque vs. time graph, C: Pressure vs. temperature graph

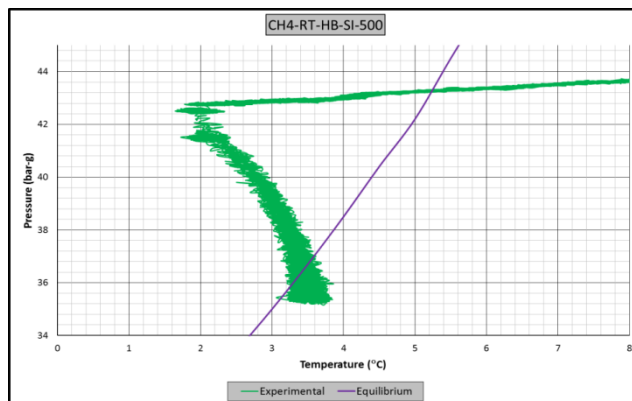
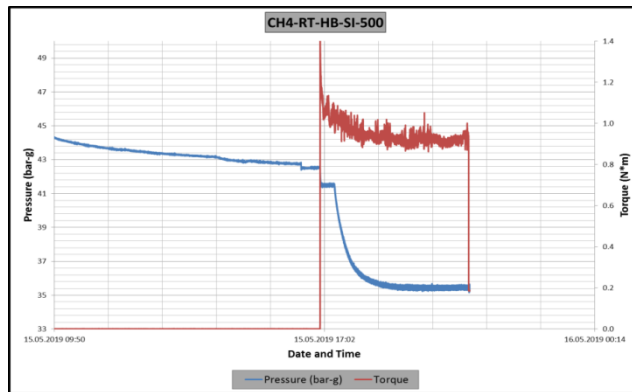
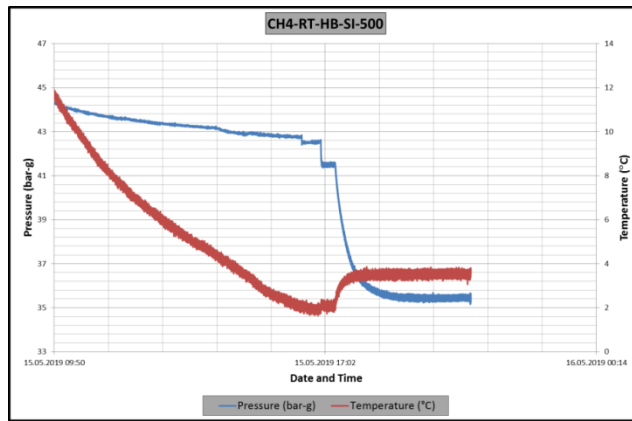


Figure A.6 Raw data of experiment CH4-RT-HB-SI-500. A: Pressure – temperature vs. time graph, B: Pressure – torque vs. time graph, C: Pressure vs. temperature graph

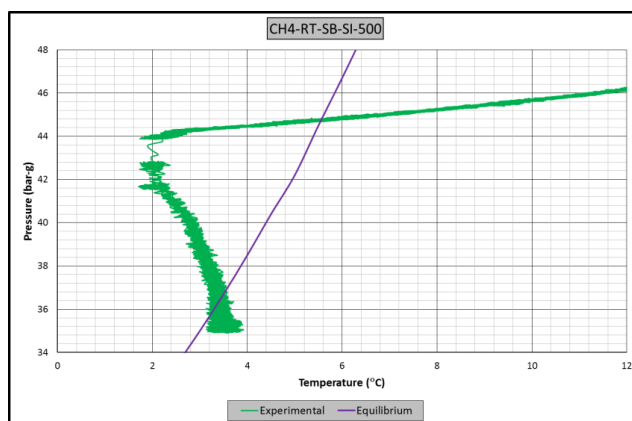
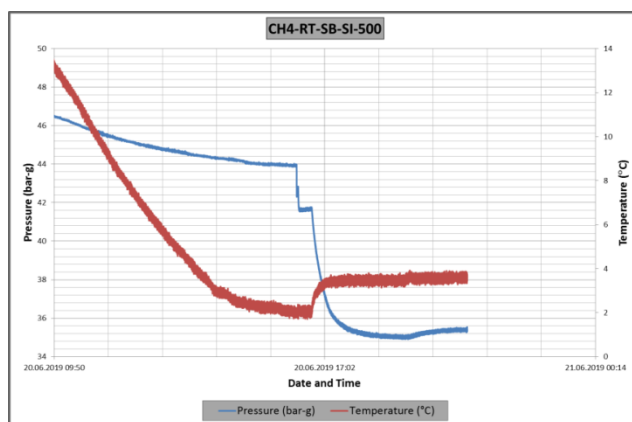
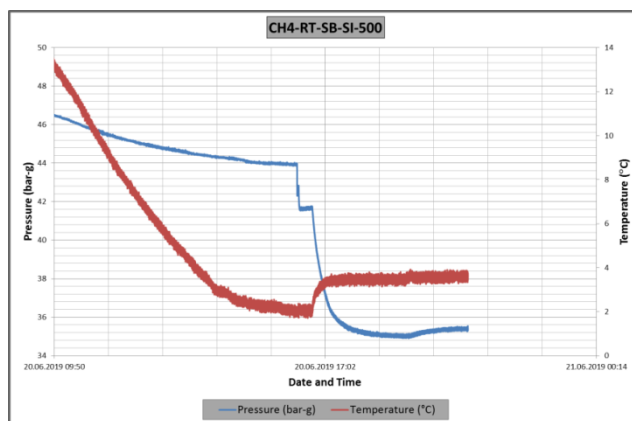


Figure A.7 Raw data of experiment CH4-RT-SB-SI-500. A: Pressure – temperature vs. time graph, B: Pressure – torque vs. time graph, C: Pressure vs. temperature graph

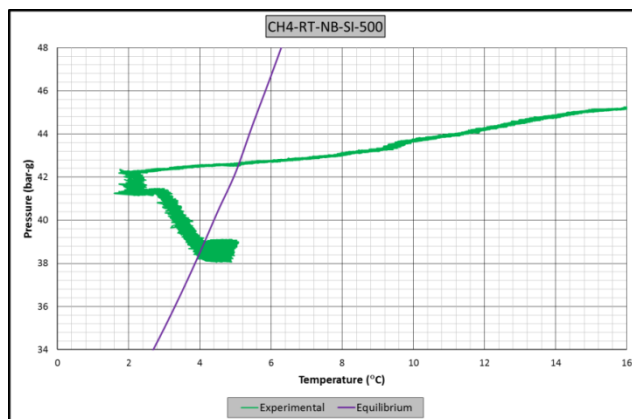
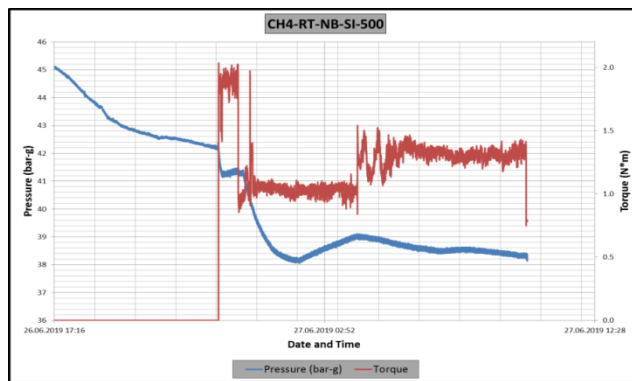
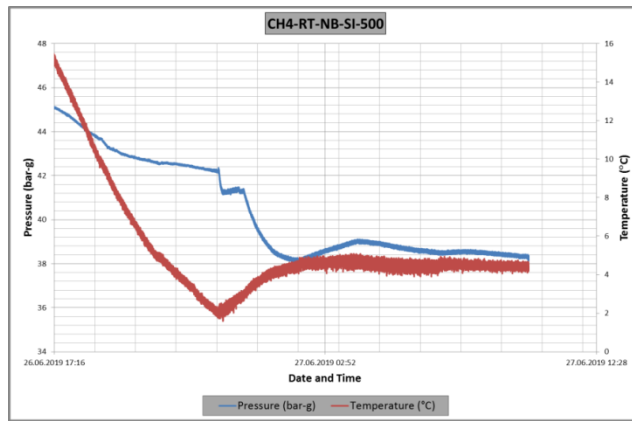


Figure A.8 Raw data of experiment CH4-RT-NB-SI-500. A: Pressure – temperature vs. time graph, B: Pressure – torque vs. time graph, C: Pressure vs. temperature graph

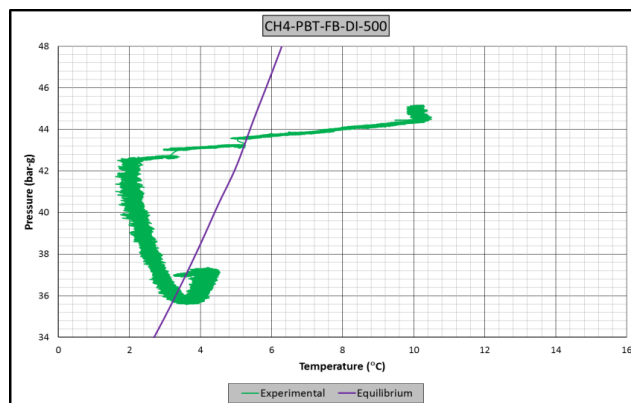
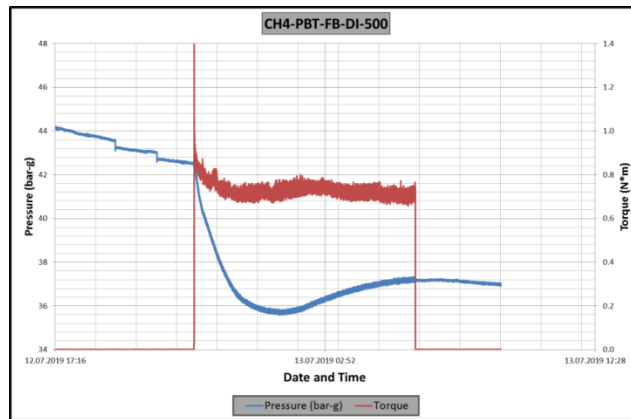
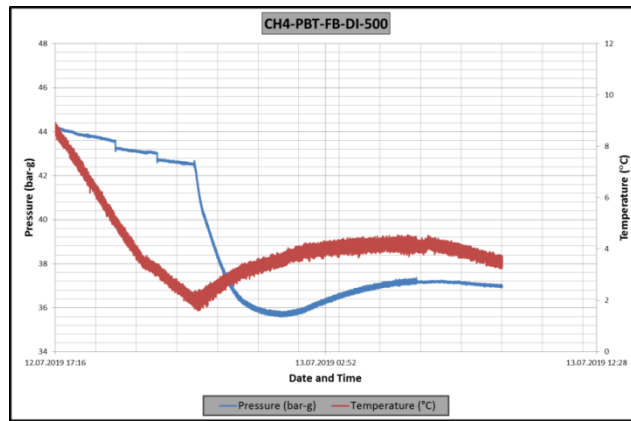


Figure A.9 Raw data of experiment CH4-PBT-FB-DI-500. A: Pressure – temperature vs. time graph, B: Pressure – torque vs. time graph, C: Pressure vs. temperature graph

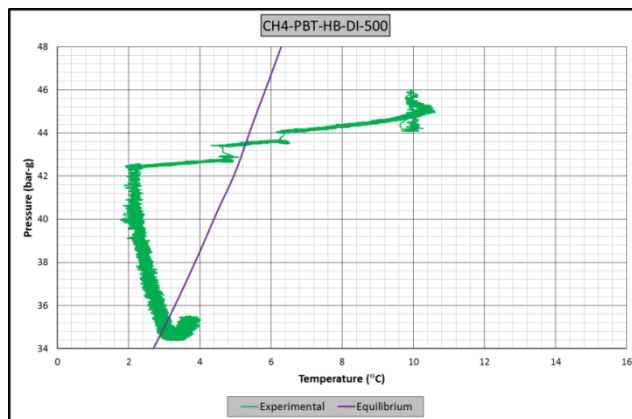
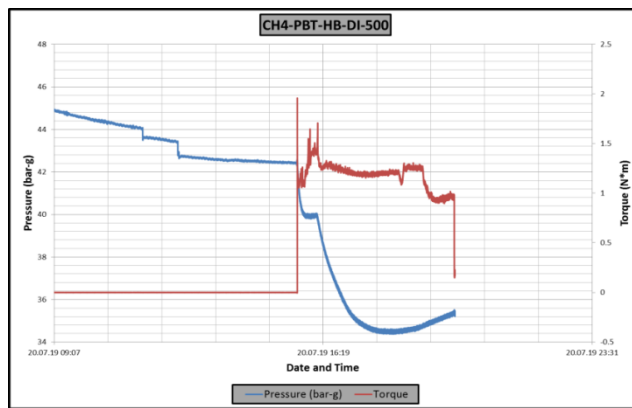
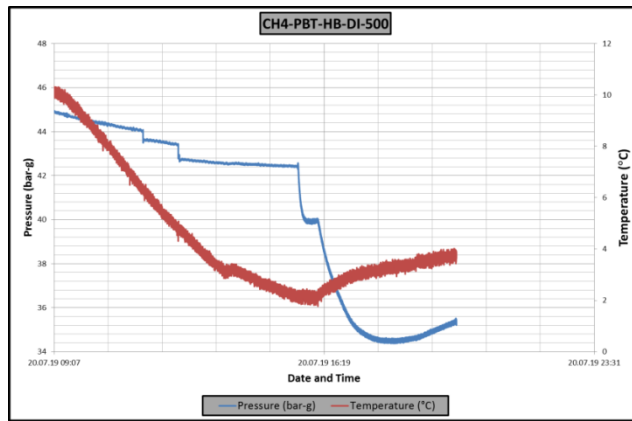


Figure A.10 Raw data of experiment CH4-PBT-HB-DI-500. A: Pressure – temperature vs. time graph, B: Pressure – torque vs. time graph, C: Pressure vs. temperature graph

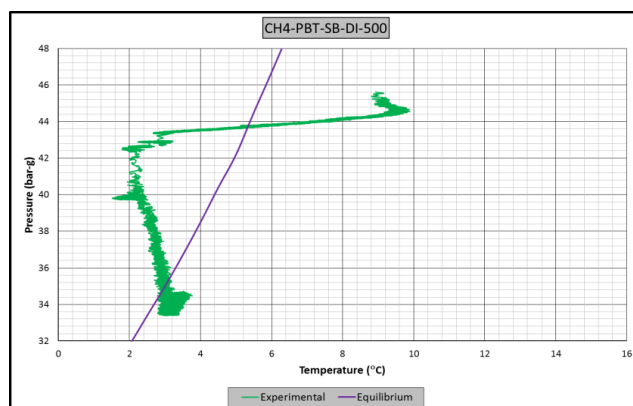
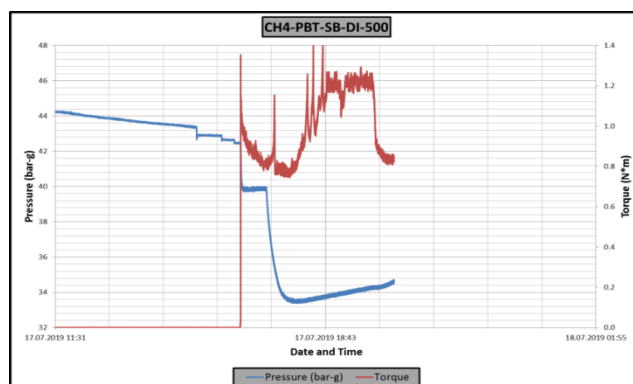
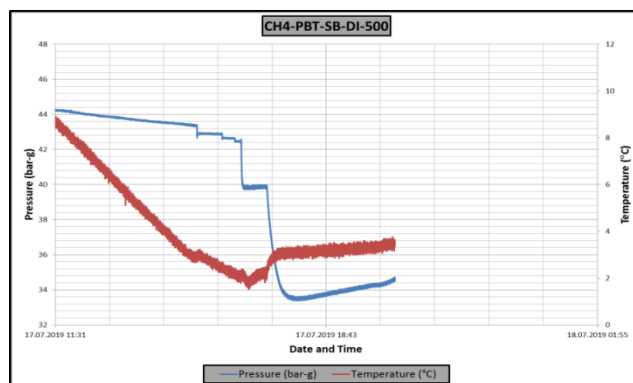


Figure A.11 Raw data of experiment CH4-PBT-SB-DI-500. A: Pressure – temperature vs. time graph, B: Pressure – torque vs. time graph, C: Pressure vs. temperature graph

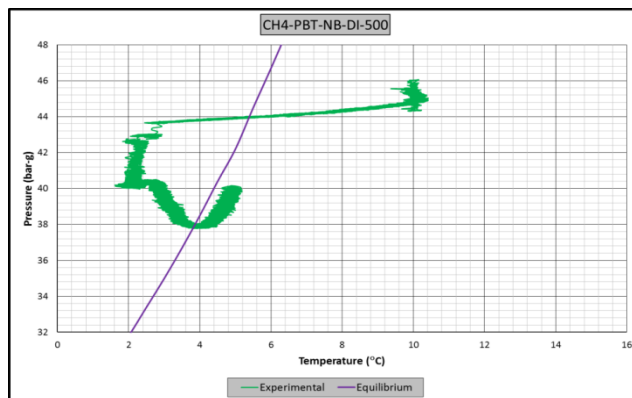
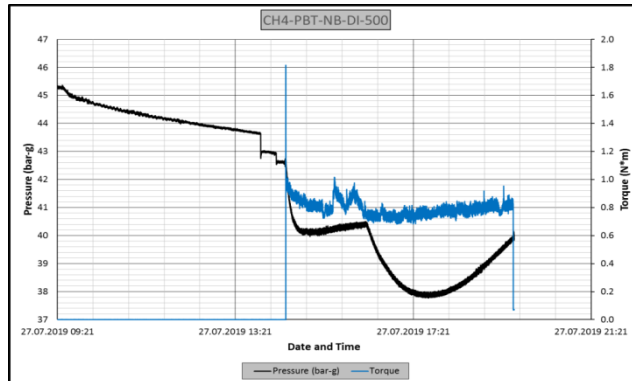
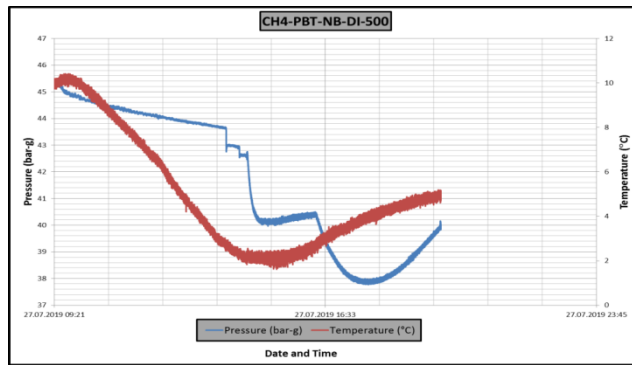


Figure A.12 Raw data of experiment CH4-PBT-NB-DI-500. A: Pressure – temperature vs. time graph, B: Pressure – torque vs. time graph, C: Pressure vs. temperature graph

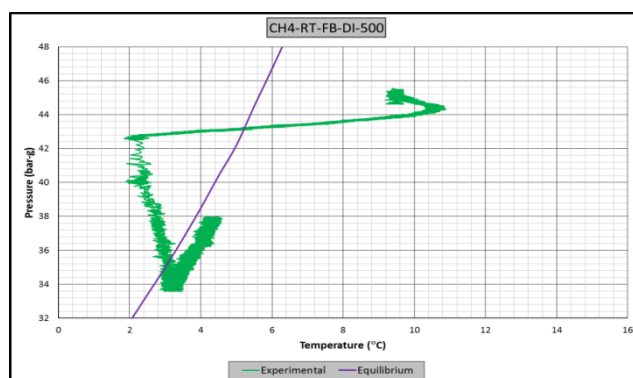
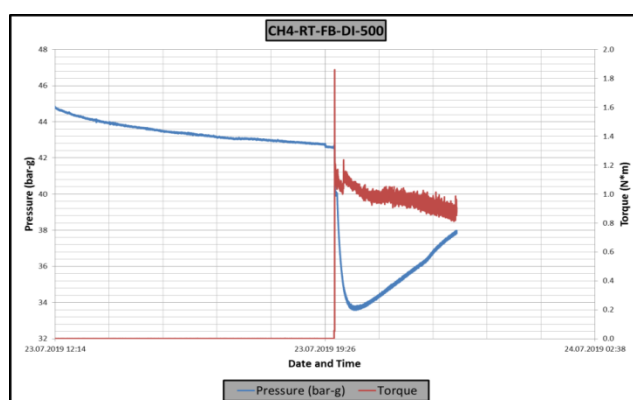
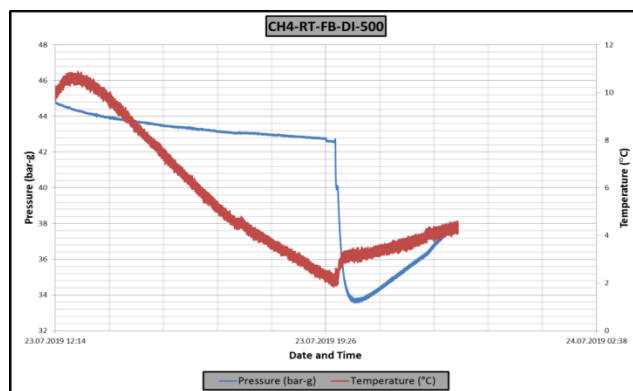


Figure A.13 Raw data of experiment CH4-RT-FB-DI-500. A: Pressure – temperature vs. time graph, B: Pressure – torque vs. time graph, C: Pressure vs. temperature graph

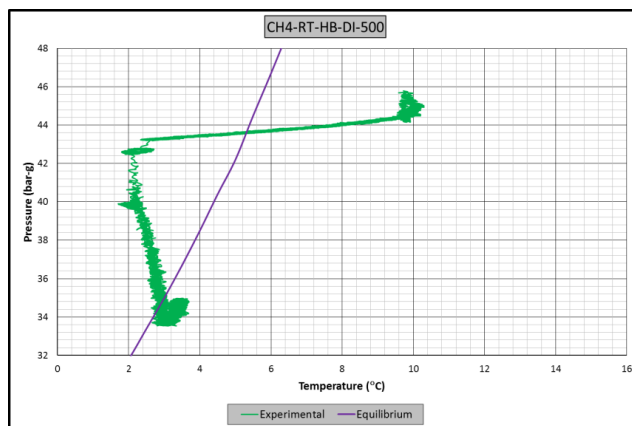
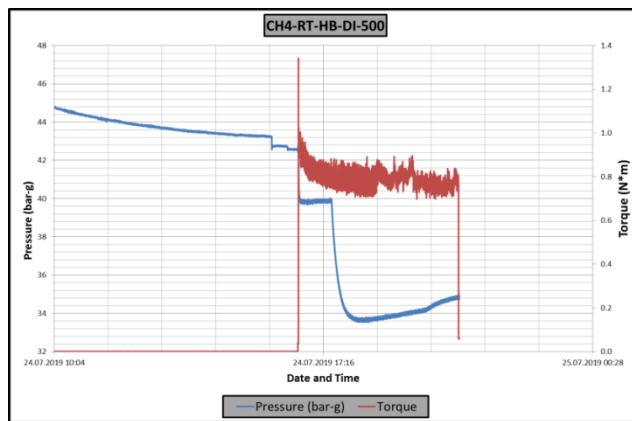
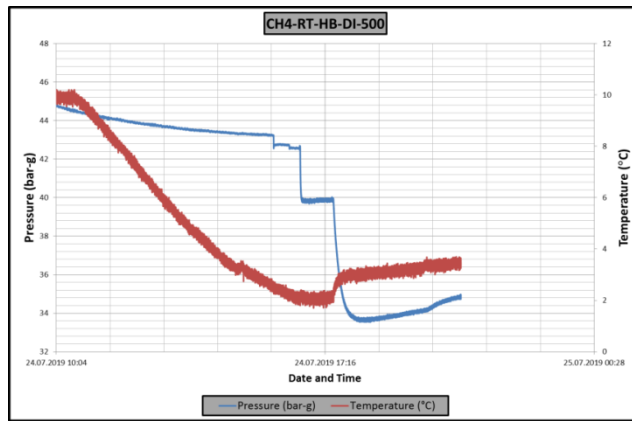


Figure A.14 Raw data of experiment CH4-RT-HB-DI-500. A: Pressure – temperature vs. time graph, B: Pressure – torque vs. time graph, C: Pressure vs. temperature graph

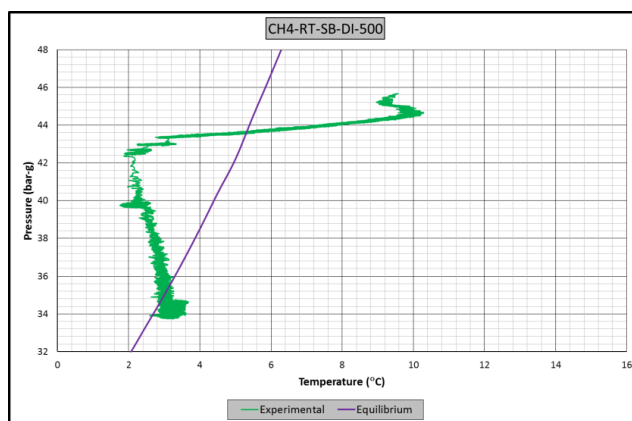
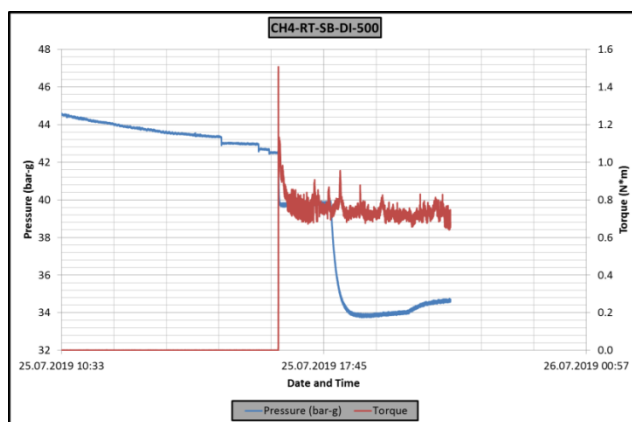
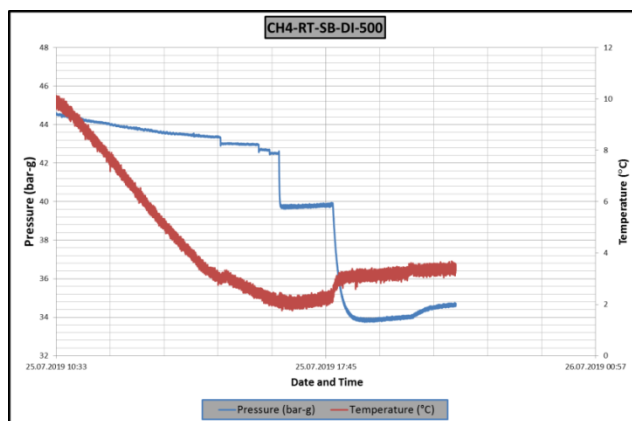


Figure A.15 Raw data of experiment CH4-RT-SB-DI-500. A: Pressure – temperature vs. time graph, B: Pressure – torque vs. time graph, C: Pressure vs. temperature graph

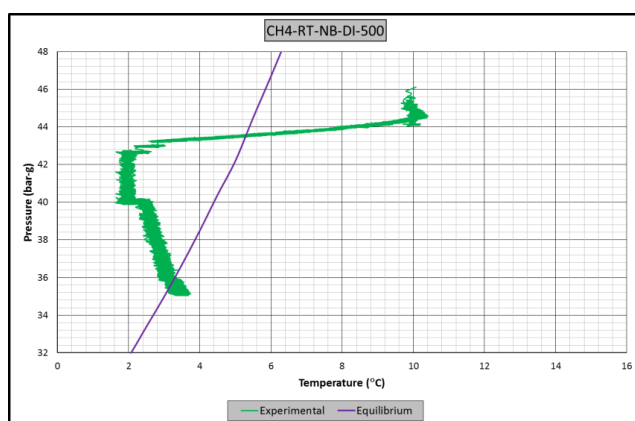
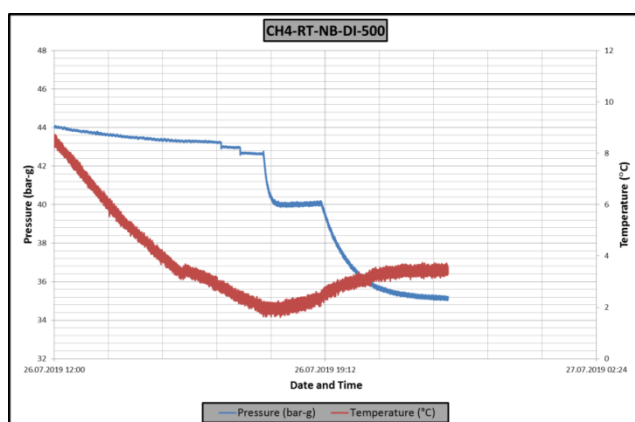
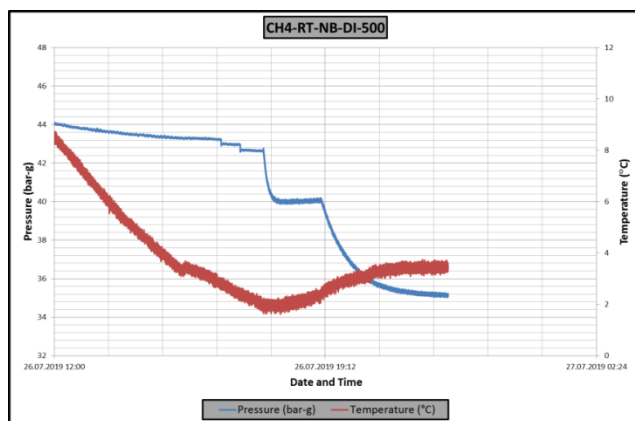


Figure A.16 Raw data of experiment CH4-RT-NB-DI-500. A: Pressure – temperature vs. time graph, B: Pressure – torque vs. time graph, C: Pressure vs. temperature graph

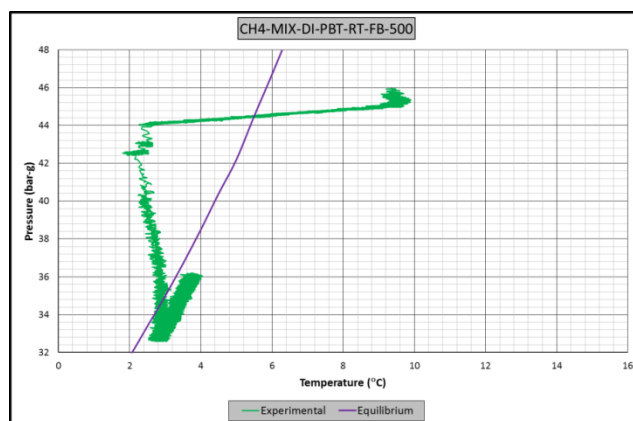
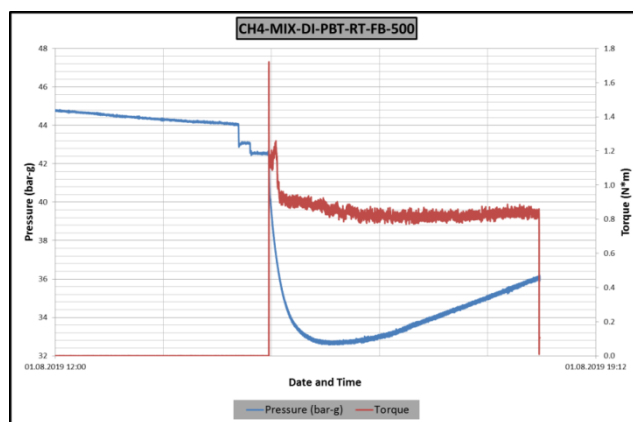
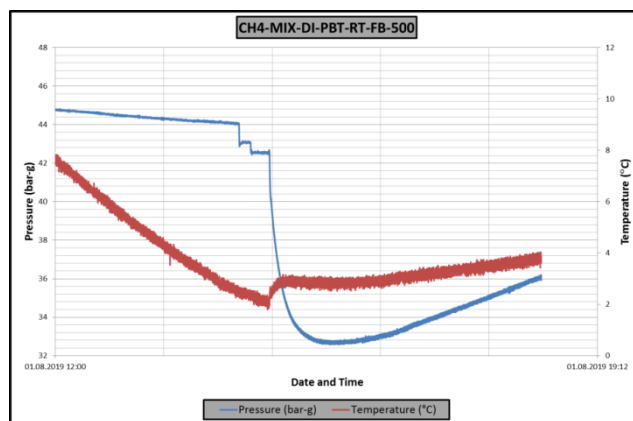


Figure A.17 Raw data of experiment CH4-PBT-RT-FB-MIX-DI-500. A: Pressure – temperature vs. time graph, B: Pressure – torque vs. time graph, C: Pressure vs. temperature graph

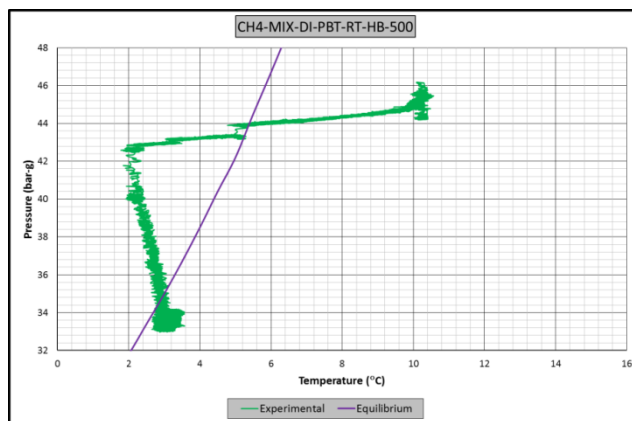
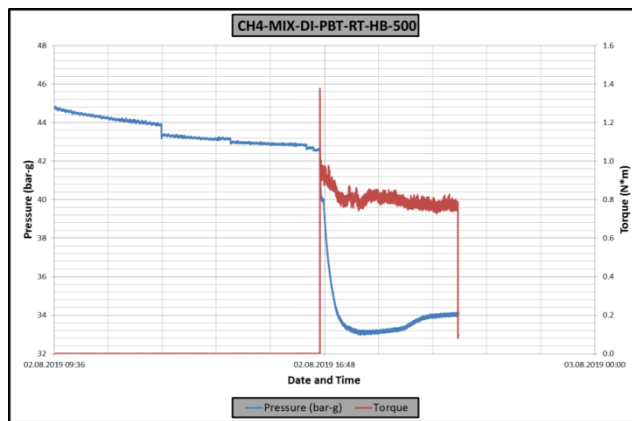
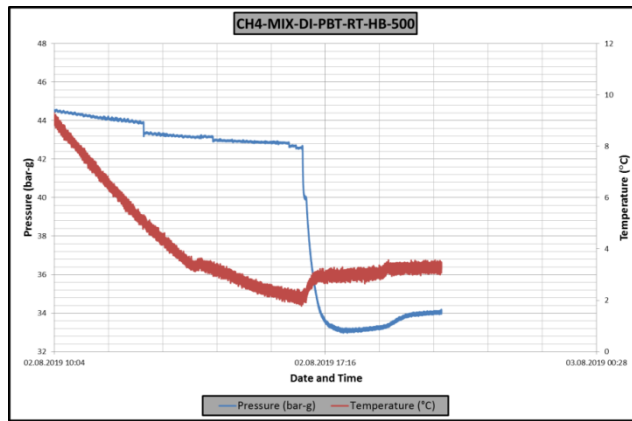


Figure A.18 Raw data of experiment CH4-PBT-RT-HB-MIX-DI-500. A: Pressure – temperature vs. time graph, B: Pressure – torque vs. time graph, C: Pressure vs. temperature graph

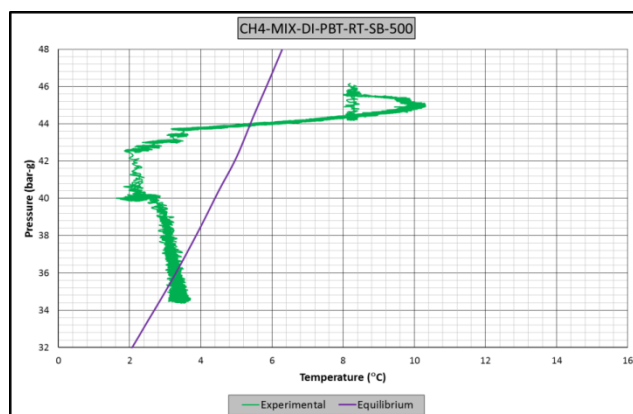
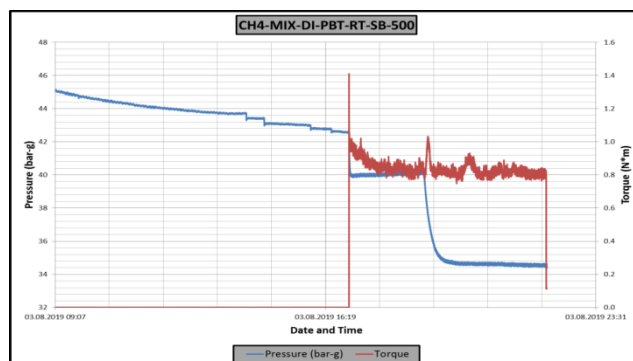
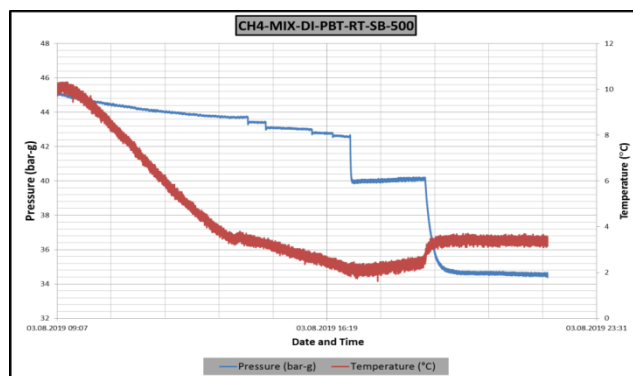


Figure A.19 Raw data of experiment CH4-PBT-RT-SB-MIX-DI-500. A: Pressure – temperature vs time graph, B: Pressure – torque vs. time graph, C: Pressure vs. temperature graph

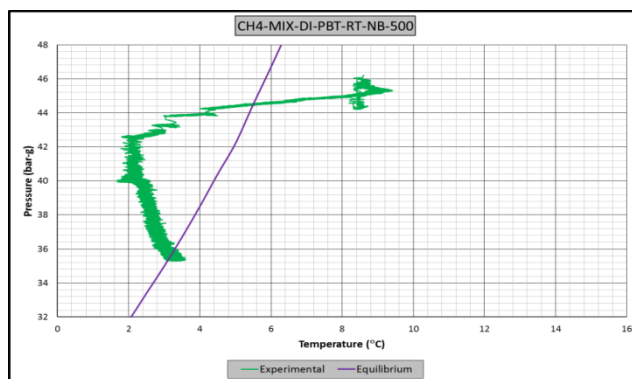
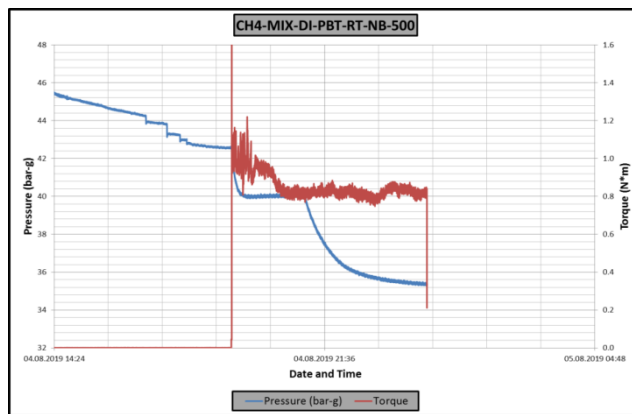
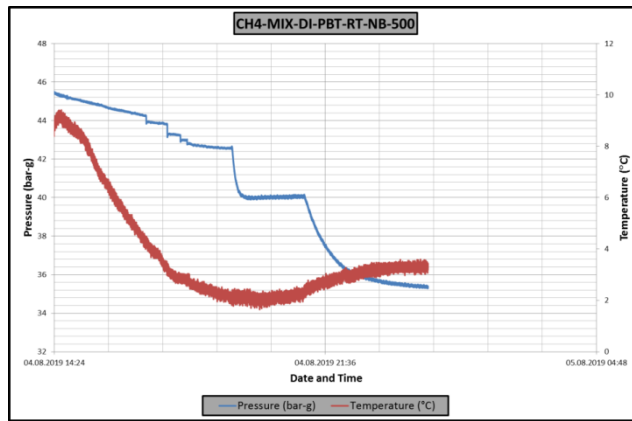


Figure A.20 Raw data of experiment CH4-PBT-RT-NB-MIX-DI-500. A: Pressure – temperature vs. time graph, B: Pressure – torque vs. time graph, C: Pressure vs. temperature graph

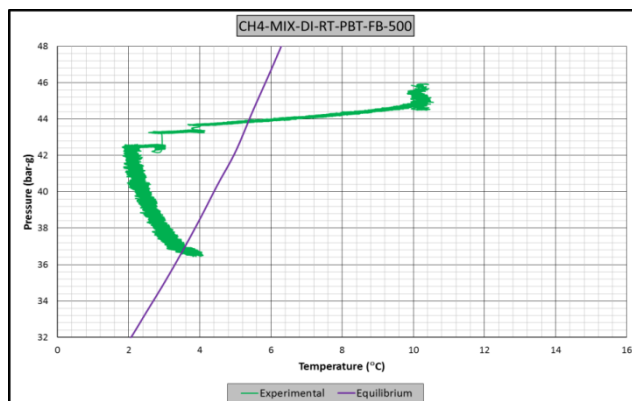
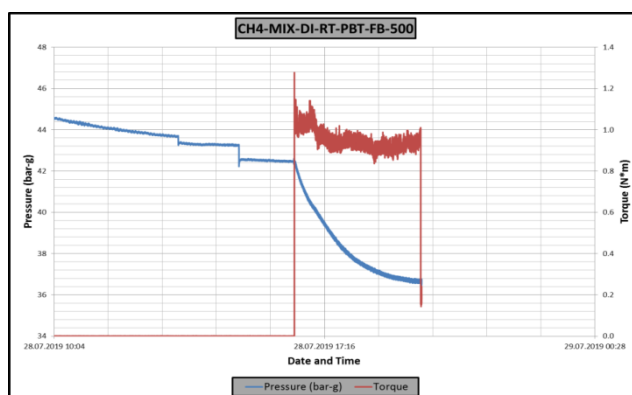
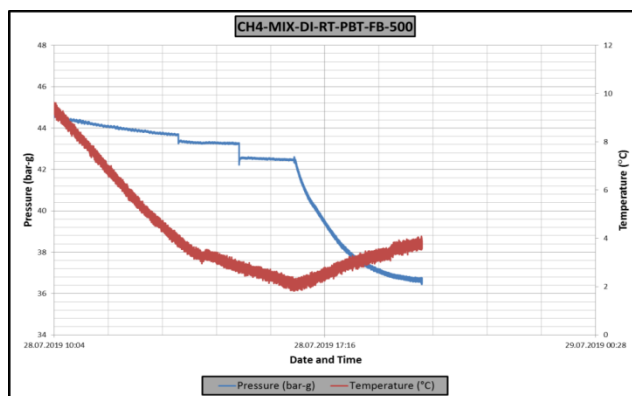


Figure A.21 Raw data of experiment CH4-RT-PBT-FB-MIX-DI-500. A: Pressure – temperature vs. time graph, B: Pressure – torque vs. time graph, C: Pressure vs. temperature graph

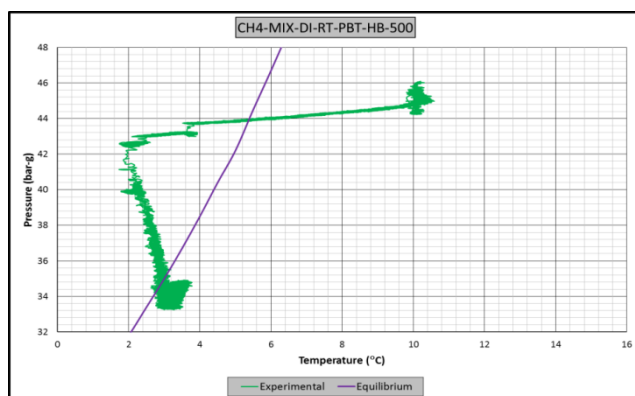
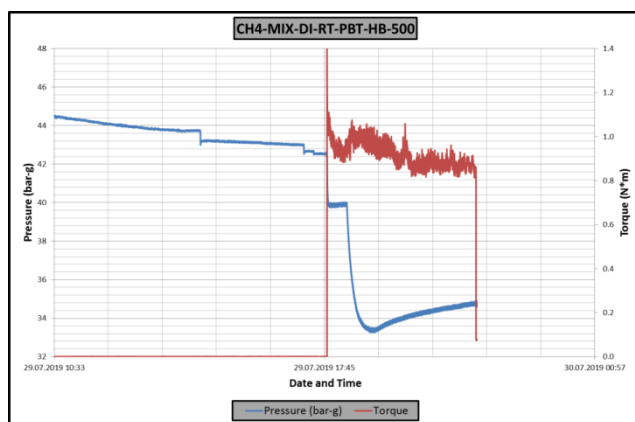
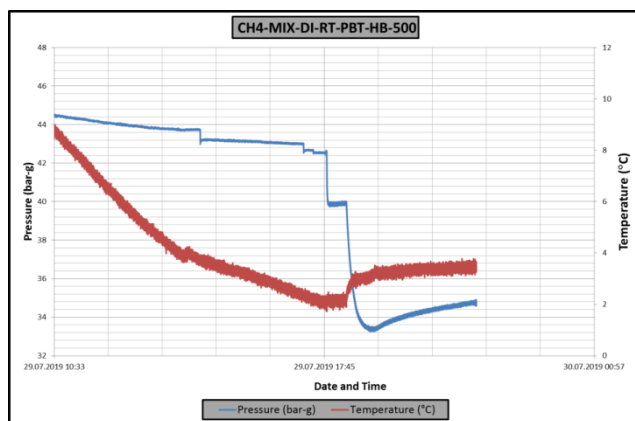


Figure A.22 Raw data of experiment CH4-RT-PBT-HB-MIX-DI-500. A: Pressure – temperature vs. time graph, B: Pressure – torque vs. time graph, C: Pressure vs. temperature graph

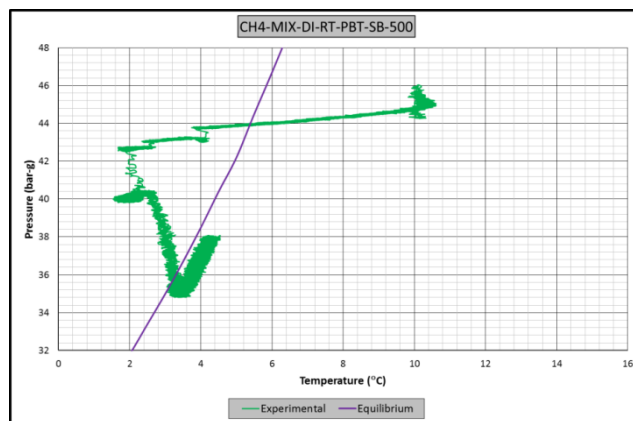
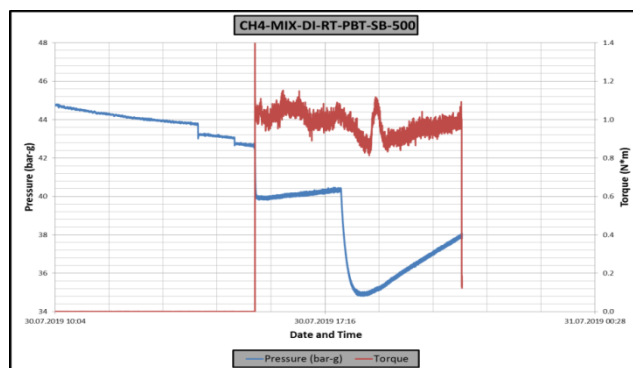
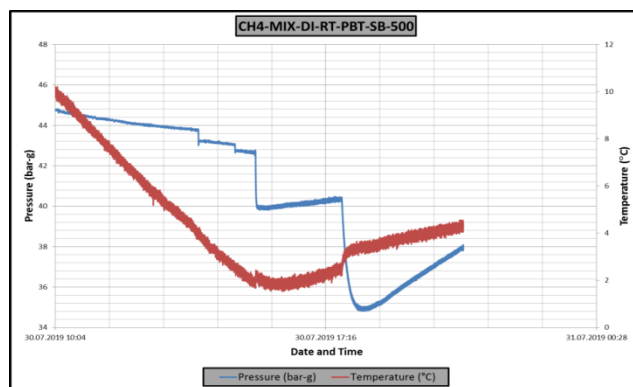


Figure A.23 Raw data of experiment CH4-RT-PBT-SB-MIX-DI-500. A: Pressure – temperature vs. time graph, B: Pressure – torque vs. time graph, C: Pressure vs. temperature graph

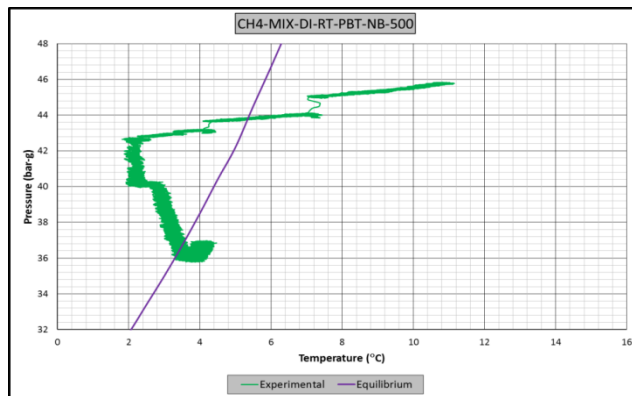
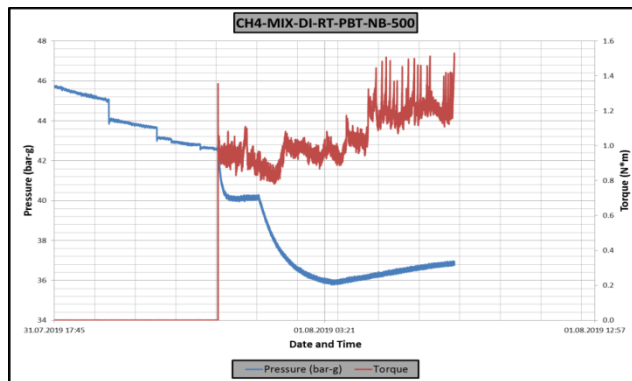
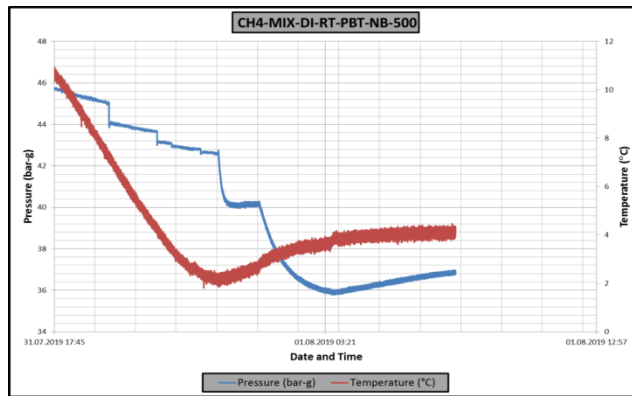


Figure A.24 Raw data of experiment CH4-RT-PBT-NB-MIX-DI-500. A: Pressure – temperature vs. time graph, B: Pressure – torque vs. time graph, C: Pressure vs. temperature graph

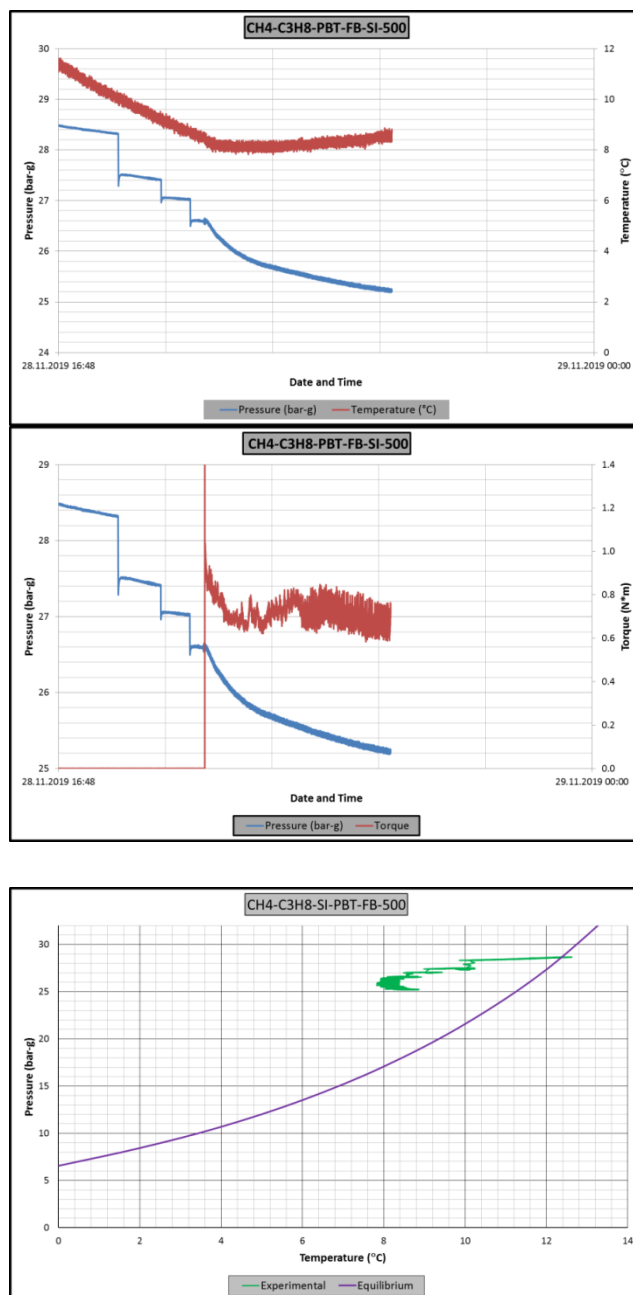


Figure A.25 Raw data of experiment CH4-C3H8-PBT-FB-SI-500. A: Pressure – temperature vs. time graph, B: Pressure – torque vs. time graph, C: Pressure vs. temperature graph. (Driving force=8.5)

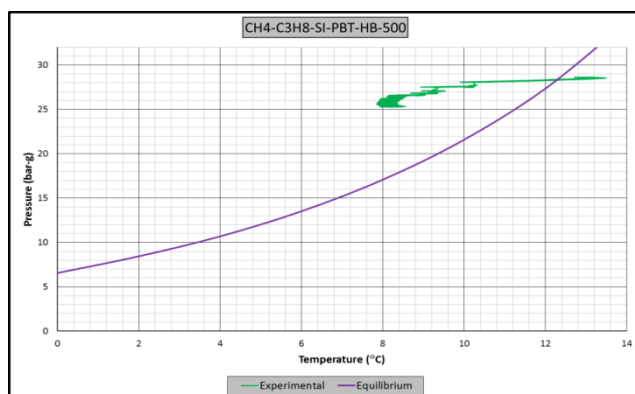
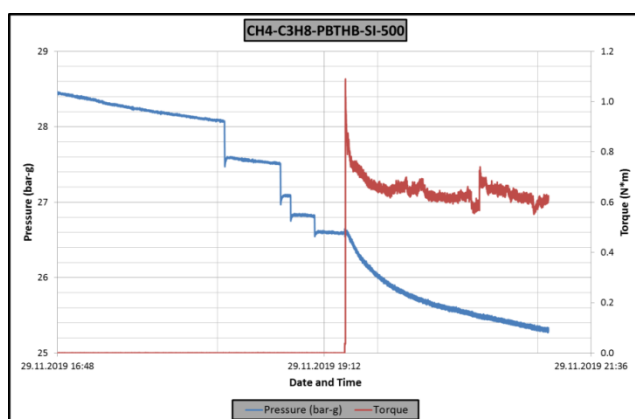
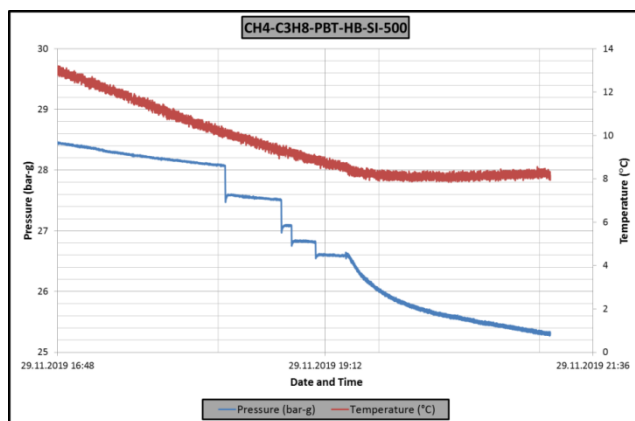


Figure A.26 Raw data of experiment CH4-C3H8-PBT-HB-SI-500. A: Pressure – temperature vs. time graph, B: Pressure – torque vs. time graph, C: Pressure vs. temperature graph. (Driving force=8.5)

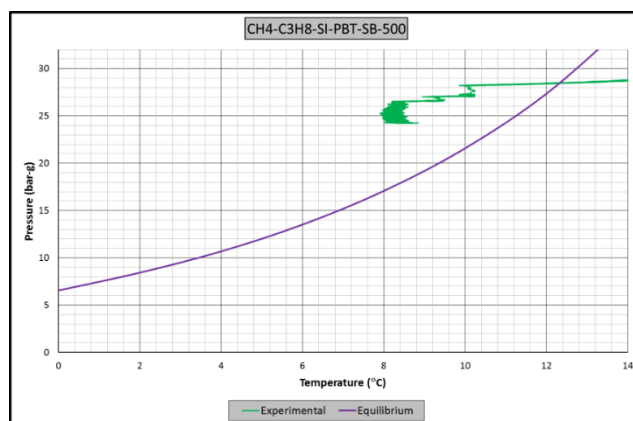
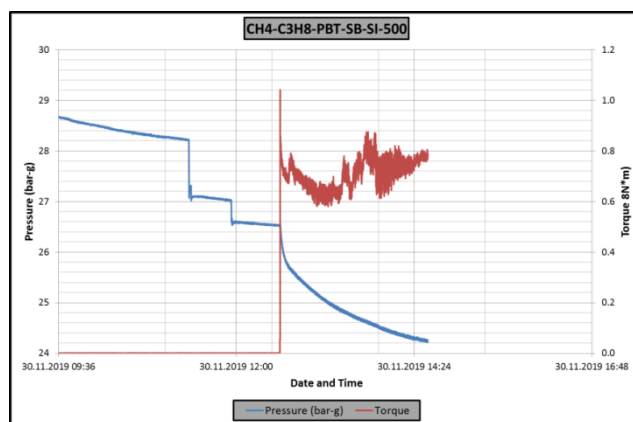
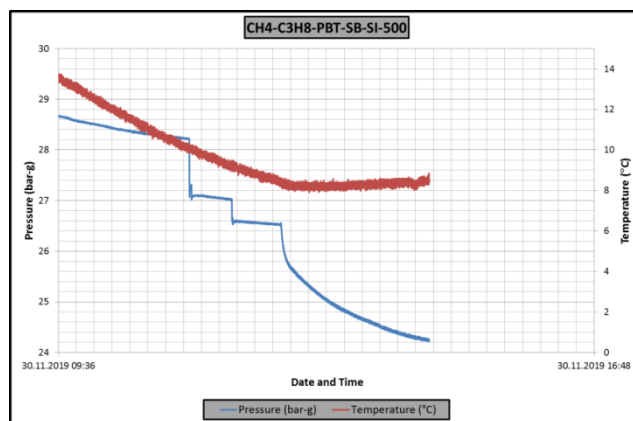


Figure A.27 Raw data of experiment CH4-C3H8-PBT-SB-SI-500. A: Pressure – temperature vs. time graph, B: Pressure – torque vs. time graph, C: Pressure vs. temperature graph. (Driving force=8.5)

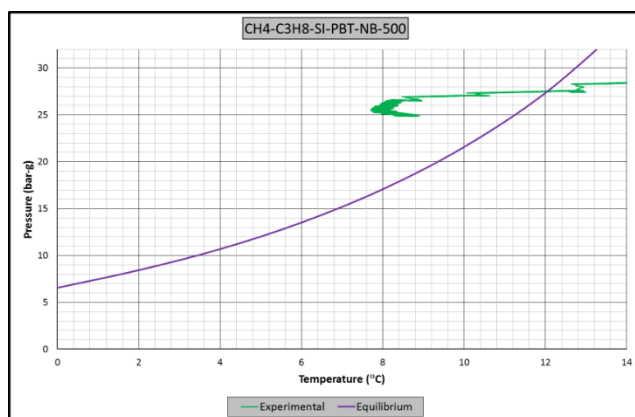
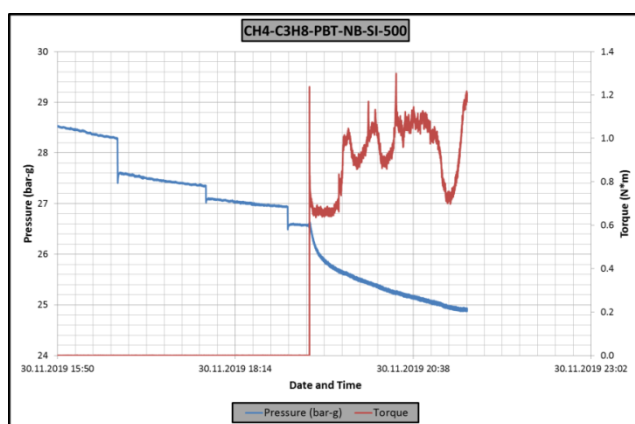
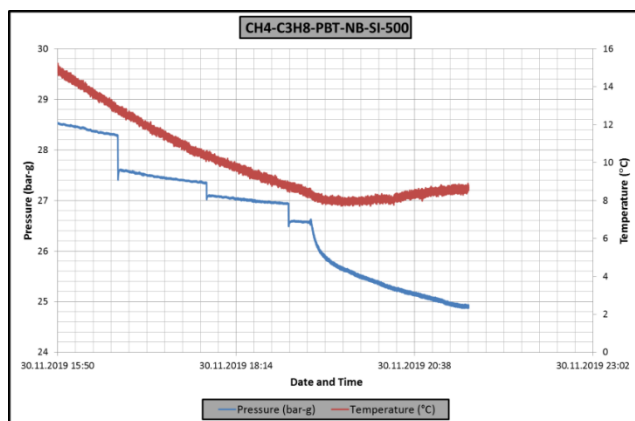


Figure A.28 Raw data of experiment CH4-C3H8-PBT-NB-SI-500. A: Pressure – temperature vs. time graph, B: Pressure – torque vs. time graph, C: Pressure vs. temperature graph. (Driving force=8.5)

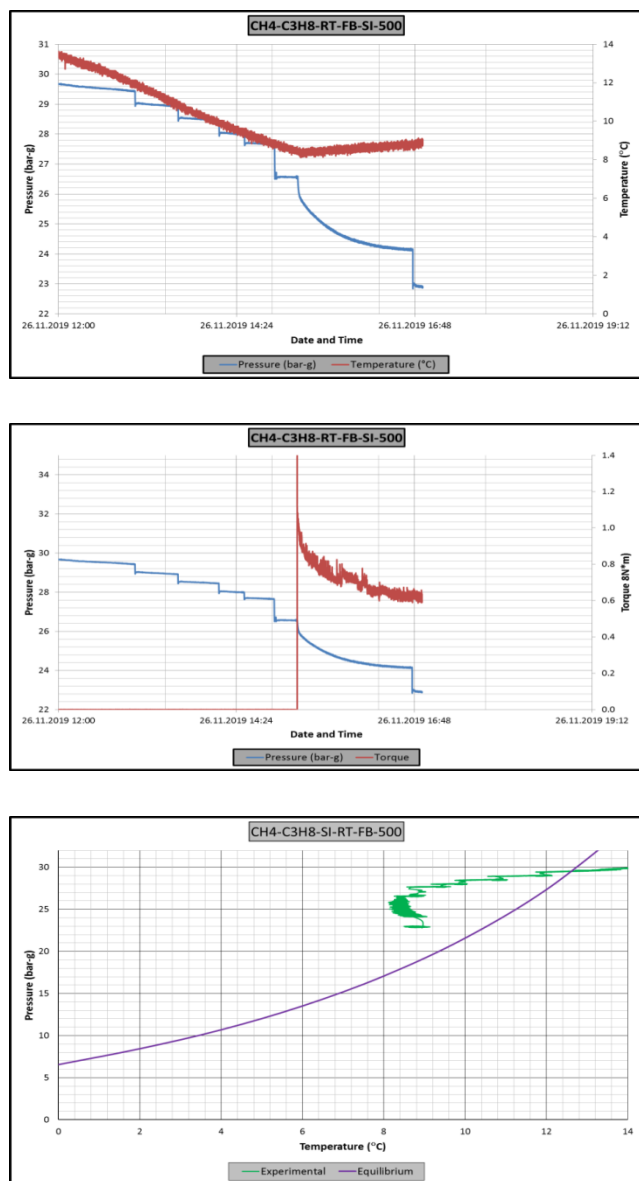


Figure A.29 Raw data of experiment CH4-C3H8-RT-FB-SI-500. A: Pressure – temperature vs. time graph, B: Pressure – torque vs. time graph, C: Pressure vs. temperature graph. (Driving force=8.5)

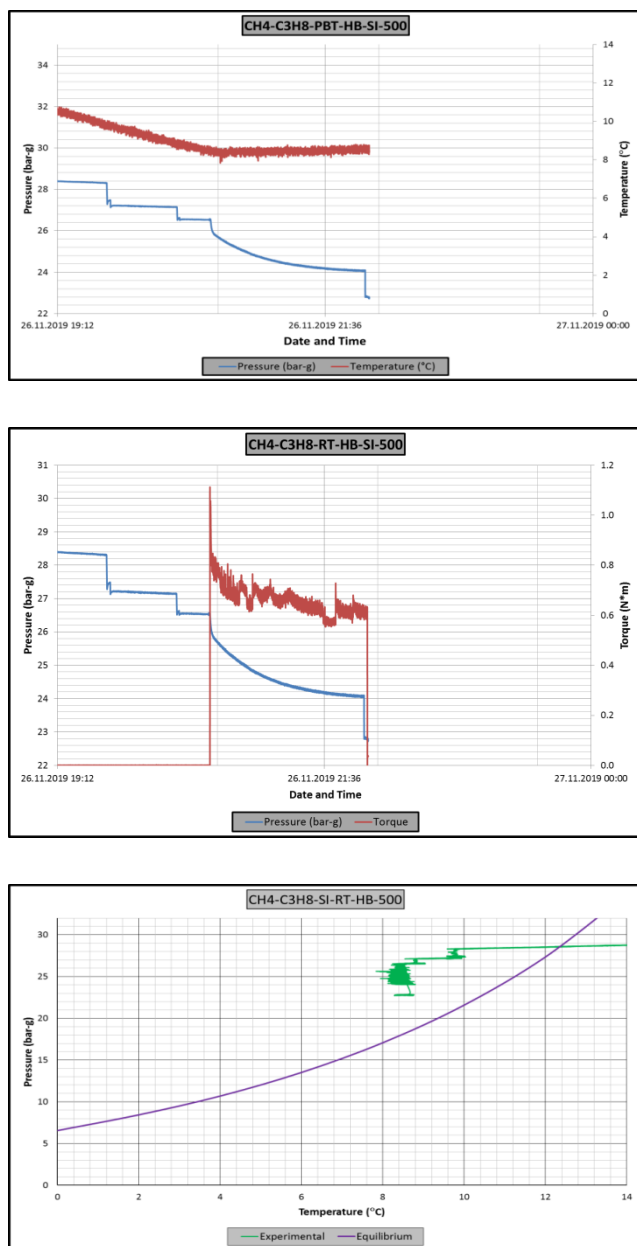


Figure A.30 Raw data of experiment CH4-C3H8-RT-HB-SI-500. A: Pressure – temperature vs. time graph, B: Pressure – torque vs. time graph, C: Pressure vs. temperature graph. (Driving force=8.5)

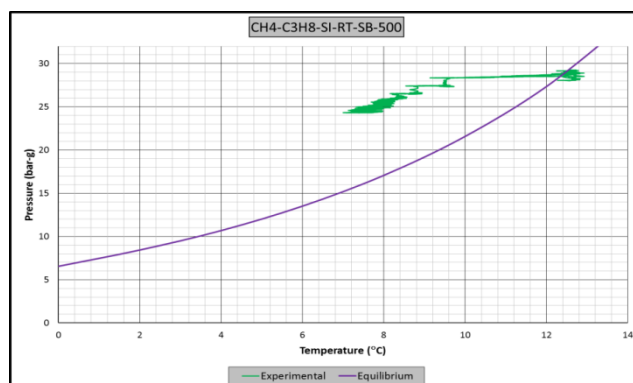
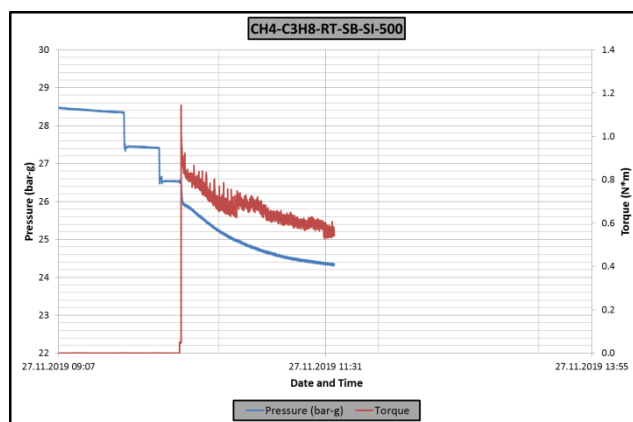
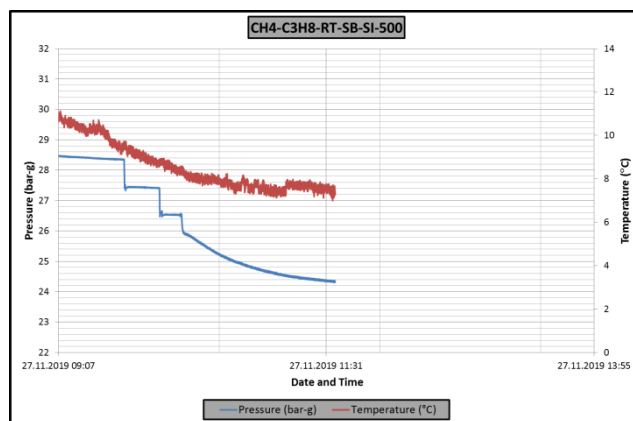


Figure A.31 Raw data of experiment CH4-C3H8-RT-SB-SI-500. A: Pressure – temperature vs. time graph, B: Pressure – torque vs. time graph, C: Pressure vs. temperature graph. (Driving force=8.5)

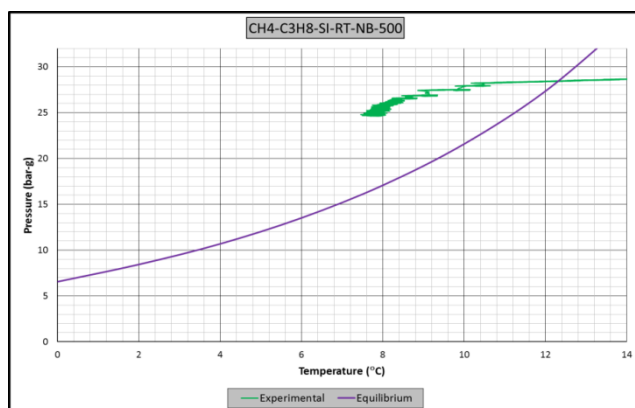
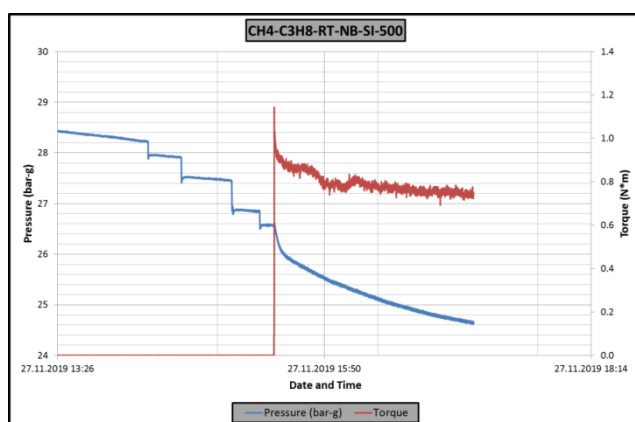
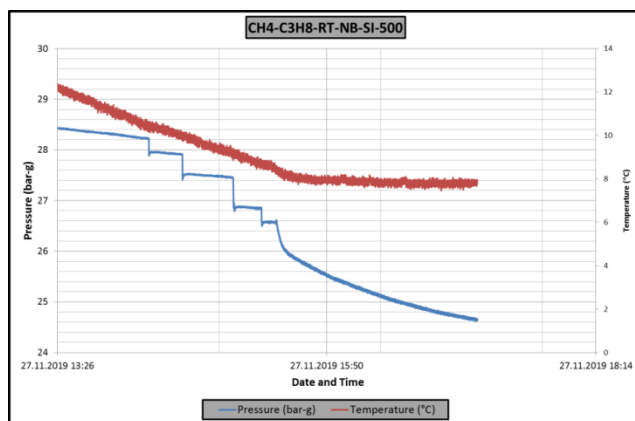


Figure A.32 Raw data of experiment CH4-C3H8-RT-NB-SI-500. A: Pressure – temperature vs. time graph, B: Pressure – torque vs. time graph, C: Pressure vs. temperature graph. (Driving force=8.5)

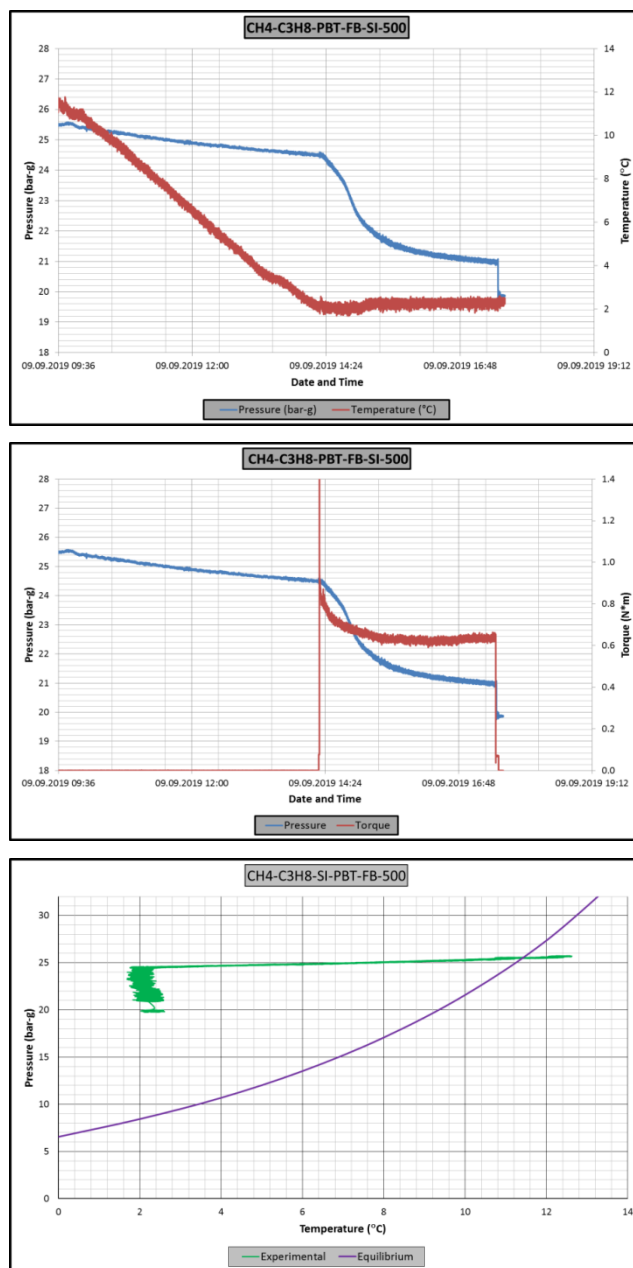


Figure A.33 Raw data of experiment CH4-C3H8-PBT-FB-SI-500. A: Pressure – temperature vs. time graph, B: Pressure – torque vs. time graph, C: Pressure vs. temperature graph. (Driving force=16)

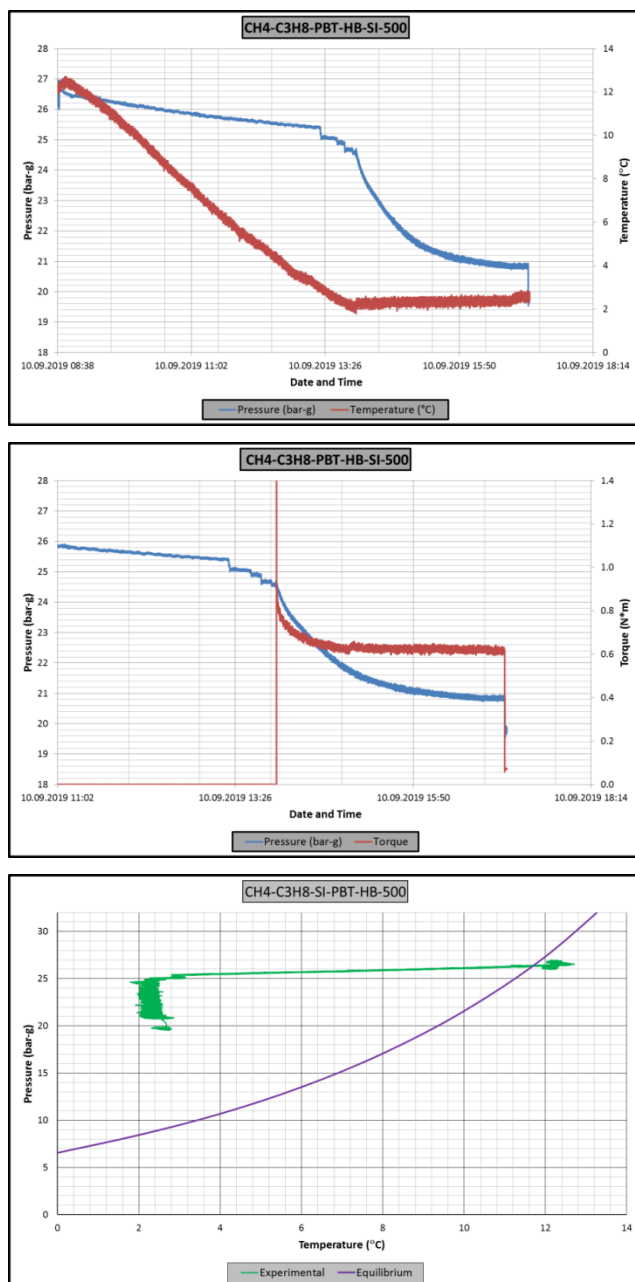


Figure A.34 Raw data of experiment CH4-C3H8-PBT-HB-SI-500. A: Pressure – temperature vs. time graph, B: Pressure – torque vs. time graph, C: Pressure vs. temperature graph. (Driving force=16)

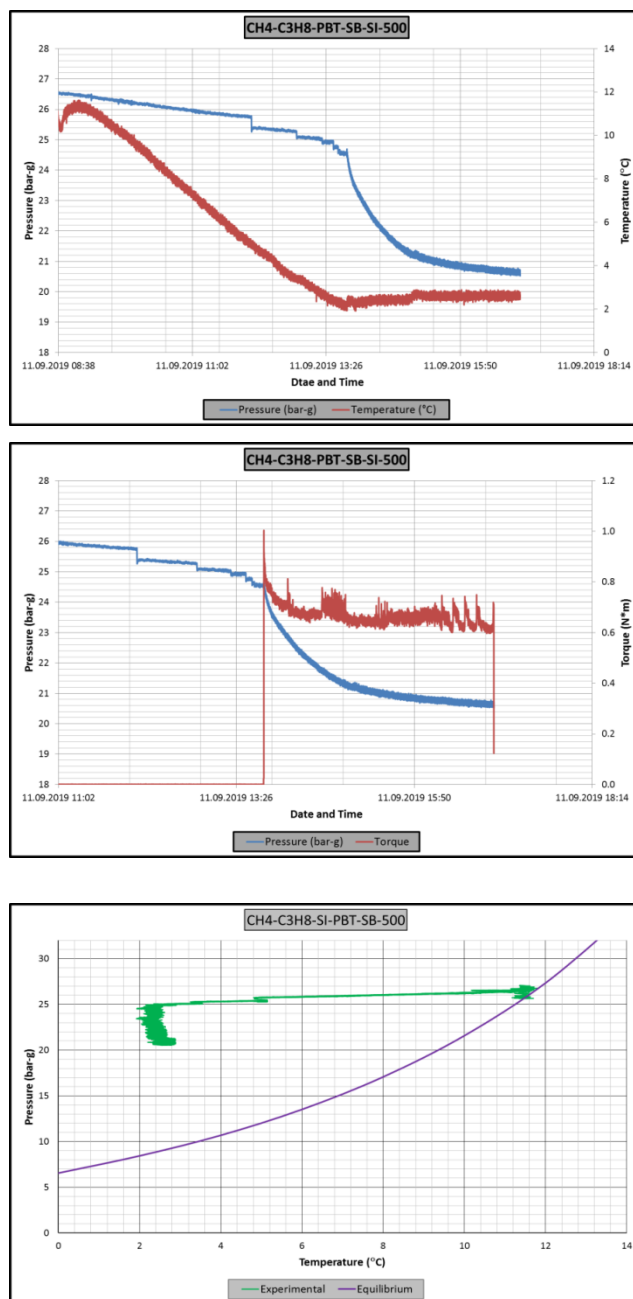


Figure A.35 Raw data of experiment CH4-C3H8-PBT-SB-SI-500. A: Pressure – temperature vs. time graph, B: Pressure – torque vs. time graph, C: Pressure vs. temperature graph. (Driving force=16)

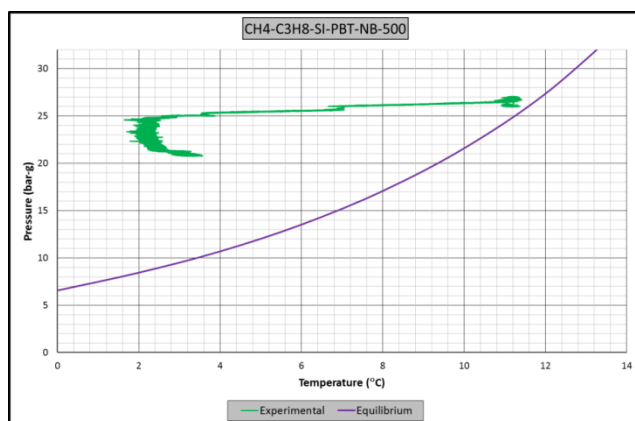
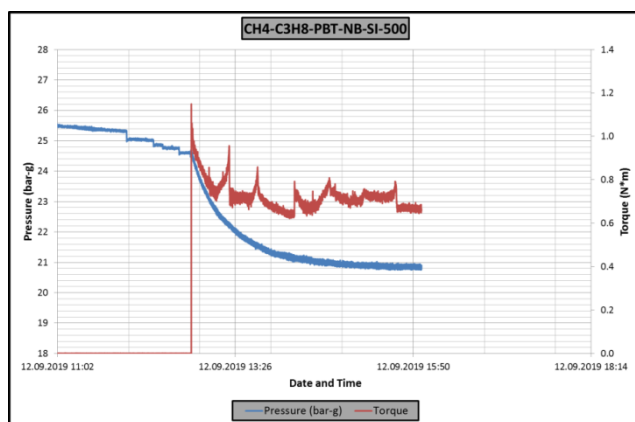
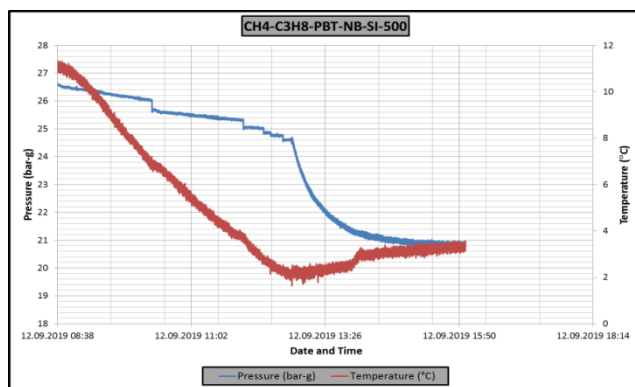


Figure A.36 Raw data of experiment CH4-C3H8-PBT-NB-SI-500. A: Pressure – temperature vs. time graph, B: Pressure – torque vs. time graph, C: Pressure vs. temperature graph. (Driving force=16)

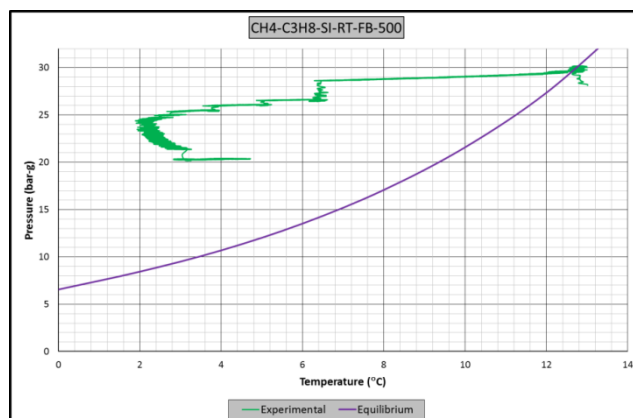
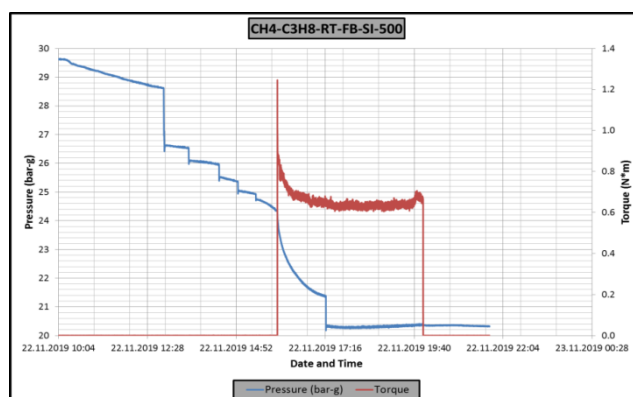
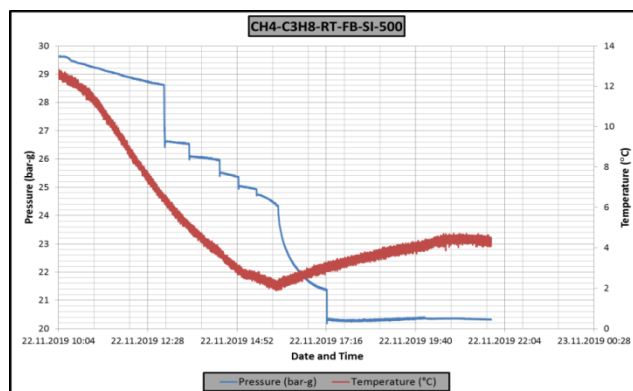


Figure A.37 Raw data of experiment CH4-C3H8-RT-FB-SI-500. A: Pressure – temperature vs. time graph, B: Pressure – torque vs. time graph, C: Pressure vs. temperature graph. (Driving force=16)

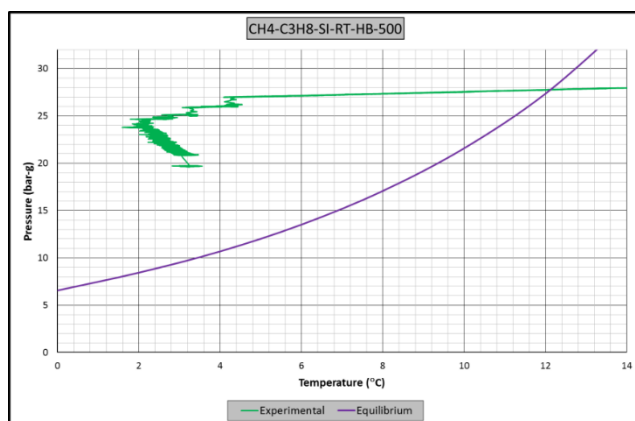
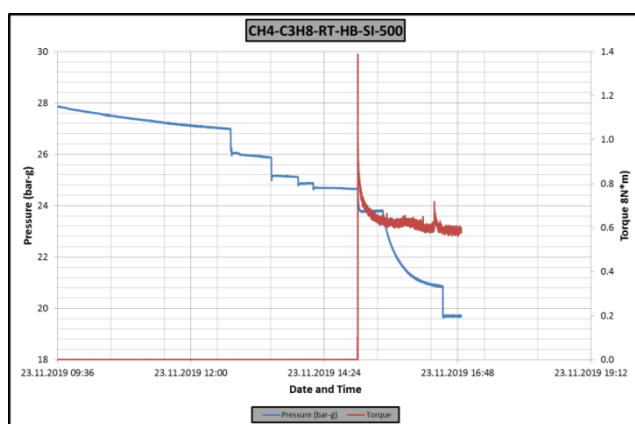
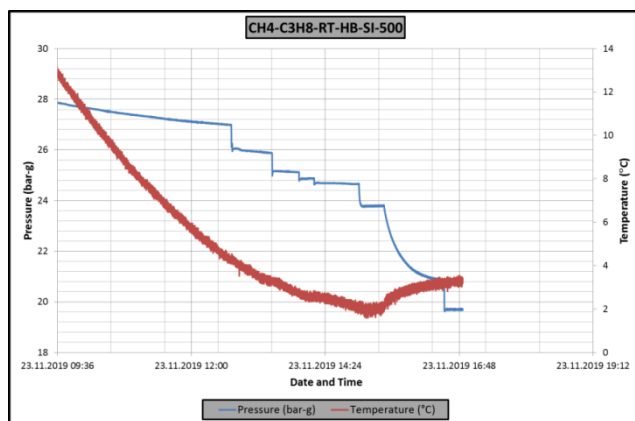


Figure A.38 Raw data of experiment CH4-C3H8-RT-HB-SI-500. A: Pressure – temperature vs. time graph, B: Pressure – torque vs. time graph, C: Pressure vs. temperature graph. (Driving force=16)

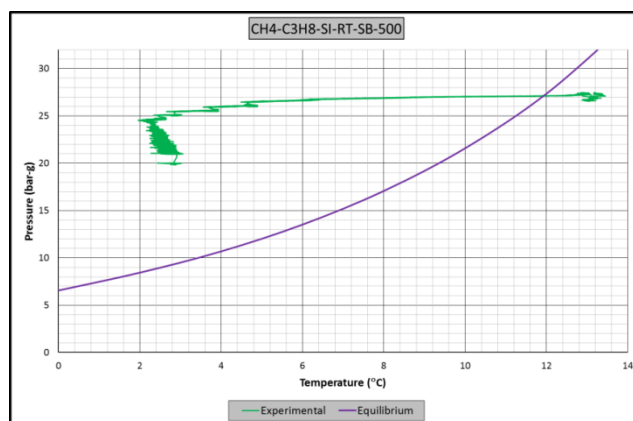
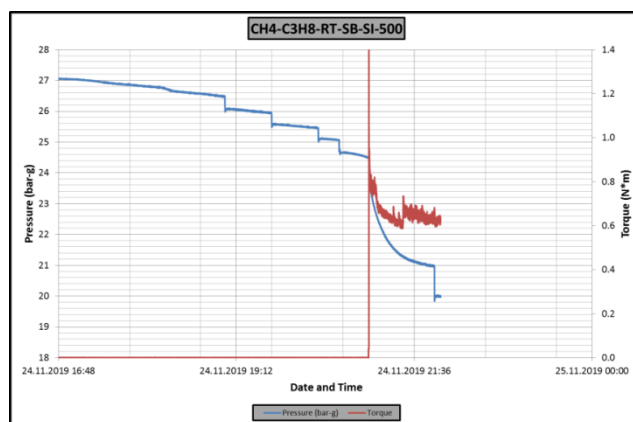
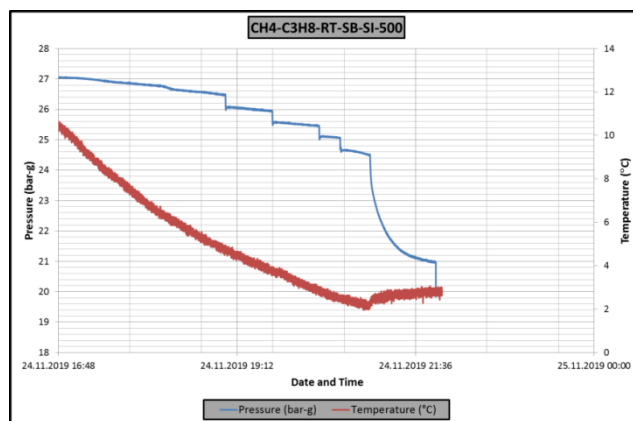


Figure A.39 Raw data of experiment CH4-C3H8-RT-SB-SI-500. A: Pressure – temperature vs. time graph, B: Pressure – torque vs. time graph, C: Pressure vs. temperature graph. (Driving force=16)

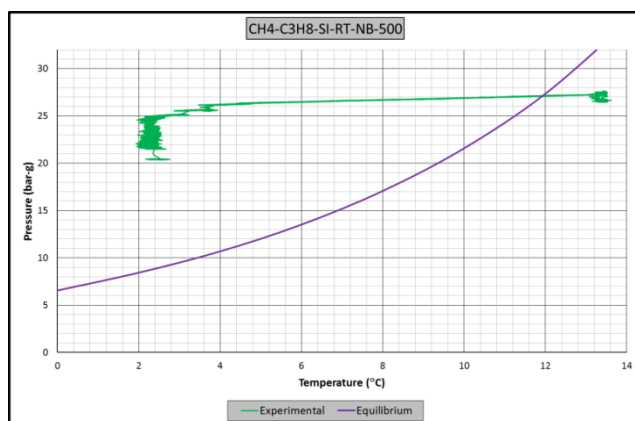
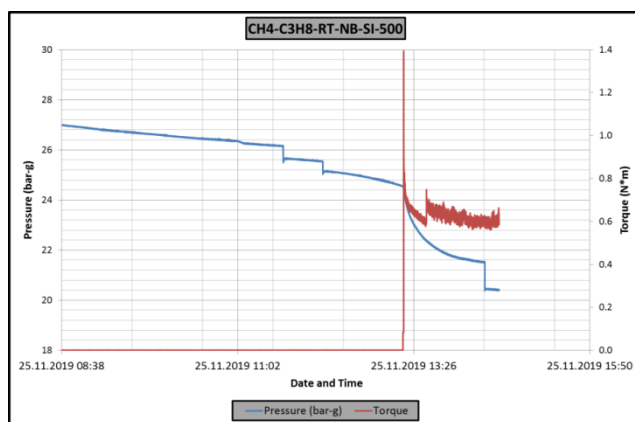
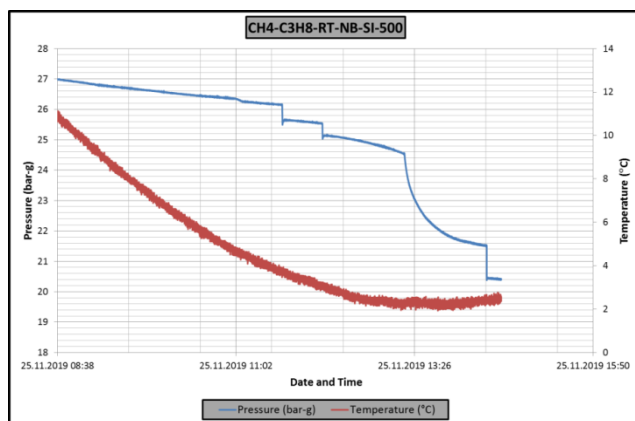


Figure A.40 Raw data of experiment CH4-C3H8-RT-NB-SI-500. A: Pressure – temperature vs. time graph, B: Pressure – torque vs. time graph, C: Pressure vs. temperature graph. (Driving force=16)

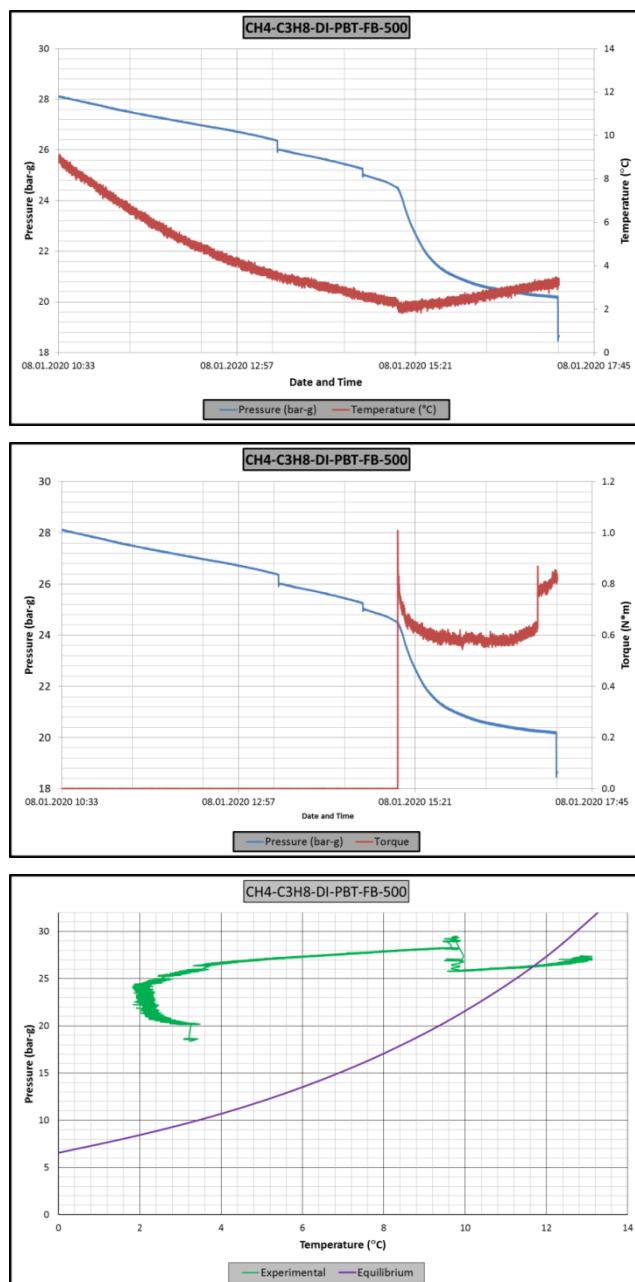


Figure A.41 Raw data of experiment CH4-C3H8-PBT-FB-DI-500. A: Pressure – temperature vs. time graph, B: Pressure – torque vs. time graph, C: Pressure vs. temperature graph. (Driving force=16)

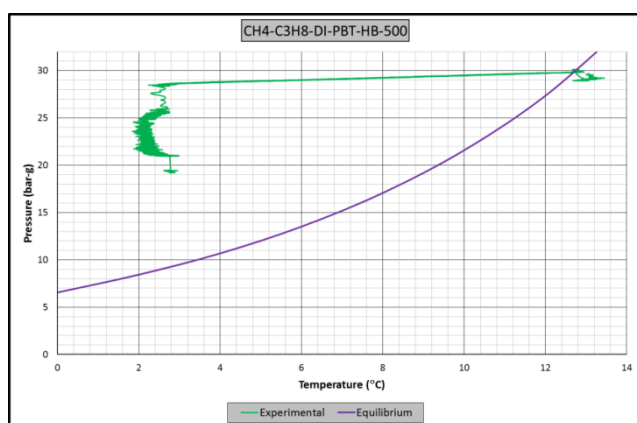
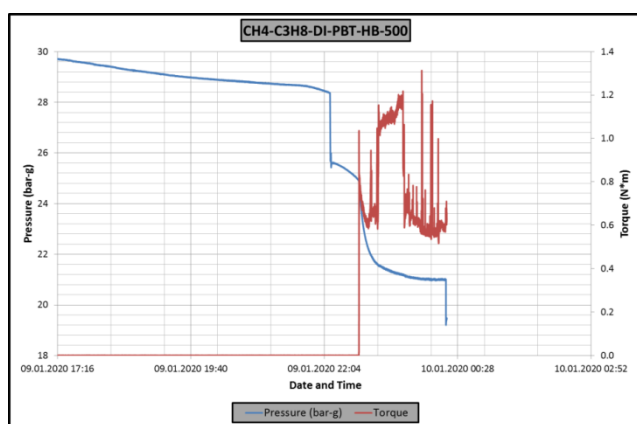
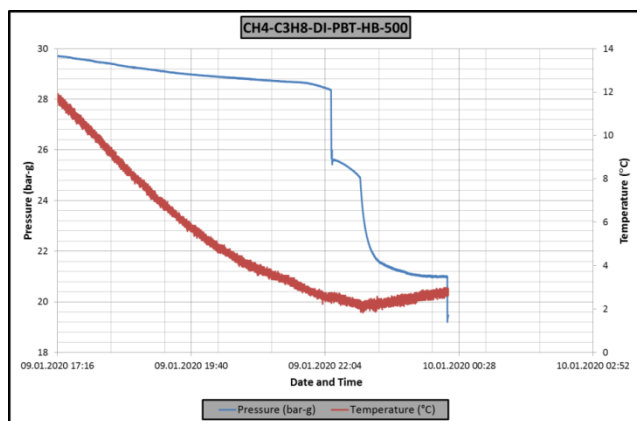


Figure A.42 Raw data of experiment CH4-C3H8-PBT-HB-DI-500. A: Pressure – temperature vs. time graph, B: Pressure – torque vs. time graph, C: Pressure vs. temperature graph. (Driving force=16)

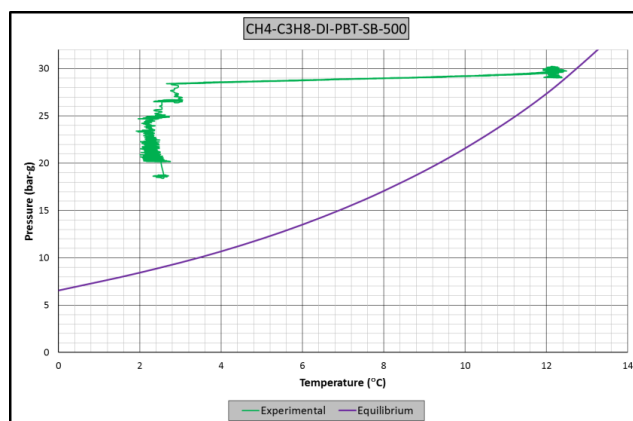
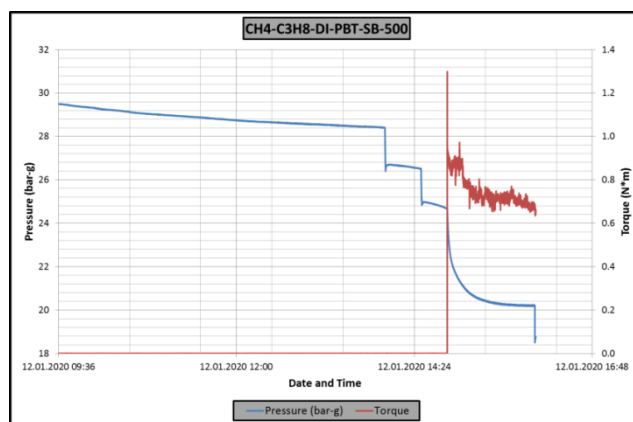
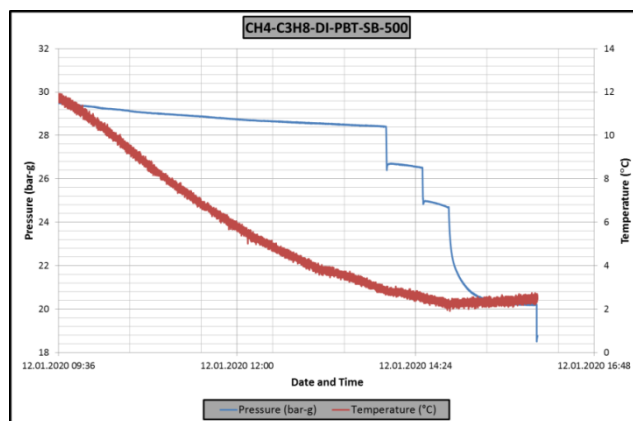


Figure A.43 Raw data of experiment CH4-C3H8-PBT-SB-DI-500. A: Pressure – temperature vs. time graph, B: Pressure – torque vs. time graph, C: Pressure vs. temperature graph. (Driving force=16)

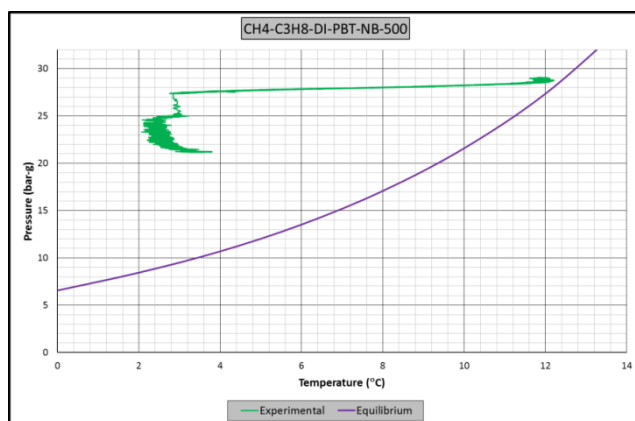
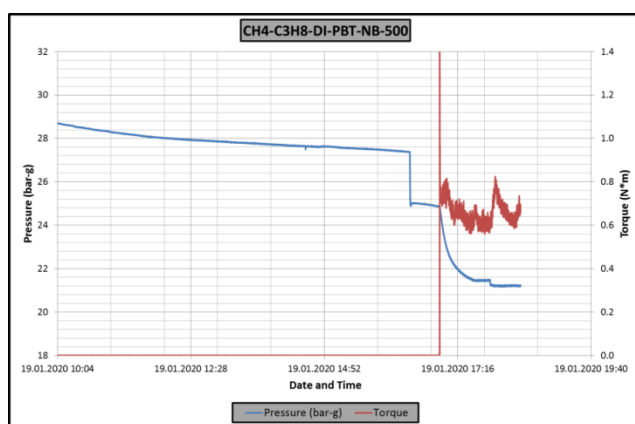
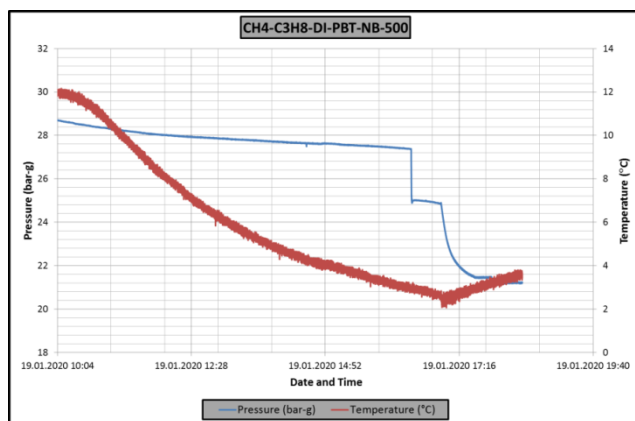


Figure A.44 Raw data of experiment CH4-C3H8-PBT-NB-DI-500. A: Pressure – temperature vs. time graph, B: Pressure – torque vs. time graph, C: Pressure vs. temperature graph. (Driving force=16)

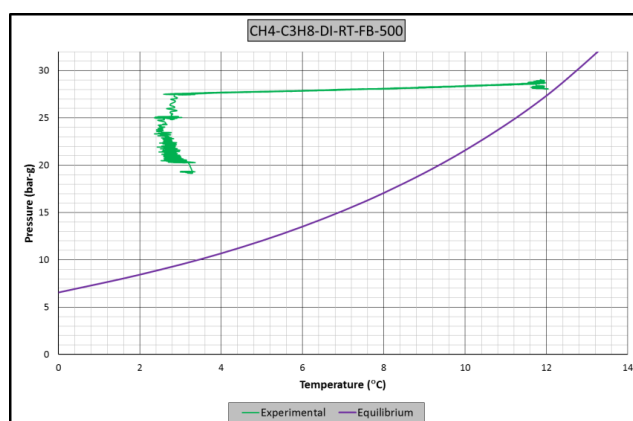
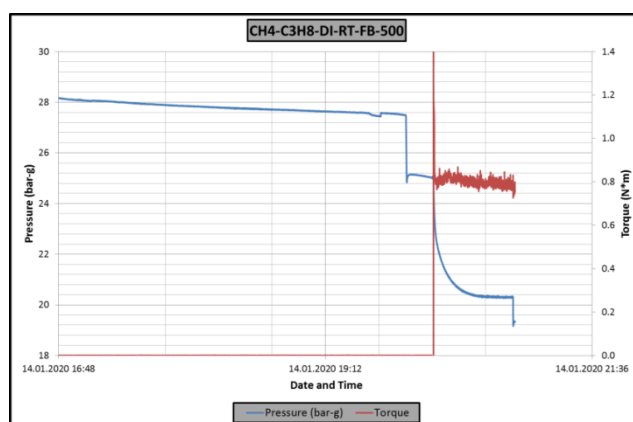
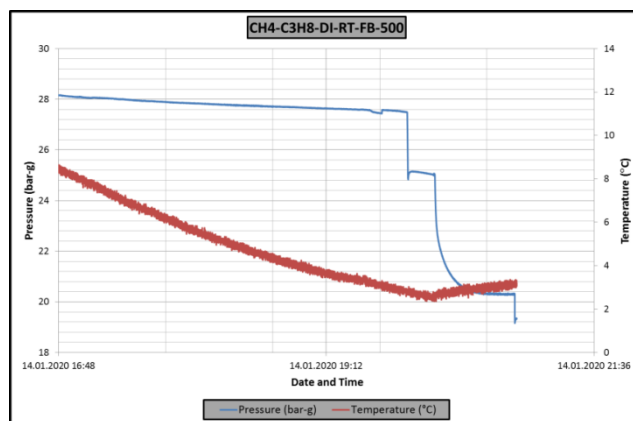


Figure A.45 Raw data of experiment CH4-C3H8-RT-FB-DI-500. A: Pressure – temperature vs. time graph, B: Pressure – torque vs. time graph, C: Pressure vs. temperature graph. (Driving force=16)

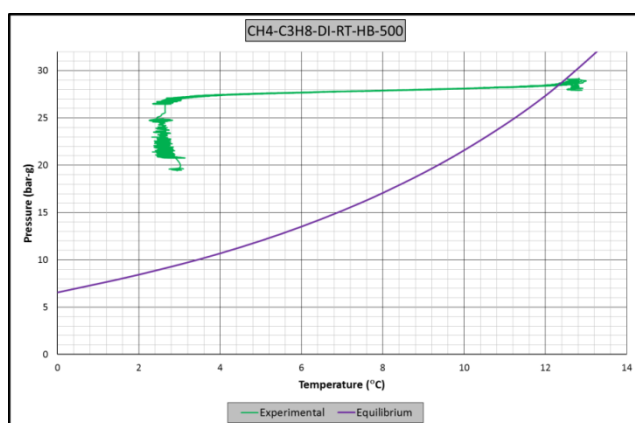
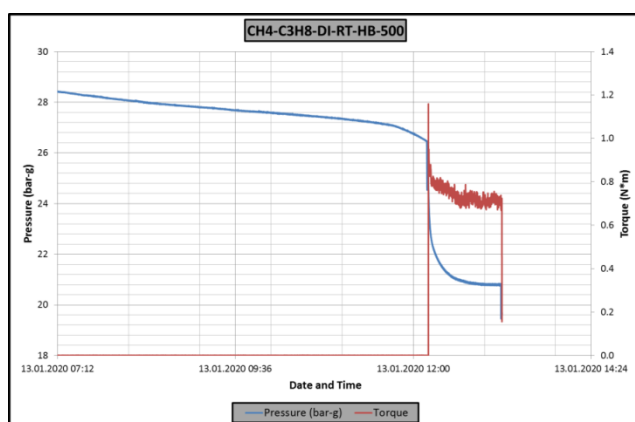
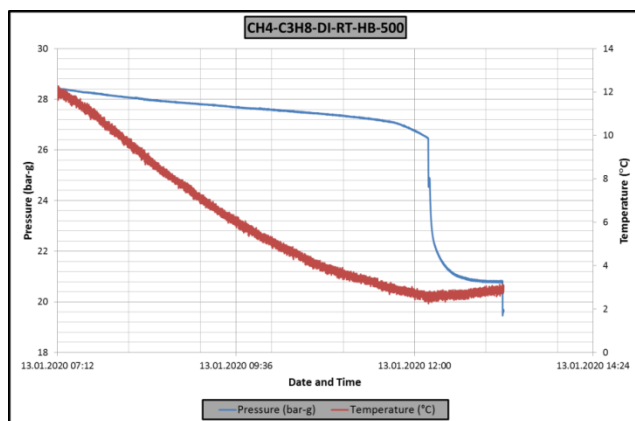


Figure A.46 Raw data of experiment CH4-C3H8-RT-HB-DI-500. A: Pressure – temperature vs. time graph, B: Pressure – torque vs. time graph, C: Pressure vs. temperature graph. (Driving force=16)

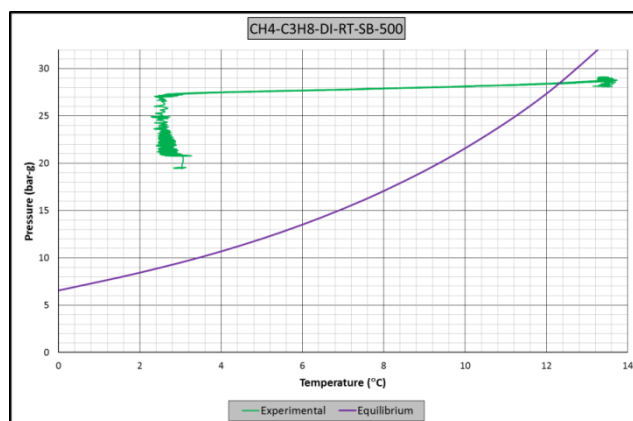
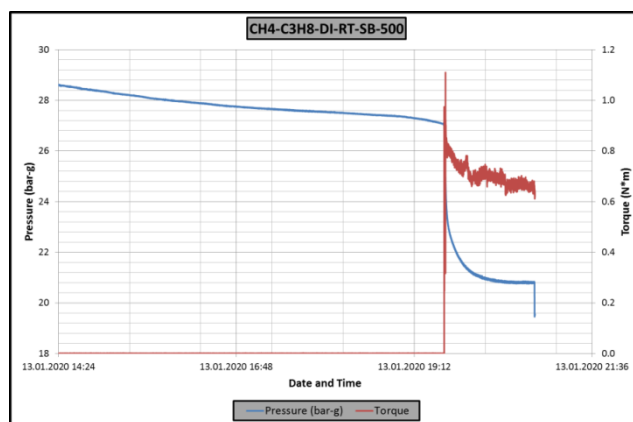
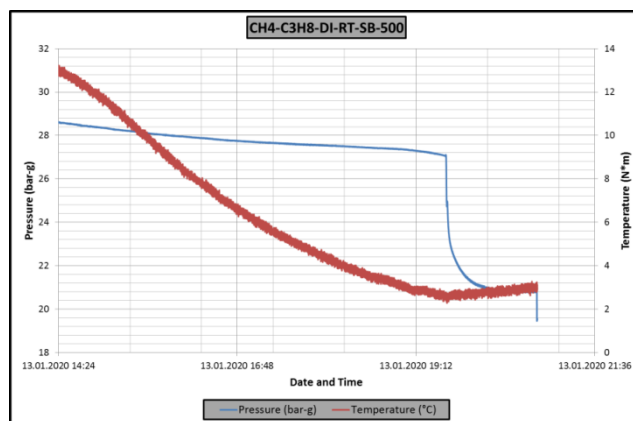


Figure A.47 Raw data of experiment CH4-C3H8--RT-SB-DI-500. A: Pressure – temperature vs. time graph, B: Pressure – torque vs. time graph, C: Pressure vs. temperature graph. (Driving force=16)

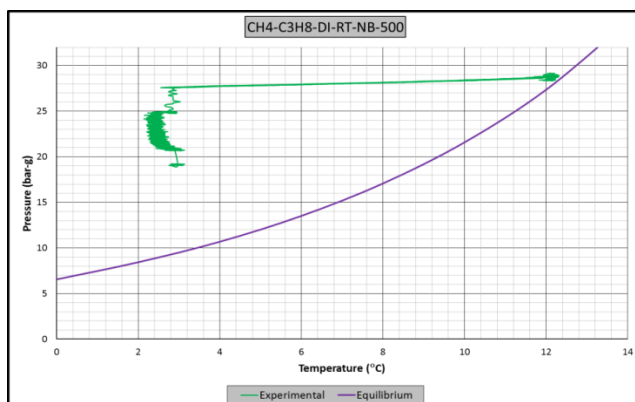
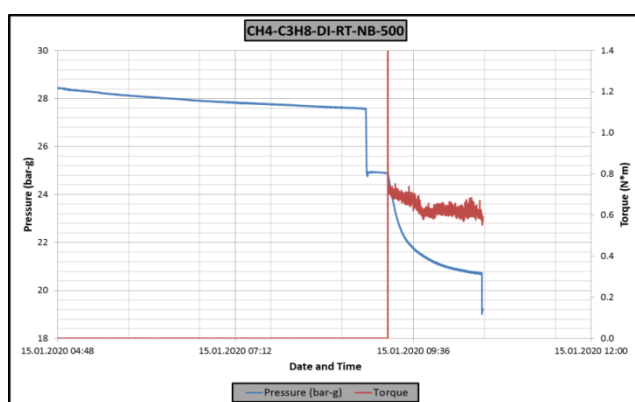
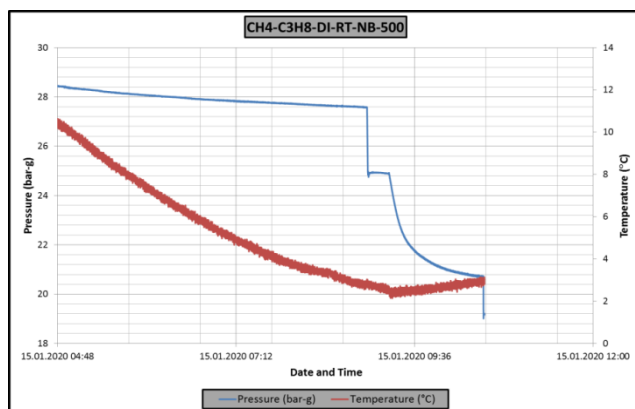


Figure A.48 Raw data of experiment CH₄-C₃H₈-RT-NB-DI-500. A: Pressure – temperature vs. time graph, B: Pressure – torque vs. time graph, C: Pressure vs. temperature graph. (Driving force=16)

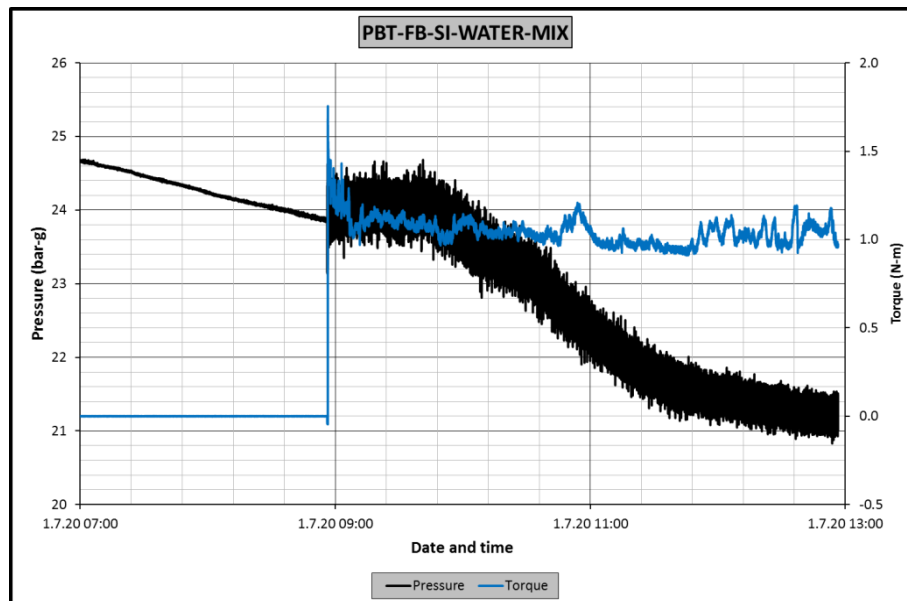
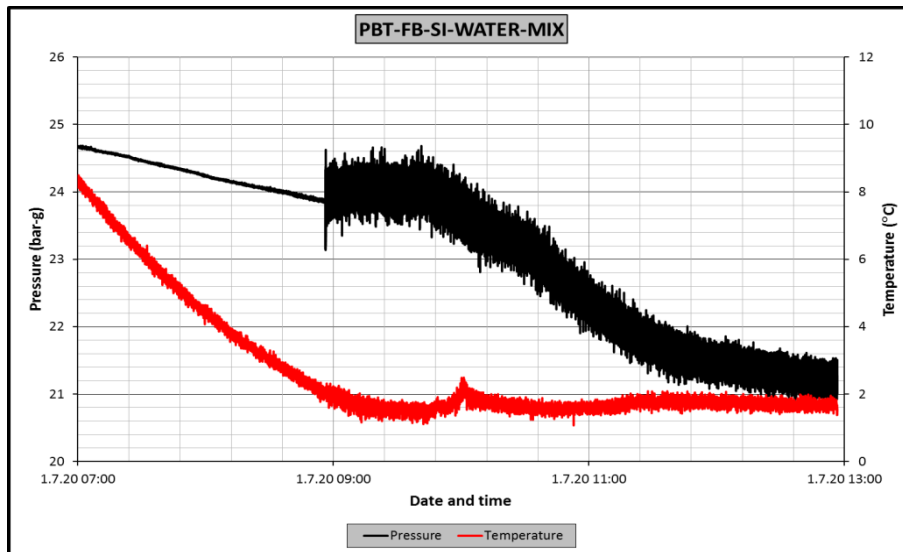


Figure A.49 Raw data experiment PBT-FB-SI-WATER-MIX, A: Pressure, temperature vs time graph, B: Pressure, torque vs time graph

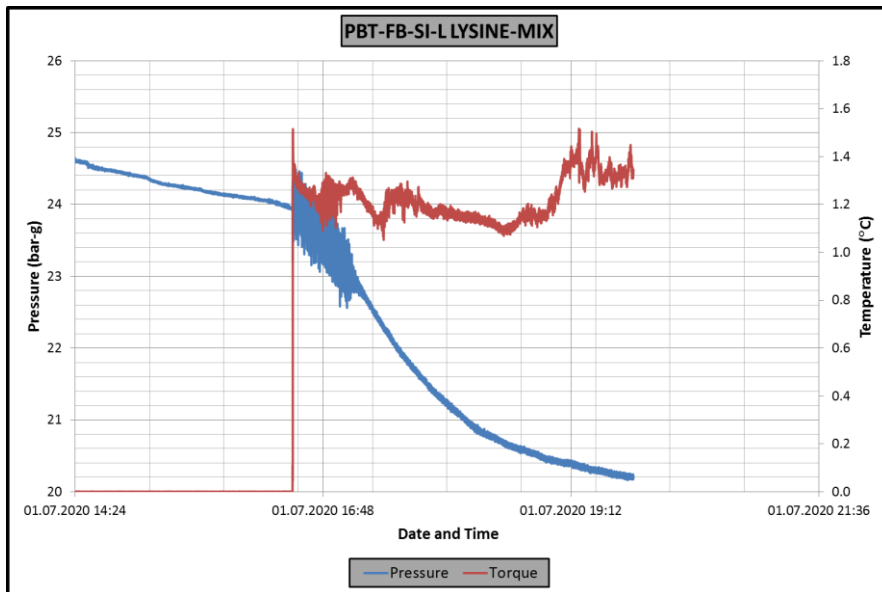
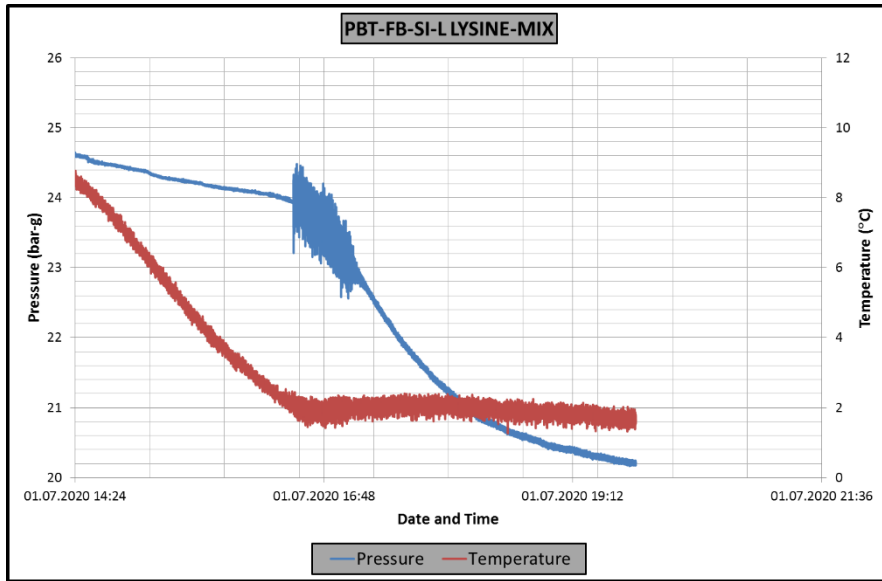


Figure A.50 Raw data experiment PBT-FB-SI-L LYSINE-MIX, A: Pressure, temperature vs time graph, B: Pressure, torque vs time graph

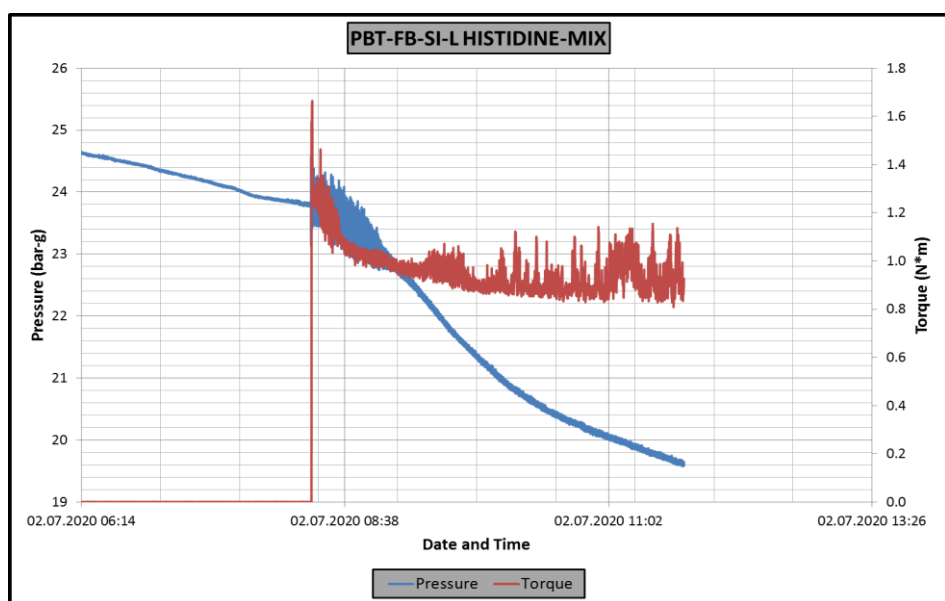
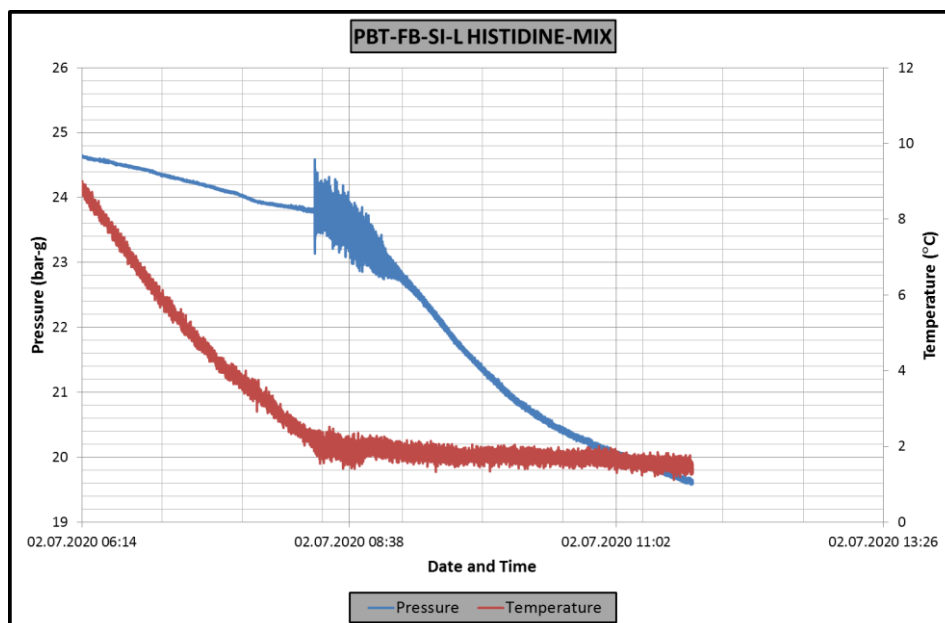


Figure A.51 Raw data experiment PBT-FB-SI-L HISTIDINE-MIX, A: Pressure, temperature vs time graph, B: Pressure, torque vs time graph

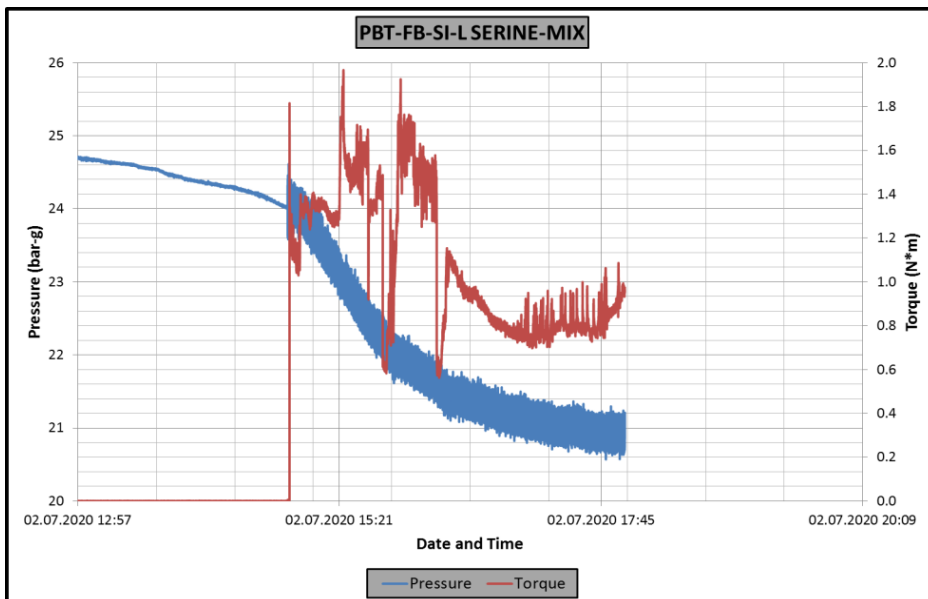
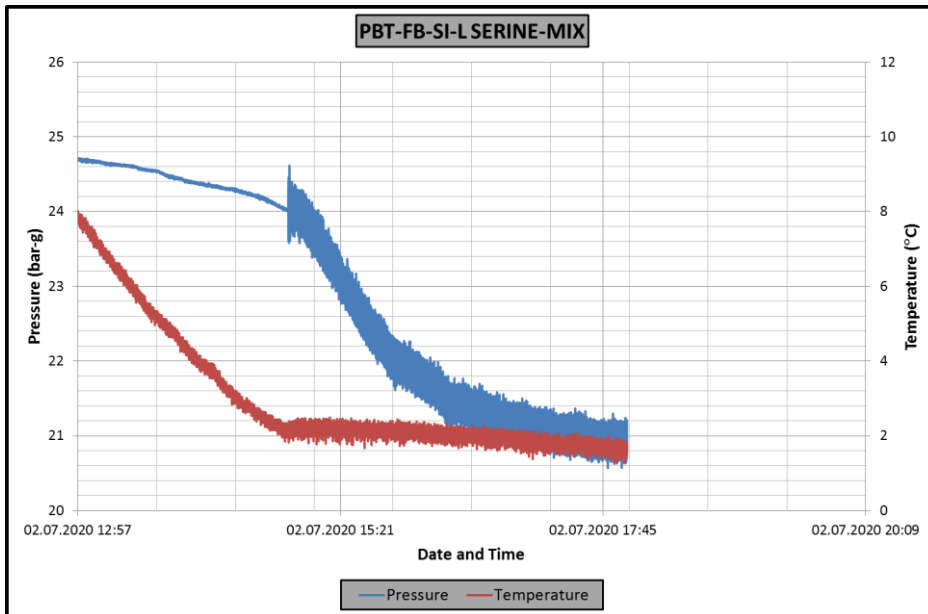


Figure A.52 Raw data experiment PBT-FB-SI-L SERINE-MIX, A: Pressure, temperature vs time graph, B: Pressure, torque vs time graph

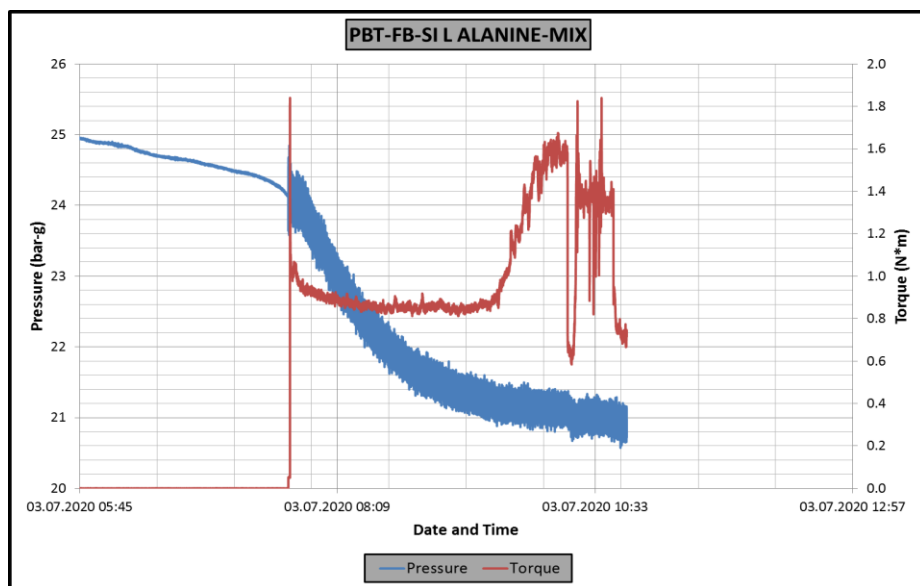
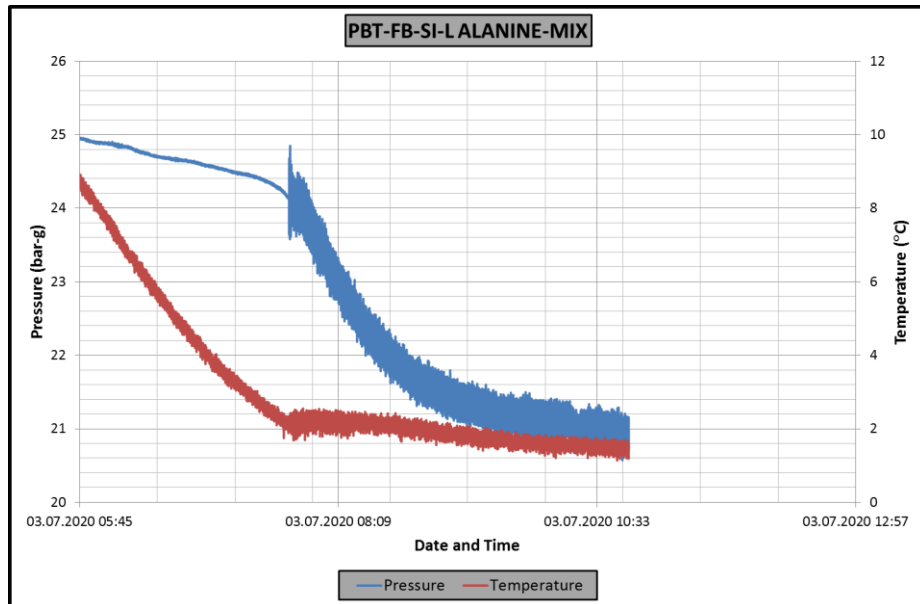


Figure A.53 Raw data experiment PBT-FB-SI-L ALANINE-MIX, A: Pressure, temperature vs time graph, B: Pressure, torque vs time graph

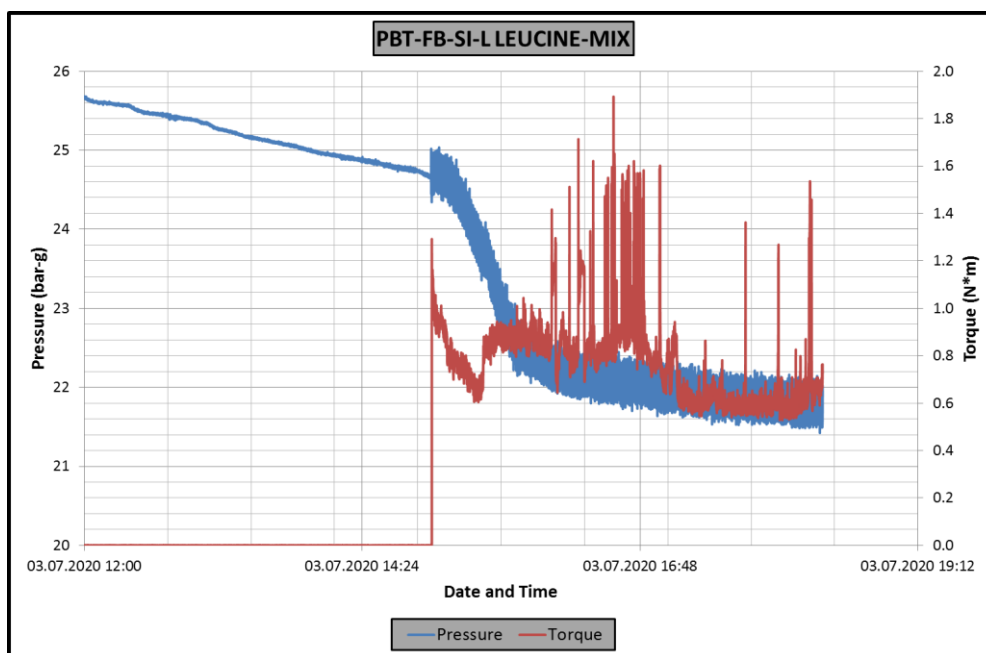
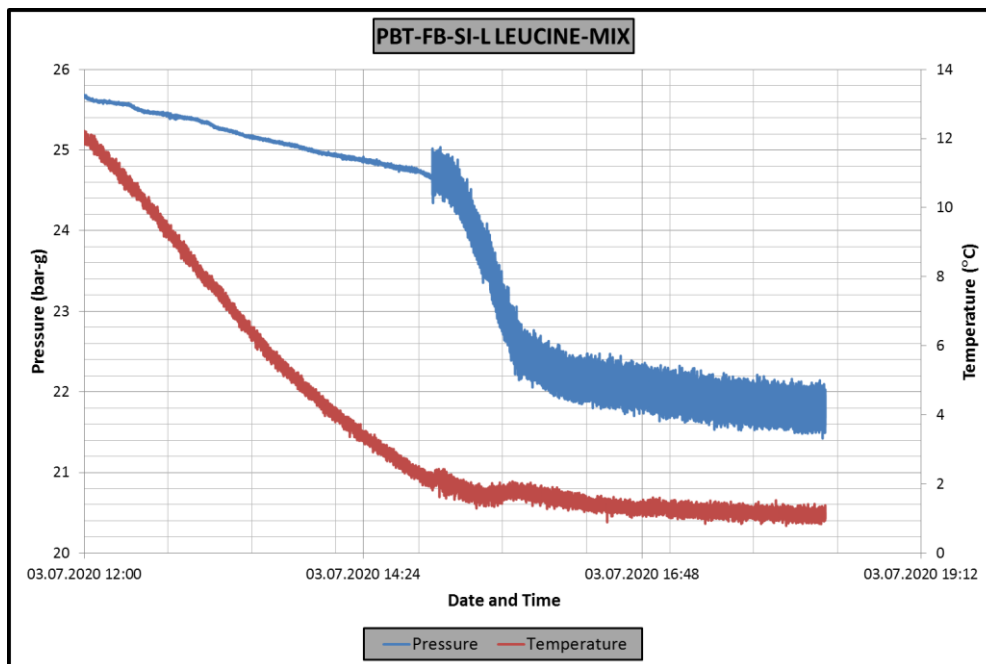


Figure A.54 Raw data experiment PBT-FB-SI-L LEUCINE-MIX, A: Pressure, temperature vs time graph, B: Pressure, torque vs time graph

APPENDIX-B

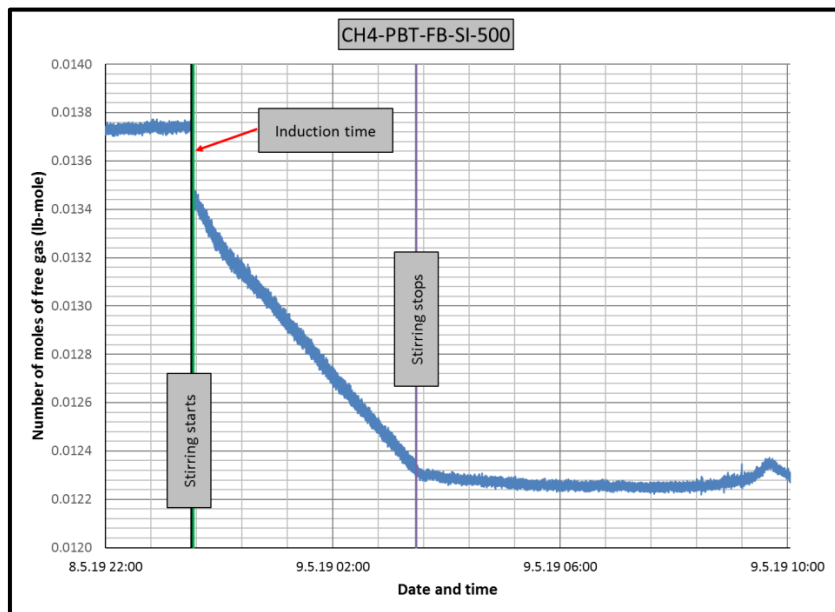


Figure B.1 Change in number of moles of free gas in CH4-PBT-FB-SI experiment.

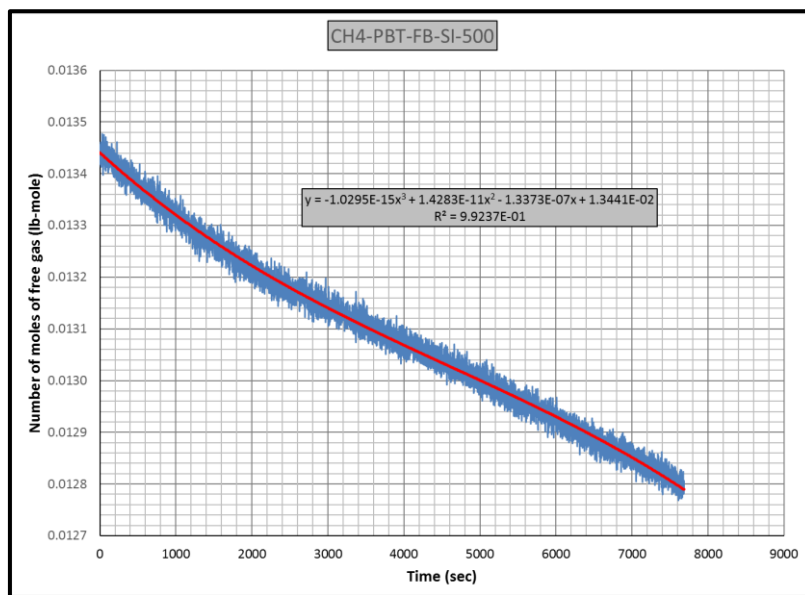


Figure B.2 Gas consumption rate equation for CH4-PBT-FB-SI experiment

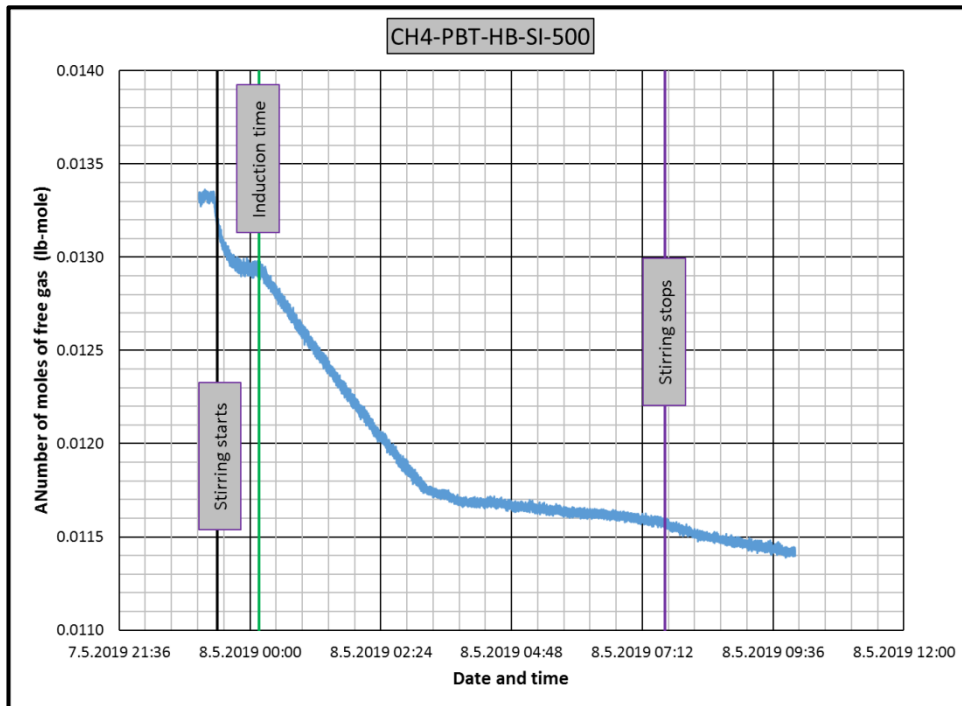


Figure B.3 Change in number of moles of free gas in CH4-PBT-HB-SI experiment

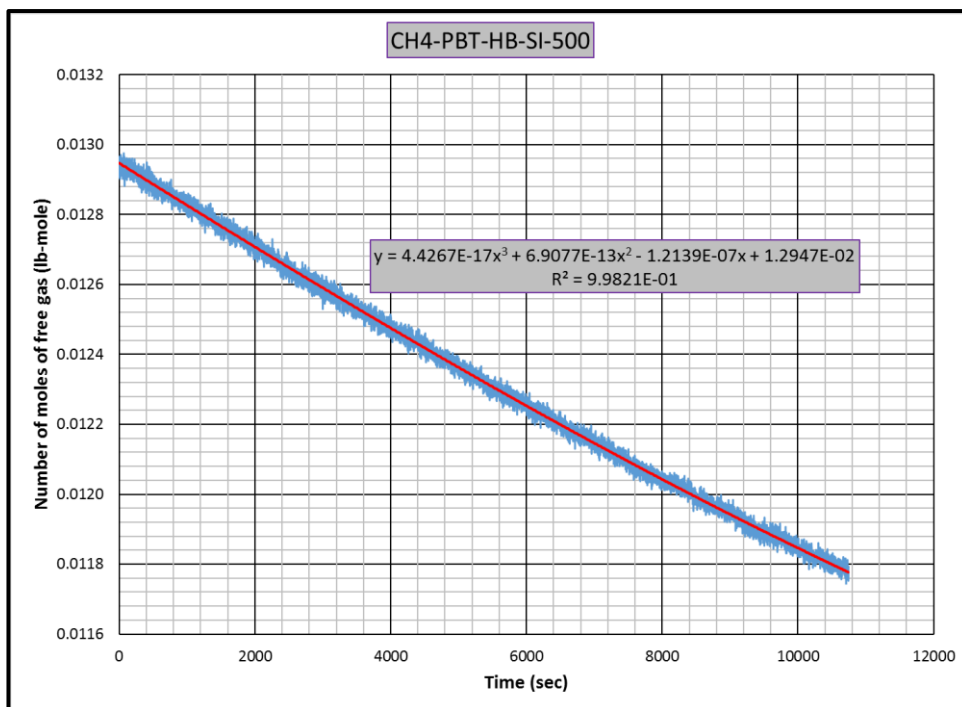


Figure B.4 Gas consumption rate equation for CH4-PBT-HB-SI experiment

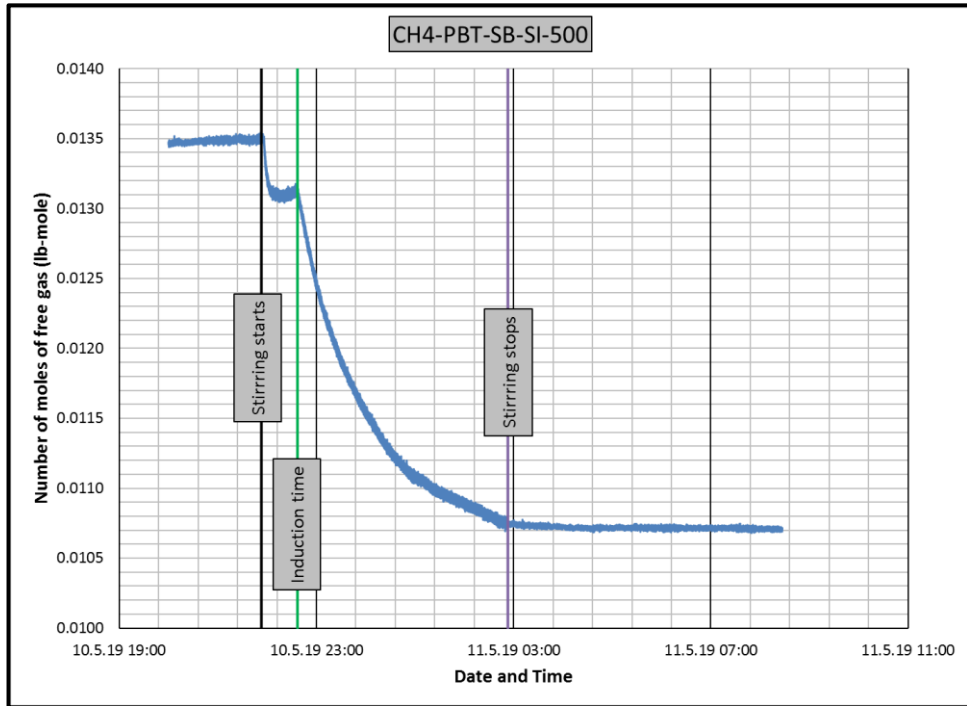


Figure B.5 Change in number of moles of free gas in CH4-PBT-SB-SI experiment

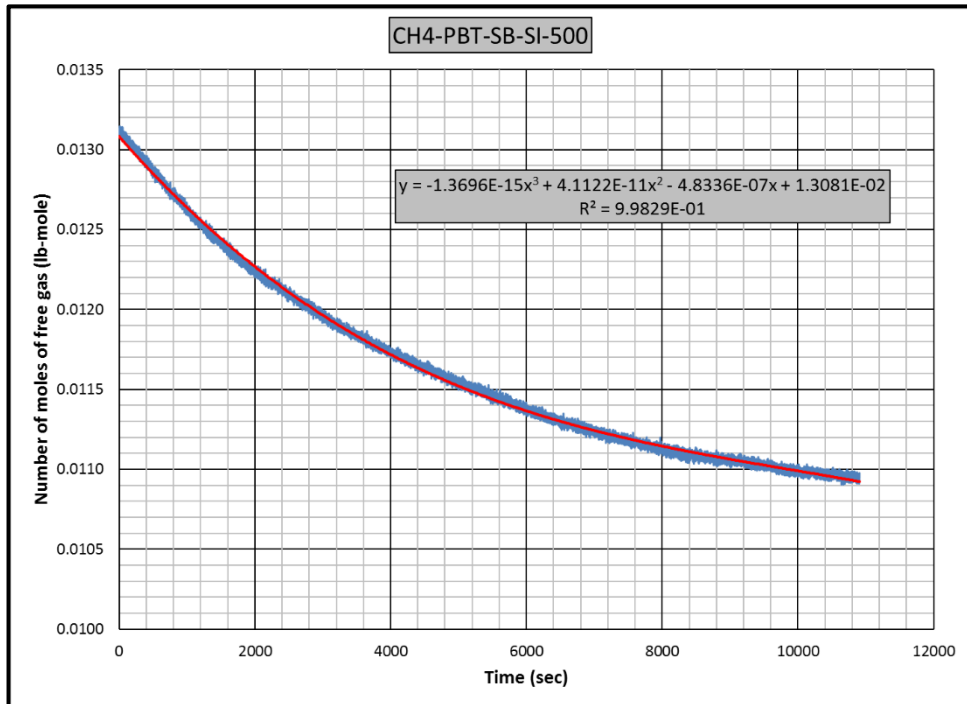


Figure B.6 Gas consumption rate equation for CH4-PBT-SB-SI experiment

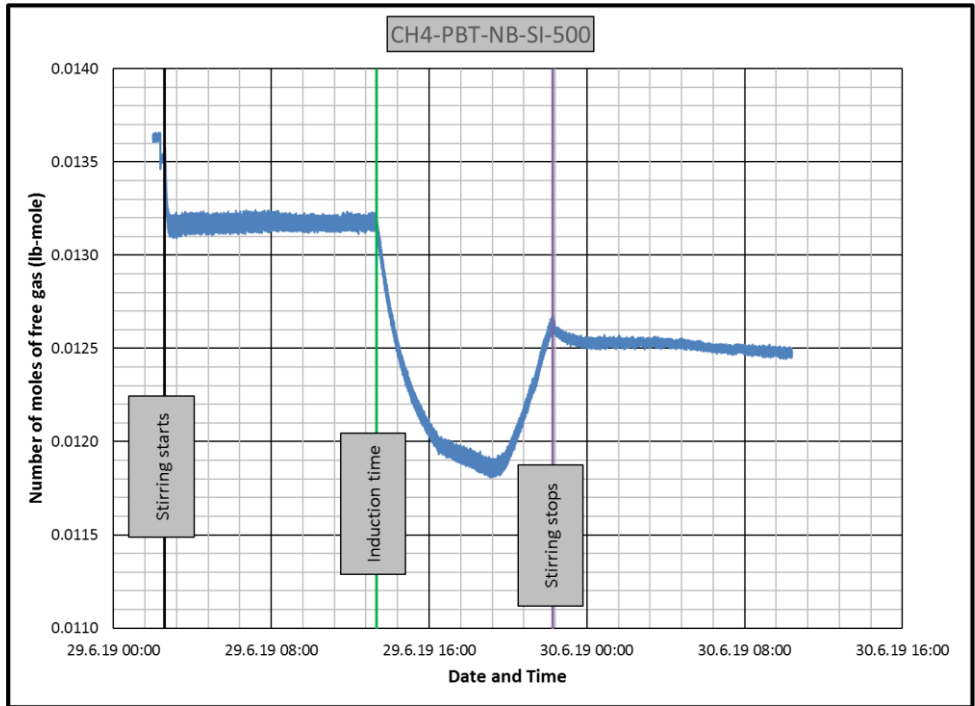


Figure B.7 Change in number of moles of free gas in CH4-PBT-NB-SI experiment

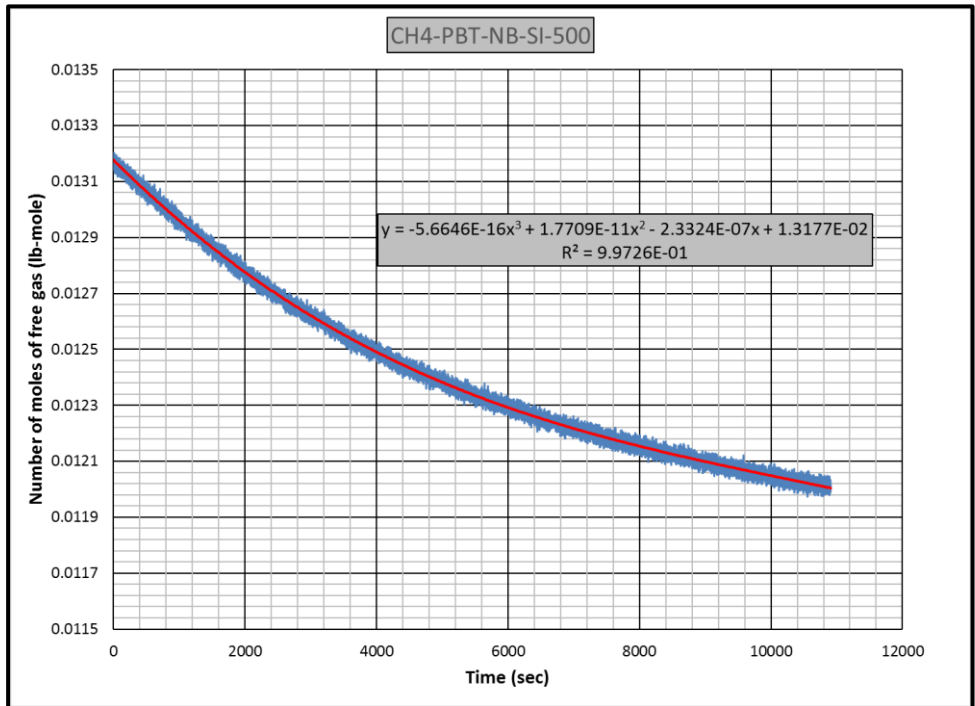


Figure B.8 Gas consumption rate equation for CH4-PBT-NB-SI experiment

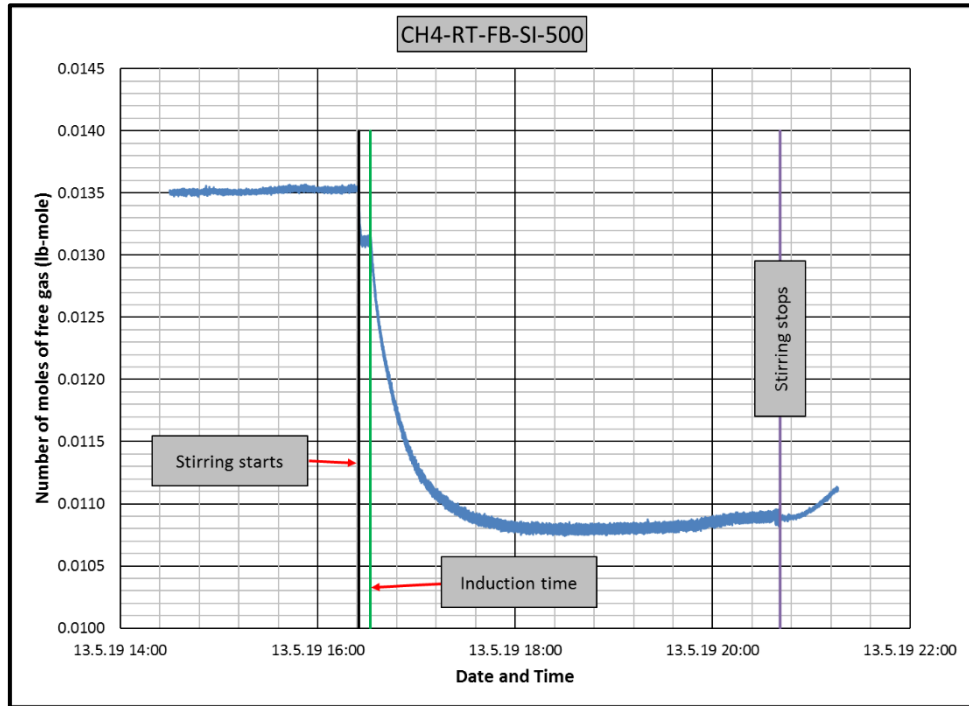


Figure B.9 Change in number of moles of free gas in CH4-RT-FB-SI experiment

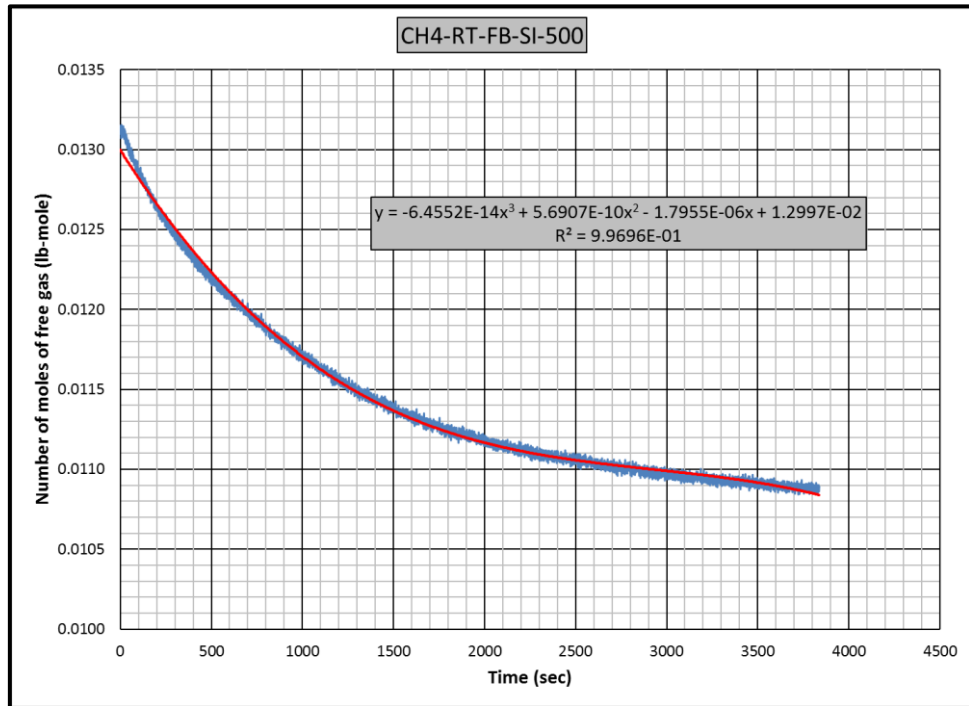


Figure B.10 Gas consumption rate equation for CH4-RT-FB-SI experiment

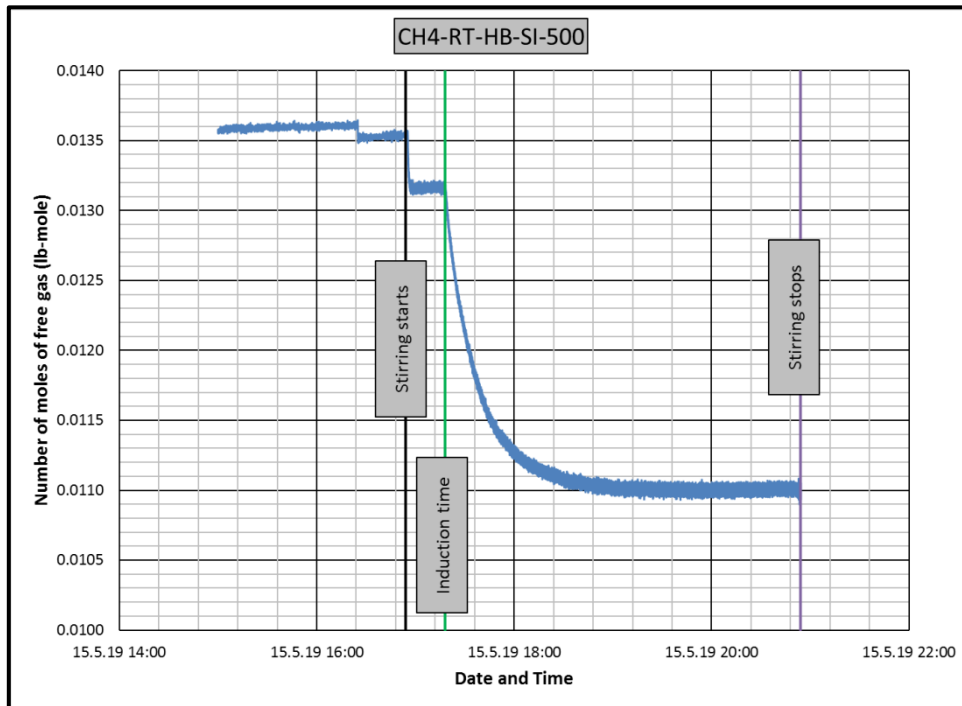


Figure B.11 Change in number of moles of free gas in CH4-RT-HB-SI experiment

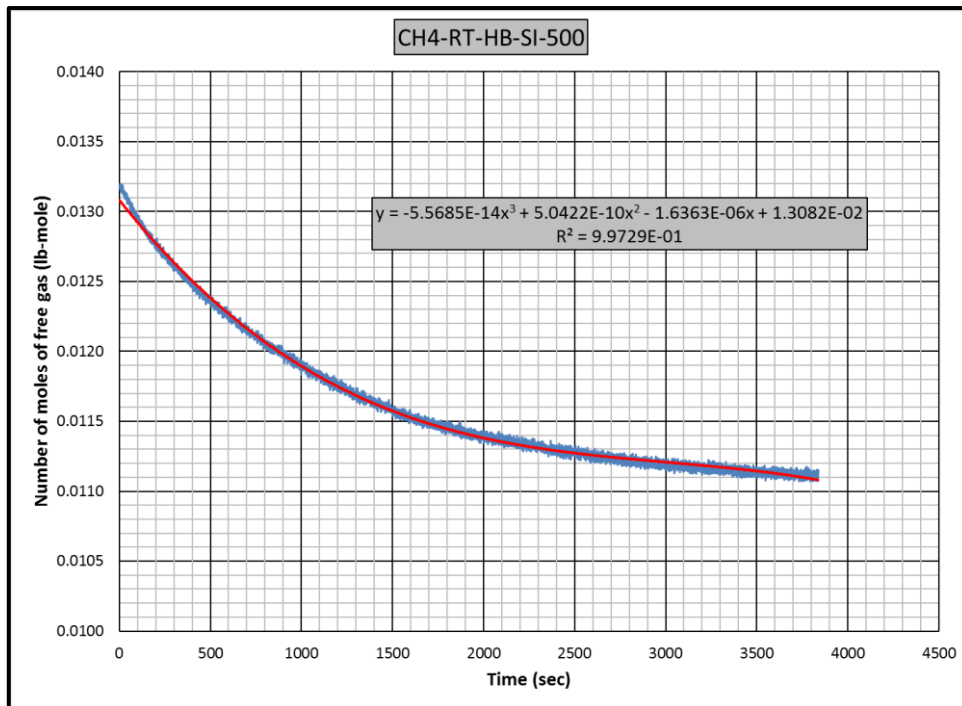


Figure B.12 Gas consumption rate equation for CH4-RT-HB-SI experiment

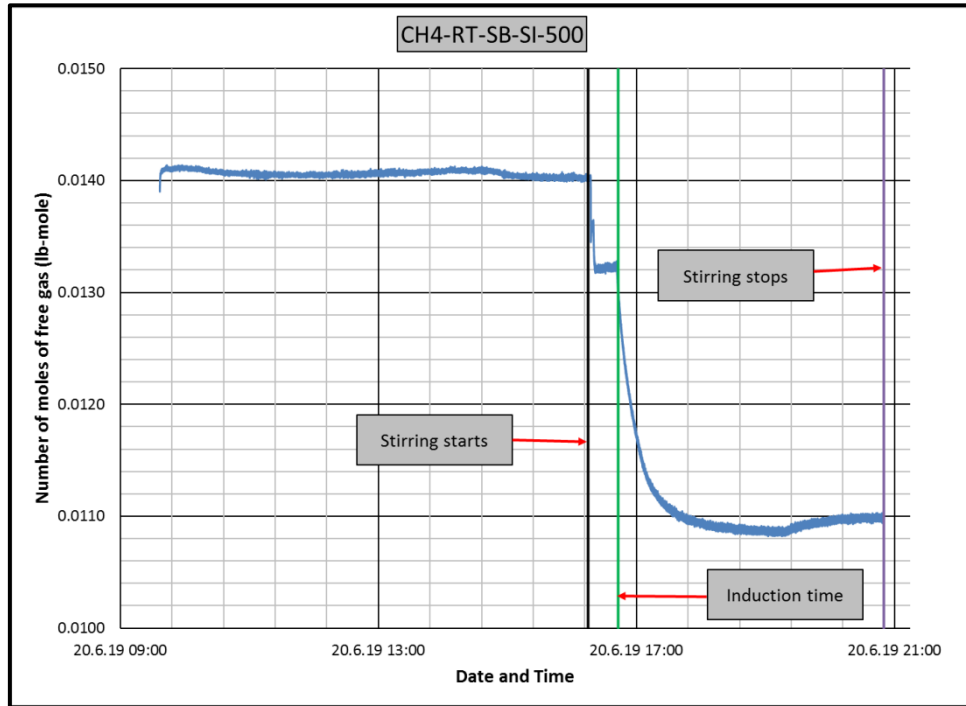


Figure B.13 Change in number of moles of free gas in CH4-RT-SB-SI experiment

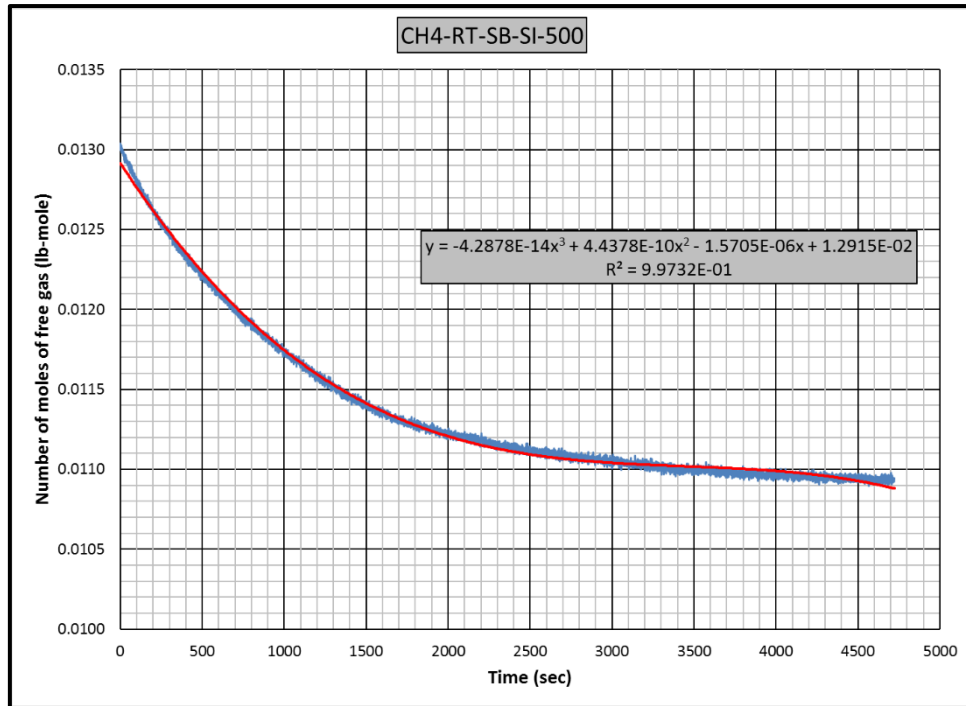


Figure B.14 Gas consumption rate equation for CH4-RT-SB-SI experiment

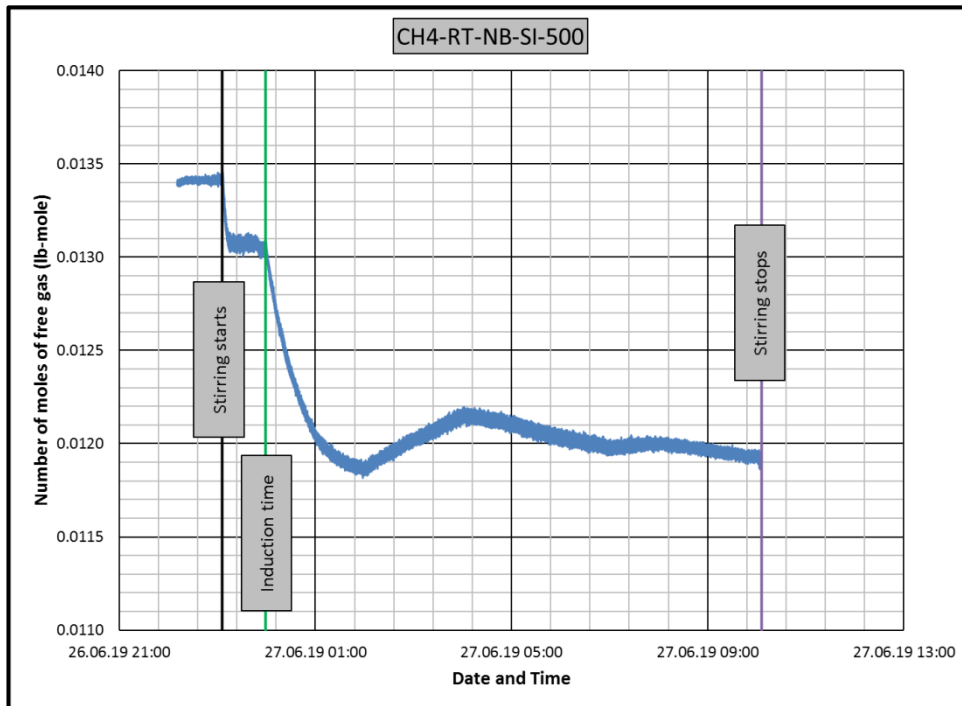


Figure B.15 Change in number of moles of free gas in CH4-RT-NB-SI experiment

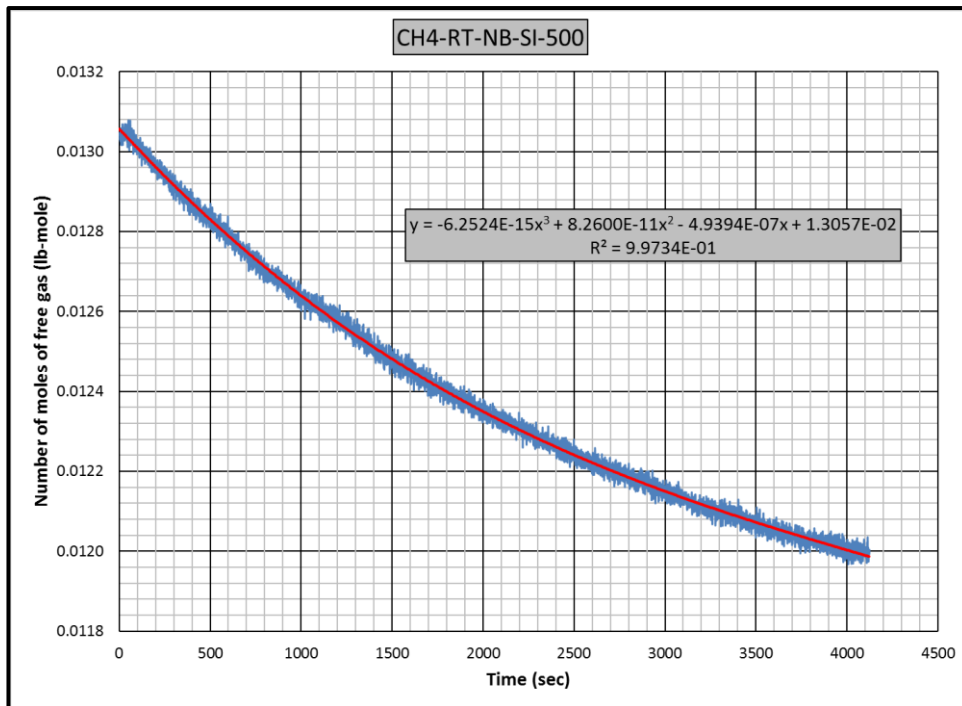


Figure B.16 Gas consumption rate equation for CH4-RT-NB-SI experiment

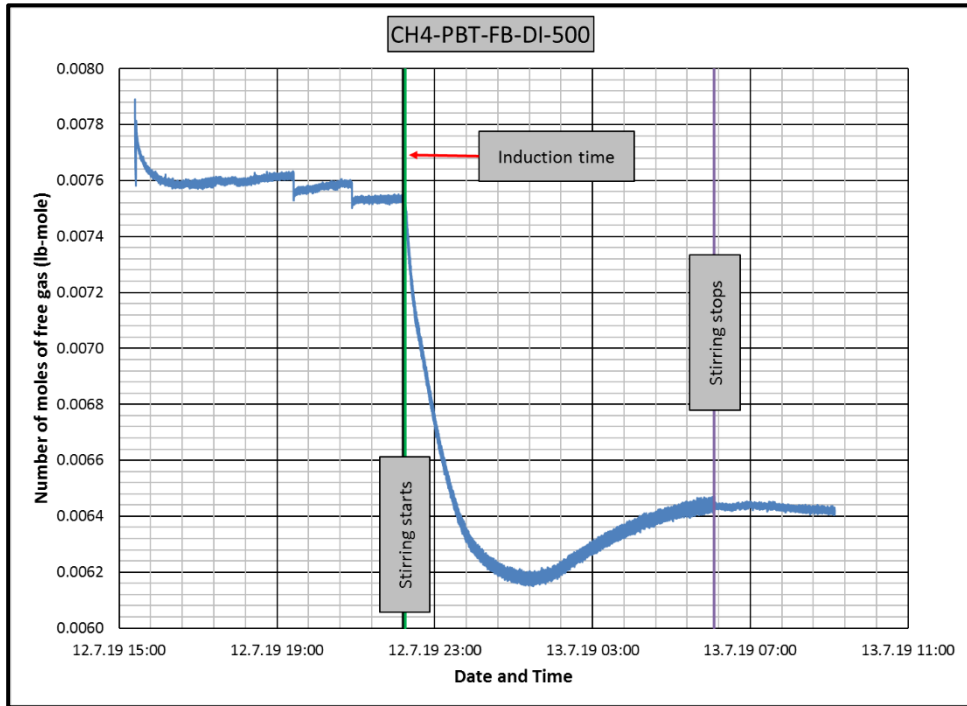


Figure B.17 Change in number of moles of free gas in CH4-PBT-FB-DI experiment

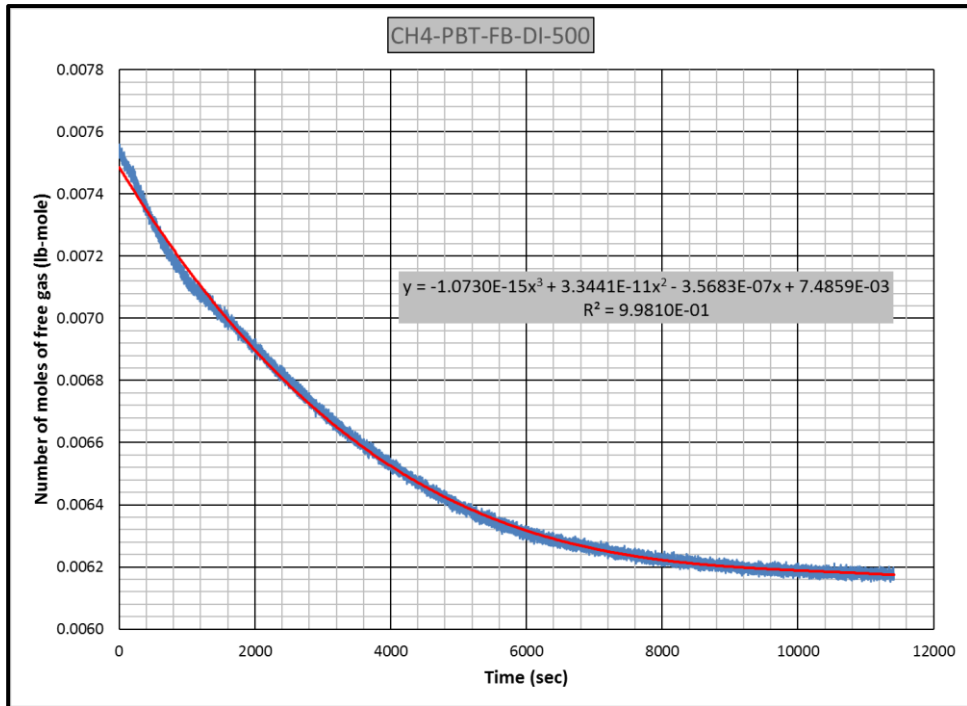


Figure B.18 Gas consumption rate equation for CH4-PBT-FB-DI experiment

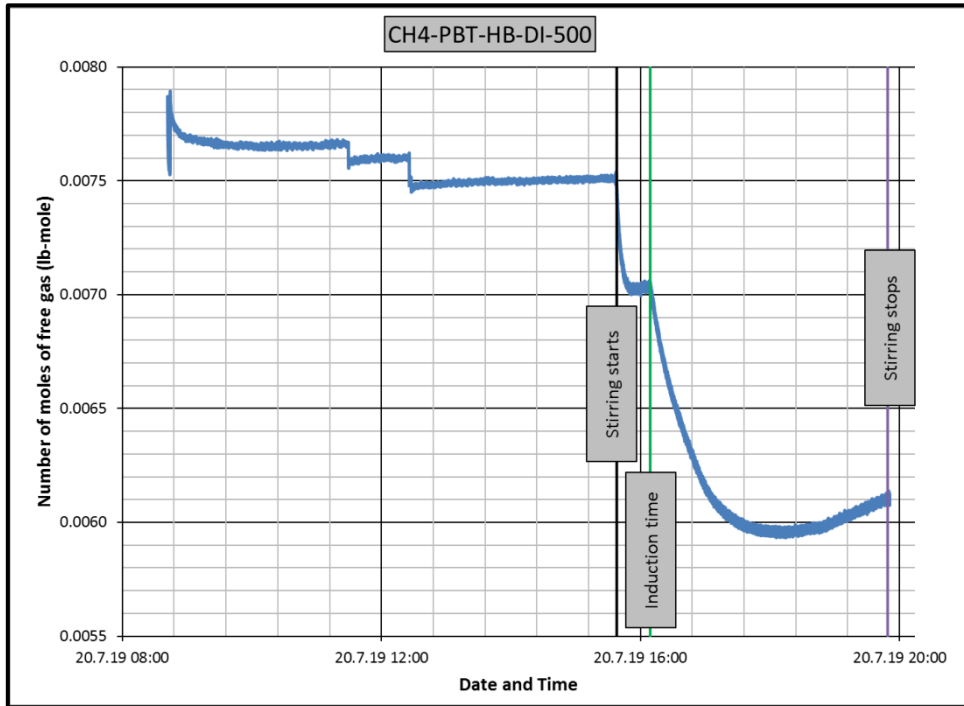


Figure B.19 Change in number of moles of free gas in CH4-PBT-HB-DI experiment

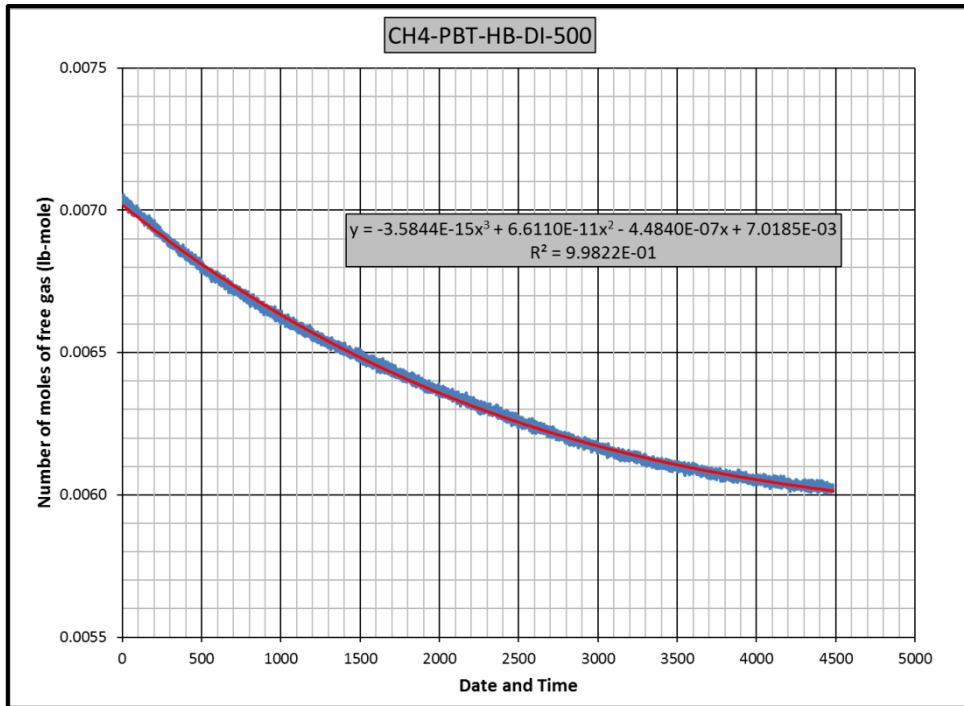


Figure B.20 Gas consumption rate equation for CH4-PBT-HB-DI experiment

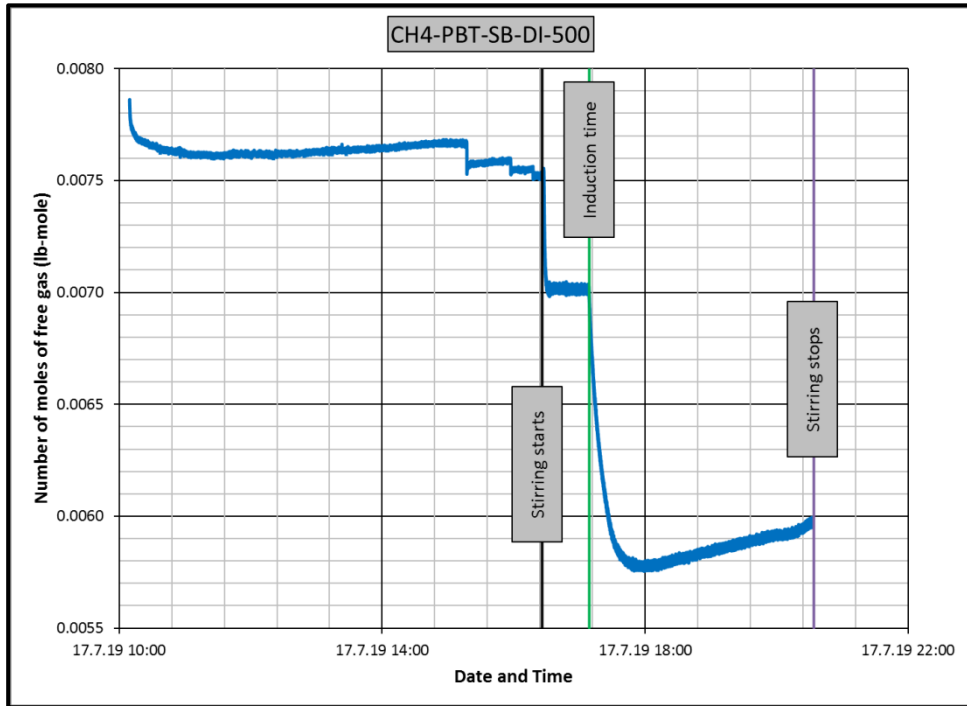


Figure B.21 Change in number of moles of free gas in CH4-PBT-SB-DI experiment

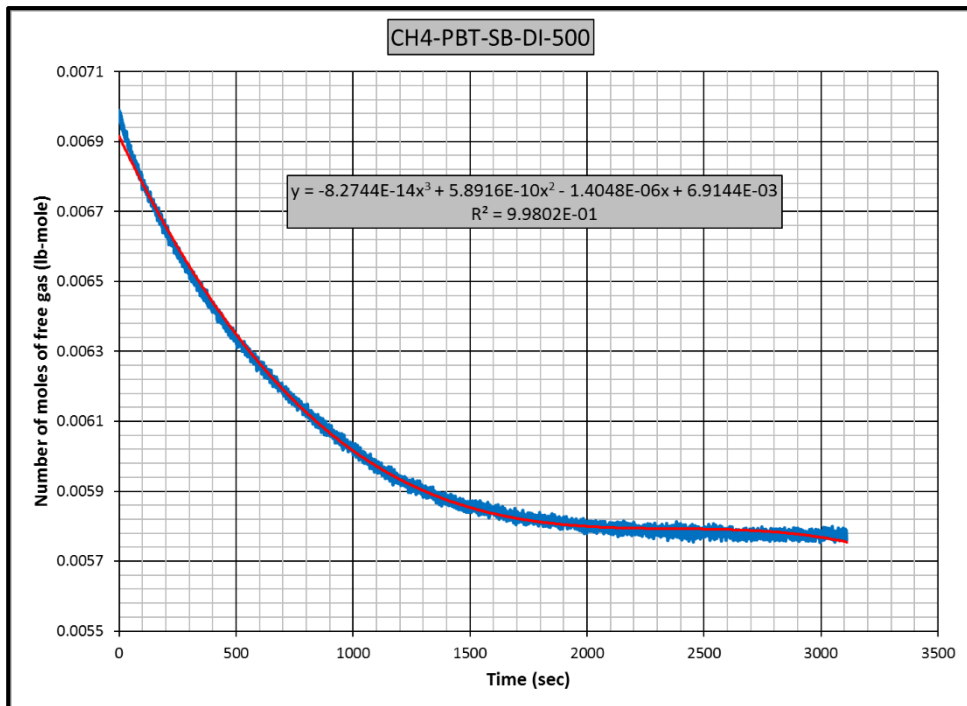


Figure B.22 Gas consumption rate equation for CH4-PBT-SB-DI experiment

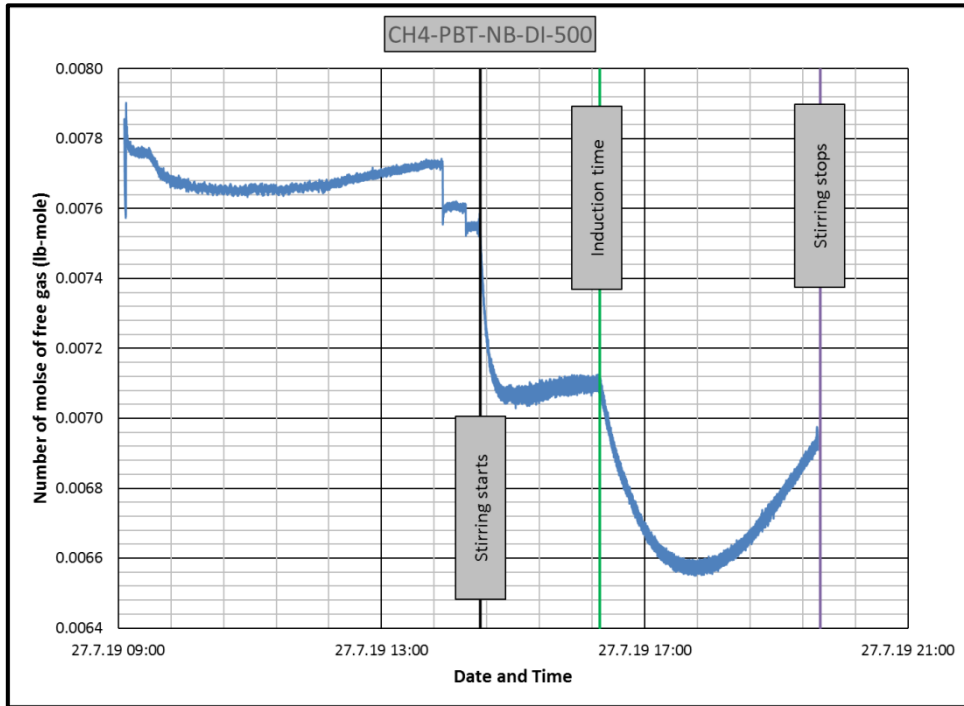


Figure B.23 Change in number of moles of free gas in CH4-PBT-NB-DI experiment

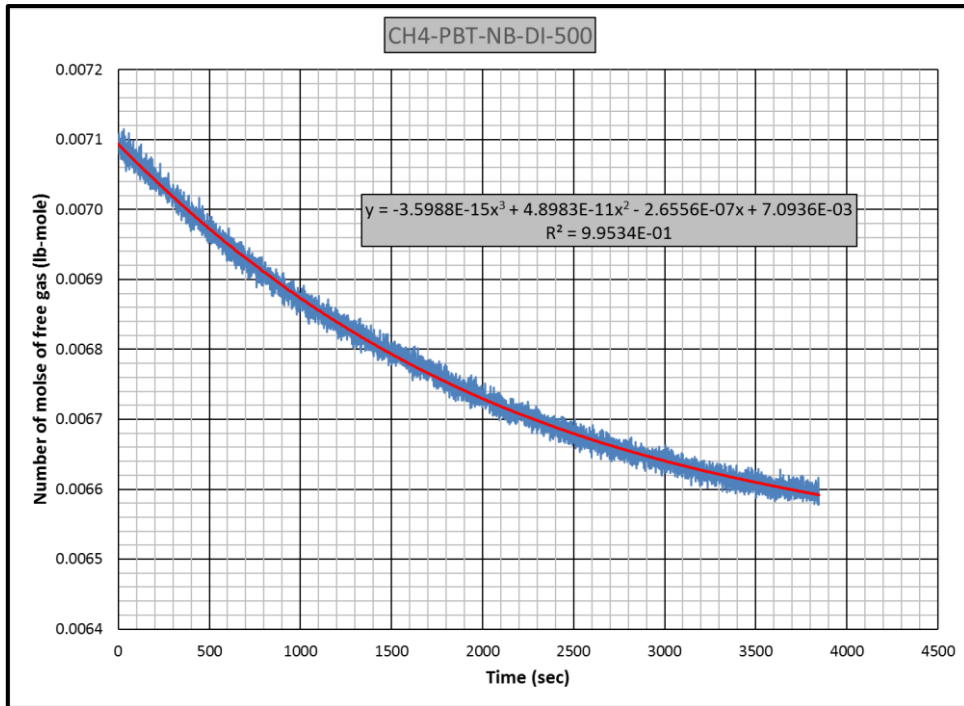


Figure B.24 Gas consumption rate equation for CH4-PBT-NB-DI experiment

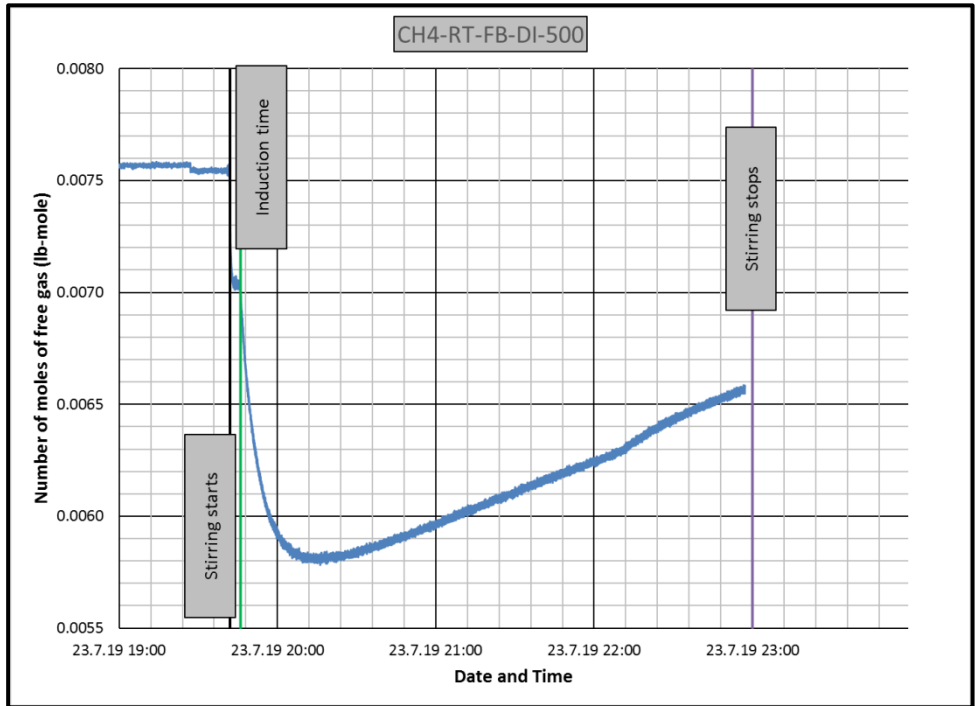


Figure B.25 Change in number of moles of free gas in CH4-RT-FB-DI experiment

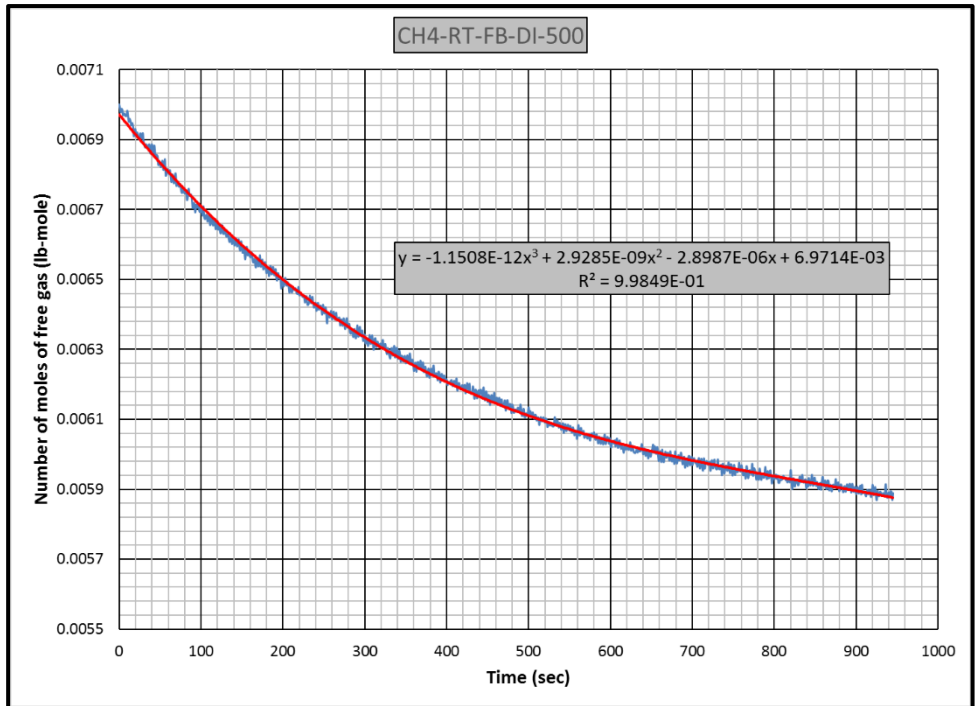


Figure B.26 Gas consumption rate equation for CH4-RT-FB-DI experiment

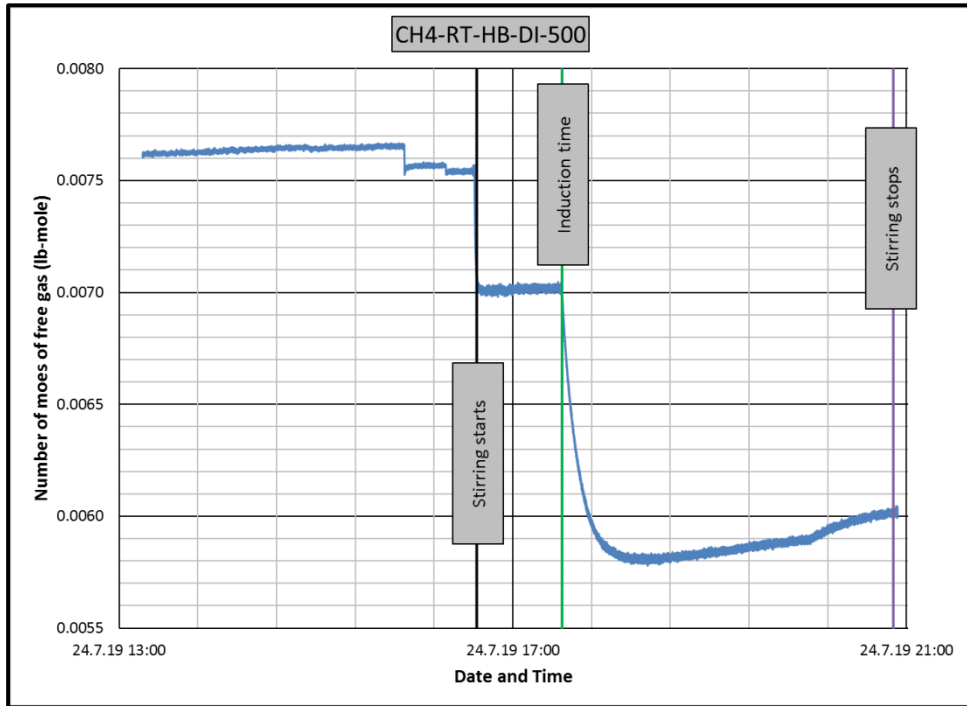


Figure B.27 Change in number of moles of free gas in CH4-RT-HB-DI experiment

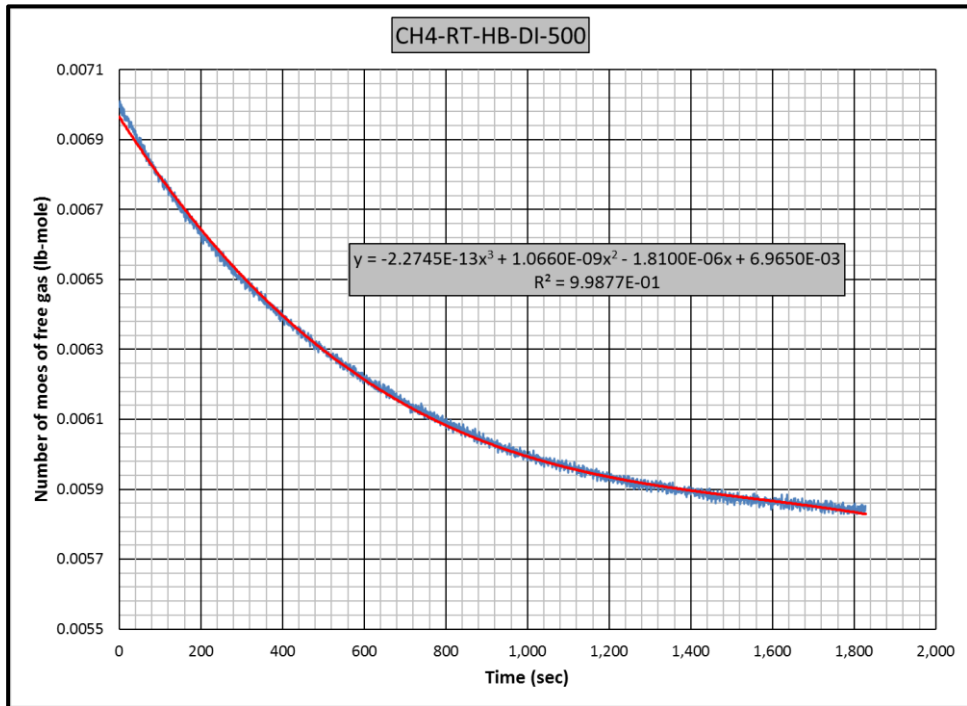


Figure B.28 Gas consumption rate equation for CH4-RT-HB-DI experiment

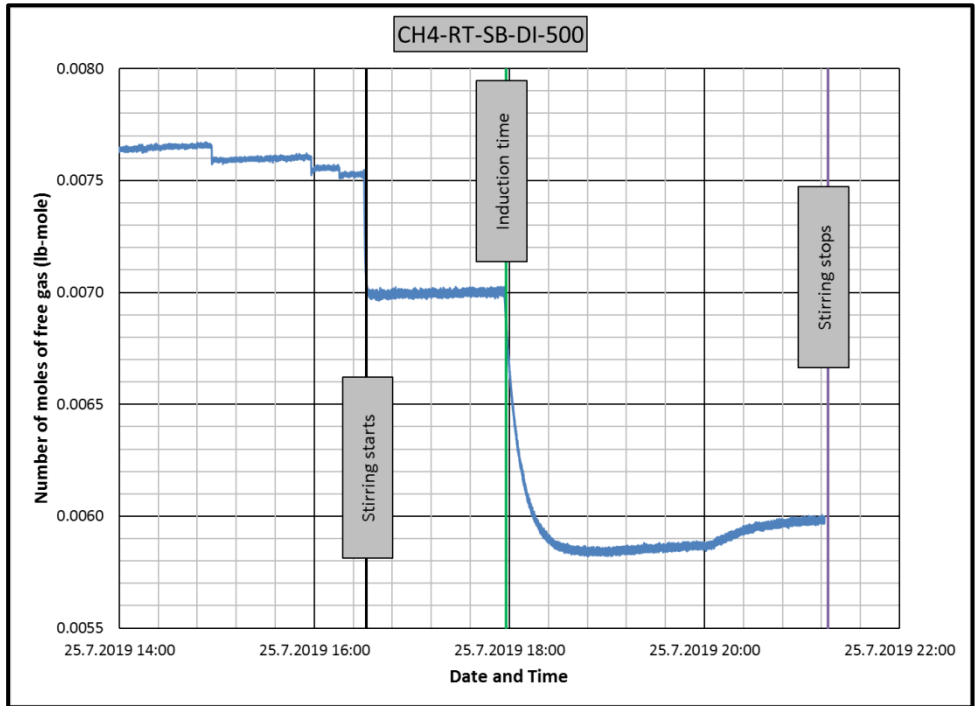


Figure B.29 Change in number of moles of free gas in CH4-RT-SB-DI experiment

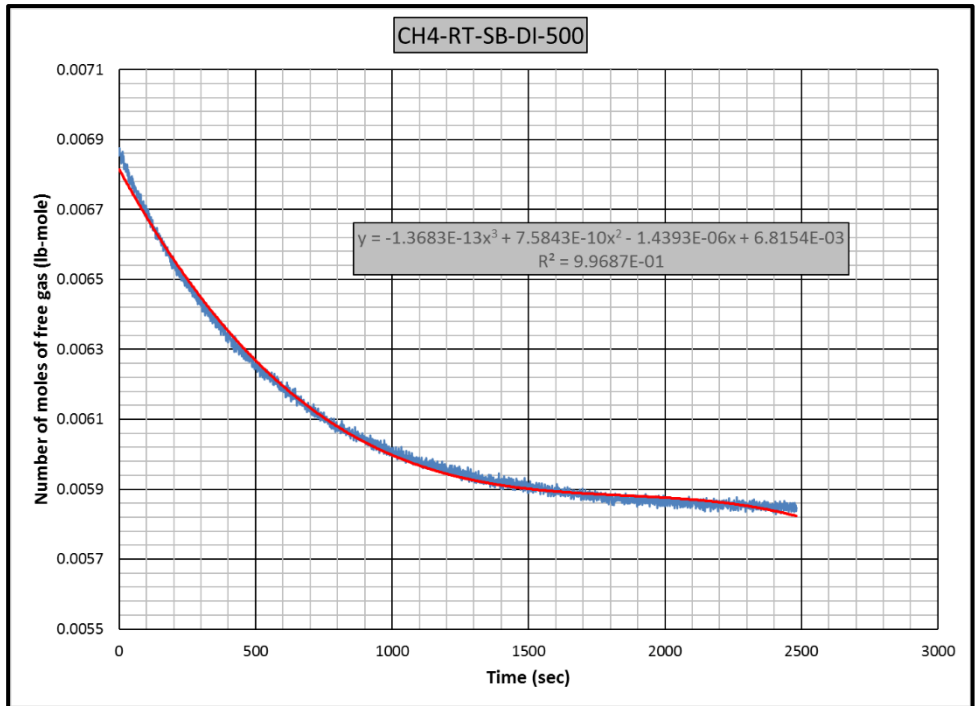


Figure B.30 Gas consumption rate equation for CH4-RT-SB-DI experiment

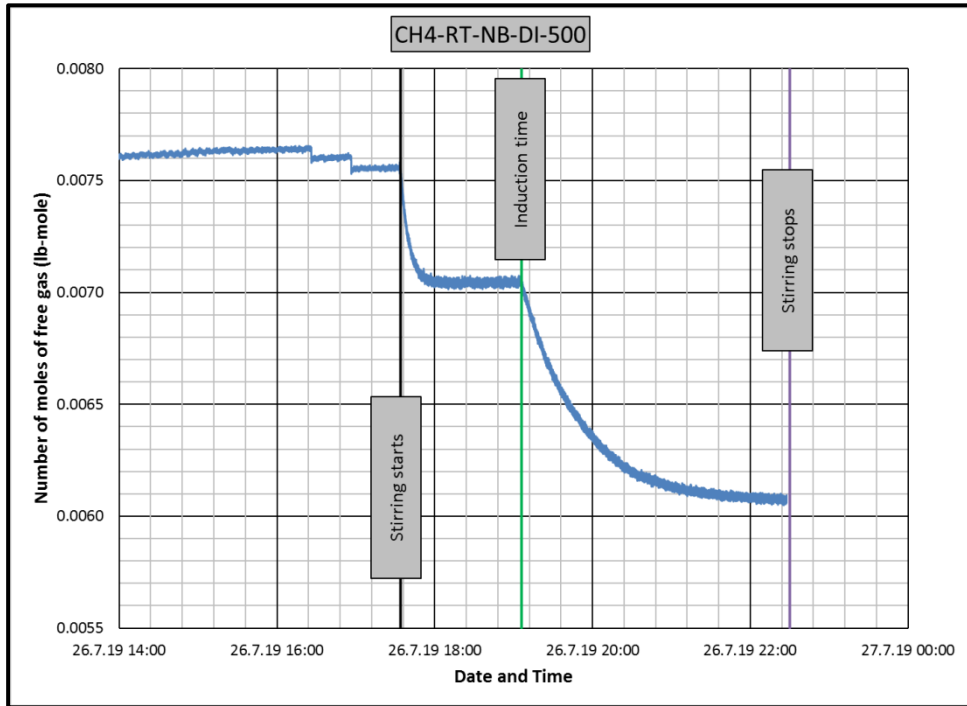


Figure B.31 Change in number of moles of free gas in CH4-RT-NB-DI experiment

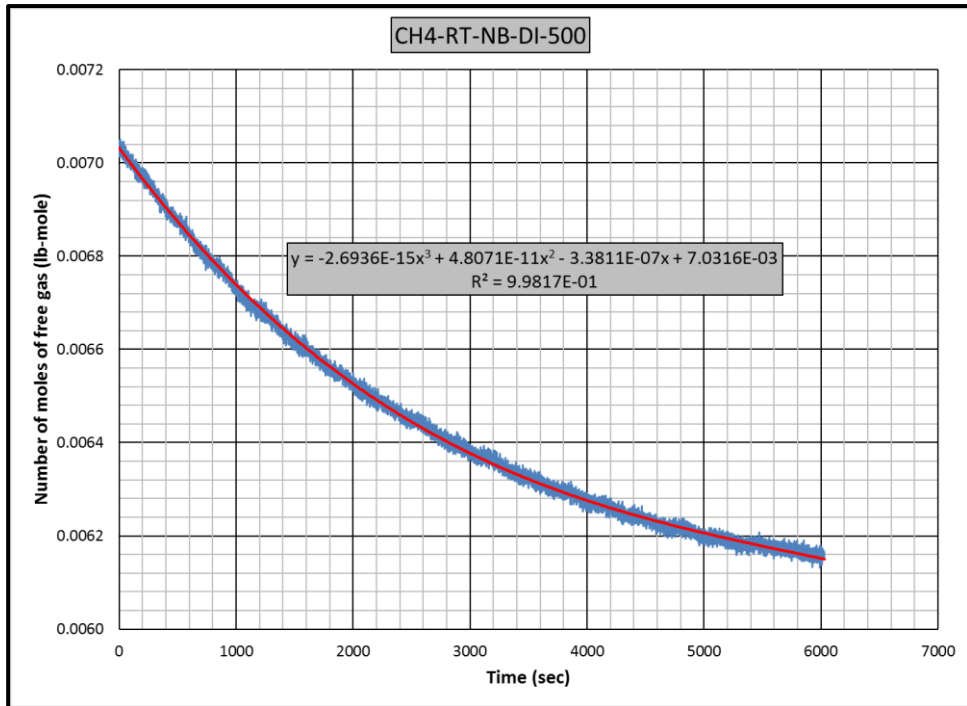


Figure B.32 Gas consumption rate equation for CH4-RT-NB-DI experiment

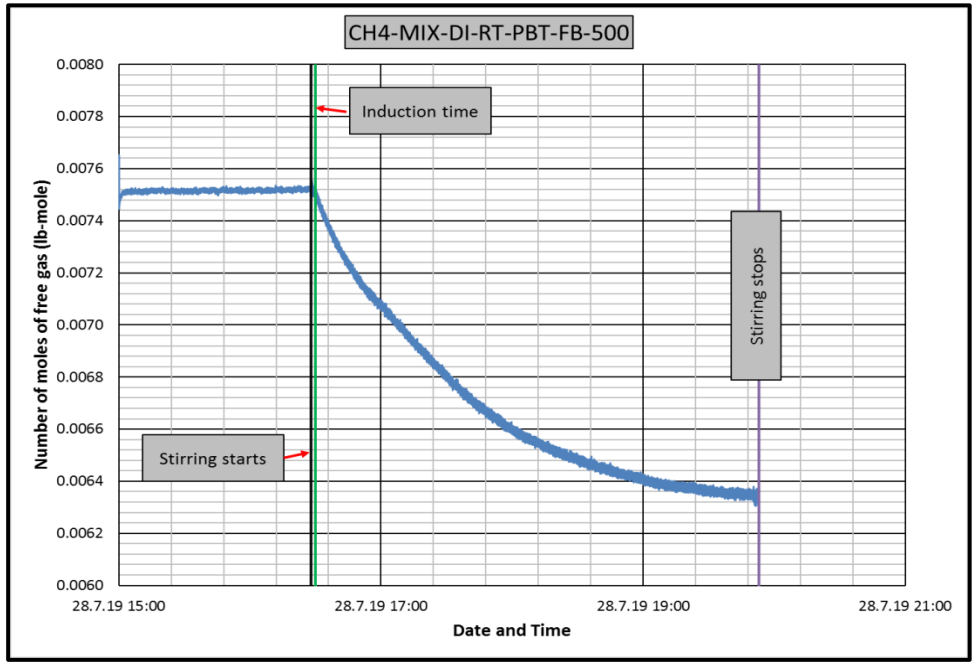


Figure B.33 Change in number of moles of free gas in CH4-MIX-RT-PBT-FB-DI experiment

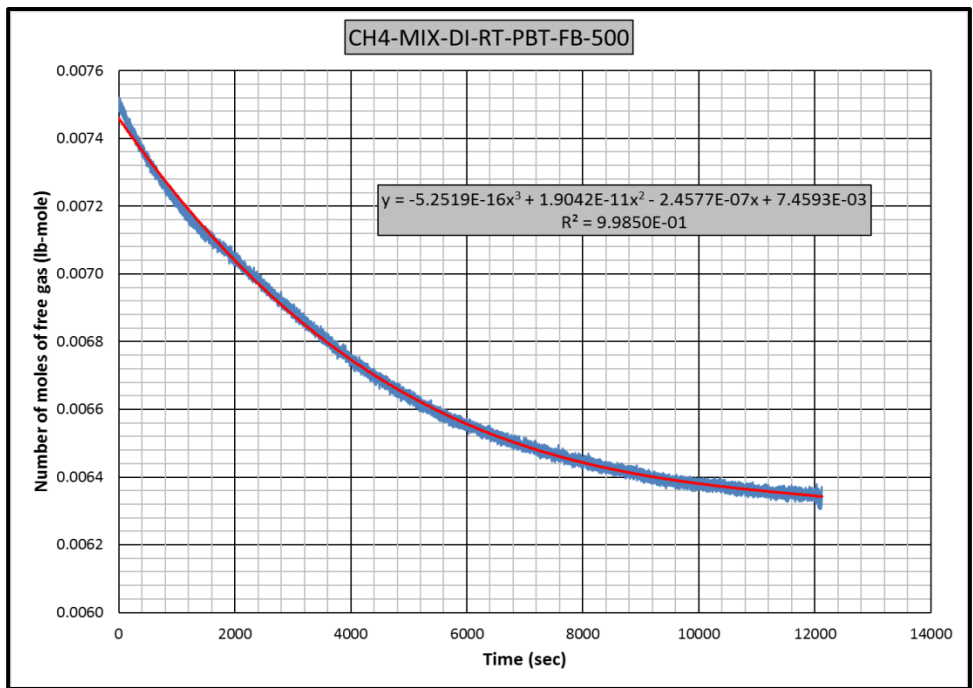


Figure B.34 Gas consumption rate equation for CH4-MIX-RT-PBT-FB-DI experiment

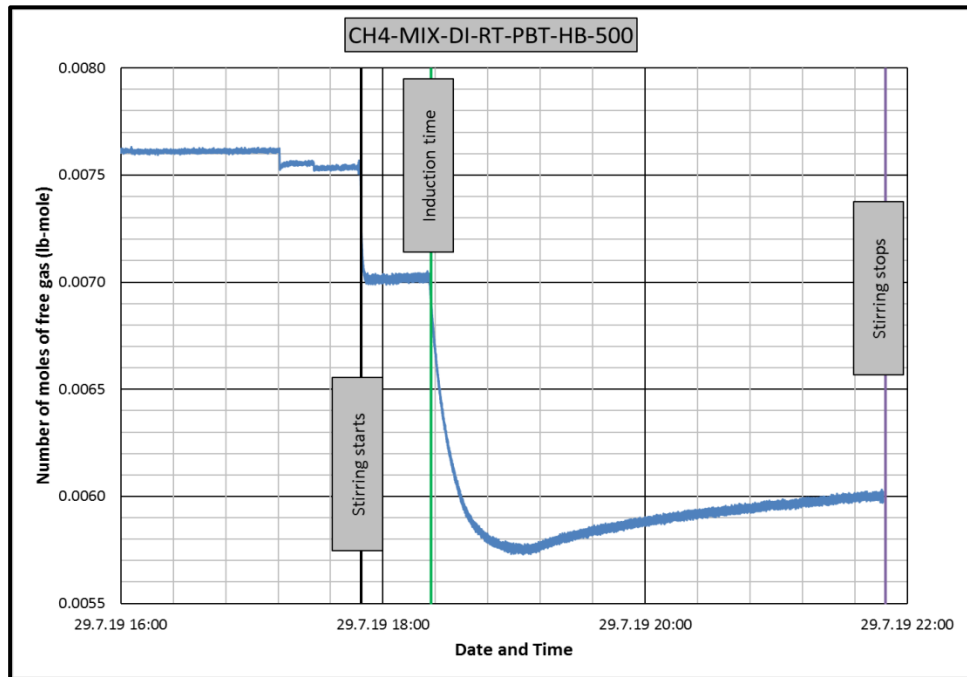


Figure B.35 Change in number of moles of free gas in CH4-MIX-RT-PBT-HB-DI experiment

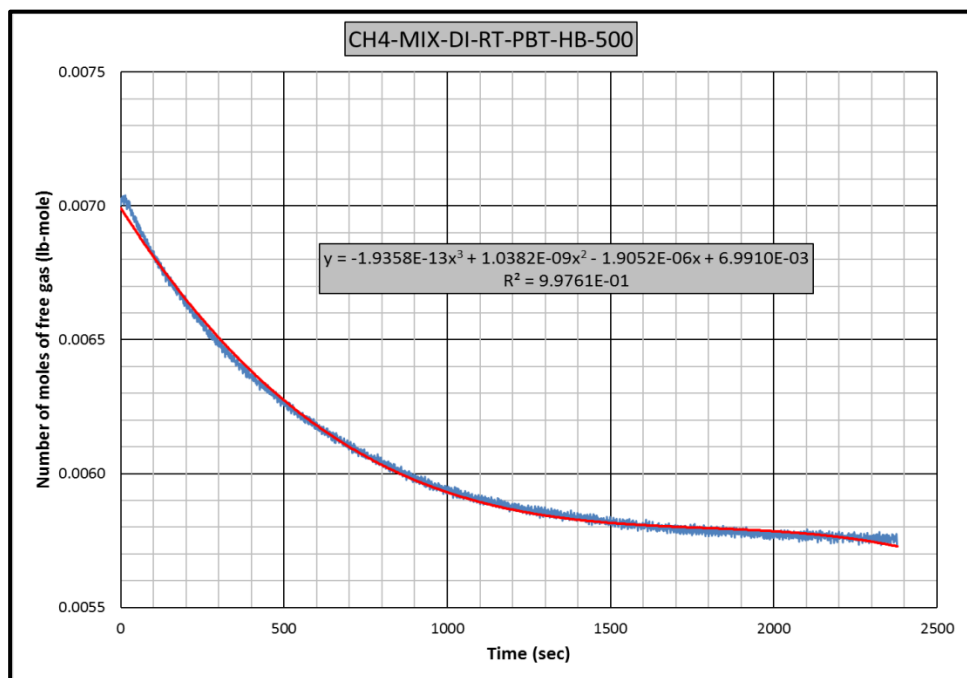


Figure B.36 Gas consumption rate equation for CH4-MIX-RT-PBT-HB-DI experiment

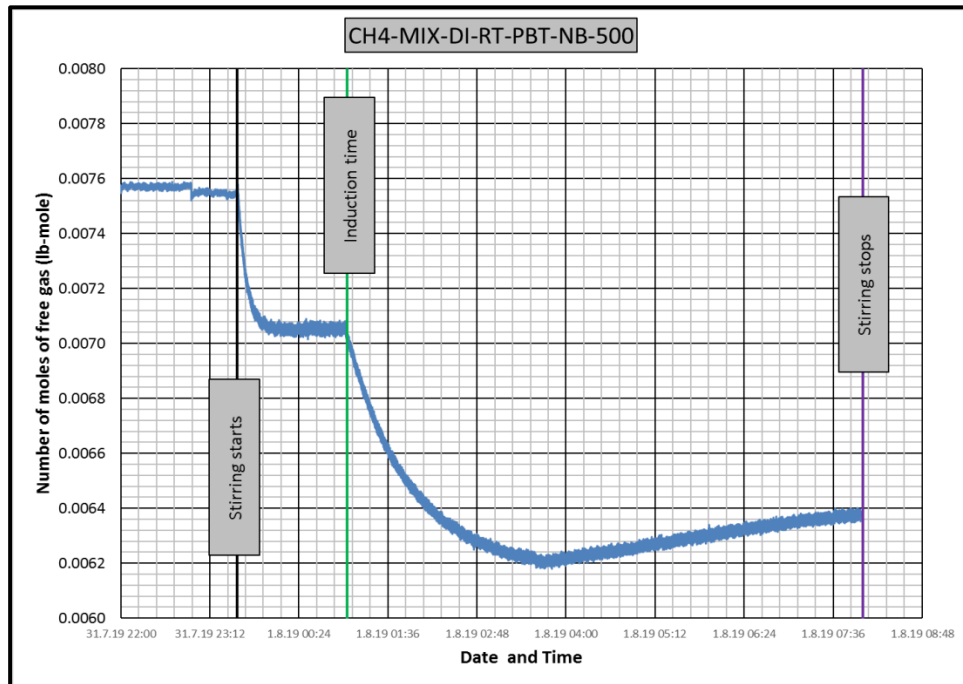


Figure B.37 Change in number of moles of free gas in CH4-MIX-RT-PBT-NB-DI experiment

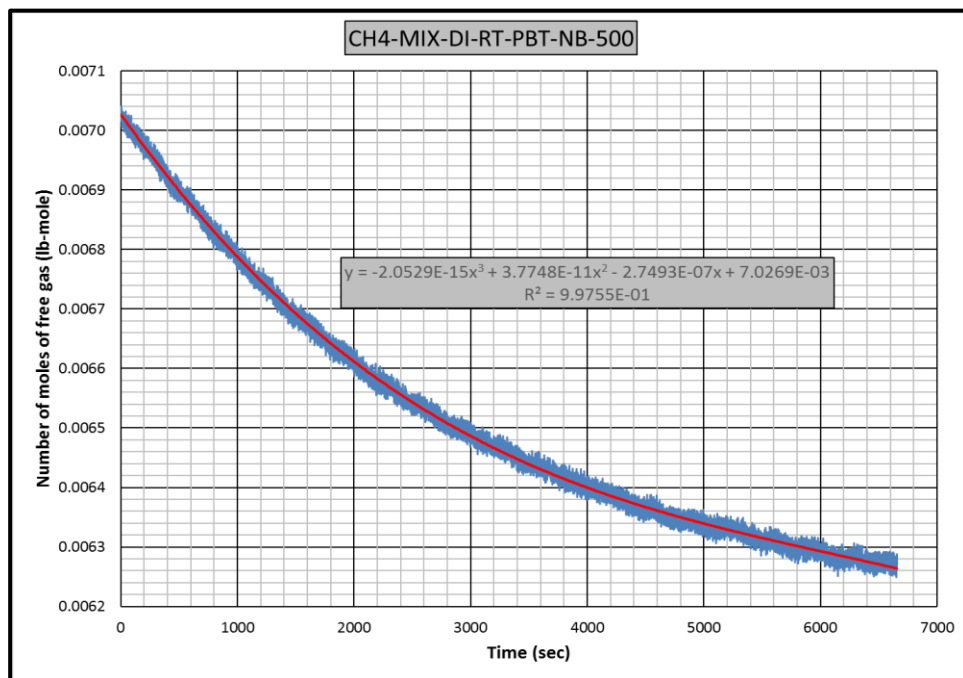


Figure B.38 Gas consumption rate equation for CH4-MIX-RT-PBT-NB-DI experiment

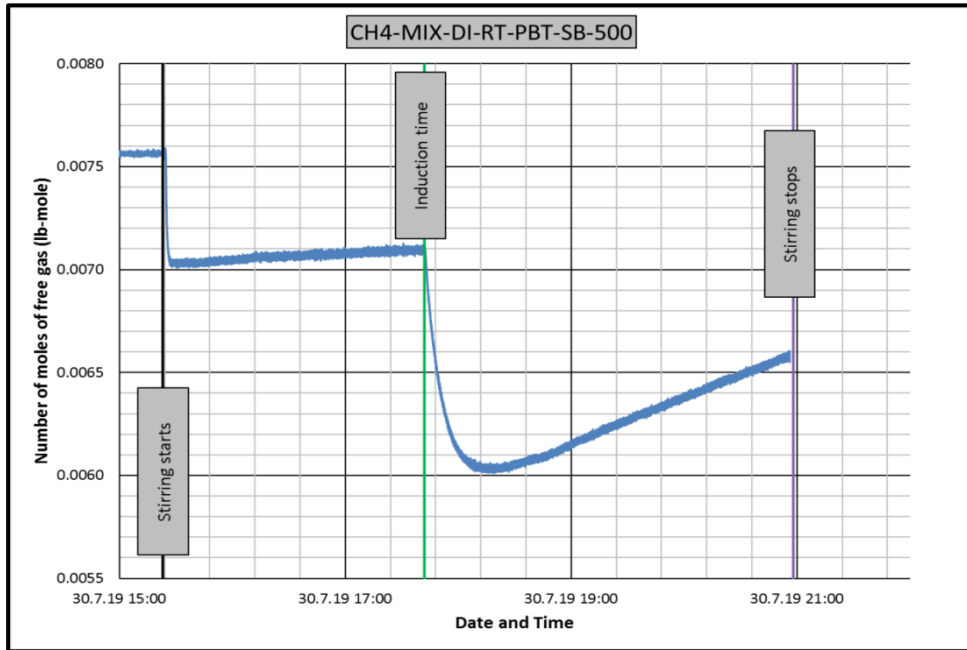


Figure B.39 Change in number of moles of free gas in CH4-MIX-RT-PBT-SB-DI experiment

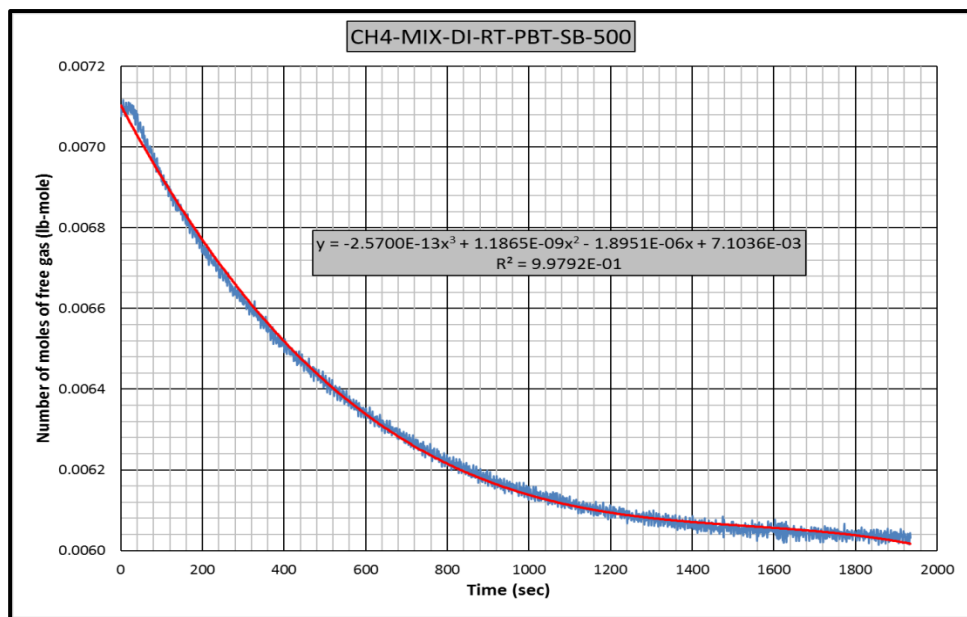


Figure B.40 Gas consumption rate equation for CH4-MIX-RT-PBT-SB-DI experiment

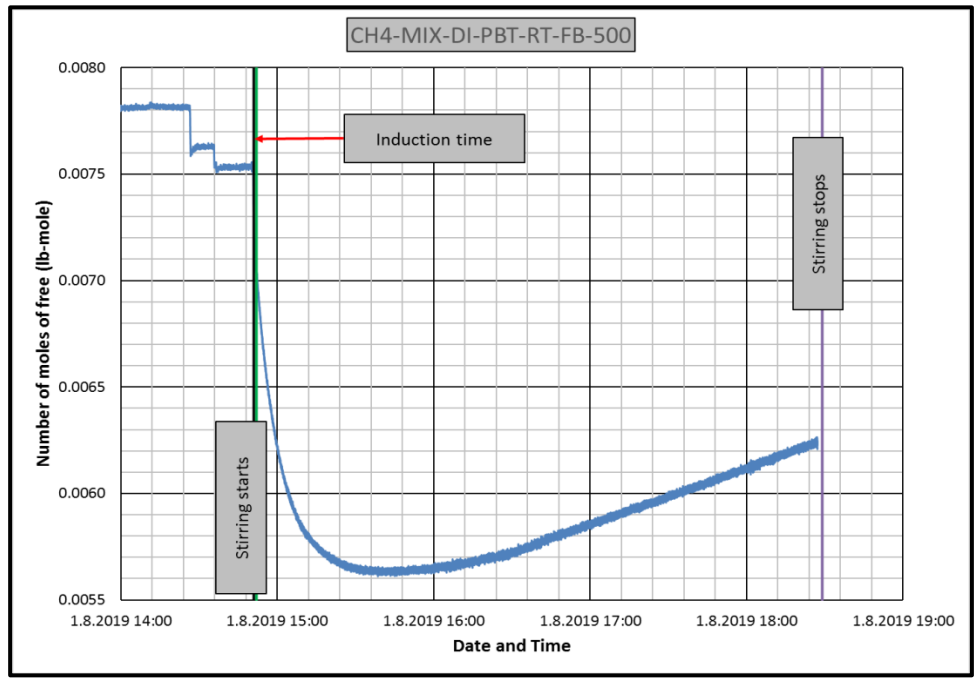


Figure B.41 Change in number of moles of free gas in CH4-MIX-PBT-RT-FB-DI experiment

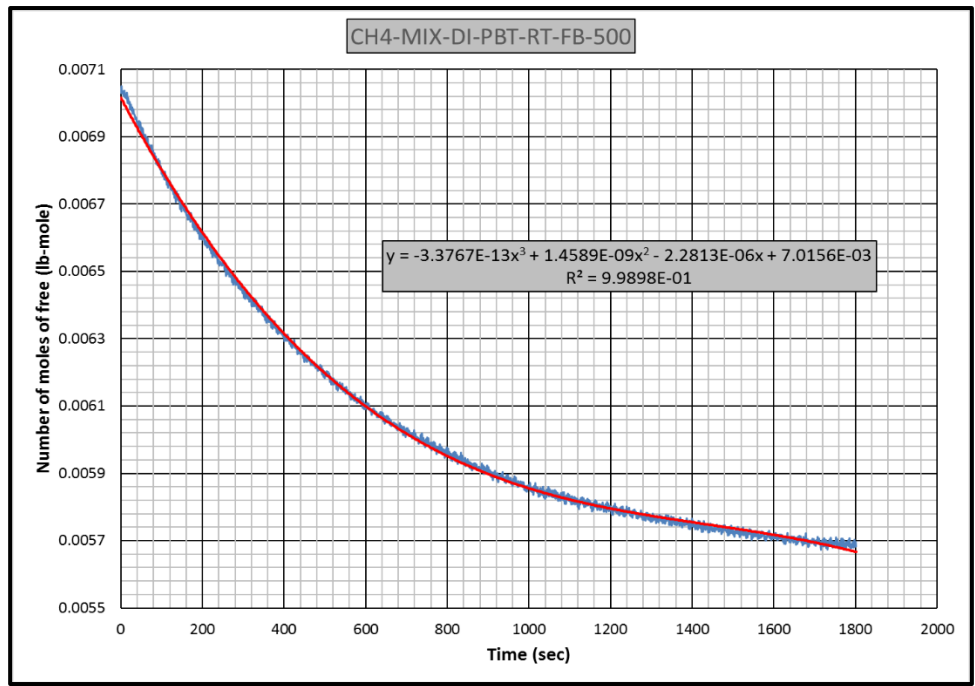


Figure B.42 Gas consumption rate equation for CH4-MIX-PBT-RT-FB-DI experiment

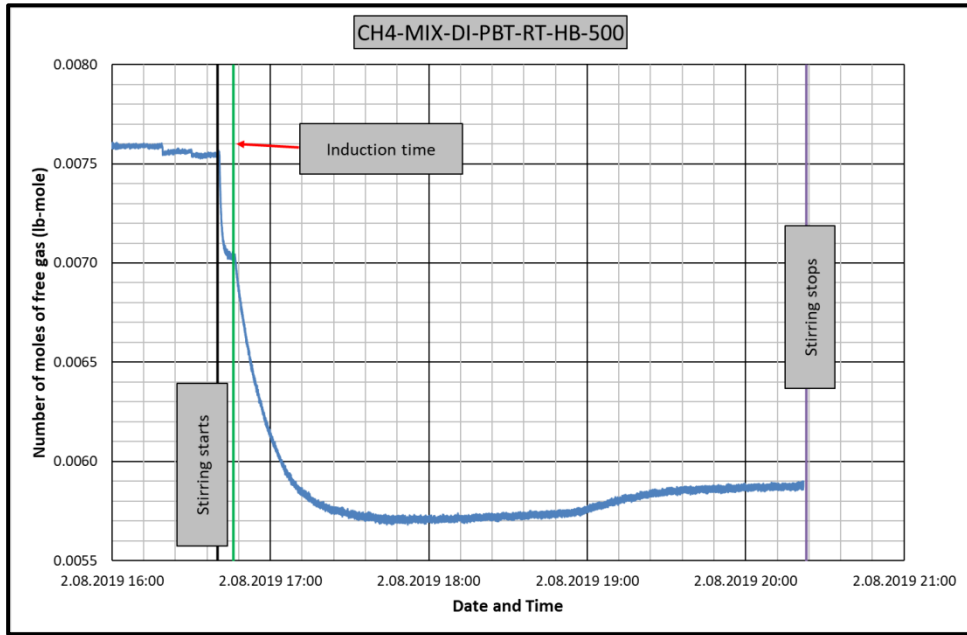


Figure B.43 Change in number of moles of free gas in CH4-MIX-PBT-RT-HB-DI experiment

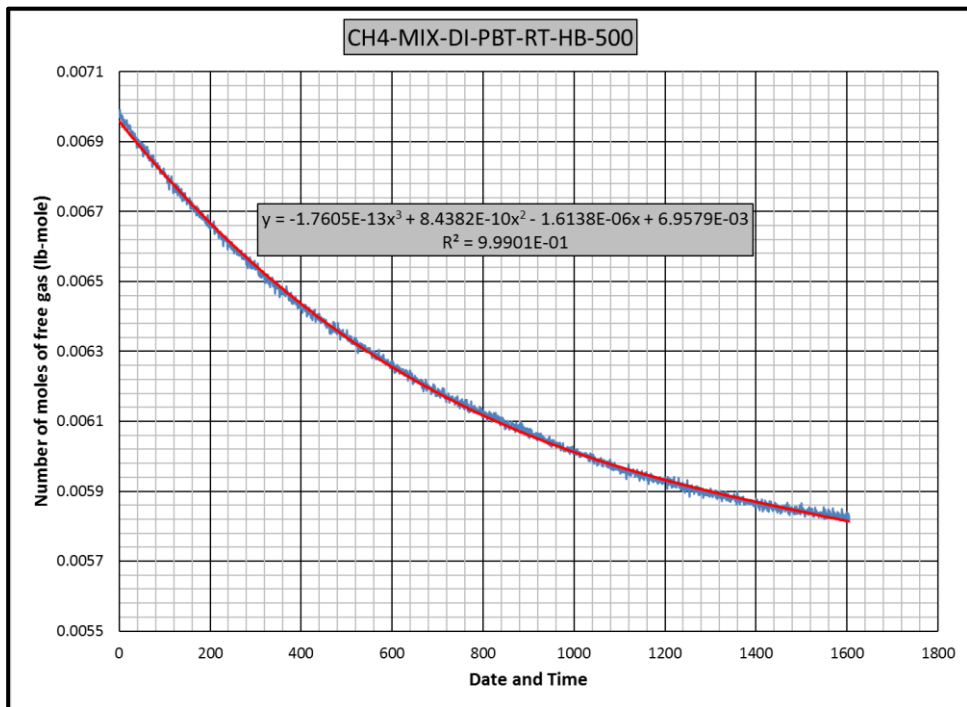


Figure B.44 Gas consumption rate equation for CH4-MIX-PBT-RT-HB-DI experiment

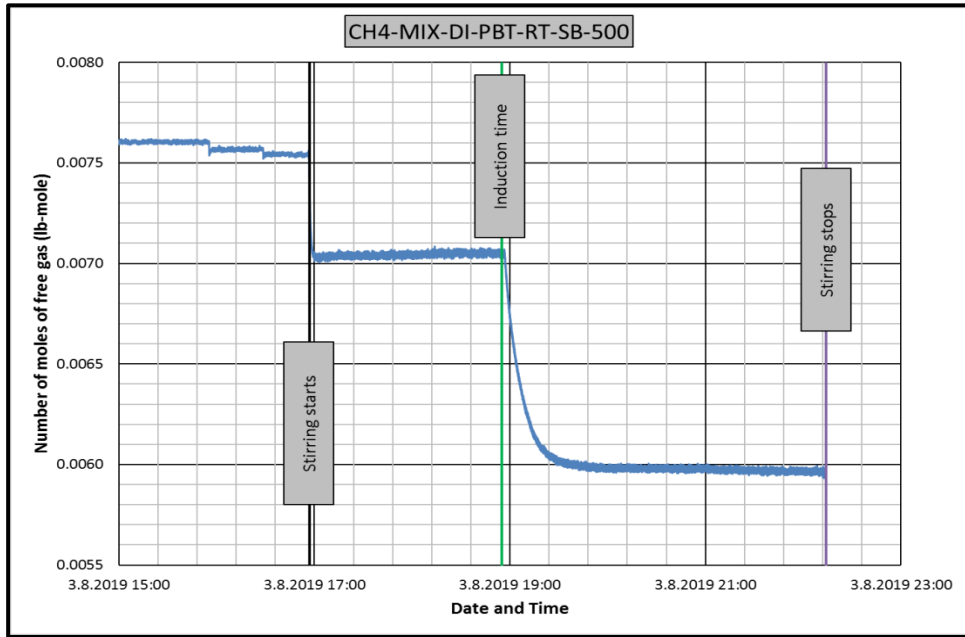


Figure B.45 Change in number of moles of free gas in CH4-MIX-PBT-RT-SB-DI experiment

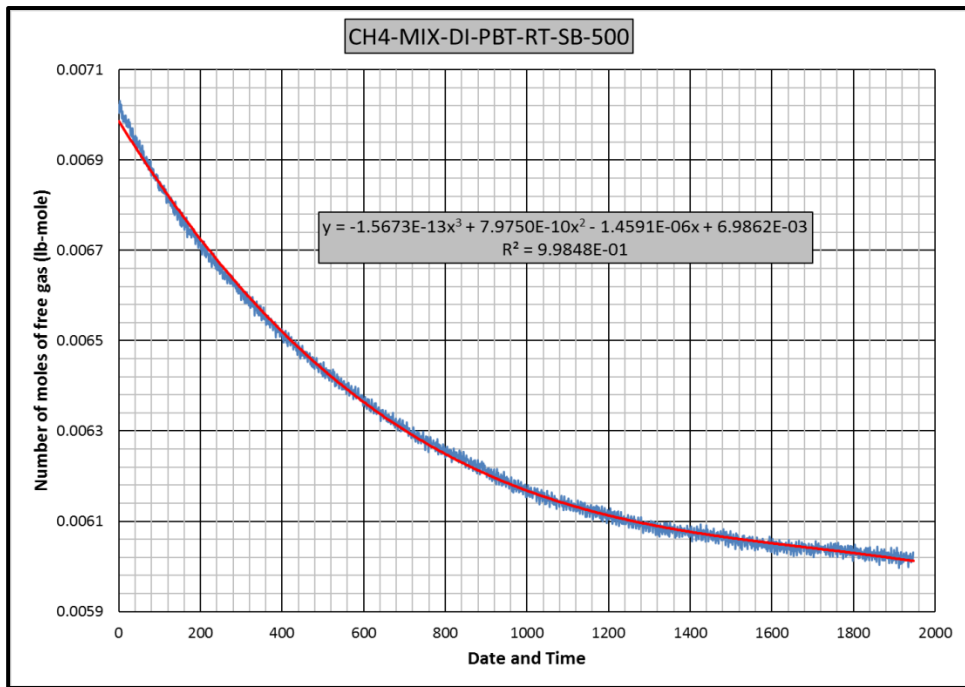


Figure B.46 Gas consumption rate equation for CH4-MIX-PBT-RT-SB-DI experiment

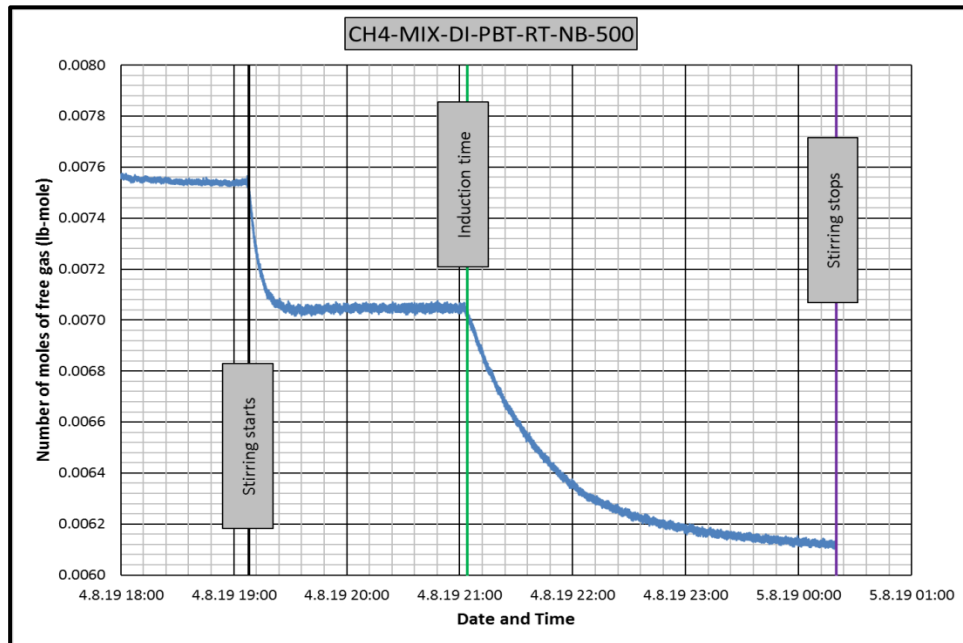


Figure B.47 Change in number of moles of free gas in CH4-MIX-PBT-RT-NB-DI experiment

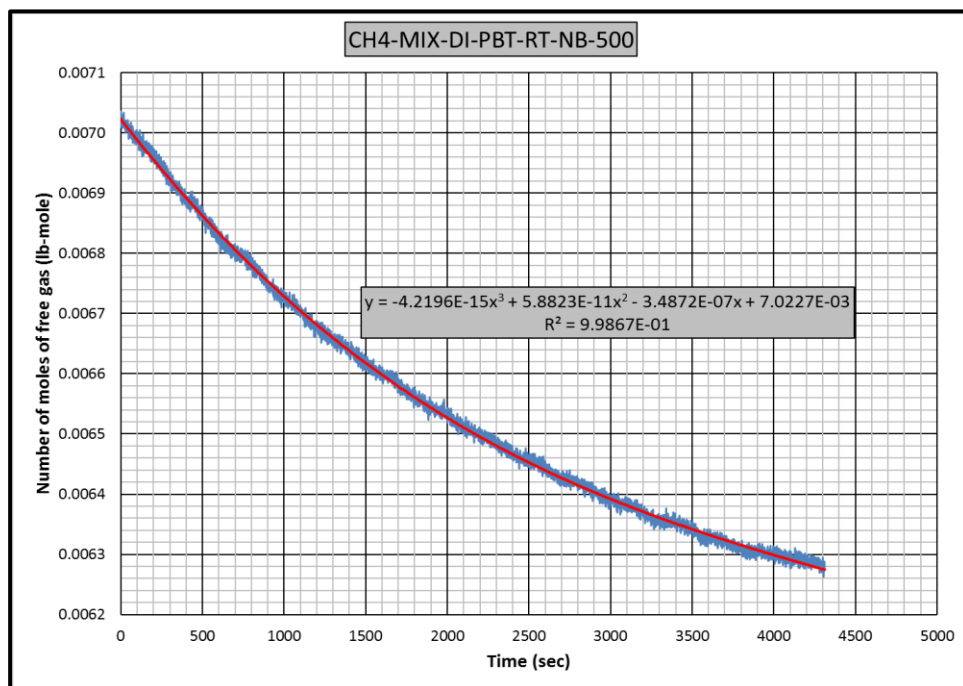


Figure B.48 Gas consumption rate equation for CH4-MIX-PBT-RT-NB-DI experiment

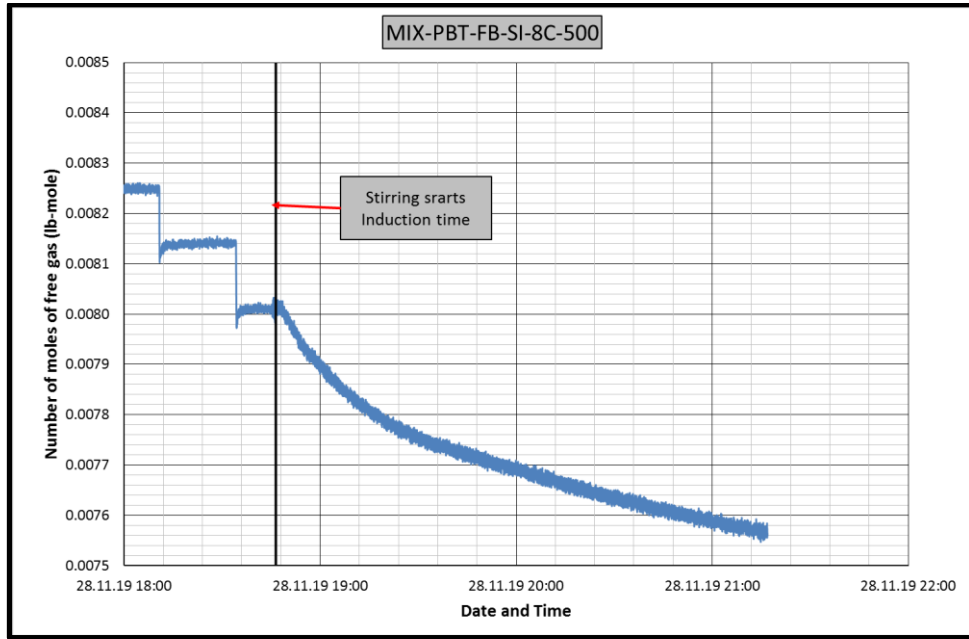


Figure B.49 Change in number of moles of free gas in CH₄-C₃H₈-PBT-FB-SI-8C experiment

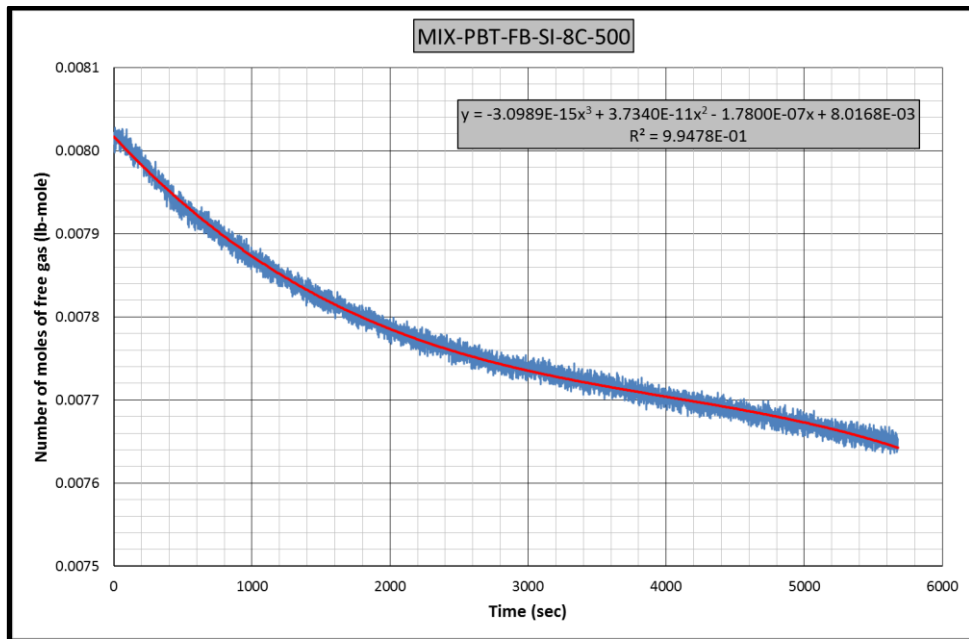


Figure B.50 Gas consumption rate equation for CH₄-C₃H₈-PBT-FB-SI-8C experiment

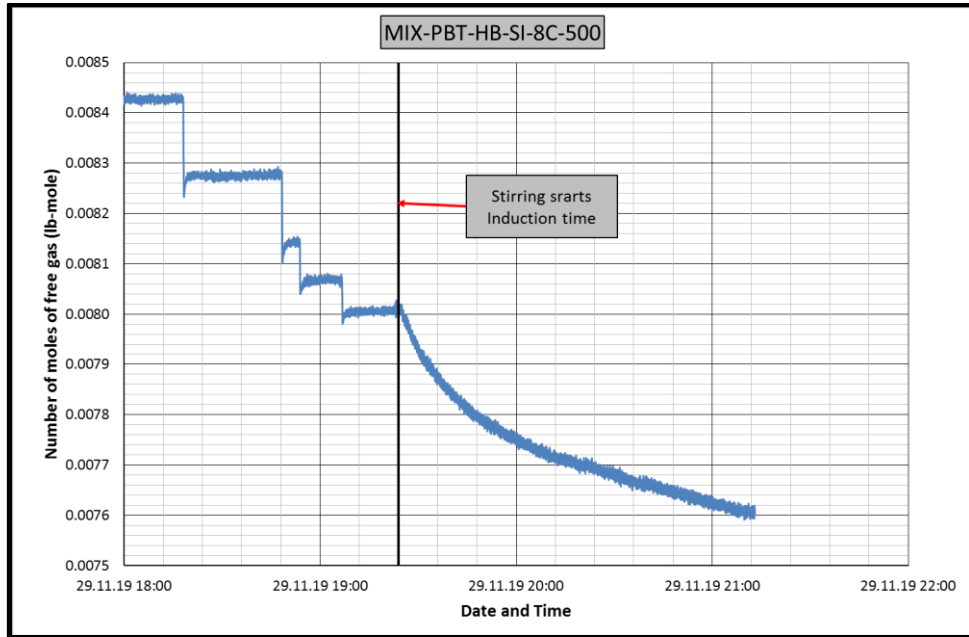


Figure B.51 Change in number of moles of free gas in CH₄-C₃H₈-PBT-HB-SI-8C experiment

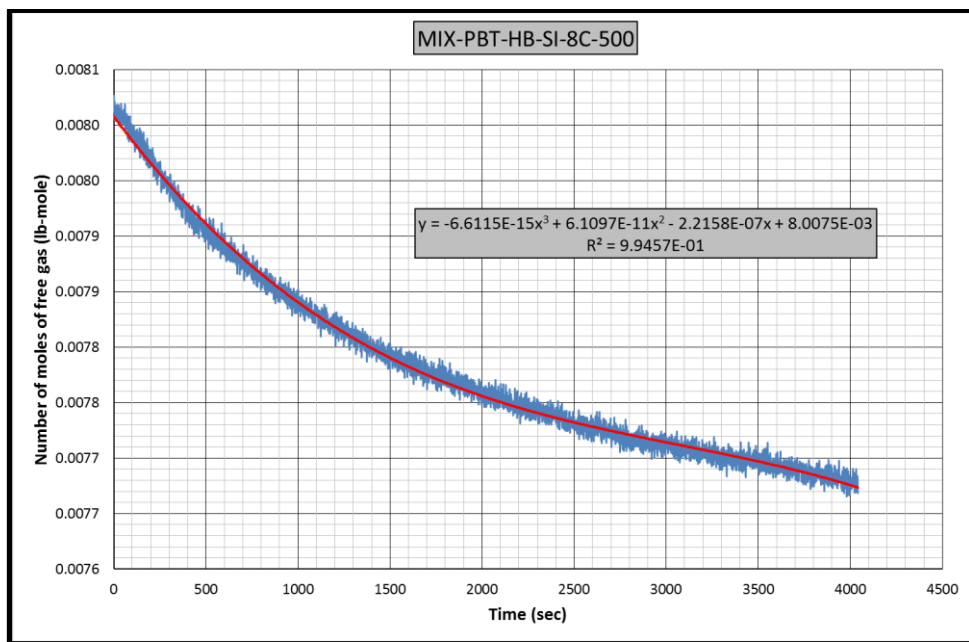


Figure B.52 Gas consumption rate equation for CH₄-C₃H₈-PBT-HB-SI-8C experiment

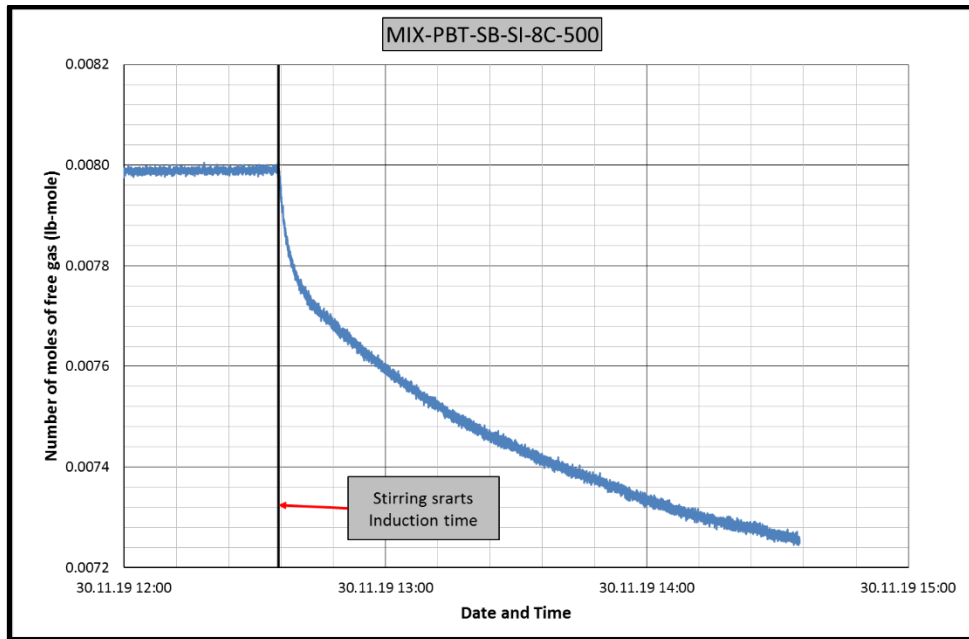


Figure B.53 Change in number of moles of free gas in CH₄-C₃H₈-PBT-SB-SI-8C experiment

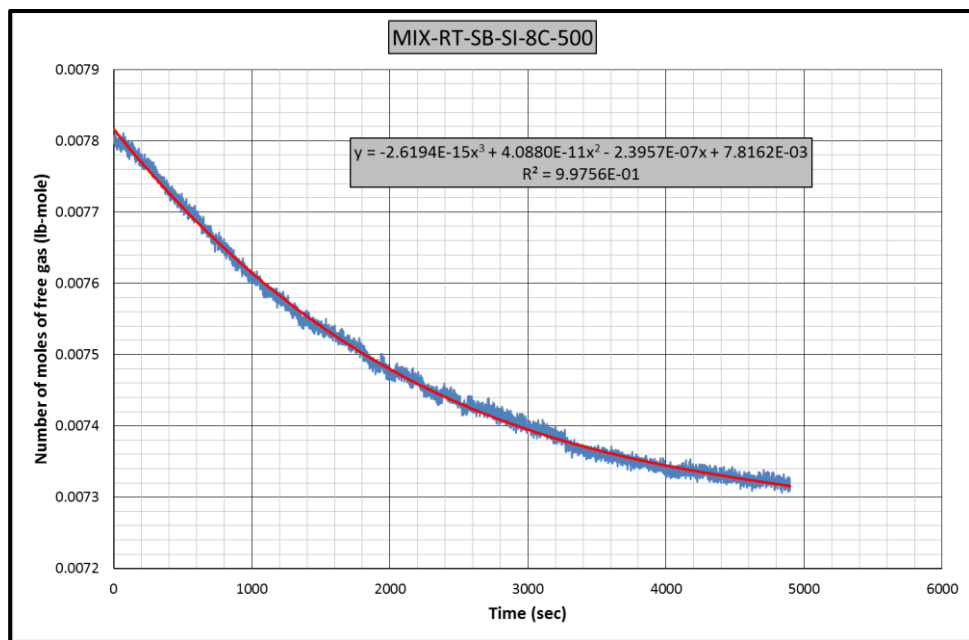


Figure B.54 Gas consumption rate equation for CH₄-C₃H₈-PBT-SB-SI-8C experiment

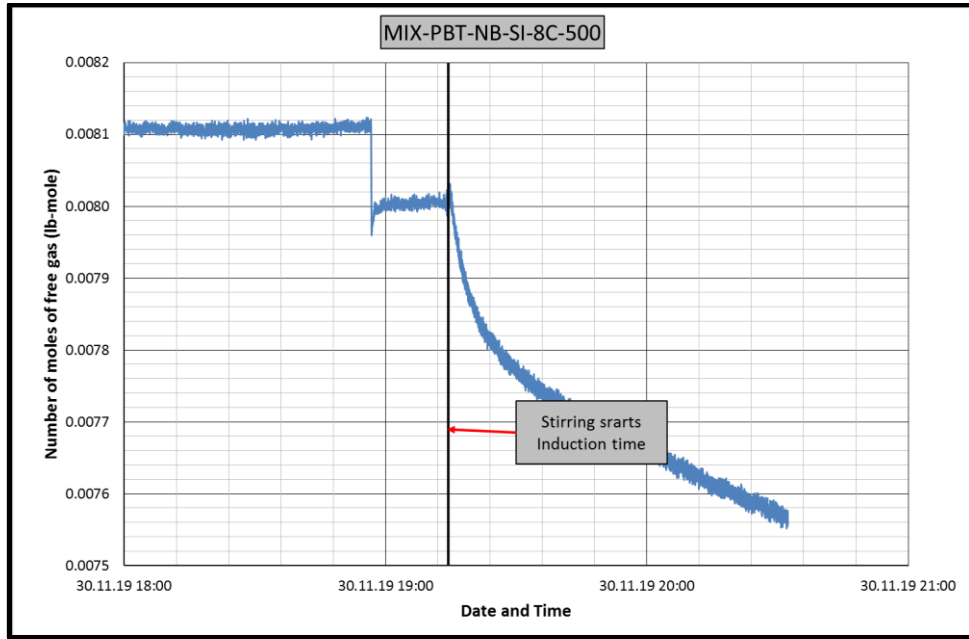


Figure B.55 Change in number of moles of free gas in CH₄-C₃H₈-PBT-NB-SI-8C experiment

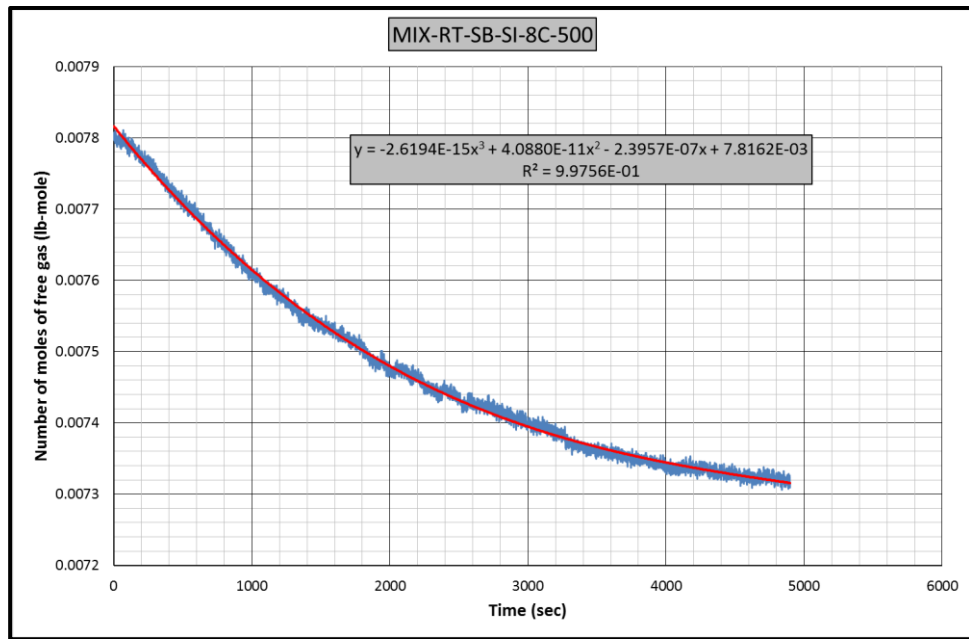


Figure B.56 Gas consumption rate equation-1 for CH₄-C₃H₈-PBT-NB-SI-8C experiment

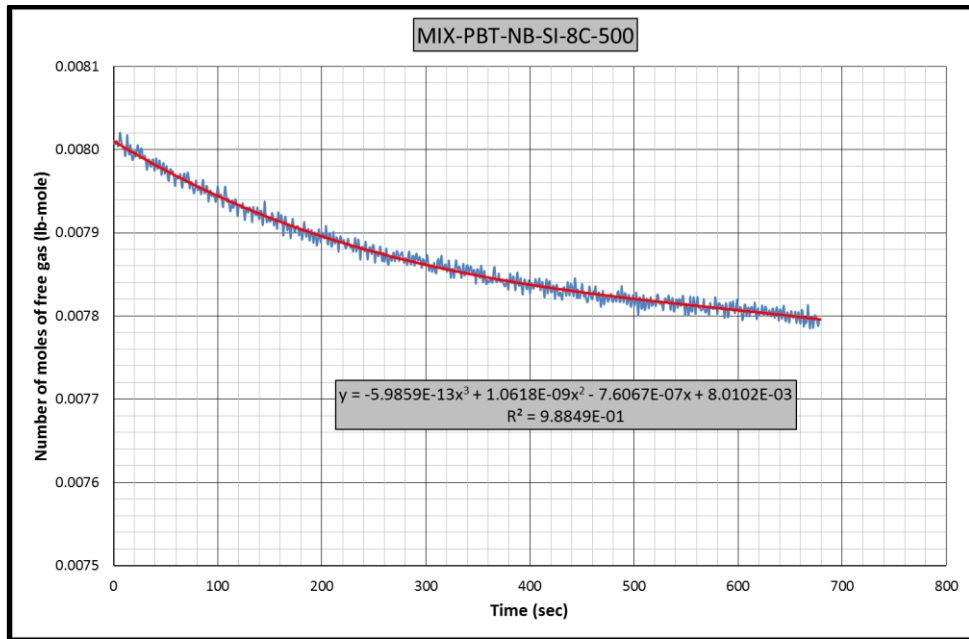


Figure B.57 Gas consumption rate equation-2 for CH₄-C₃H₈-PBT-NB-SI-8C experiment

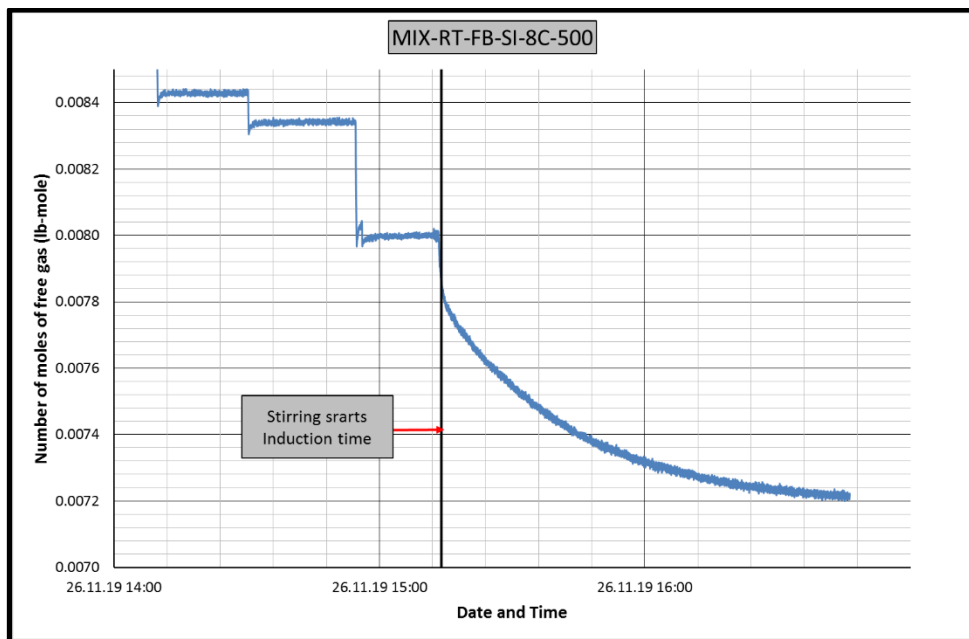


Figure B.58 Change in number of moles of free gas in CH₄-C₃H₈-RT-FB-SI-8C experiment

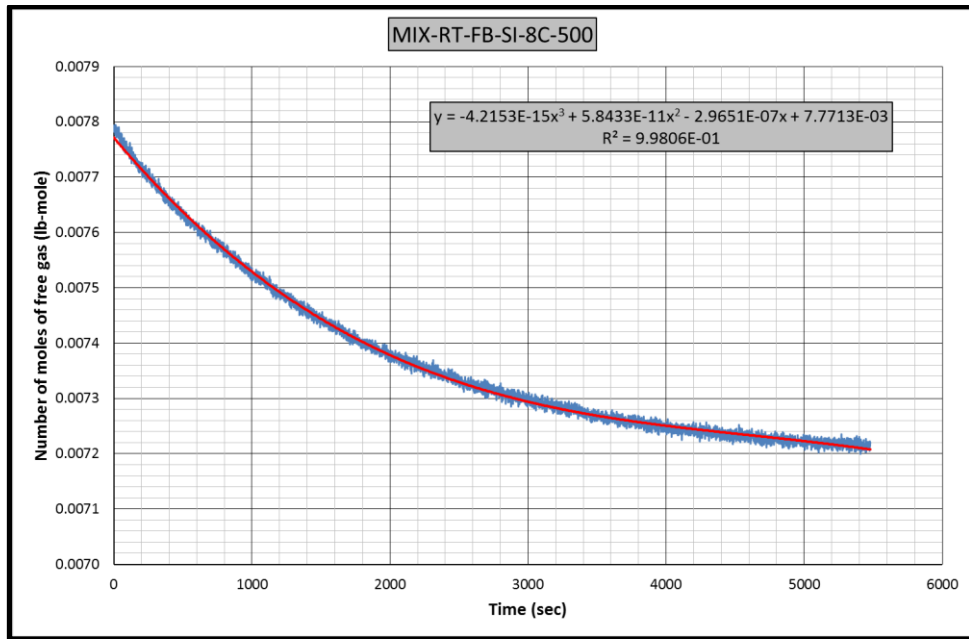


Figure B.59 Gas consumption rate equation for CH₄-C₃H₈-RT-FB-SI-8C experiment

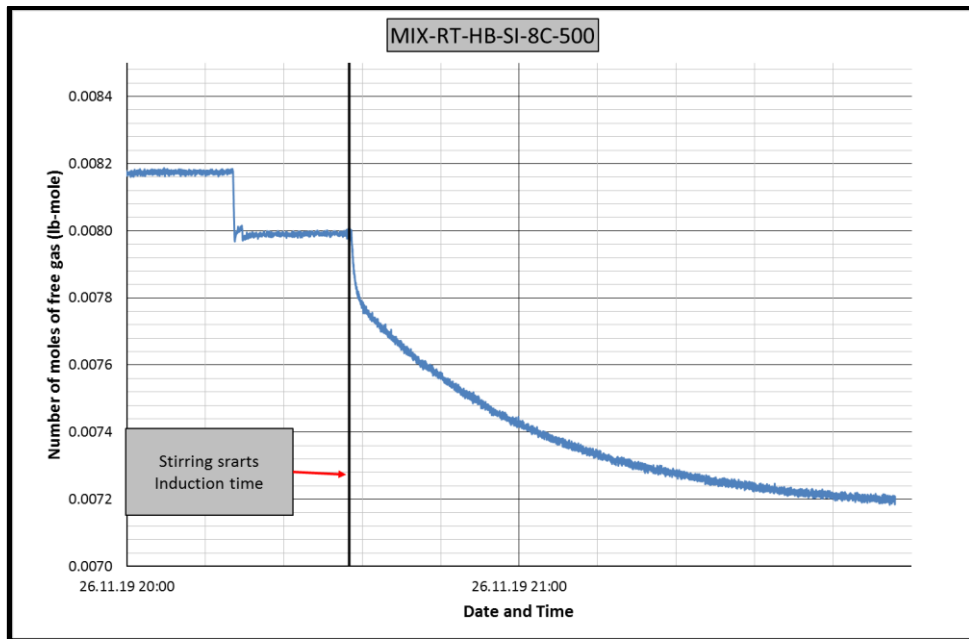


Figure B.60 Change in number of moles of free gas in CH₄-C₃H₈-RT-HB-SI-8C experiment

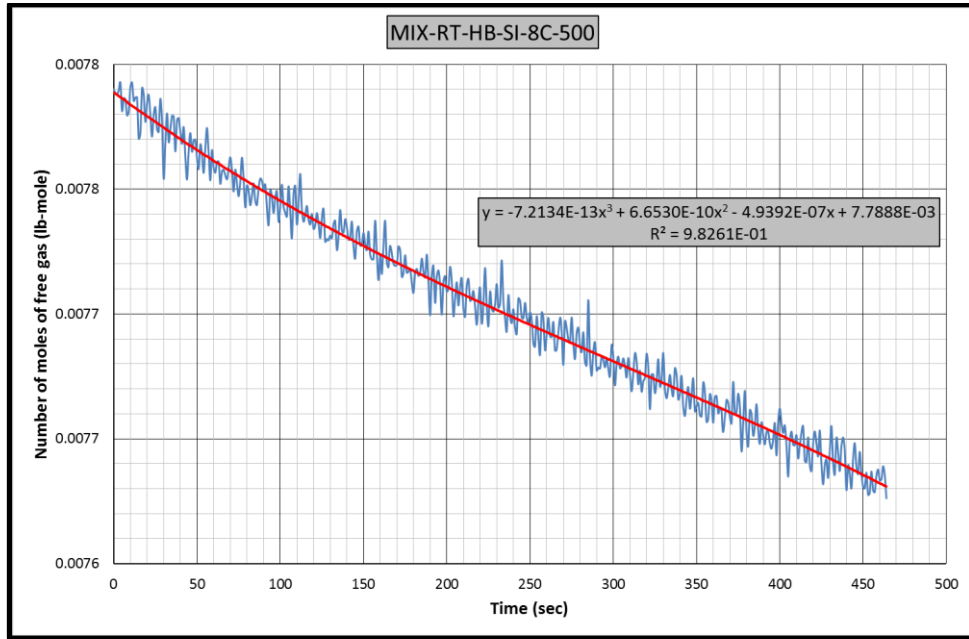


Figure B.61 Gas consumption rate equation-1 for CH₄-C₃H₈-RT-HB-SI-8C experiment

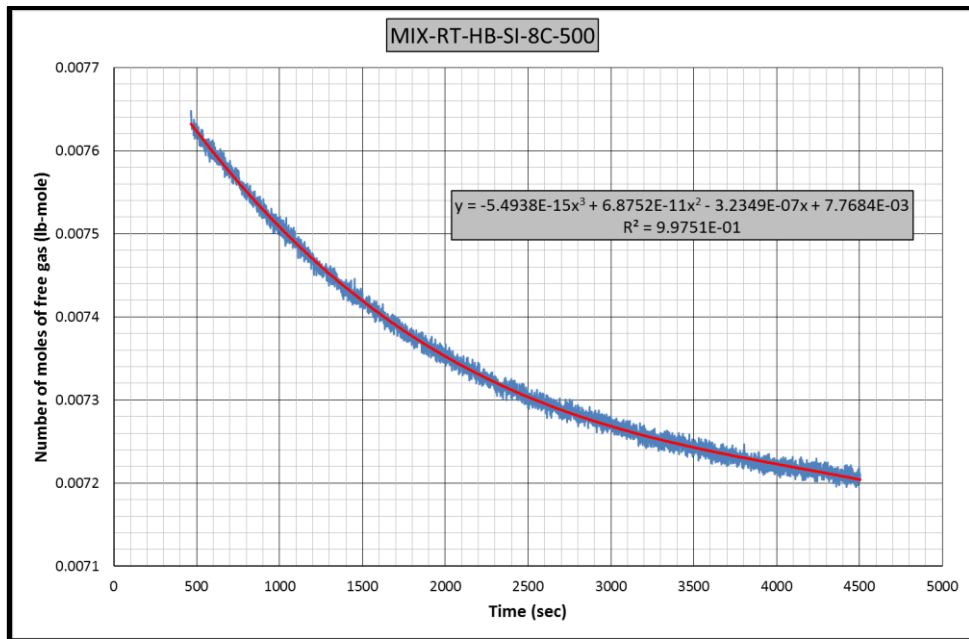


Figure B.62 Gas consumption rate equation-2 for CH₄-C₃H₈-RT-HB-SI-8C experiment

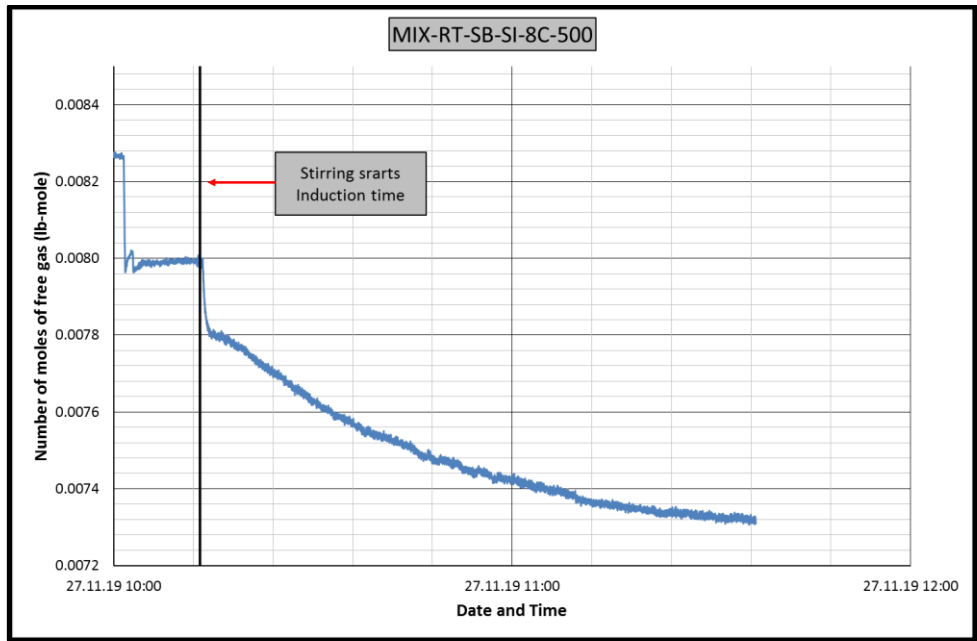


Figure B.63 Change in number of moles of free gas in CH4-C3H8-RT-SB-SI-8C experiment

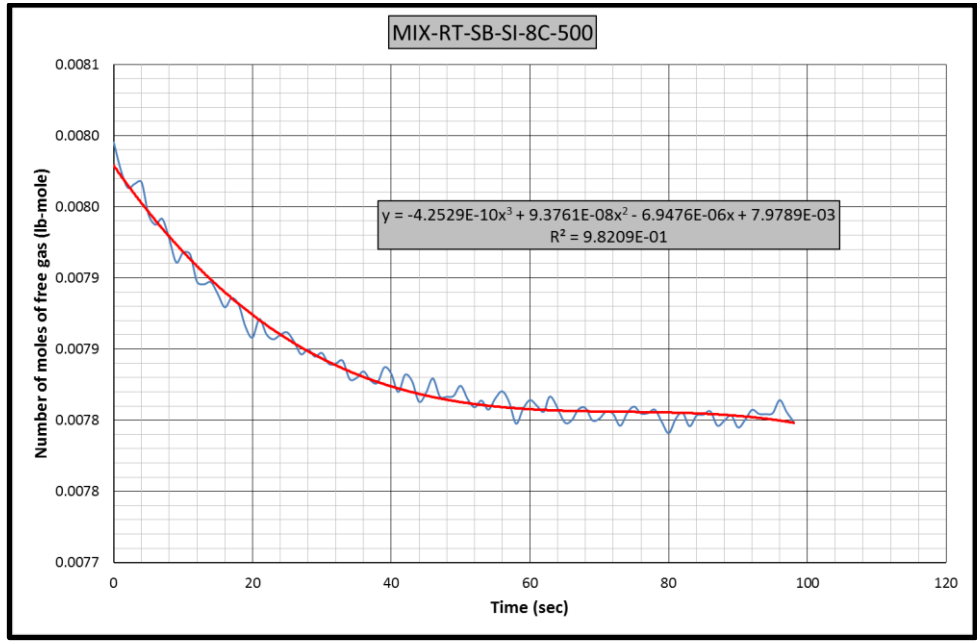


Figure B.64 Gas consumption rate equation-1 for CH4-C3H8-RT-SB-SI-8C experiment

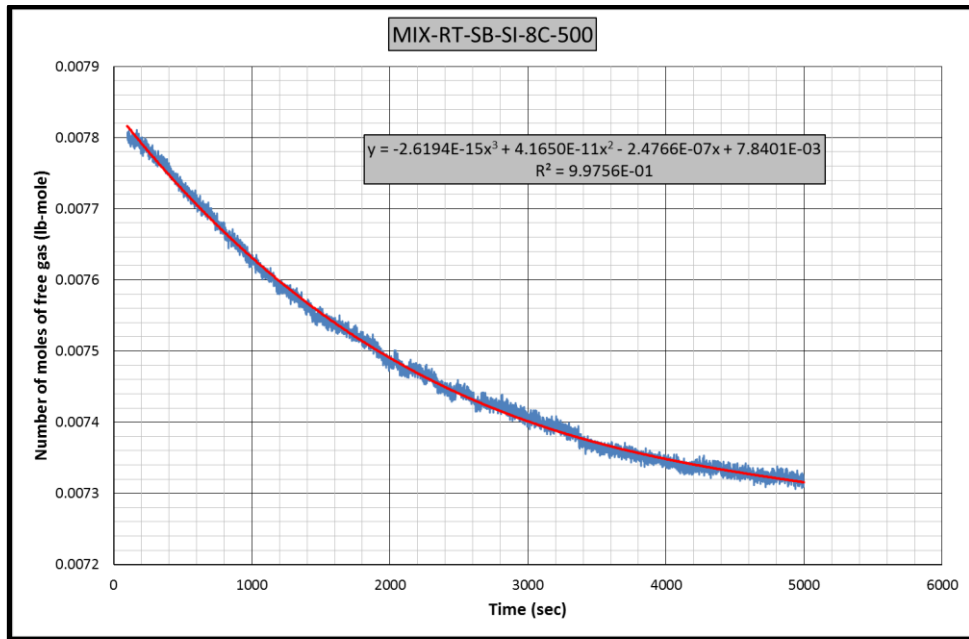


Figure B.65 Gas consumption rate equation-2 for CH₄-C₃H₈-RT-SB-SI-8C experiment

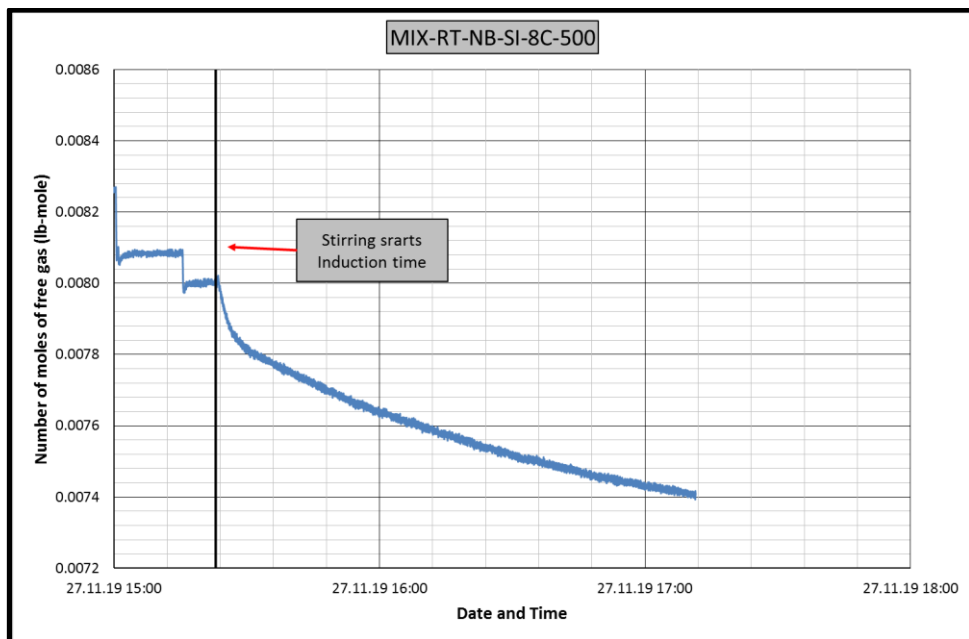


Figure B.66 Change in number of moles of free gas in CH₄-C₃H₈-RT-NB-SI-8C experiment

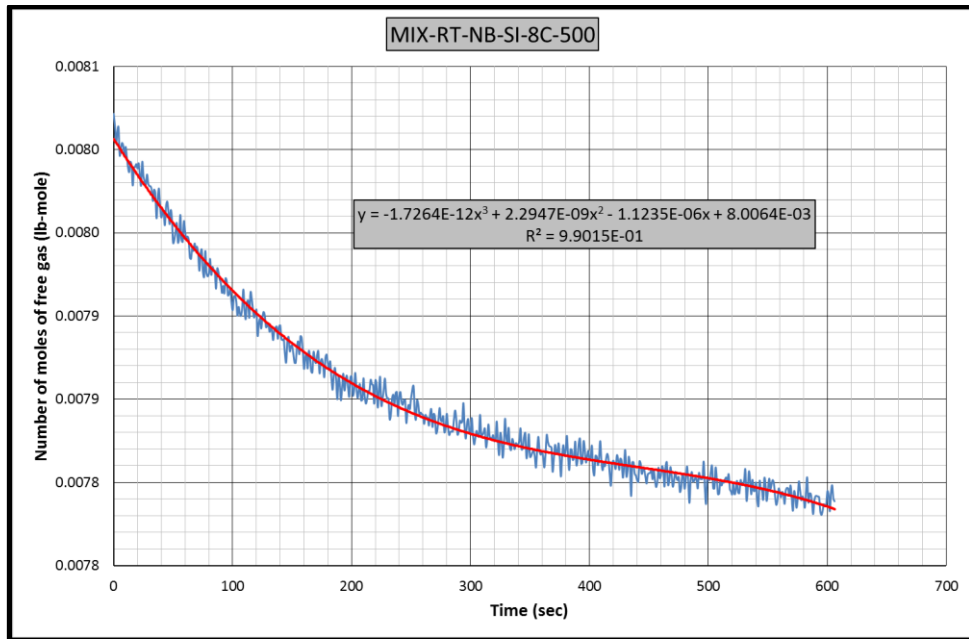


Figure B.67 Gas consumption rate equation-1 for CH₄-C₃H₈-RT-NB-SI-8C experiment

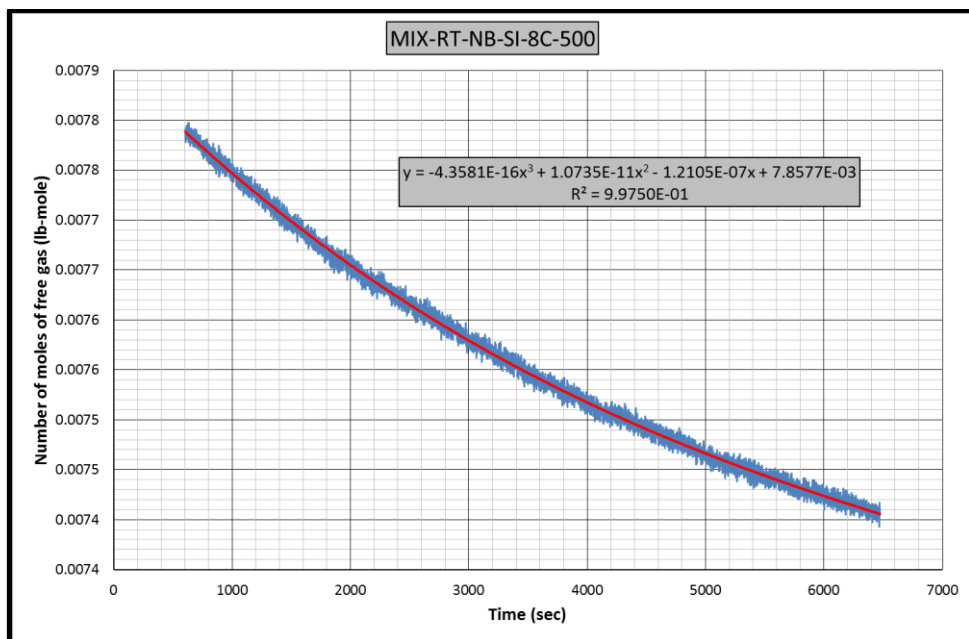


Figure B.68 Gas consumption rate equation-2 for CH₄-C₃H₈-RT-NB-SI-8C experiment

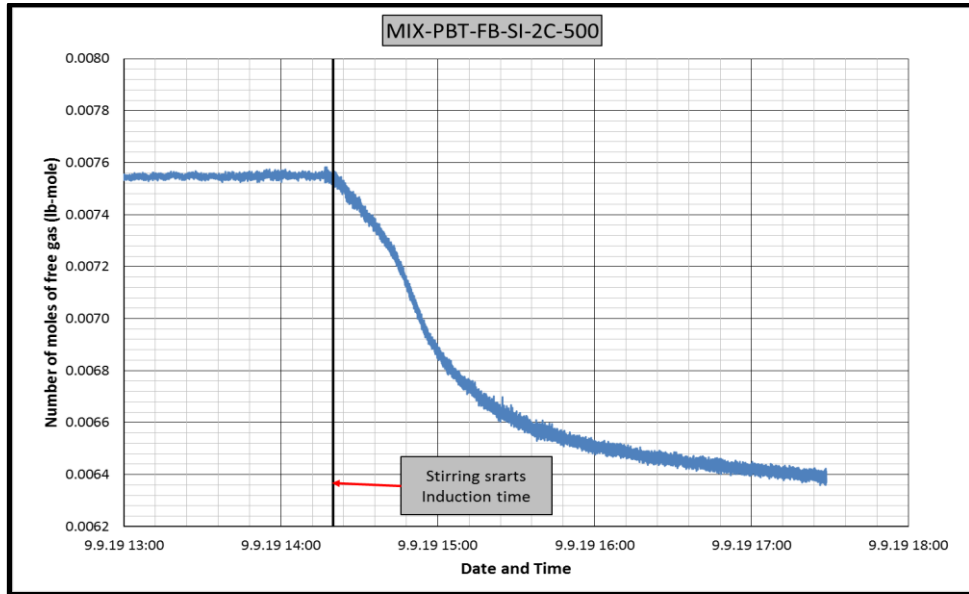


Figure B.69 Change in number of moles of free gas in CH₄-C₃H₈-PBT-FB-SI-2C experiment

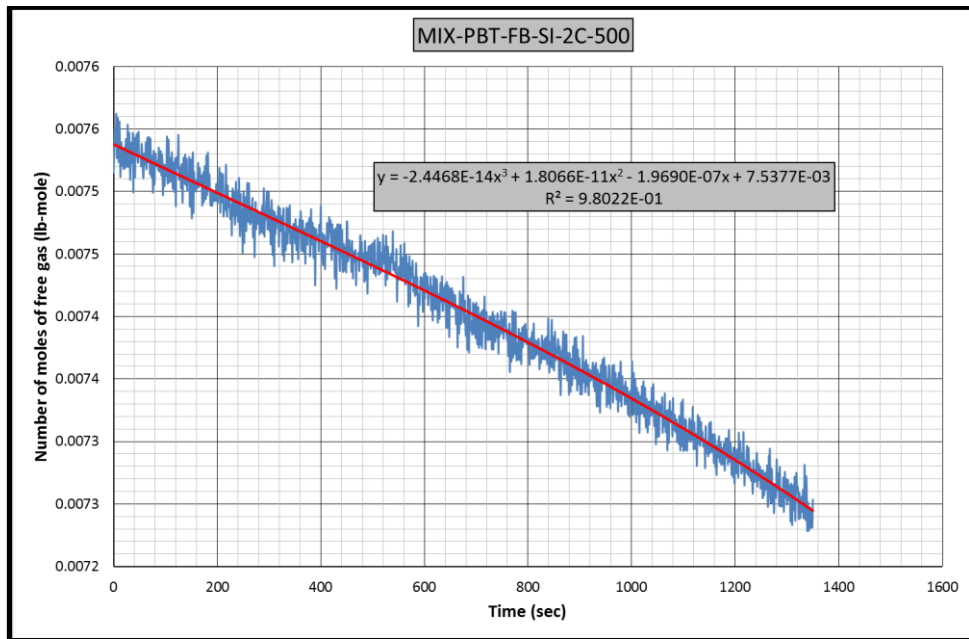


Figure B.70 Gas consumption rate equation-1 for CH₄-C₃H₈-PBT-FB-SI-2C experiment

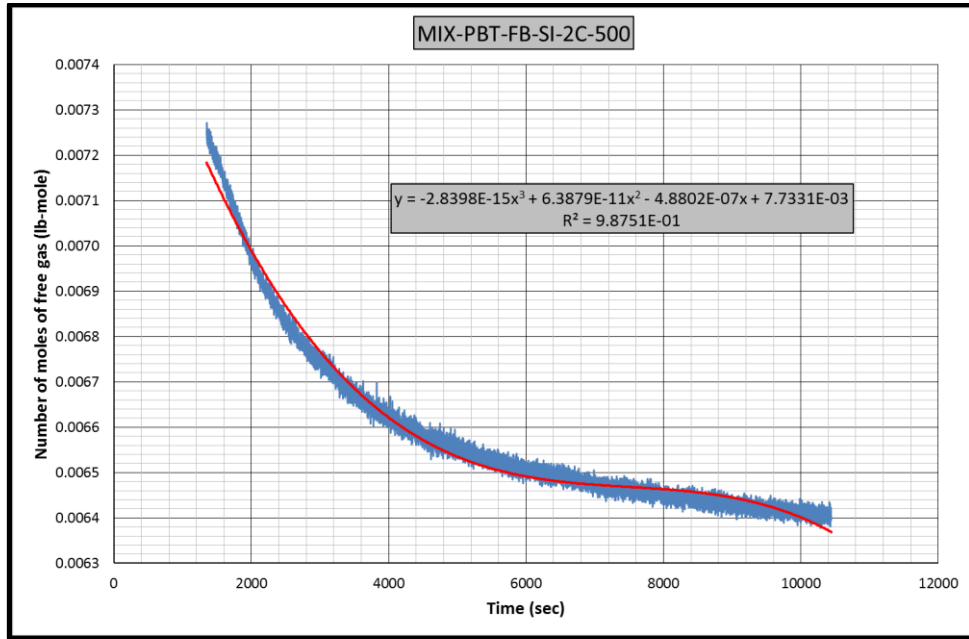


Figure B.71 Gas consumption rate equation-2 for CH₄-C₃H₈-PBT-FB-SI-2C experiment

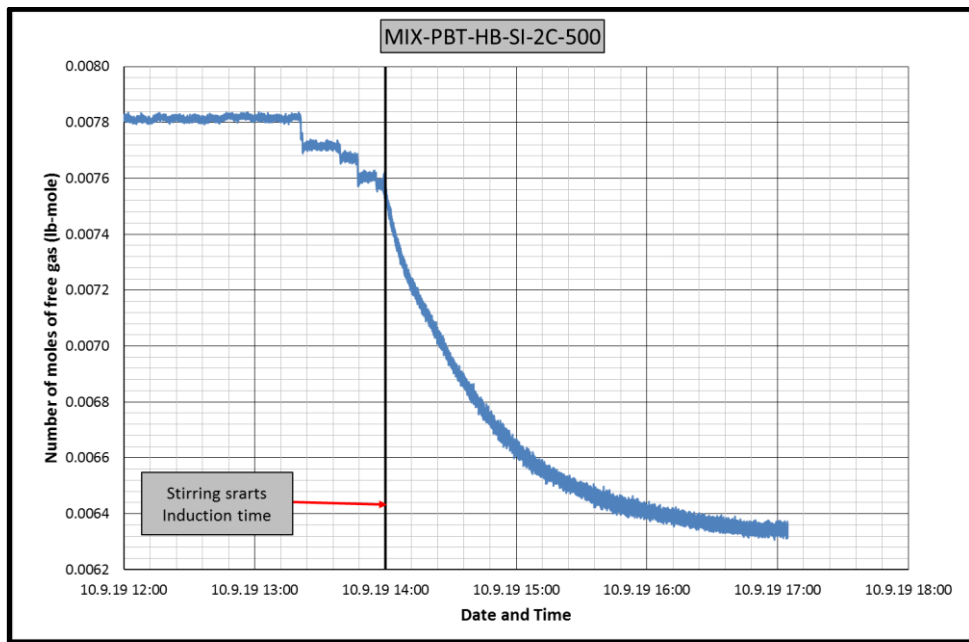


Figure B.72 Change in number of moles of free gas in CH₄-C₃H₈-PBT-HB-SI-2C experiment

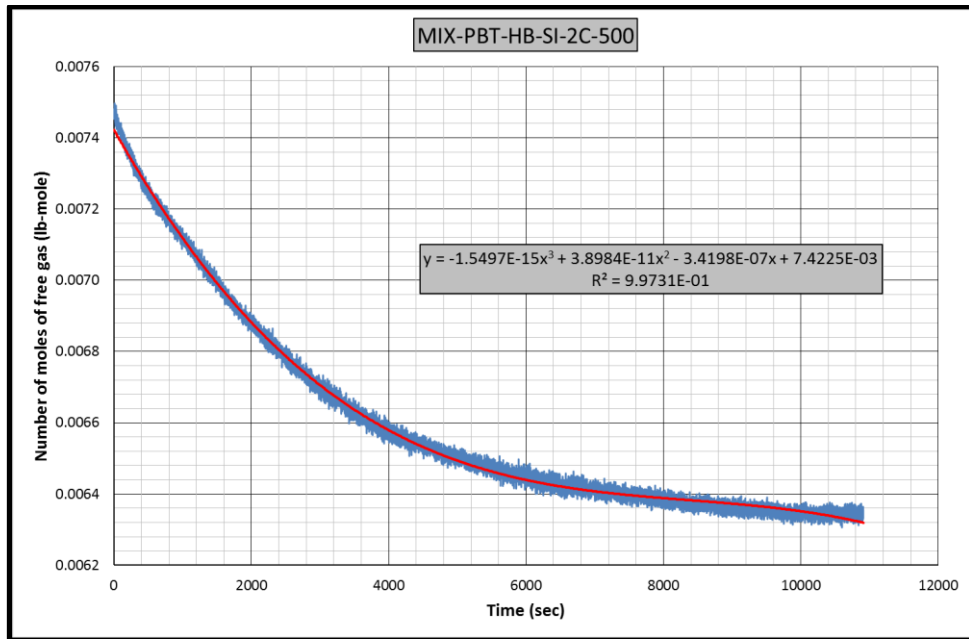


Figure B.73 Gas consumption rate equation for CH₄-C₃H₈-PBT-HB-SI-2C experiment

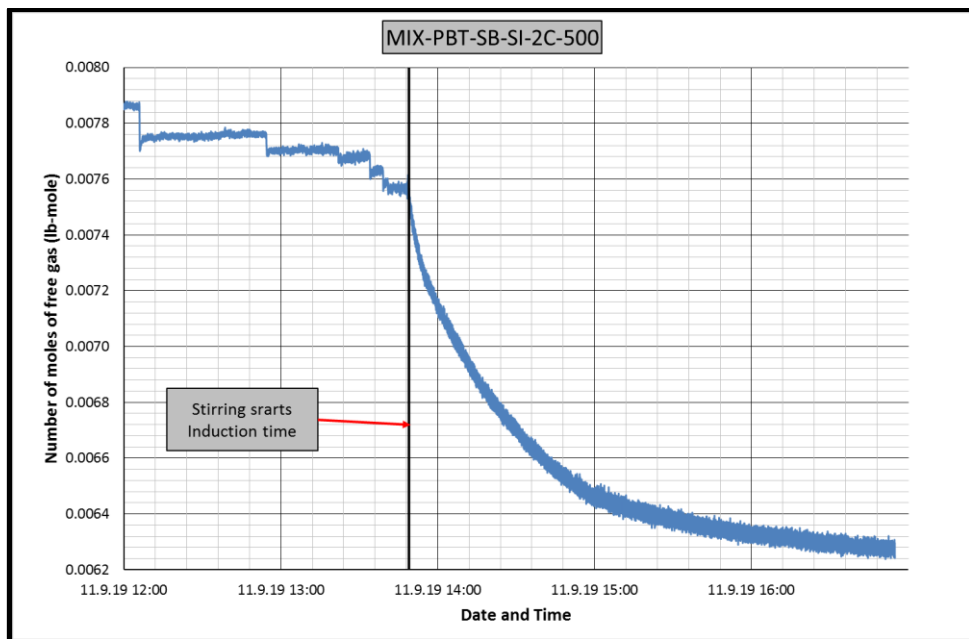


Figure B.74 Change in number of moles of free gas in CH₄-C₃H₈-PBT-SB-SI-2C experiment

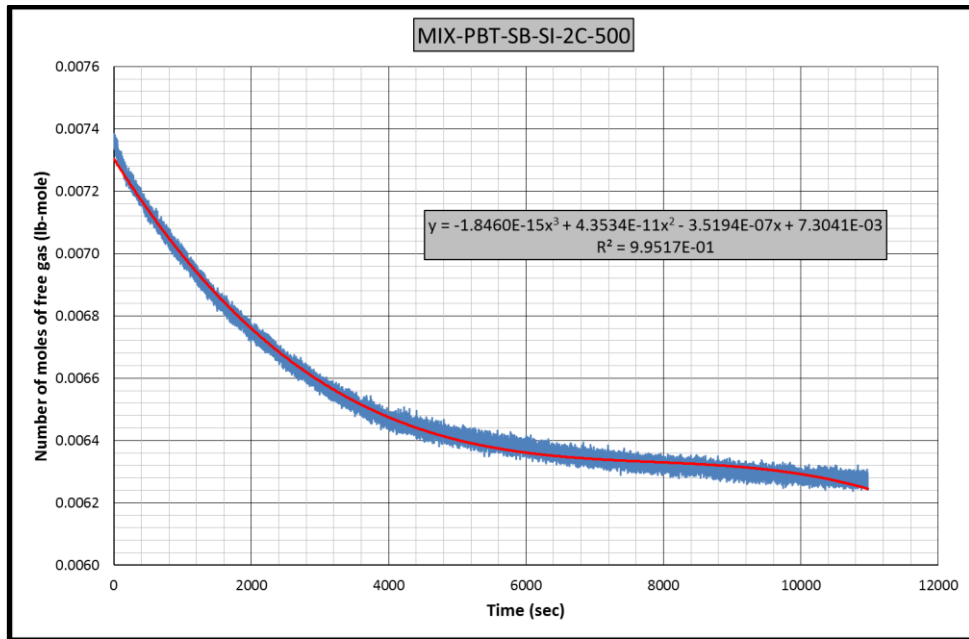


Figure B.75 Gas consumption rate equation for CH₄-C₃H₈-PBT-SB-SI-2C experiment

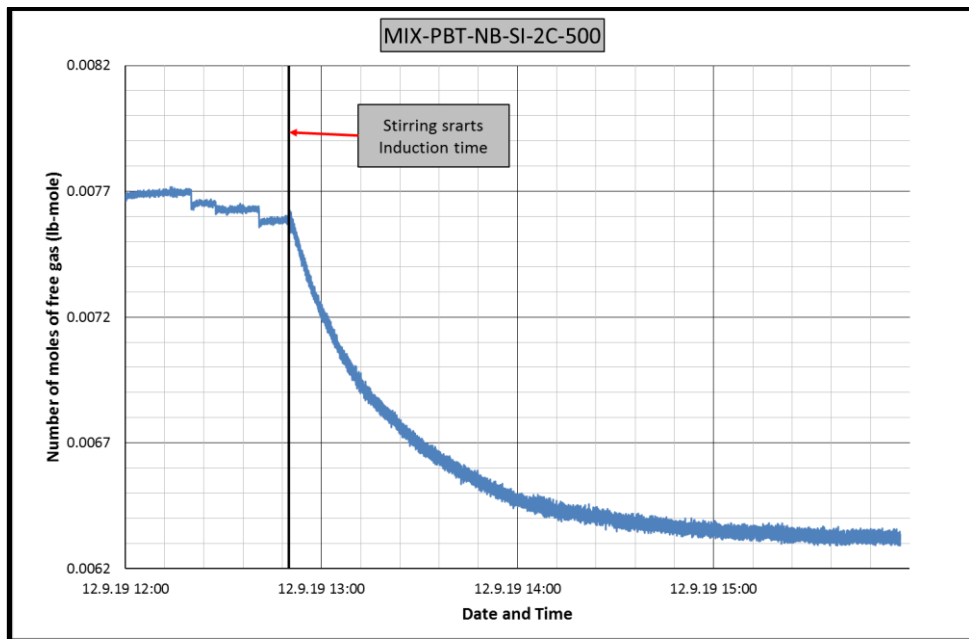


Figure B.76 Change in number of moles of free gas in CH₄-C₃H₈-PBT-NB-SI-2C experiment

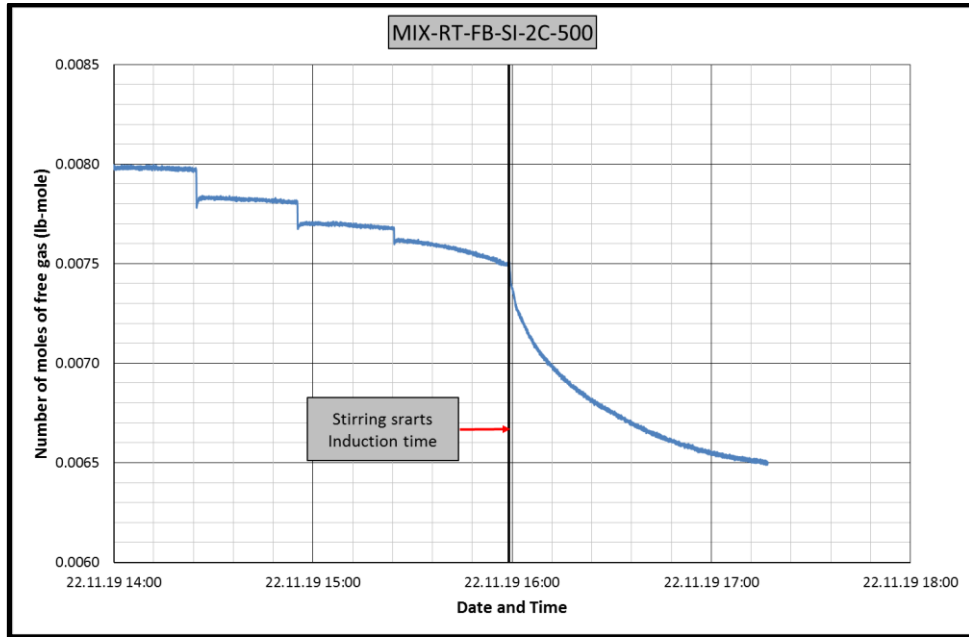


Figure B.77 Change in number of moles of free gas in CH₄-C₃H₈-RT-FB-SI-2C experiment

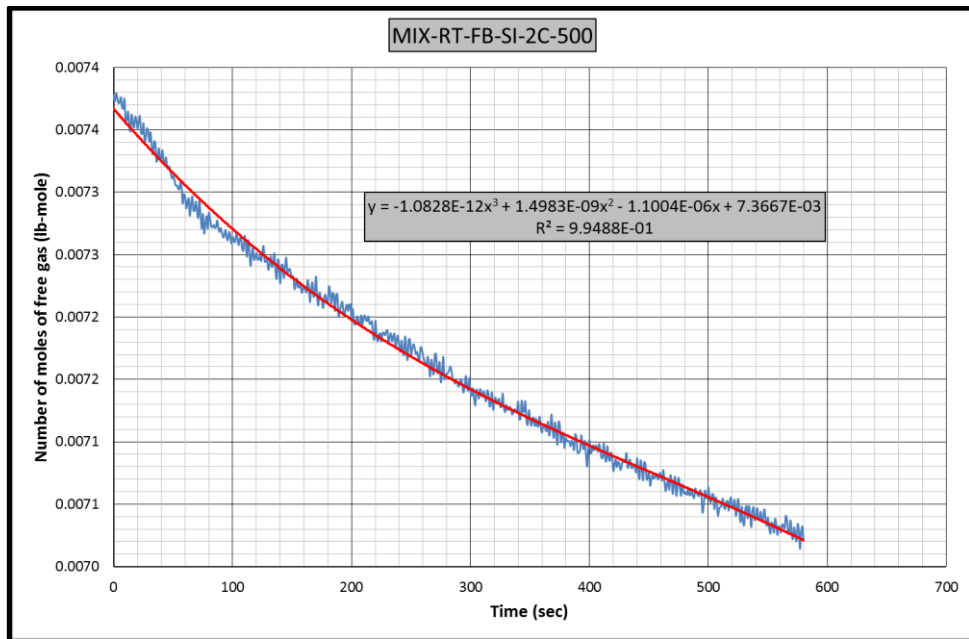


Figure B.78 Gas consumption rate equation-1 for CH₄-C₃H₈-RT-FB-SI-2C experiment

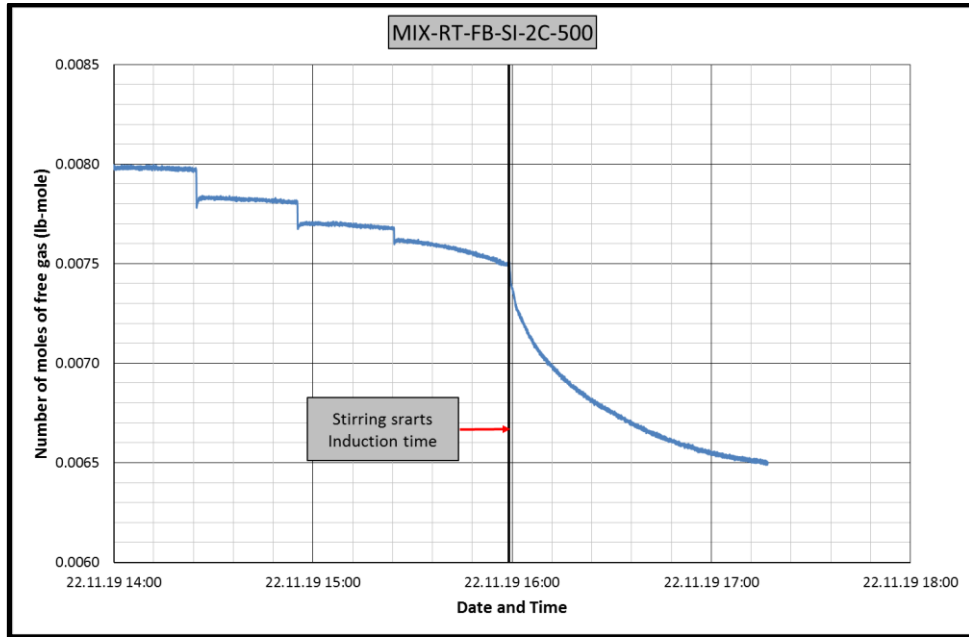


Figure B.79 Change in number of moles of free gas in CH₄-C₃H₈-RT-FB-SI-2C experiment

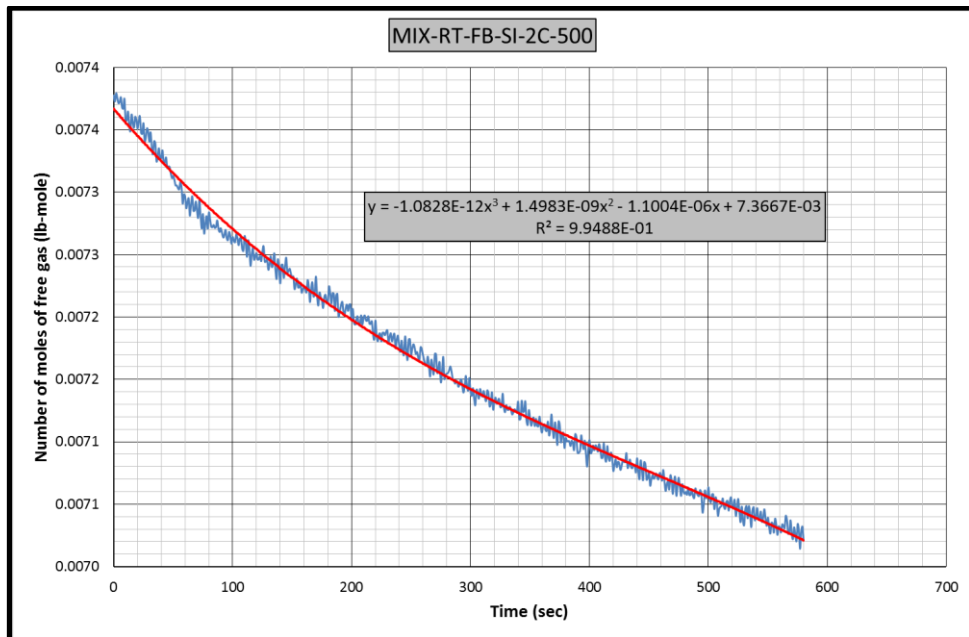


Figure B.80 Gas consumption rate equation-1 for CH₄-C₃H₈-RT-FB-SI-2C experiment

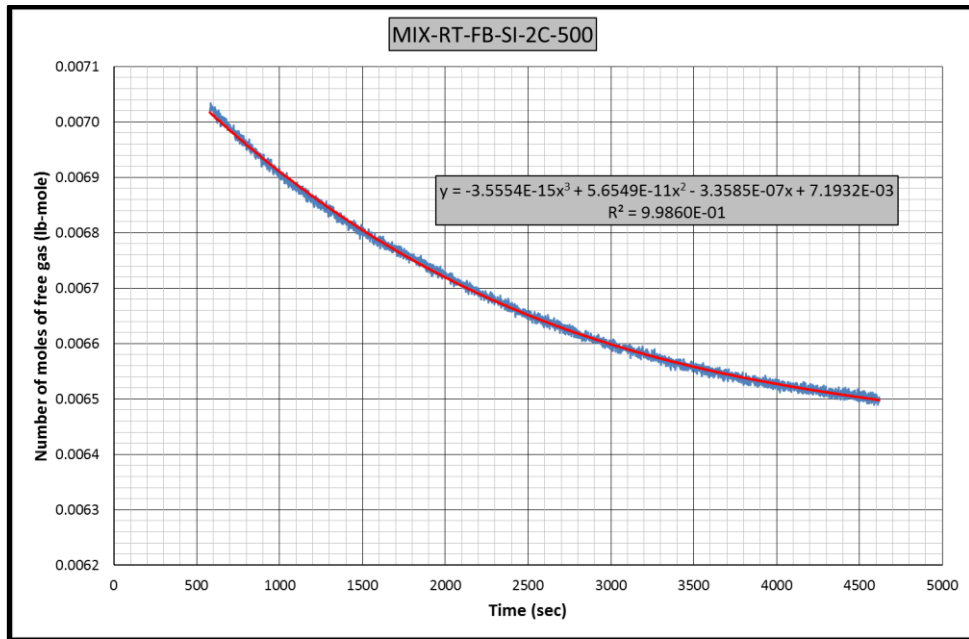


Figure B.81 Gas consumption rate equation-2 for CH₄-C₃H₈-RT-FB-SI-2C experiment

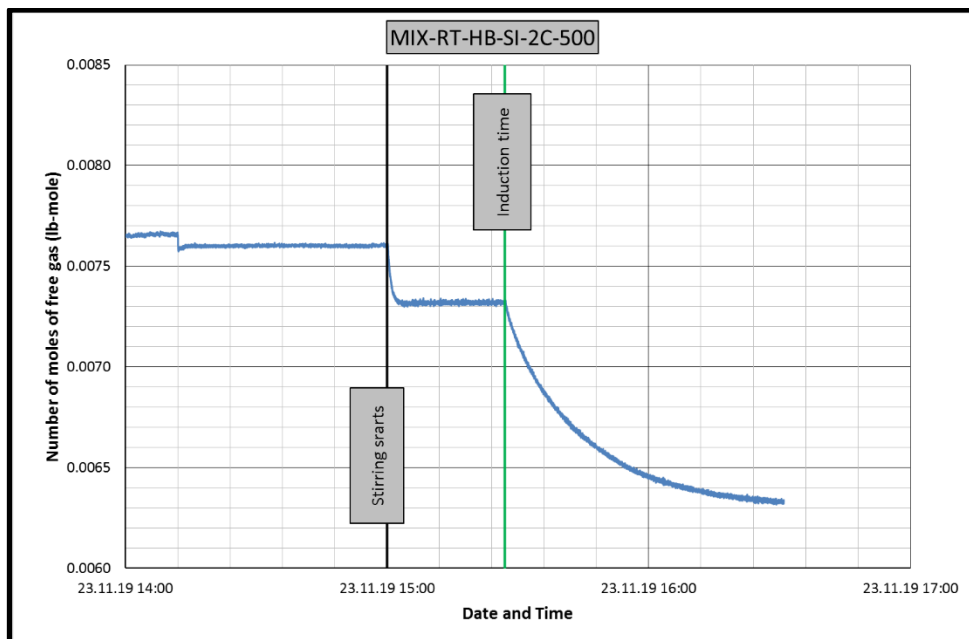


Figure B.82 Change in number of moles of free gas in CH₄-C₃H₈-RT-HB-SI-2C experiment

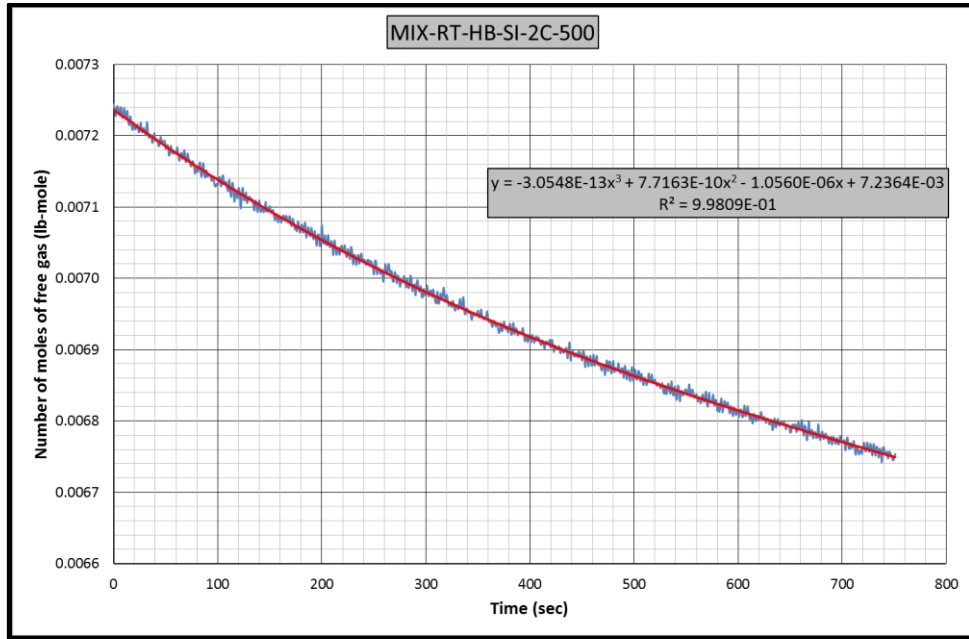


Figure B.83 Gas consumption rate equation-1 for CH₄-C₃H₈-RT-HB-SI-2C experiment

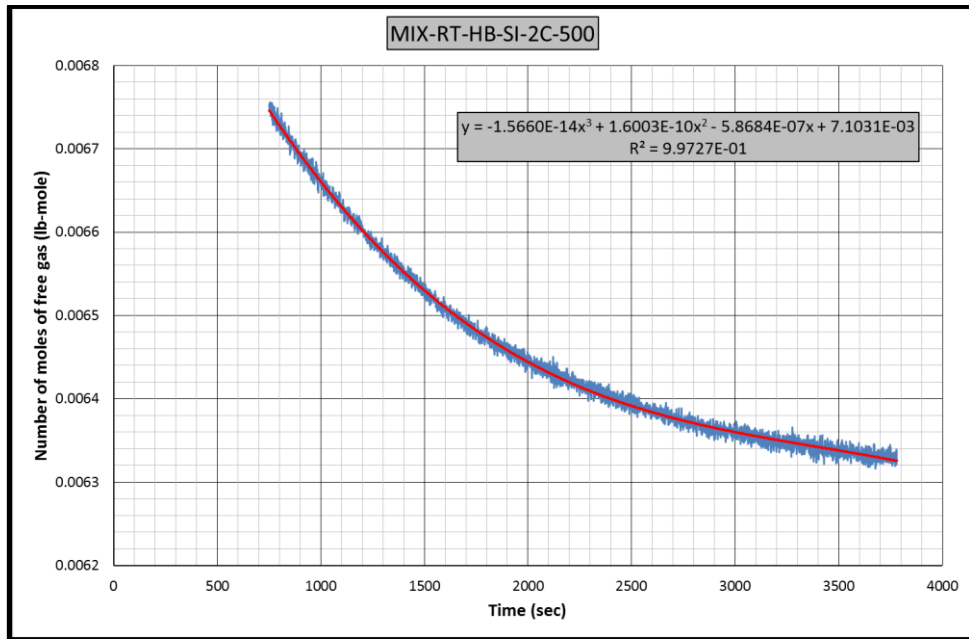


Figure B.84 Gas consumption rate equation-2 for CH₄-C₃H₈-RT-HB-SI-2C experiment

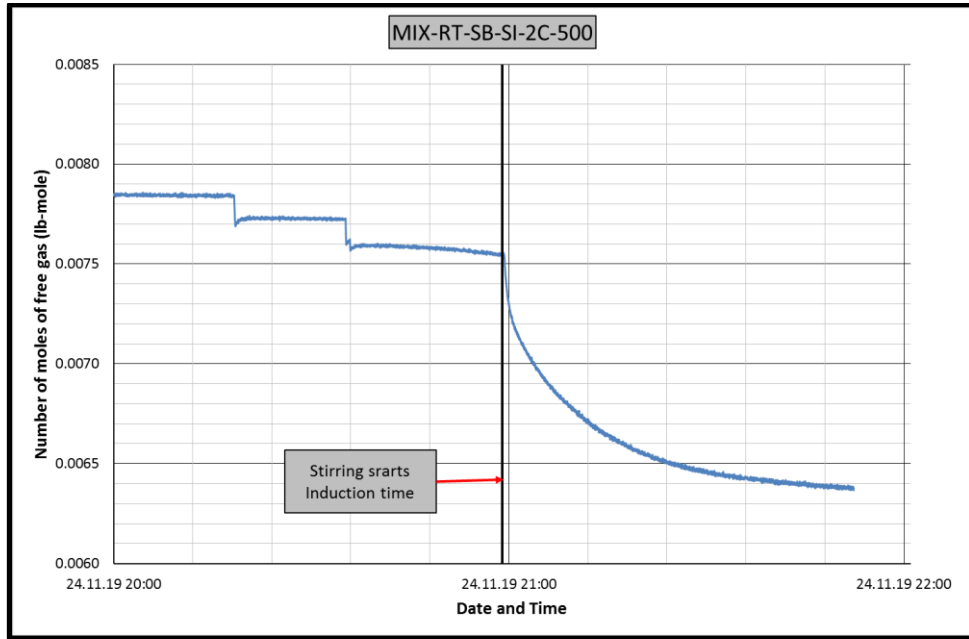


Figure B.85 Change in number of moles of free gas in CH₄-C₃H₈-RT-SB-SI-2C experiment

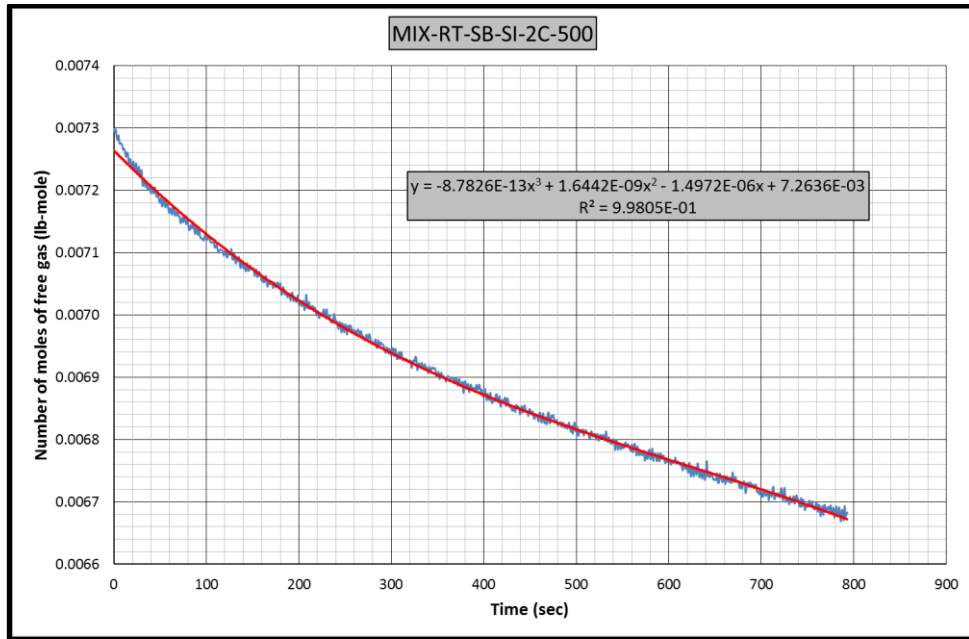


Figure B.86 Gas consumption rate equation-1 for CH₄-C₃H₈-RT-SB-SI-2C experiment

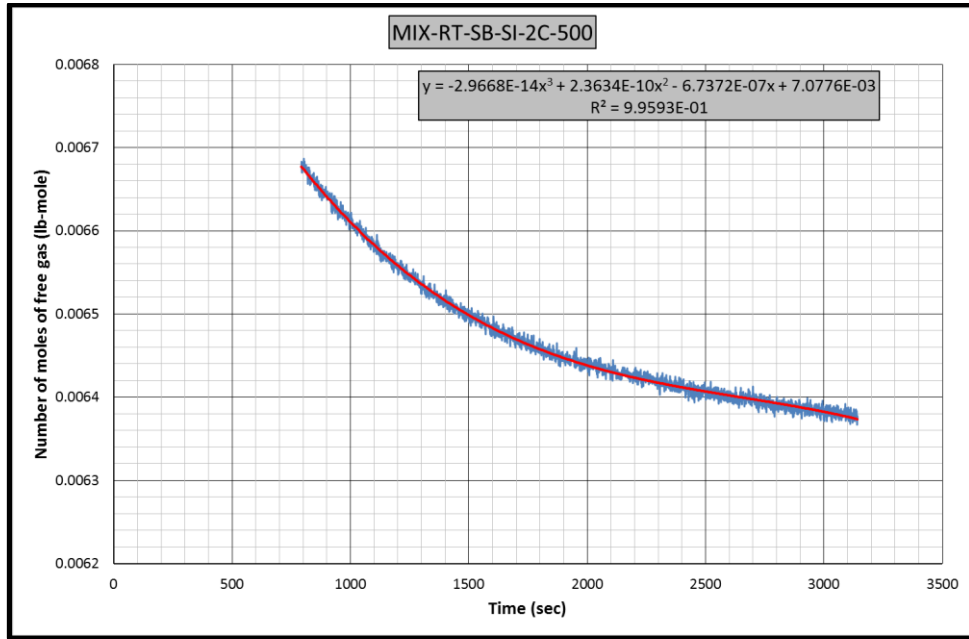


Figure B.87 Gas consumption rate equation-2 for CH₄-C₃H₈-RT-SB-SI-2C experiment

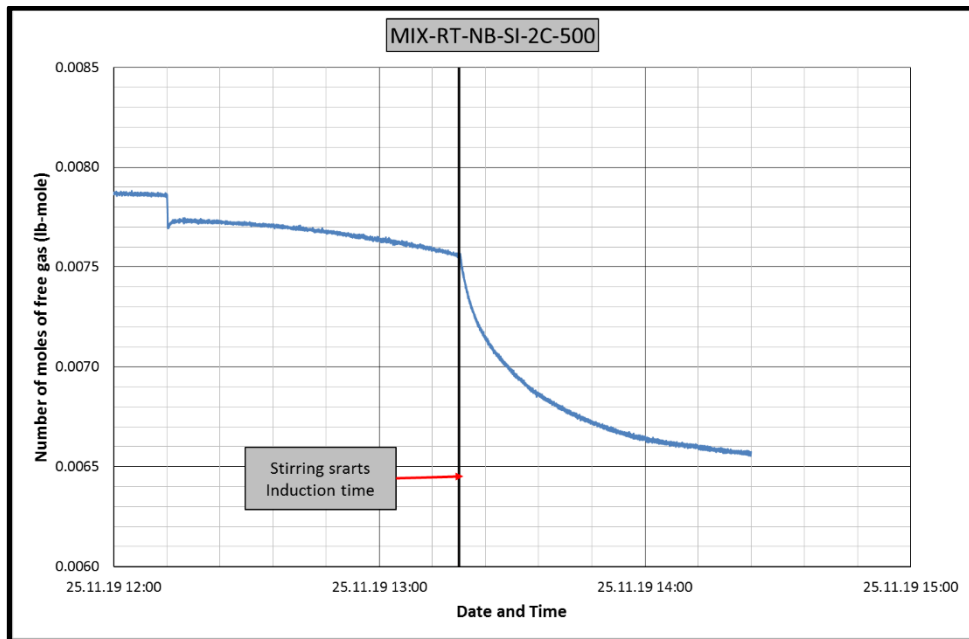


Figure B.88 Change in number of moles of free gas in CH₄-C₃H₈-RT-NB-SI-2C experiment

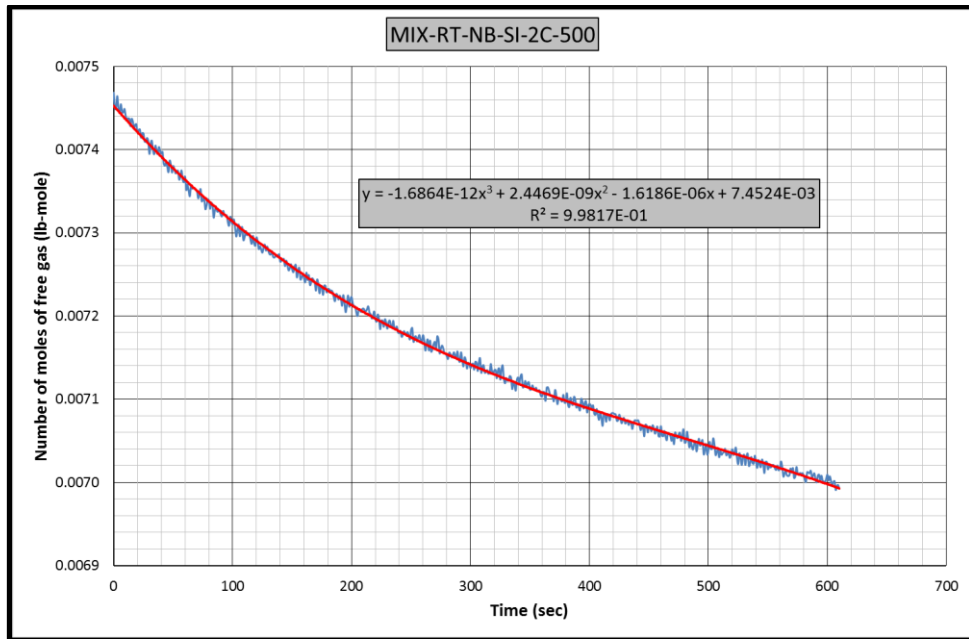


Figure B.89 Gas consumption rate equation-1 for CH₄-C₃H₈-RT-NB-SI-2C experiment

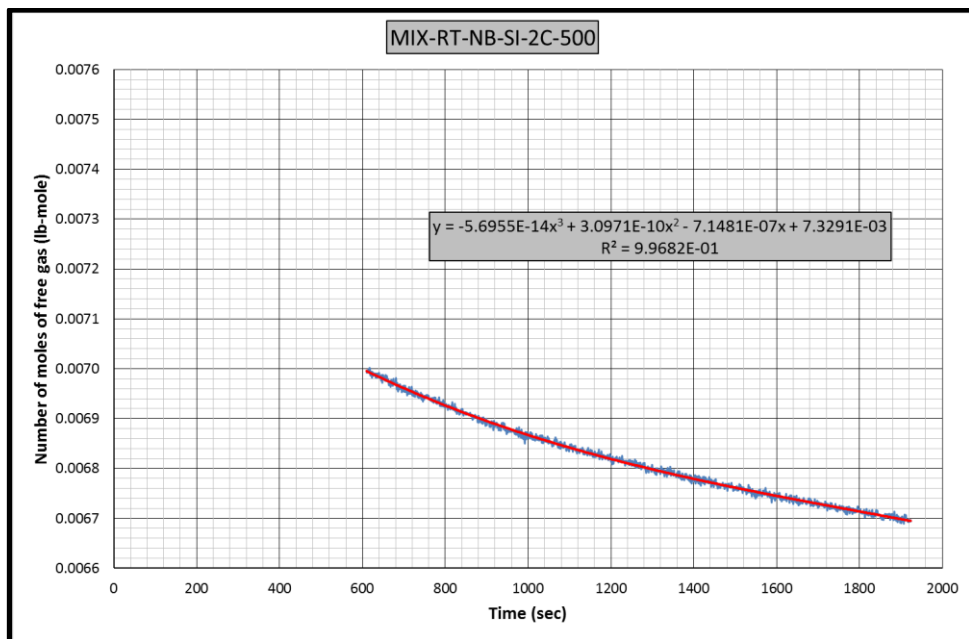


Figure B.90 Gas consumption rate equation-2 for CH₄-C₃H₈-RT-NB-SI-2C experiment

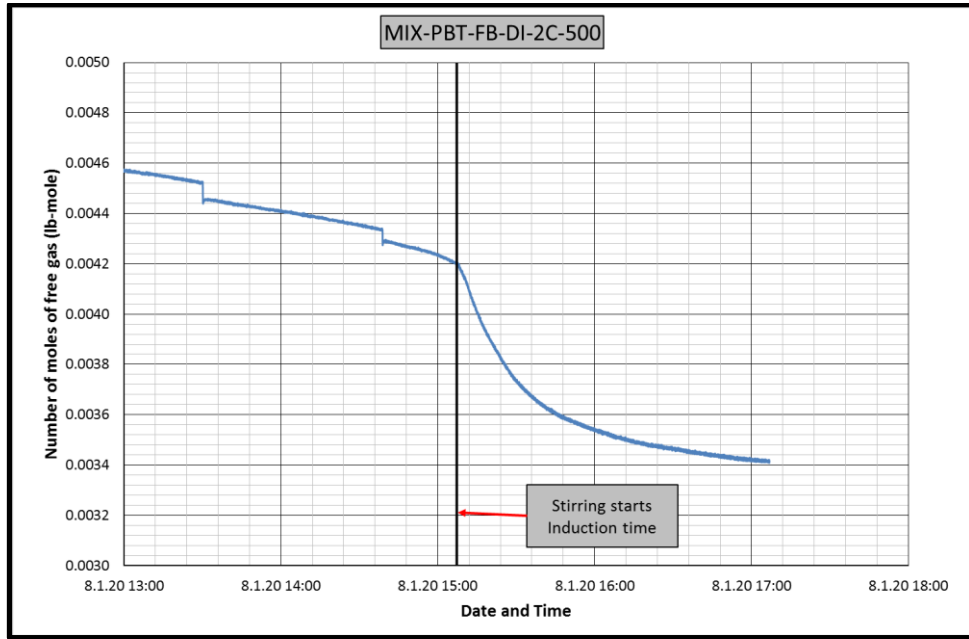


Figure B.91 Change in number of moles of free gas in CH₄-C₃H₈-PBT-FB-DI-2C experiment

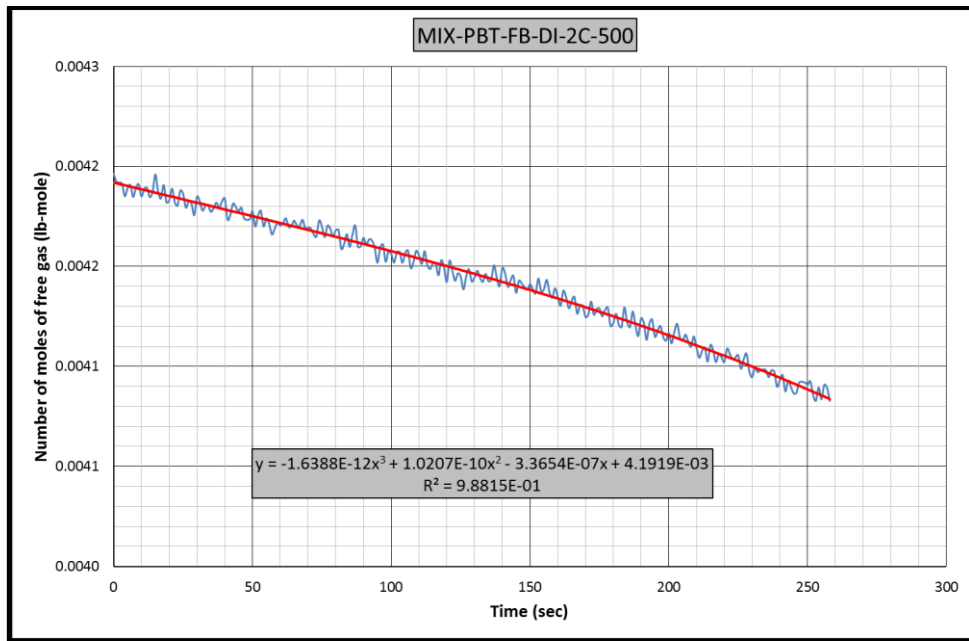


Figure B.92 Gas consumption rate equation-1 for CH₄-C₃H₈-PBT-FB-DI-2C experiment

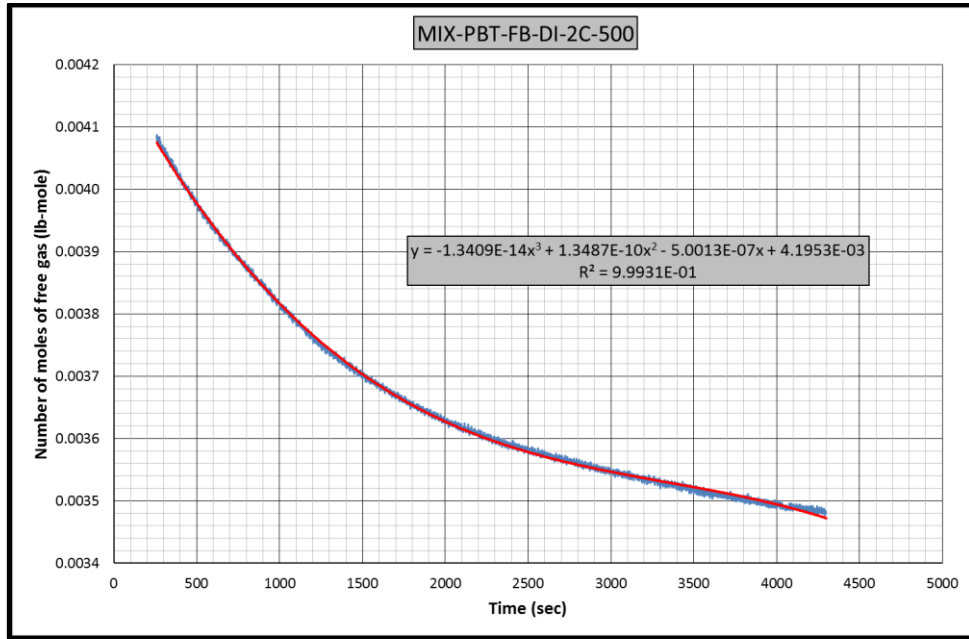


Figure B.93 Gas consumption rate equation-2 for CH₄-C₃H₈-PBT-FB-DI-2C experiment

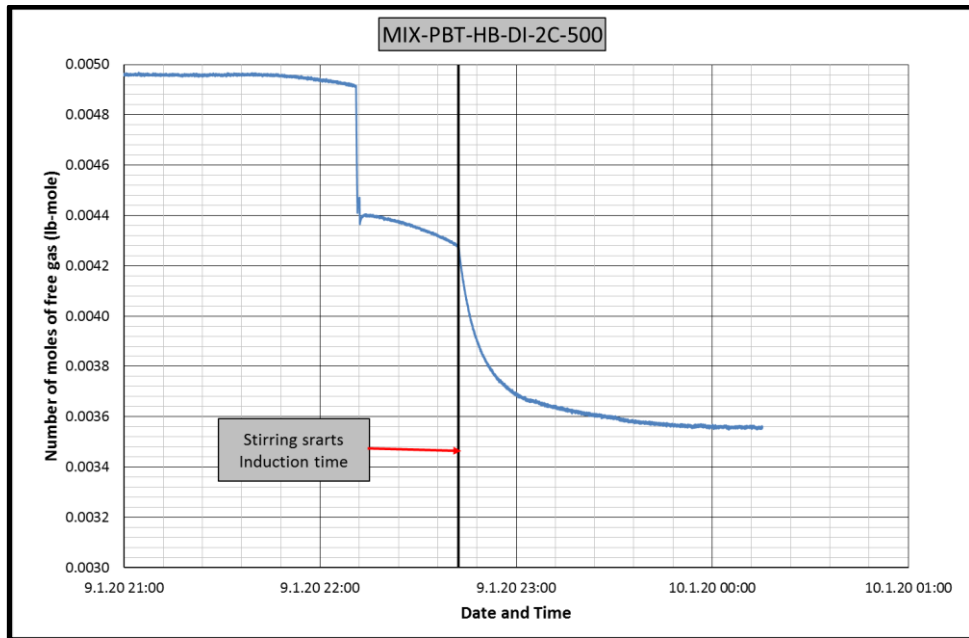


Figure B.94 Change in number of moles of free gas in CH₄-C₃H₈-PBT-HB-DI-2C experiment

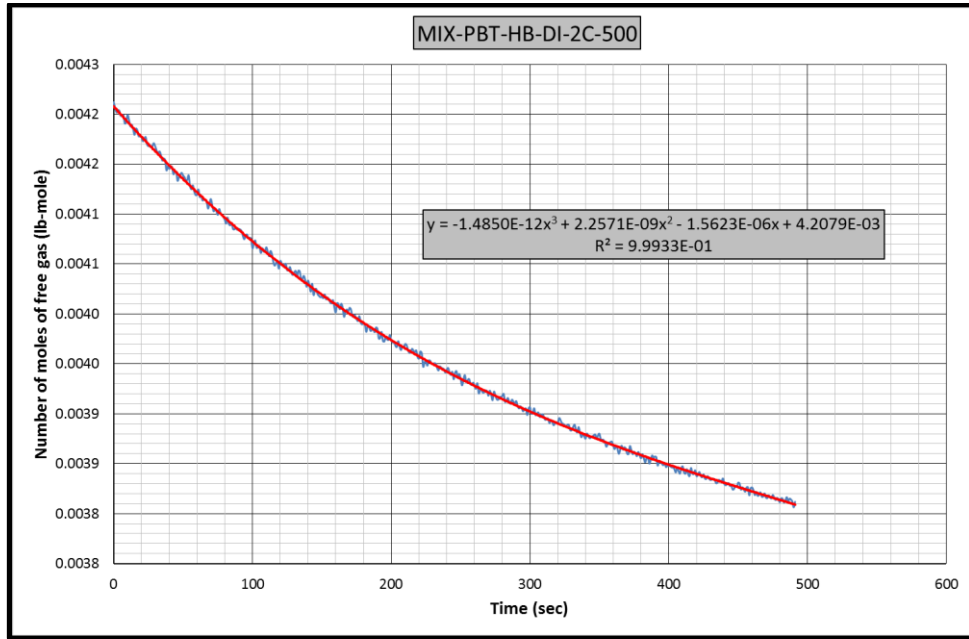


Figure B.95 Gas consumption rate equation-1 for CH₄-C₃H₈-PBT-HB-DI-2C experiment

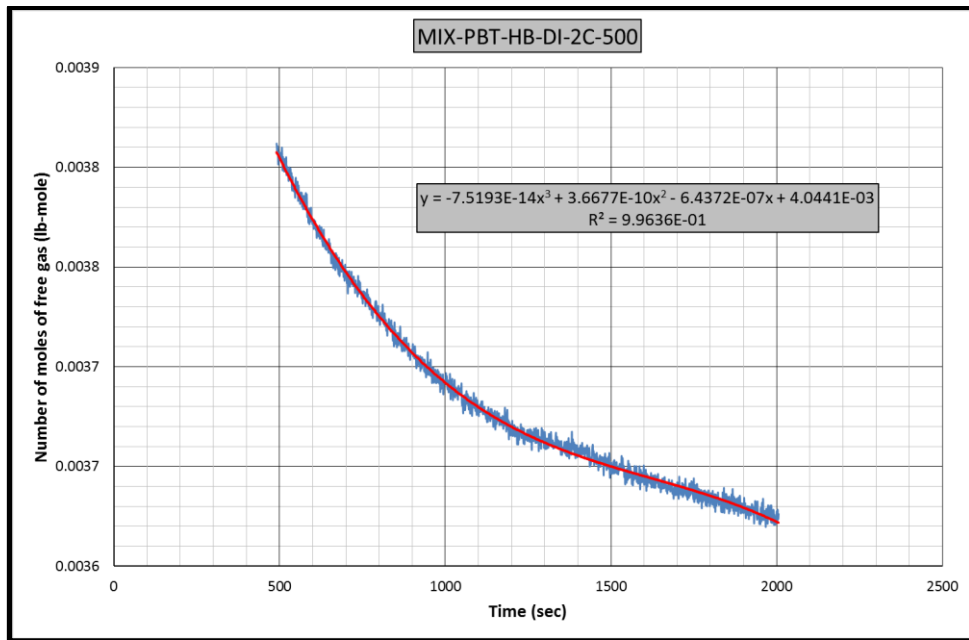


Figure B.96 Gas consumption rate equation-2 for CH₄-C₃H₈-PBT-HB-DI-2C experiment

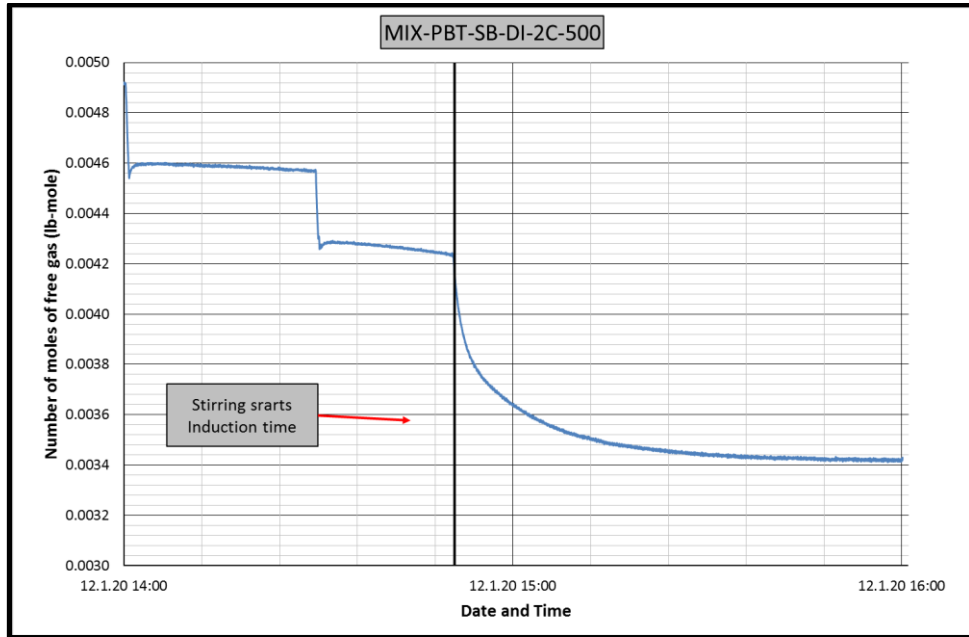


Figure B.97 Change in number of moles of free gas in CH₄-C₃H₈-PBT-SB-DI-2C experiment

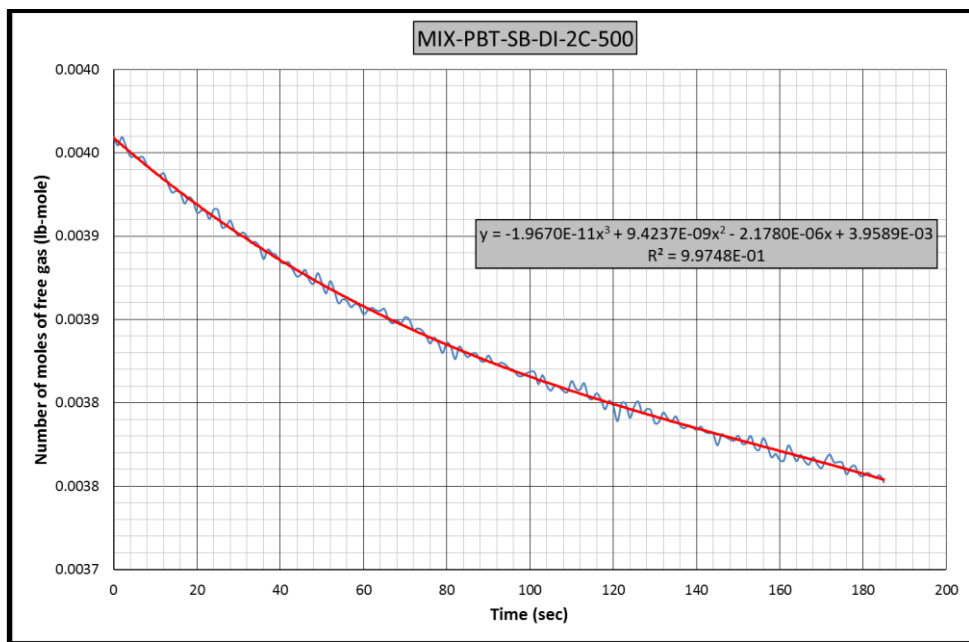


Figure B.98 Gas consumption rate equation-1 for CH₄-C₃H₈-PBT-SB-DI-2C experiment

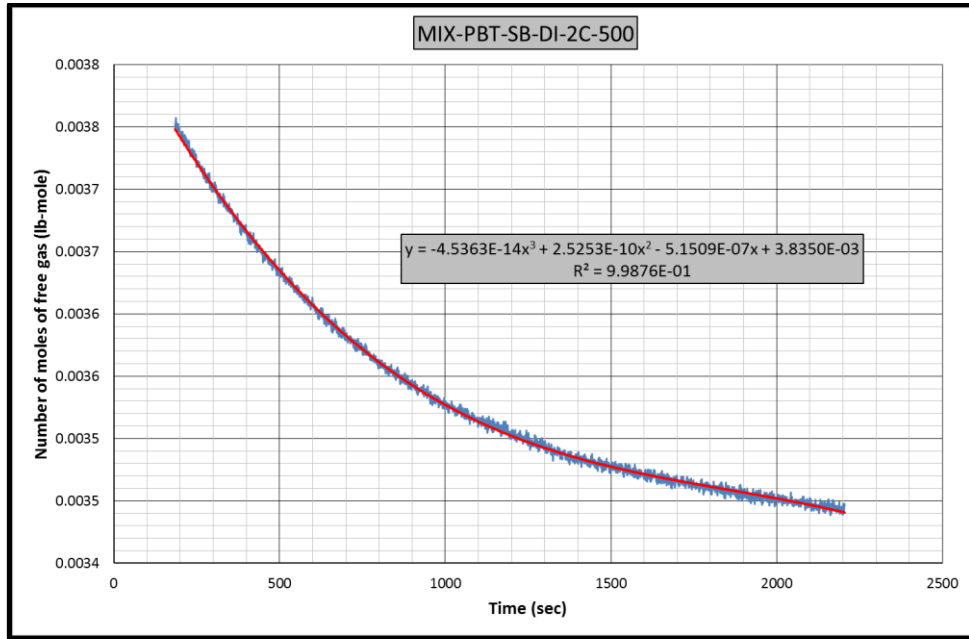


Figure B.99 Gas consumption rate equation-2 for CH₄-C₃H₈-PBT-SB-DI-2C experiment

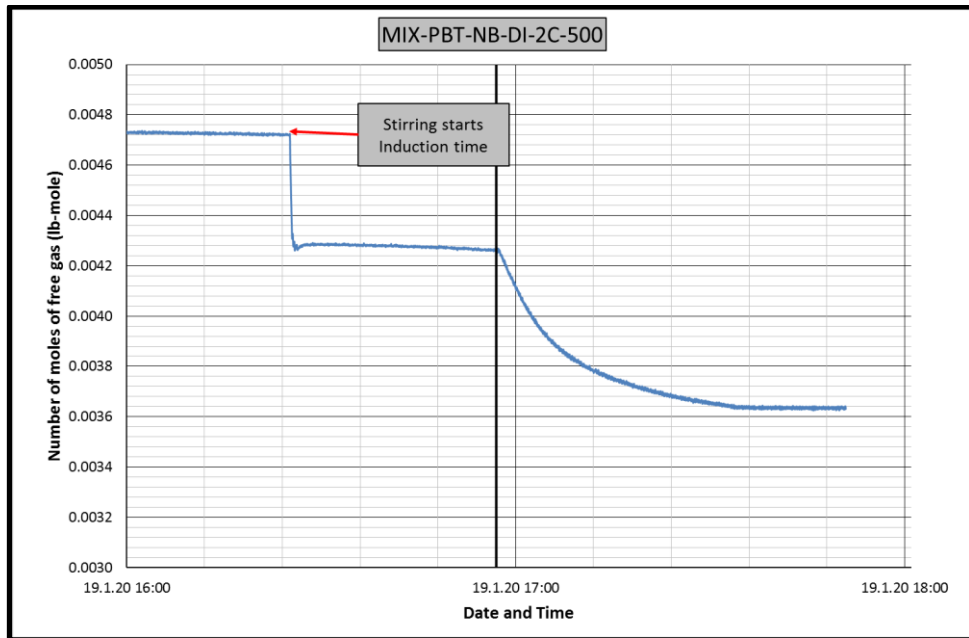


Figure B.100 Change in number of moles of free gas in CH₄-C₃H₈-PBT-NB-DI-2C experiment

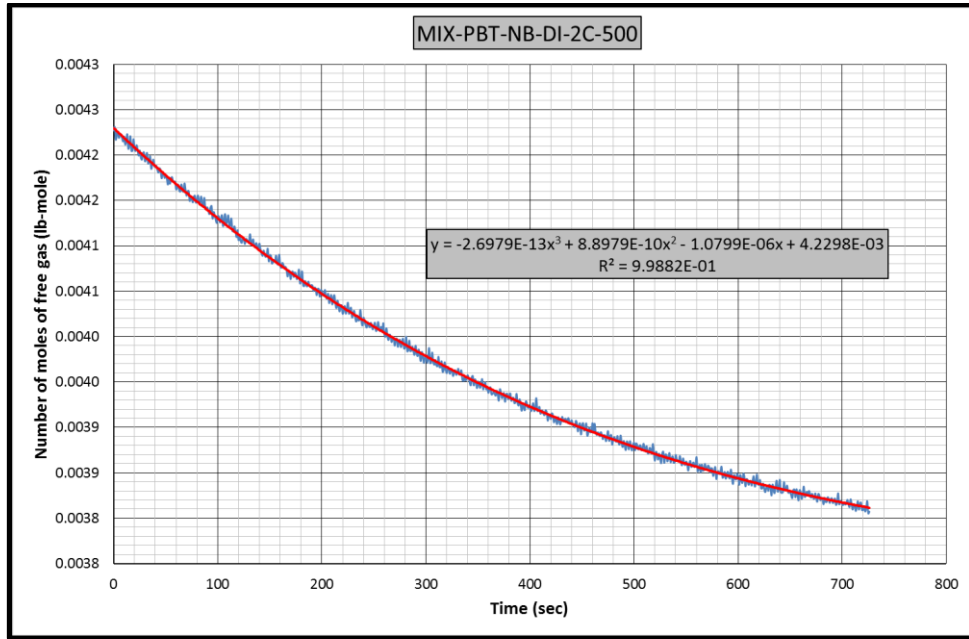


Figure B.101 Gas consumption rate equation-1 for CH₄-C₃H₈-PBT-NB-DI-2C experiment

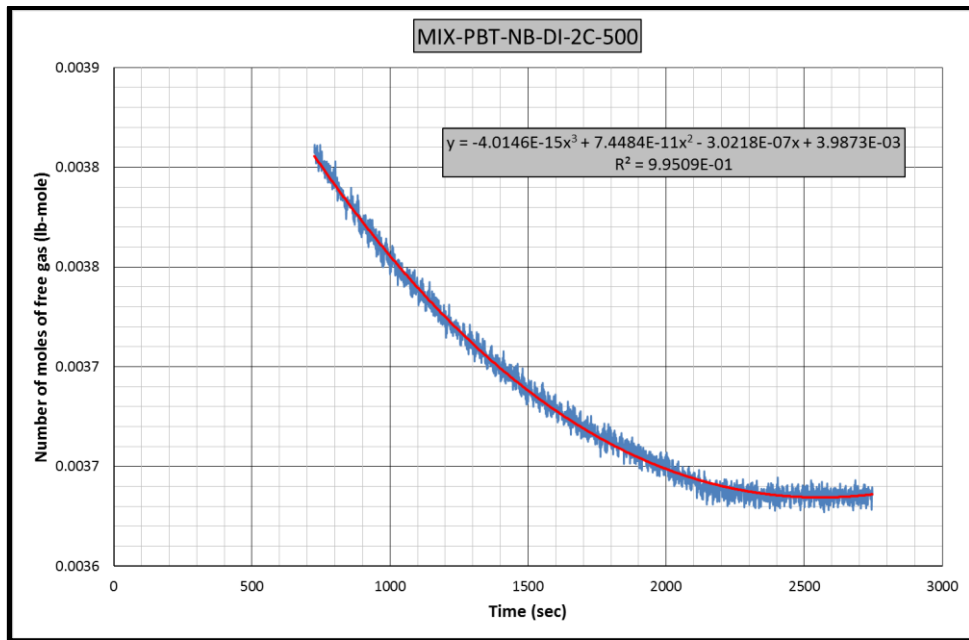


Figure B.102 Gas consumption rate equation-2 for CH₄-C₃H₈-PBT-NB-DI-2C experiment

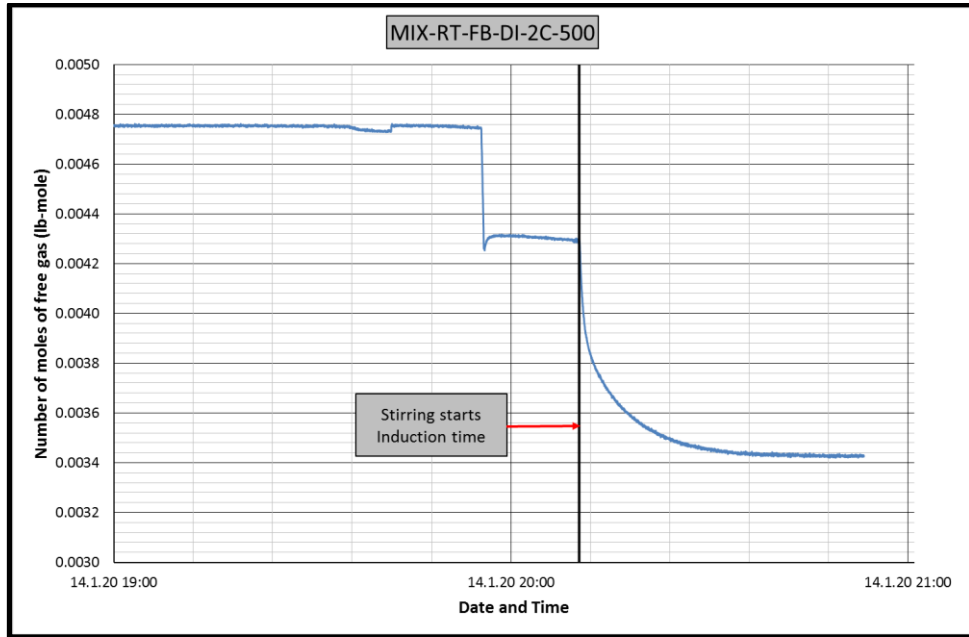


Figure B.103 Change in number of moles of free gas in CH₄-C₃H₈-RT-FB-DI-2C experiment

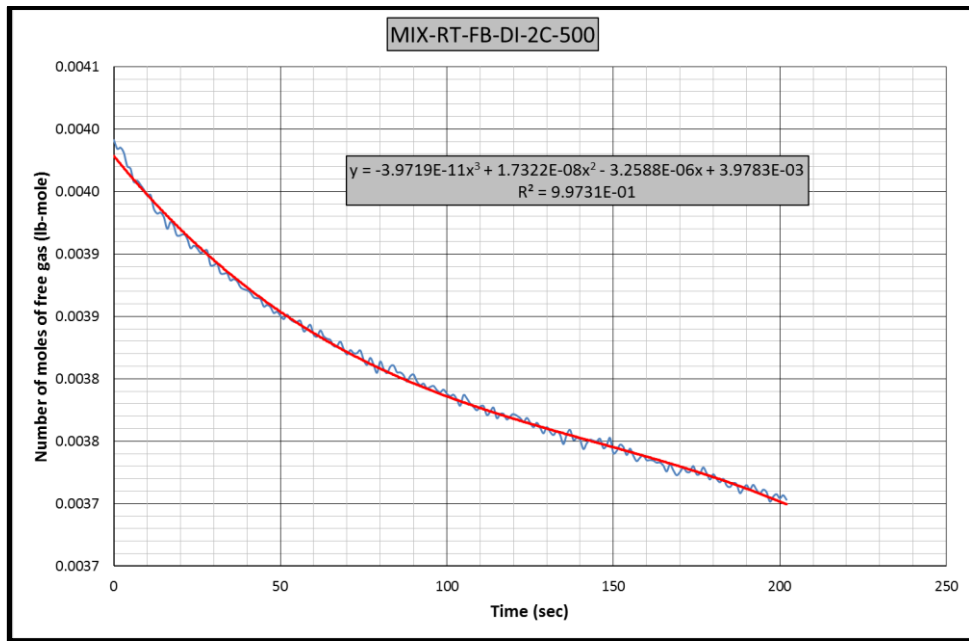


Figure B.104 Gas consumption rate equation-1 for CH₄-C₃H₈-RT-FB-DI-2C experiment

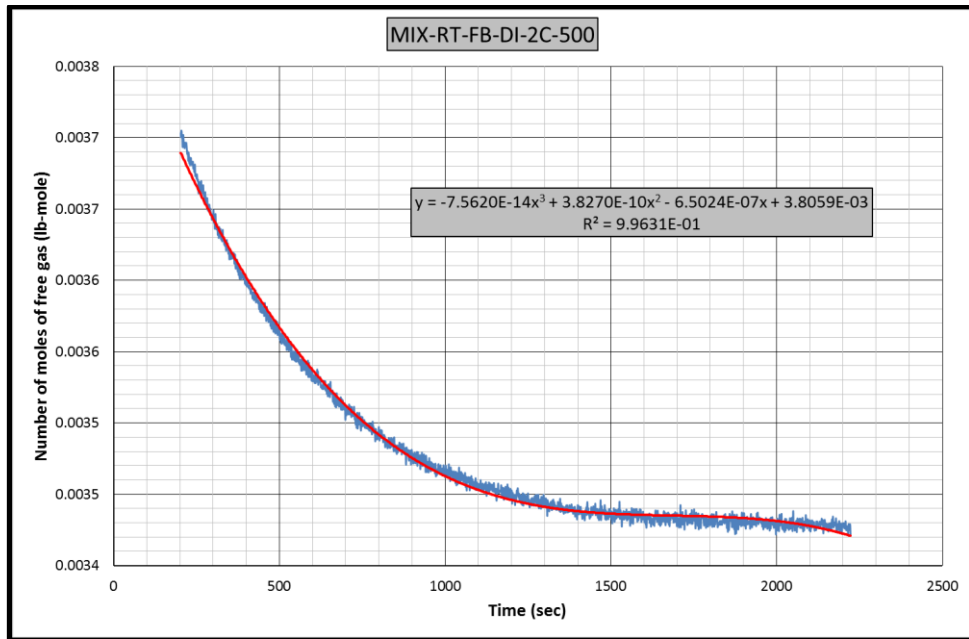


Figure B.105 Gas consumption rate equation-2 for CH₄-C₃H₈-RT-FB-DI-2C experiment

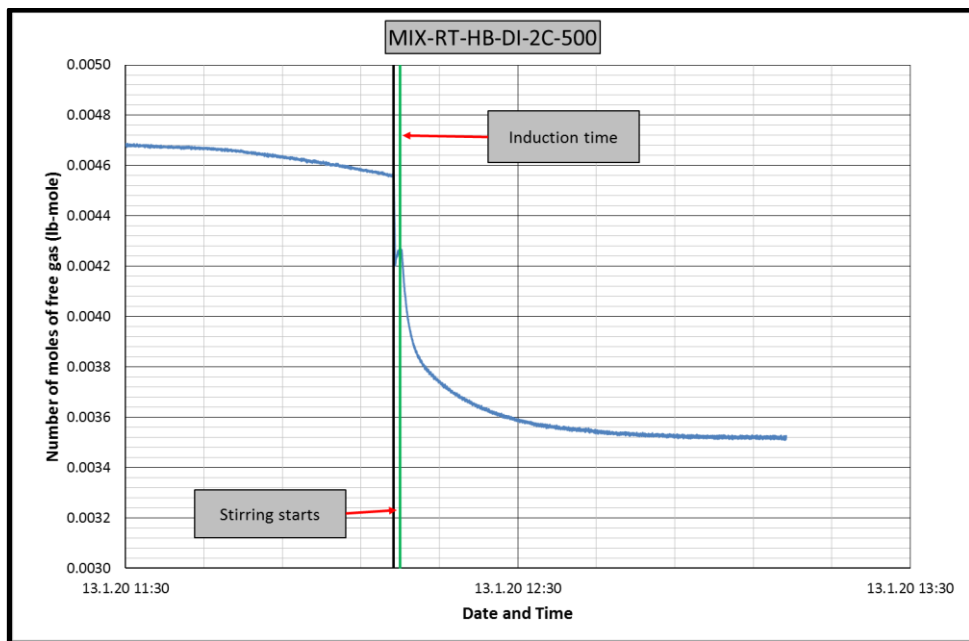


Figure B.106 Change in number of moles of free gas in CH₄-C₃H₈-RT-HB-DI-2C experiment

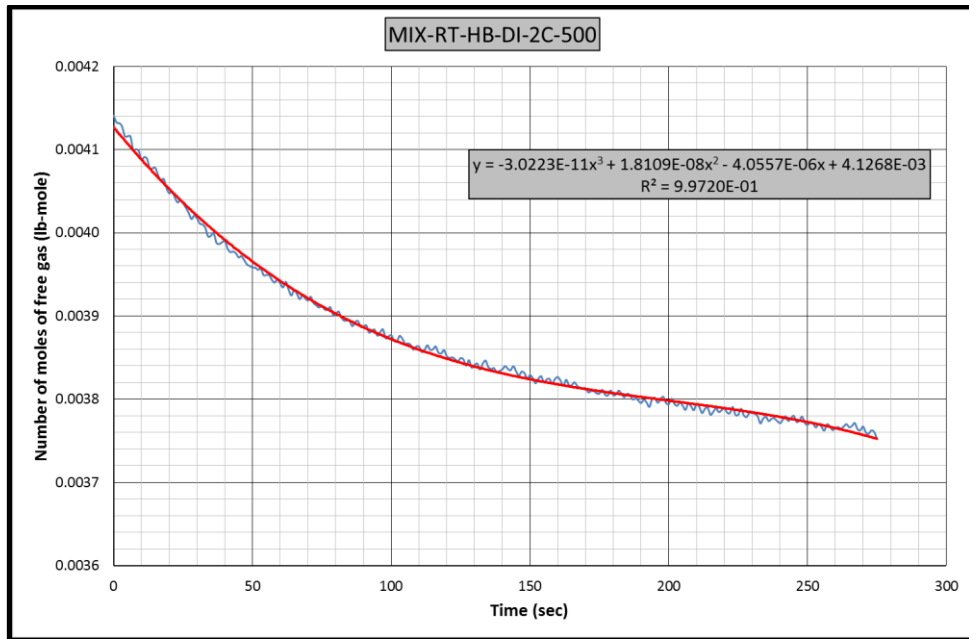


Figure B.107 Gas consumption rate equation-1 for CH₄-C₃H₈-RT-HB-DI-2C experiment

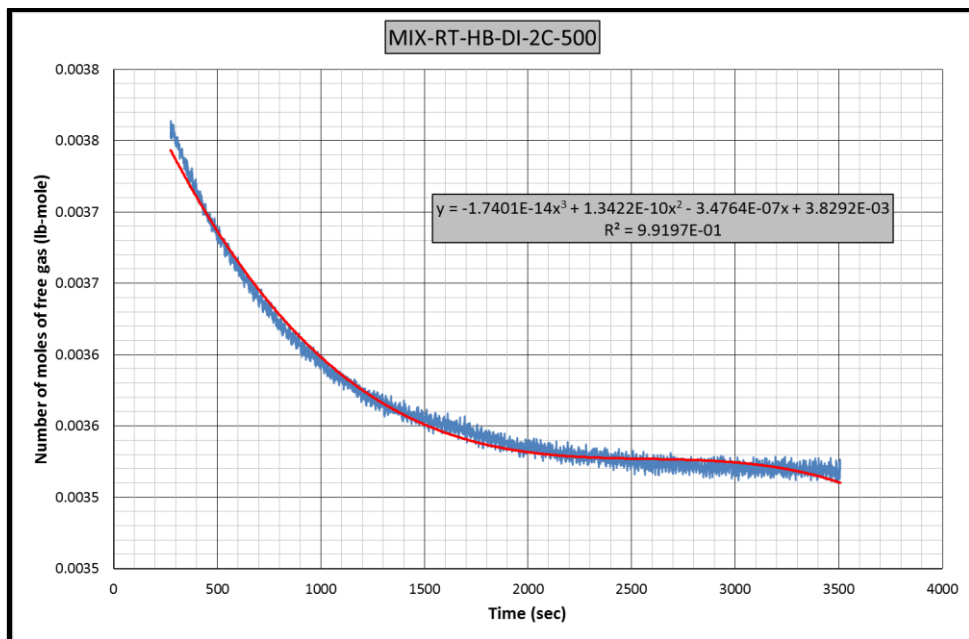


Figure B.108 Gas consumption rate equation-2 for CH₄-C₃H₈-RT-HB-DI-2C experiment

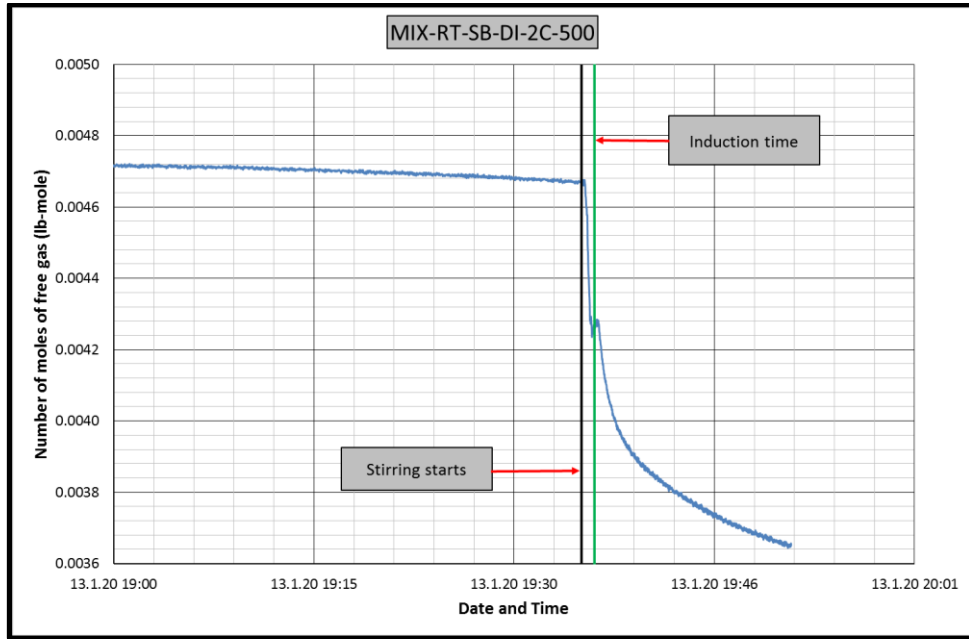


Figure B.109 Change in number of moles of free gas in CH₄-C₃H₈-RT-SB-DI-2C experiment

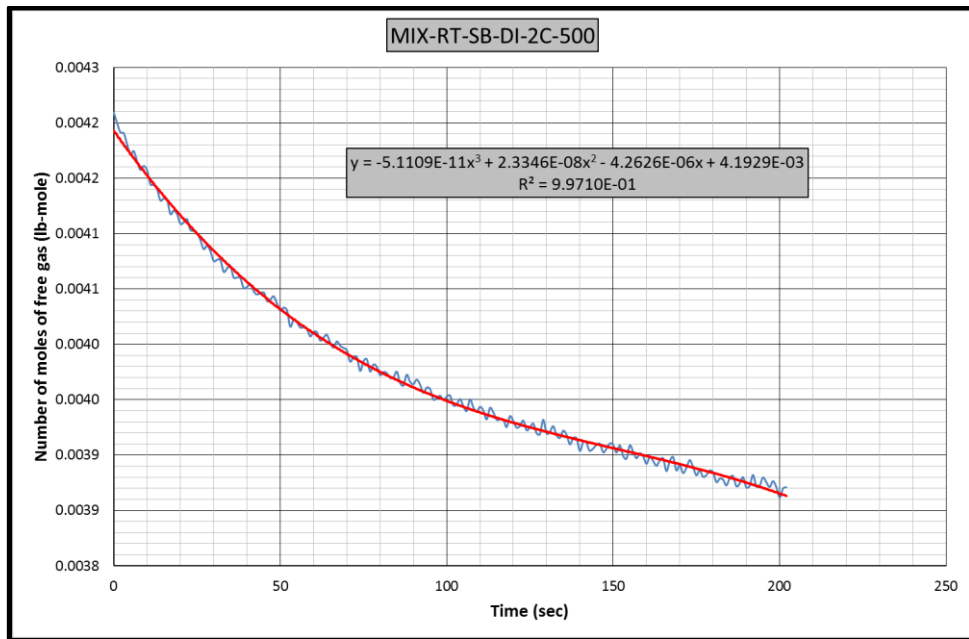


Figure B.110 Gas consumption rate equation-1 for CH₄-C₃H₈-RT-SB-DI-2C experiment

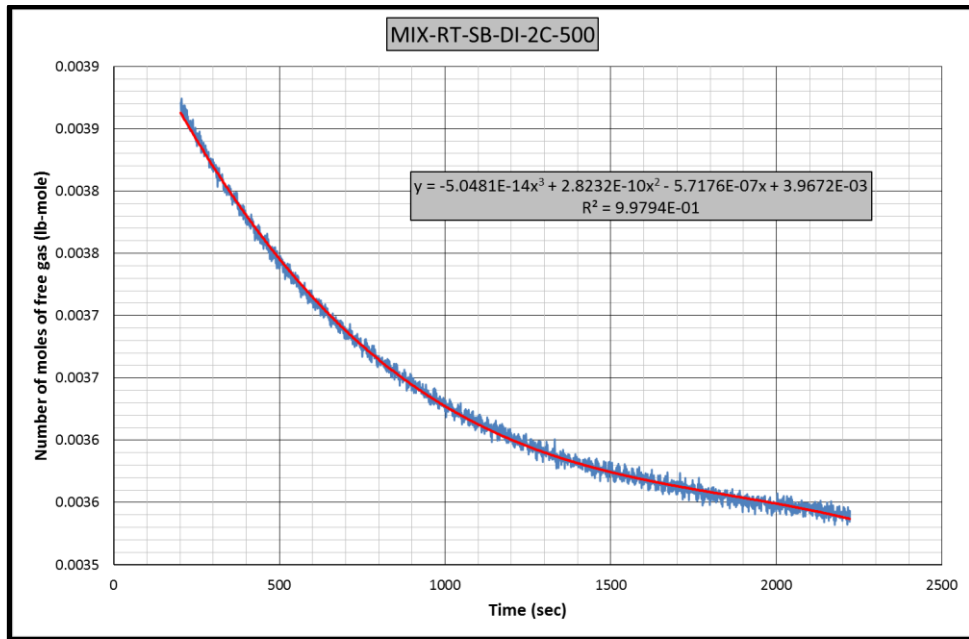


Figure B.111 Gas consumption rate equation-2 for CH₄-C₃H₈-RT-SB-DI-2C experiment

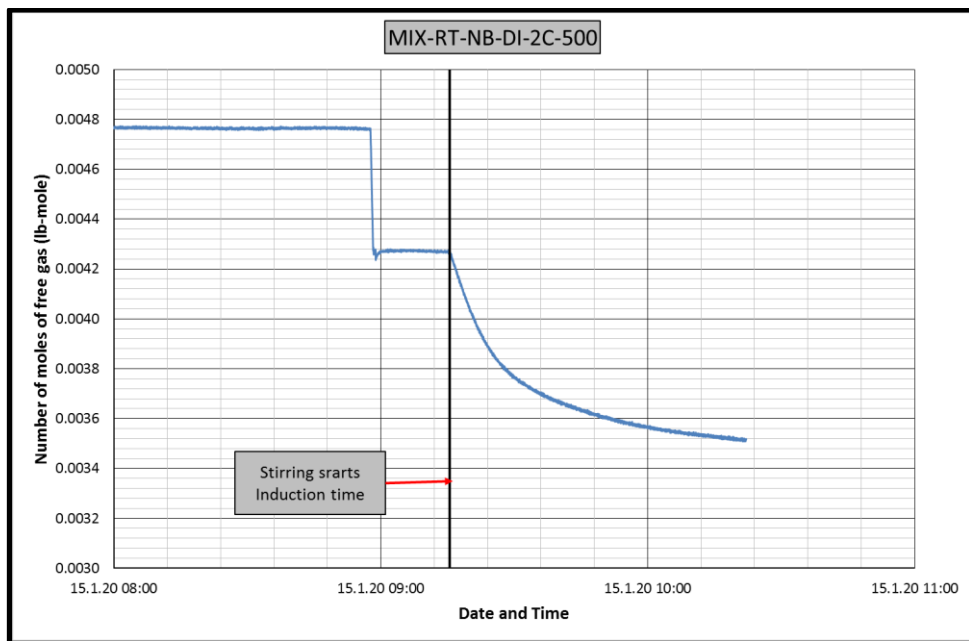


Figure B.112 Change in number of moles of free gas in CH₄-C₃H₈-RT-NB-DI-2C experiment

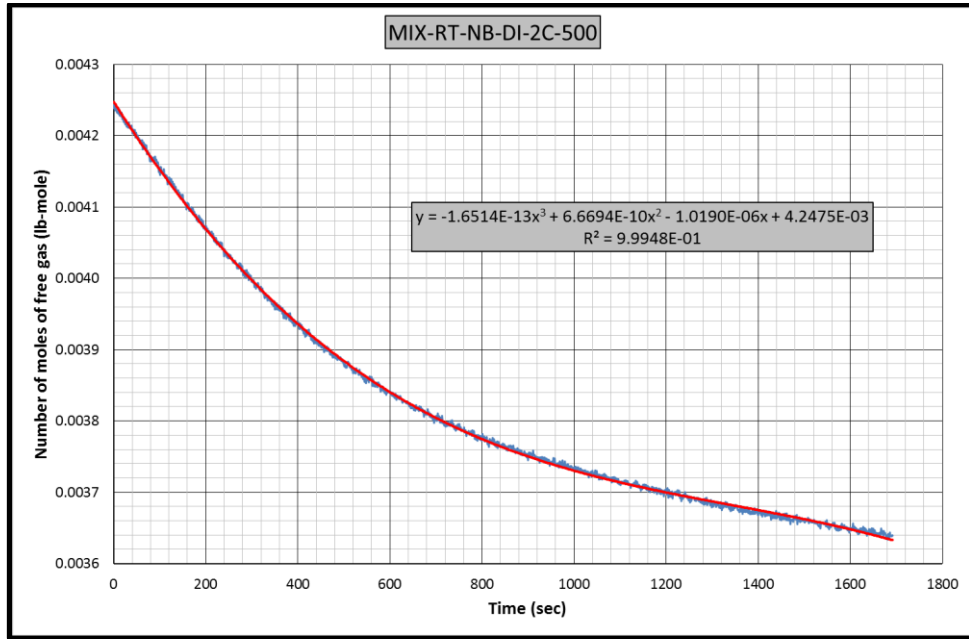


Figure B.113 Gas consumption rate equation for CH₄-C₃H₈-RT-NB-DI-2C experiment

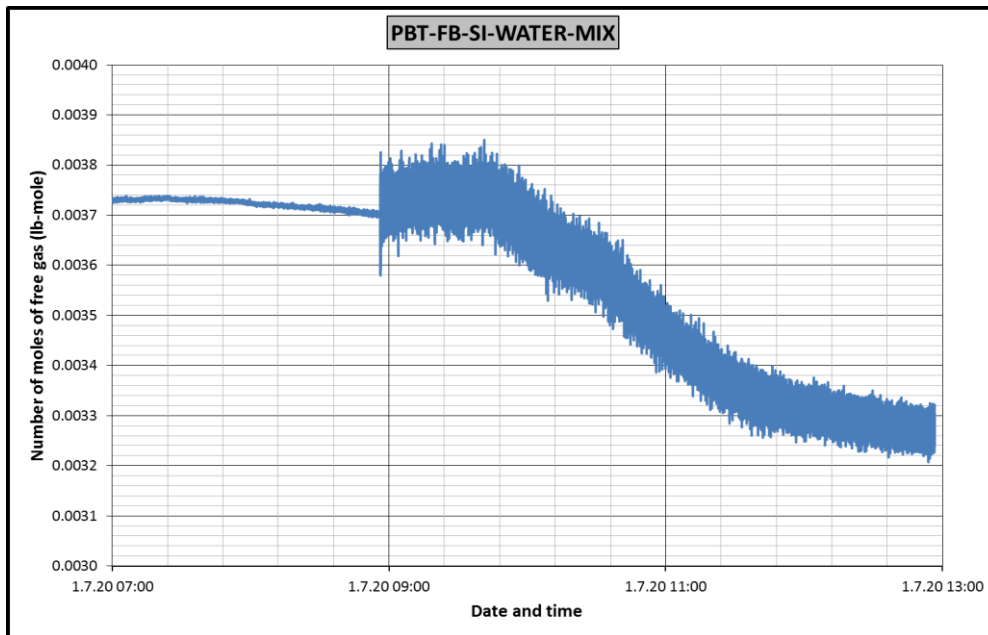


Figure B.114 Change in number of moles of free gas in PBT-FB-SI-WATER-MIX experiment

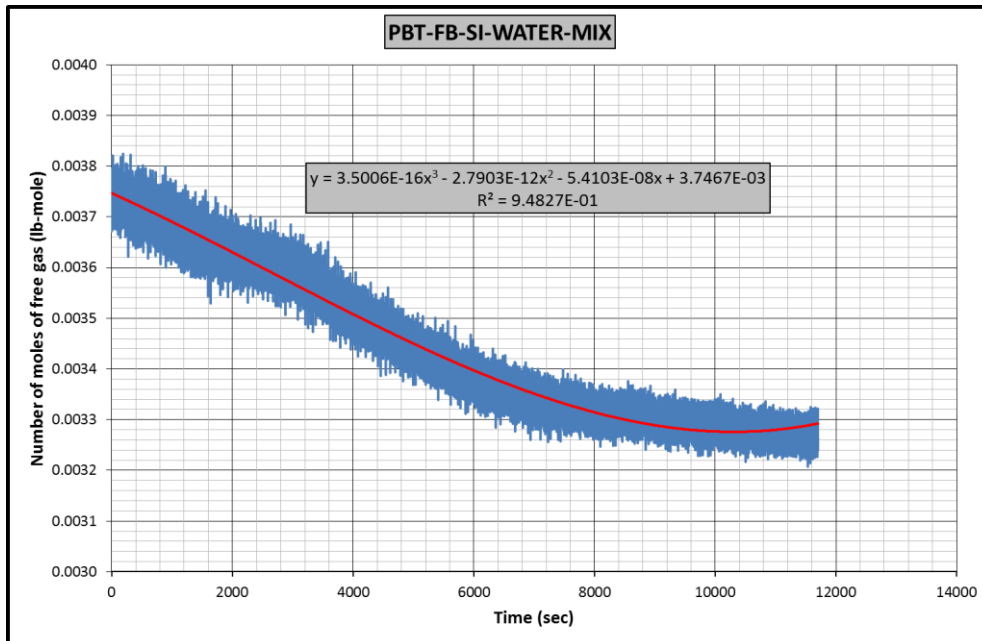


Figure B.115 Gas consumption rate equation for PBT-FB-SI-WATER-MIX experiment

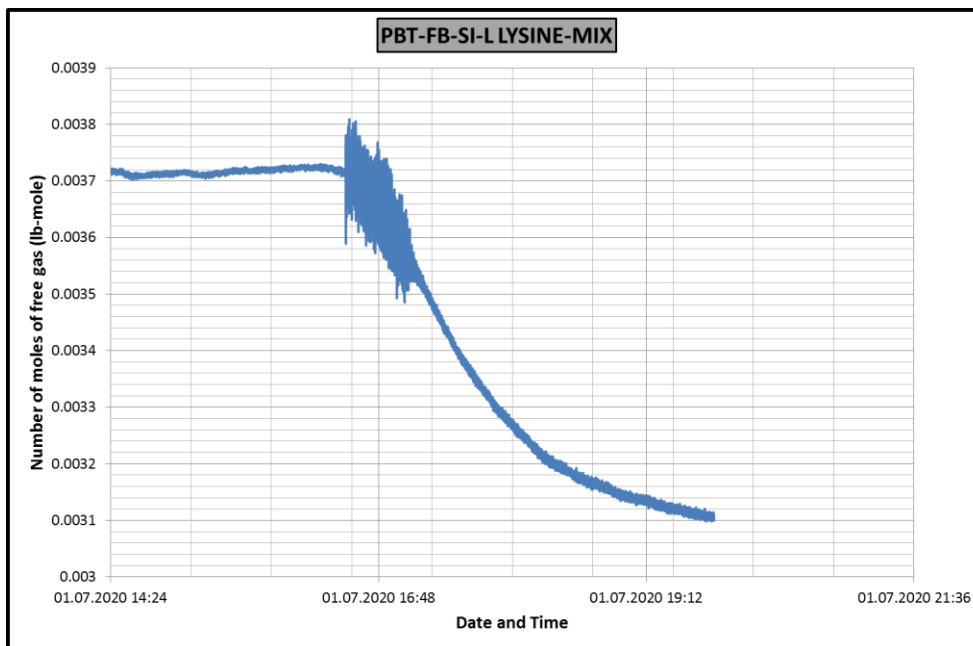


Figure B.116 Change in number of moles of free gas in PBT-FB-SI-L LYSINE-MIX experiment

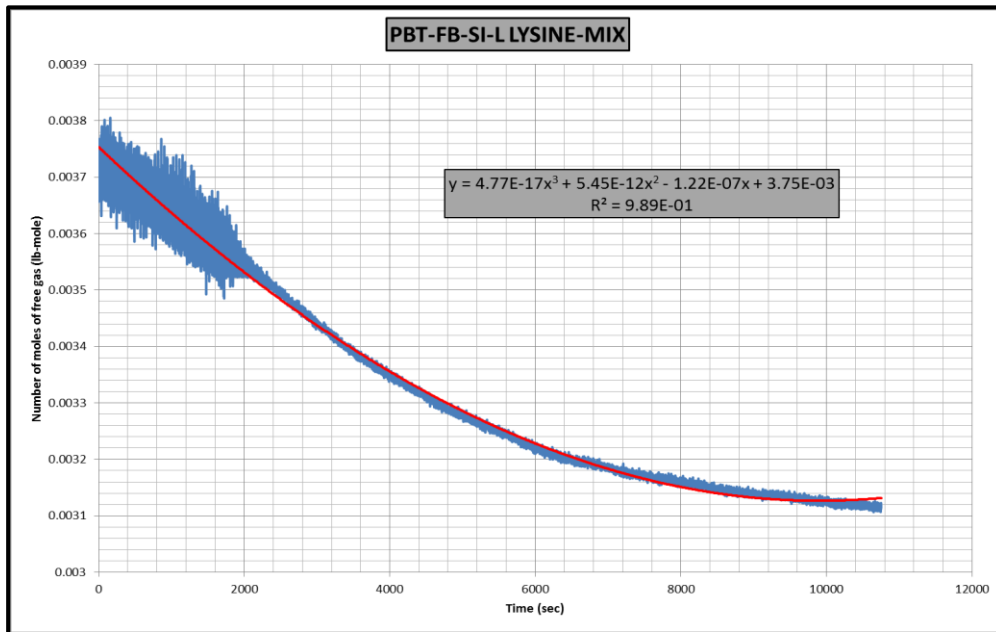


Figure B.117 Gas consumption rate equation for PBT-FB-SI-L LYSINE-MIX experiment

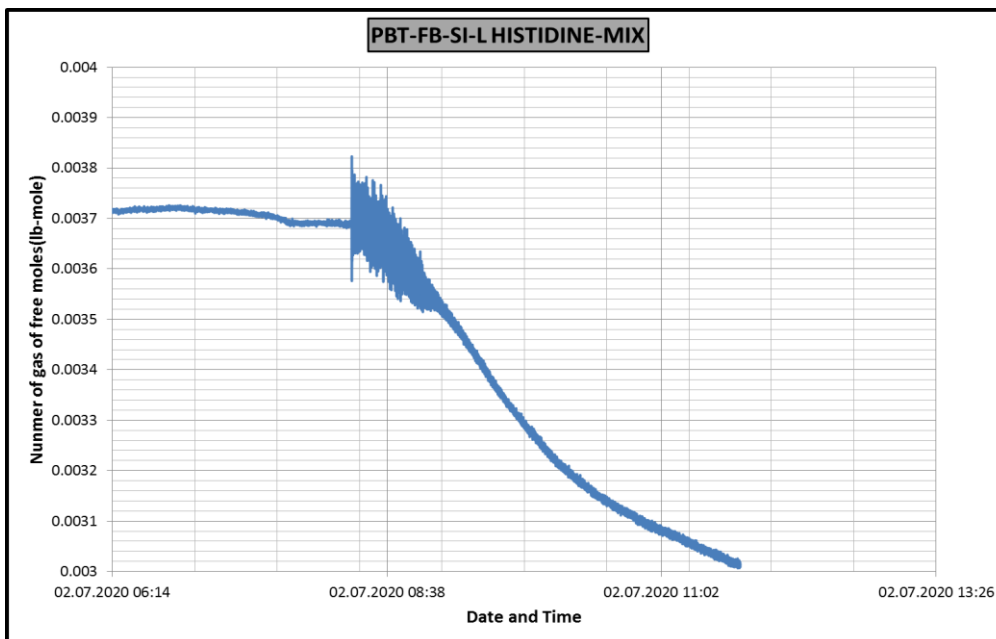


Figure B.118 Change in number of moles of free gas in PBT-FB-SI-LHISTIDINE-MIX experiment

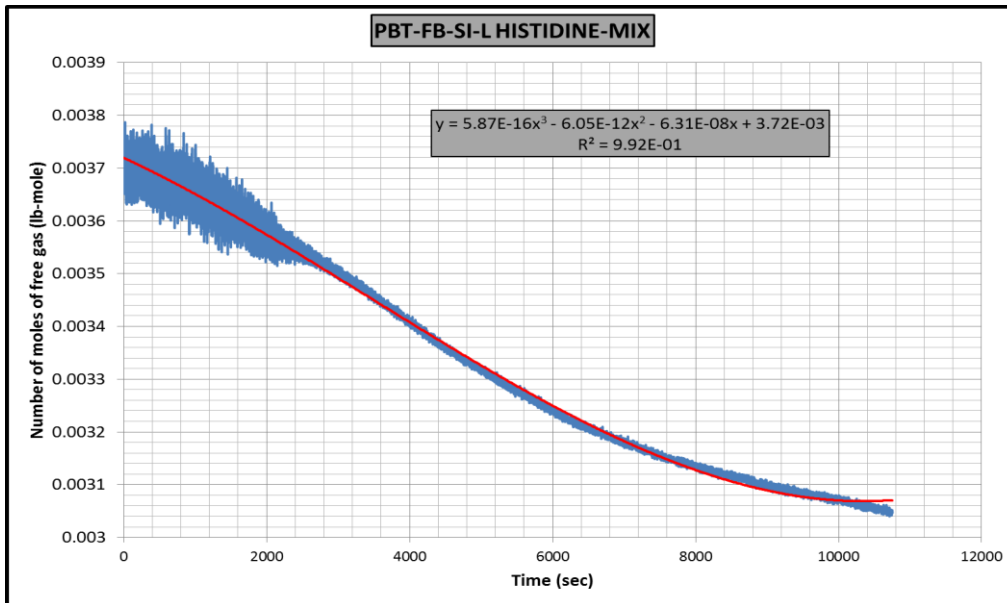


Figure B.119 Gas consumption rate equation for PBT-FB-SI-L HISTIDINE-MIX experiment

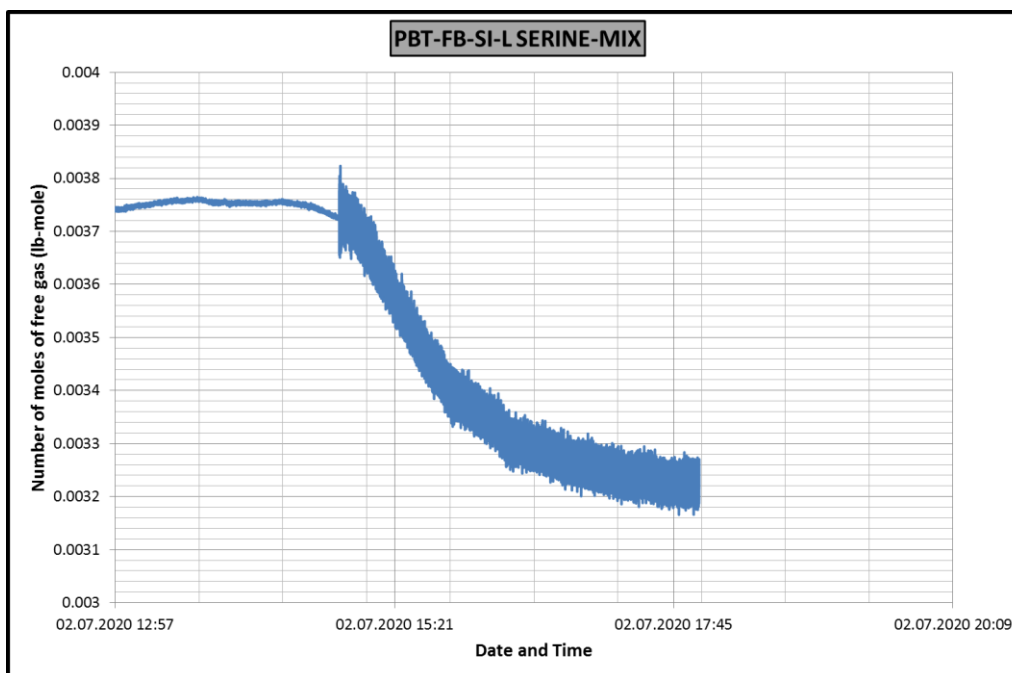


Figure B.120 Change in number of moles of free gas in PBT-FB-SI-L SERINE-MIX experiment

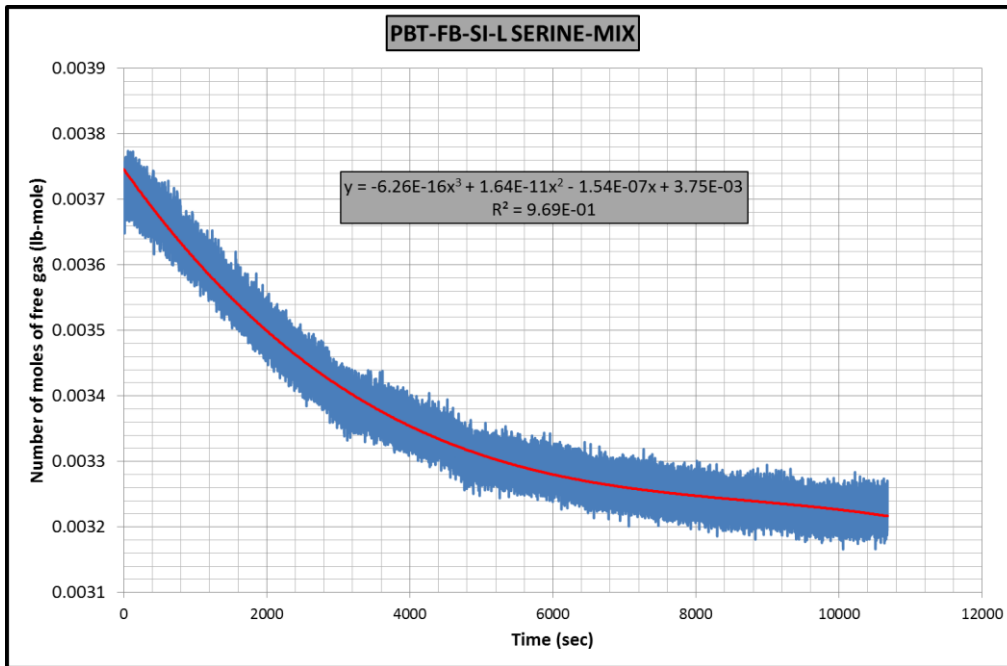


Figure B.121 Gas consumption rate equation for PBT-FB-SI-L SERINE-MIX experiment

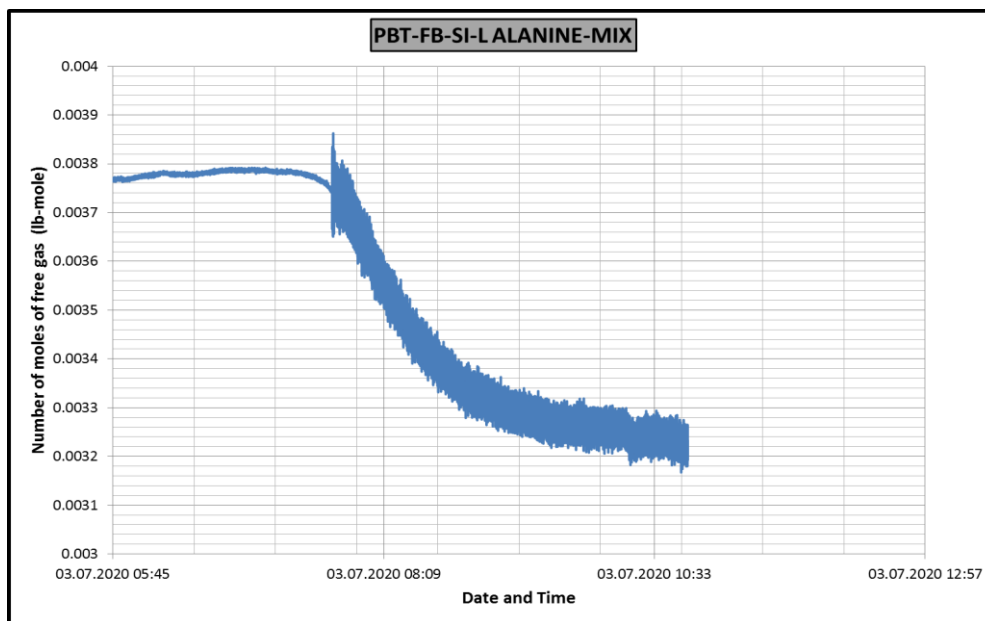


Figure B.122 Change in number of moles of free gas in PBT-FB-SI-L ALANINE-MIX experiment

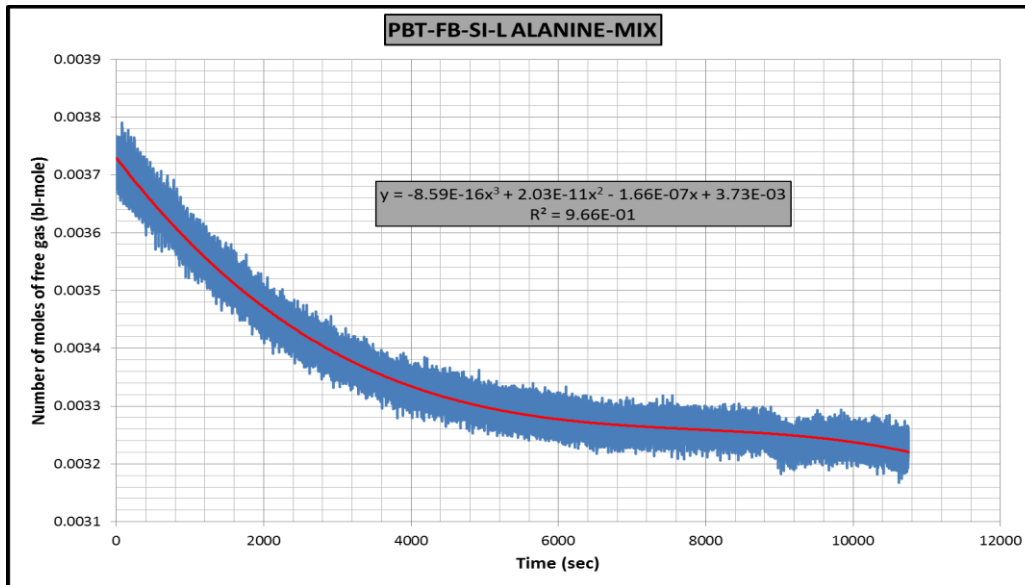


Figure B.123 Gas consumption rate equation for PBT-FB-SI-L ALANINE-MIX experiment

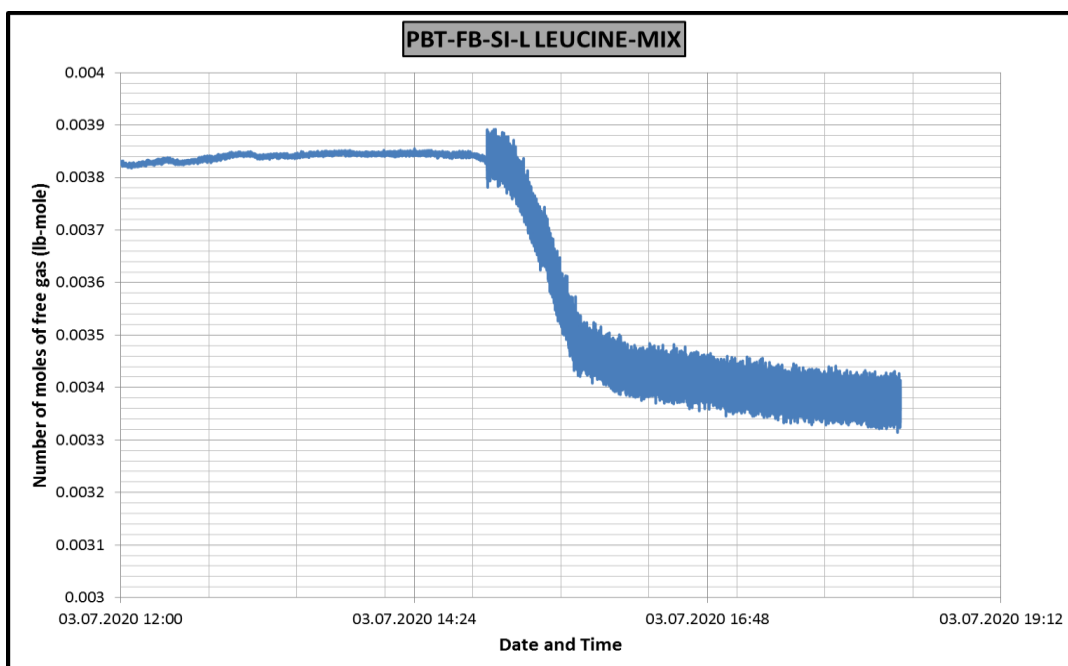


Figure B.124 Change in number of moles of free gas in PBT-FB-SI-L LEUCINE-MIX experiment

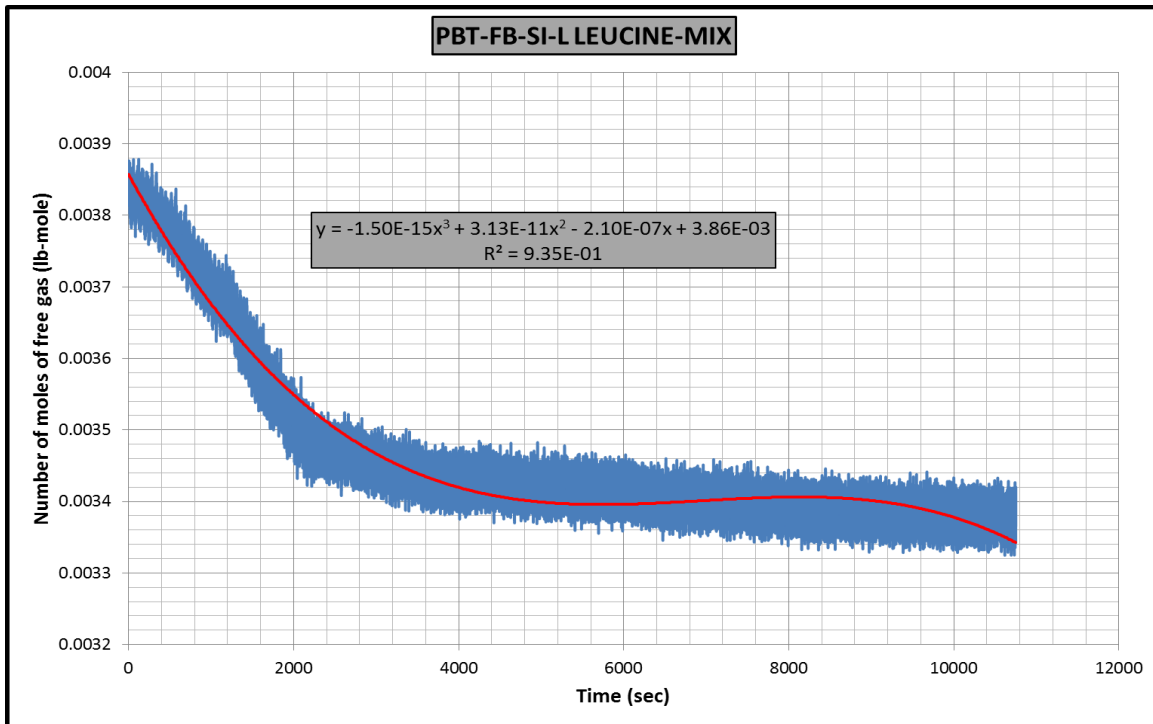


Figure B.125 Gas consumption rate equation for PBT-FB-SI-L LEUCINE-MIX experiment

CURRICULUM VITAE

Name Sotirios LONGINOS

Email s.n.longinos@gmail.com

Nationality Hellenic

EDUCATION

B.Sc.

2000– 2004: Technological Educational Institute of Central Greece (T.E.I.), Lamia, Electrical Engineering Department (4-year curriculum)

Diploma

2007– 2011: National Technical University of Athens (N.T.U.A.), Athens. School of Chemical Engineering (5 year curriculum, MSc equivalent)

M.Sc.

2012– 2013: University of Aberdeen (UOA), Aberdeen, School of Engineering, Master in Oil and Gas Engineering

Ph.D.

2014– 2020: Middle East Technical University (METU), Ankara Department of Petroleum and Natural Gas Engineering

EXPERIENCE

- | | |
|-------------------|---|
| 10/2003 – 03/2004 | Electrical Engineer Trainee,
Piraeus Port Authority S.A., Port Services, GR |
| 07/2010 –09/2010 | Chemical Engineer Trainee,
Hellenic Petroleum S.A., Aspropyrgos, Attica, GR
(Refinery's Conversion Units Department) |
| 09/2009-07/2012 | Research Assistant, School of Chemical Engineering, School of Chemical Engineering (Fuels and Lubricants Technology Laboratory) |

09/2011-09/2012

Project Manager,

Local Host LTD, Liverpool, UK

Publications (Journal Articles)

- [J7] Sukru Merey, **Sotirios Nik. Longinos**, The Gas Hydrate Potential of the Eastern Mediterranean Sea, Bull. Min. Res. Exp. (2019) 159?
- [J6] Sükrü Merey, **Sotirios Nik Longinos**, 'The Role of Natural Gas Hydrates During Natural Gas Transportation', OHU J. Eng. Sci., 7(2): 937-953, 2018
- [J5] Sükrü Merey, **Sotirios Nik Longinos**, 'Investigation of gas seepages in Thessaloniki mud volcano in the Mediterranean Sea'', Journal of Petroleum Science and Engineering 168, pp.81-97, 2018
- [J4] Sükrü Merey, **Sotirios Nik Longinos**, 'Does the Mediterranean Sea Have Potential for Producing Gas Hydrates?', Journal of Natural Gas Science and Engineering 55, pp. 113–134, 2018
- [J3] Sükrü Merey, **Sotirios Nik Longinos**, "Numerical simulations of gas production from Class 1 hydrate and Class 3 hydrate in the Nile Delta of the Mediterranean Sea", Journal of Natural. Gas Science and Engineering 52, pp. 248–266, 2018
- [J2] **Sotirios. Nik. Longinos**, Yahya. Muh. QADRI and Mahmut PARLAKTUNA, "Health and Safety Conditions in Four Major Industrial Sectors of Pakistan from 2010 to 2015", International Journal of Petroleum and Petrochemical Engineering (IJPPE), Volume 3, Issue 4, pp. 102-110, 2017
- [J1] G.S Dodos, T. Konstantakakos, **S. Longinos**, F. Zannikos "Effects of microbiological contamination in the quality of biodiesel fuels", Global NEST Journal, Vol 14, No 2, pp 175-182, 2012

Publications (Conference Articles)

- [C8] **Sotirios Nik. Longinos**, Sevtac Bulbul, Mahmut Parlaktuna, Potential Effects of Methane Hydrates to the Environment, PESXM-12th Panhellenic Scientific Conference in Chemical Engineering, Athens 2019, Greece
- [C7] **Sotirios Nik. Longinos**, Can Bakiler, Mahmut Parlaktuna, 'The Role of Greek Chemical Engineer in Future Upstream Activities in Greece', PESXM-12th Panhellenic Scientific Conference in Chemical Engineering, Athens 2019, Greece

[C6] **Sotirios Nik. Longinos**, Sevtac Bulbul, Mahmut Parlaktuna, ‘Methane’s Gas hydrates Possible Consequences in the Environment’, ICERAT-4th International Congress on Environmental Research & Technology, Athens 2018, Greece

[C5] **Sotirios Nik. Longinos**, Sukru Merey, ‘CO₂ Sequestration in the Mature Oil Fields: A Case Study of Bati Raman Oil Field, Turkey’, ENRES-1st International Conference on Energy Research, Alanya 2018, Turkey

Books-Book Chapters

[B3] Achinas S, **Longinos S**, Achinas V, Euverink GJW. Scale-up operations for biogas production: Analysis on critical factors governing large scale operations. In: Balagurusamy (Ed.), Biogas production, Springer (in press).

[B2] **Sotirios Nik. Longinos**, Dionysia-Dimitra Longinou, Spyridon Achinas, Natural Gas Hydrates: Possible Environmental Issues, in Contemporary Environmental Issues and Challenges in Era of Climate Change, Singh P., Singh R.P., Srivastava V. (Edit.), Springer, 2020

[B1] **Sotirios Longinos**, Potential Environmental Challenges for Gas Hydrates, LAP LAMBERT Academic Publishing (Edit.), 2019

Reviewer

2017-present Journal of Natural Gas Engineering and Science

2017-present Journal of Petroleum Engineering and Science

2017-present Journal of Environmental Geotechnics

2019-present Journal of Waste Management and Research

Additional Information

Affiliations Society of Petroleum Engineers • Energy Institute • Scientific Society of Technological Education Engineers (EETEM) • Institute of Corrosion • Society of Greek Chemical Engineers

Computer Skills Windows, Word, Excel, PowerPoint, Internet

Languages **Greek** : Fluent written and oral communication skills (native speaker)

English : Excellent written and oral communication skills (Certificate of Proficiency)

Italian : Good written and oral communication skills

Arabic : Good written and oral communication skills

Military Obligations Fulfilled: Signals Division • Hellenic Army (2004 – 2005)

Interests President of Undergraduate Student Association (N.T.U.A. & T.E.I.)

Representative in Rector Council & Senate (N.T.U.A & T.E.I.)

Student Representative in School Council (University of Aberdeen)

Soccer (U16 National Team until 1997) • Sailing (member of sailing team - par

• Literature • Music